INFORMATION TO USERS

This manuscript has been reproduced from the microfilm master. UMI films the text directly from the original or copy submitted. Thus, some thesis and dissertation copies are in typewriter face, while others may be from any type of computer printer.

The quality of this reproduction is dependent upon the quality of the copy submitted. Broken or indistinct print, colored or poor quality illustrations and photographs, print bleedthrough, substandard margins, and improper alignment can adversely affect reproduction.

In the unlikely event that the author did not send UMI a complete manuscript and there are missing pages, these will be noted. Also, if unauthorized copyright material had to be removed, a note will indicate the deletion.

Oversize materials (e.g., maps, drawings, charts) are reproduced by sectioning the original, beginning at the upper left-hand corner and continuing from left to right in equal sections with small overlaps. Each original is also photographed in one exposure and is included in reduced form at the back of the book.

Photographs included in the original manuscript have been reproduced xerographically in this copy. Higher quality 6" x 9" black and white photographic prints are available for any photographs or illustrations appearing in this copy for an additional charge. Contact UMI directly to order.

UMI

A Bell & Howell Information Company
300 North Zeeb Road, Ann Arbor MI 48106-1346 USA
313/761-4700 800/521-0600

SEISMIC ARRAY PROCESSING AND COMPUTATIONAL INFRASTRUCTURE FOR IMPROVED MONITORING OF ALASKAN AND ALEUTIAN SEISMICITY AND VOLCANOES

A
THESIS

Presented to the Faculty
of the University of Alaska Fairbanks

in Partial Fulfillment of the Requirements
for the Degree of

DOCTOR OF PHILOSOPHY
By

Kent Gordon Lindquist, B.A., M.S.

Fairbanks, Alaska

May 1998

SEISMIC ARRAY PROCESSING AND COMPUTATIONAL INFRASTRUCTURE FOR IMPROVED MONITORING OF ALASKAN AND ALEUTIAN SEISMICITY AND VOLCANOES

By

Kent Gordon Lindquist

RECOMMENDED:

Prof. Max Wyss

Assoc. Prof. Douglas Christensen

Research Prof. Stephen McNutt

Research Prof. Roger Hansen
Advisory Committee Chair

Assoc. Prof. Paul Layer
Department Head

APPROVED:

Prof. Paul Reichardt
Dean, College of Natural Sciences,
Engineering, and Mathematics

Prof. Joseph Kan
Dean of the Graduate School

Date

Abstract

We constructed a near-real-time system, called Iceworm, to automate seismic data collection, processing, storage, and distribution at the Alaska Earthquake Information Center (AEIC). Phase-picking, phase association, and interprocess communication components come from Earthworm [U.S. Geological Survey]. A new generic, internal format for digital data supports unified handling of data from diverse sources. A new infrastructure for applying processing algorithms to near-real-time data streams supports automated information extraction from seismic wavefields. Integration of Datascope [U. of Colorado] provides relational database management of all automated measurements, parametric information for located hypocenters, and waveform data from Iceworm. Data from 1997 yield 329 earthquakes located by both Iceworm and the AEIC. Of these, 203 have location residuals under 22 km, sufficient for hazard response.

Regionalized inversions for local magnitude in Alaska yield M_L calibration curves ($\log A_0$) that differ from the Californian Richter magnitude. The new curve is 0.2 M_L units more attenuative than the Californian curve at 400 km for earthquakes north of the Denali fault. South of the fault, and for a region north of Cook Inlet, the difference is 0.4 M_L. A curve for deep events differs by 0.6 M_L at 650 km.

We expand geographic coverage of Alaskan regional seismic monitoring to the Aleutians, the Bering Sea, and the entire Arctic by initiating the processing of four short-period, Alaskan seismic arrays. To show the array stations' sensitivity, we detect and locate two microearthquakes that were missed by the AEIC. An empirical study of the location sensitivity of the arrays predicts improvements over the Alaskan regional network that are shown as map-view contour plots. We verify these predictions by detecting an M_L 3.2 event near Unimak Island with one array. The detection and location of four representative earthquakes illustrates the expansion of geographic coverage from array processing. Measurements at the arrays of systematic azimuth residuals, between 5° and 50° from 203 Aleutian events, reveal significant effects of heterogeneous structure on wavefields. Finally, algorithms to automatically detect earthquakes in continuous array data are demonstrated with the detection of an Aleutian earthquake.

Table of Contents

List of Figures

List of Tables

Acknowledgments

There are a great many people without whose support this thesis work would not have been accomplished. First, we thank Dan Quinlan and Danny Harvey, authors of Datascope and the Datascope Seismic Application Package, for their software contributions to the world of seismology, and for years of productive advice, help, and collaboration. Second, the Iceworm system which leads this work was begun as an extension of the Earthworm project of the United States Geological Survey. We are indebted to the Earthworm Team of Menlo Park, including Alex Bittenbinder, Barbara Bogaert, Lynn Dietz, and Will Kohler for providing their source code and for useful discussions and visits. The staff of the seismology lab at the University of Nevada Reno, including Ken Smith, Glenn Biasi, and David von Seggern have provided a very helpful beta-test site, and with the contributions of David Chavez as well our work has gained a great deal. At the Alaska Earthquake Information Center and Alaska Volcano Observatory, we thank the faculty, staff, and graduate students for extensive discussion and collaboration during the development of this work. While all here deserve thanks, special mention goes to Mitch Robinson for his enthusiastic maintenance and improvement of our computer network, plus productive collaboration on hardware and software system design; and to John Benoit and Dr. Stephen McNutt, who deserve a large share of credit for the volcano monitoring work presented here. Several students participating in the National Science Foundation's Research Experience for Undergraduates program (grant number EAR95-31601) have

contributed to this work. Suzanne Floyd helped in the initial stages of the local-magnitude automation. Cristyn Presley and Elizabeth Wolf aided in empirical studies of predicted array performance, and in preparing for array processing at the AEIC. Janae Deverell made an impressive contribution during the summer of 1997 to our initial studies with the Alaskan array data. Regrettably it is not possible to thank by name the many people whose advice and help were invaluable to the completion of this work. However, it is the author's pleasure to thank Dr. Roger Hansen for years of patient coaching, support, and instruction, as well as Drs. Douglas Christensen, Max Wyss, Stephen McNutt, and Paul Layer for their instruction and discussions during the past three years. Finally, the author thanks his family for their dedicated support.

Chapter 1

Introduction

Regional seismic networks serve a variety of functions, with variable emphasis depending on their locations, seismicity levels, hardware deployment, and funding justification. Quick response to the hazard of large earthquakes is one of the most prominent reasons for public interest in funding seismic networks, both for determining the strong ground shaking caused by these events and for ameliorating the impact of secondary effects such as tsunami. Similarly, seismology with networks of stations on volcanoes provides the ability to monitor and sometimes forecast volcanic eruptions, mitigating the hazard to air traffic of airborne ash clouds and the hazard to population centers from pyroclastic flows and lahars. Related to hazard response, hazard assessment is another frequent focus for seismology with regional networks. Study of the seismic and volcanic potential of a region is made possible by the development of earthquake catalogs, along with more sophisticated measures. Another aspect of regional seismology important to the general public is nuclear test-ban verification, now made more important by the recent passage of the Comprehensive Test-Ban Treaty (CTBT) [Monastersky, 1996]. Especially in the topics of CTBT and volcano monitoring, one can extend the capability of a regional seismic network to include similar data streams and processing techniques for infrasound

propagation in the atmosphere. Complementing the applications of regional seismic networks that are of direct value to the daily lives of the public, regional networks are essential to scientific measurement of the earth. At the most rudimentary level this involves data archival and the production of catalogs of earthquake locations, magnitudes, and detected phases. Further measurements are often derived from these basic elements by individual scientists or scientific groups, however the work is customized by each scientist for each application.

Many factors contribute to the success of a regional seismic network in its public-hazard-response goals and, if applicable, treaty-verification goals; and as well, many factors influence the ability of a regional network to achieve its full scientific potential. Chief among these is the software infrastructure available to receive, process, store, and distribute the data and scientific measurements. Network processing is a broad problem which touches on geophysical signal processing, association algorithms, computer science, and wavefield modelling. Nowhere is the importance of a well-designed infrastructure for seismic data handling and processing more clear than in Alaska.

Alaska provides great potential for the study of regional earth processes, seismic wave propagation in complex, heterogeneous media, and the understanding of tectonic processes. Equally interesting are the extensive scientific insights to be gained and the potential for improving the safety of human communities in the face of hazardous volcanic eruptions, with their pyroclastic flows, volcano-induced tsunamis and ash clouds hazardous to air transportation; and the seismic and tsunamigenic hazard from some of the

world's largest earthquakes. Coupled with the solid-earth monitoring, infrasonic waves from volcanic eruptions can be considered in the same processing context. The understanding of regional-wave propagation characteristics is especially important in the context of earthquake hazard assessment as well as the CTBT for the development of transportable discriminants. One of the key issues here is the use of array processing for regional monitoring, and great value could come from an understanding of the use of teleseismic arrays in a regional context. The crustal complexity of Alaska provides an ideal testbed for studying array-based wavefield monitoring.

With approximately 6000 earthquakes reported each year by the Alaska Earthquake Information Center, the Alaskan regional network provides 11% of the earthquakes located in the world and 52% of the earthquakes reported in the United States. The events reported include a transition of strike-slip to subduction-zone events from the Western to Eastern Aleutians all the way into central Alaska, and transform faulting near the Alaskan panhandle [Biswas *et al.*, 1980; Taber *et al.*, 1991; Page *et al.*, 1991; Gedney, 1980]. Earthquakes extend from the surface to depths greater than 150 km [Page *et al.*, 1980]. The distribution of events located by the Alaskan network is shown in Figure 1.1. While extensive, a comparison of this set of events with the catalog of Preliminary Determination of Epicenters (PDE) by the Global network (Figure 1.2) suggests that much of the Aleutian seismicity is being missed.

Improvement of earthquake detection in the Aleutian Chain is one of the principal areas for improvement in Alaskan regional network processing. In the current work, we

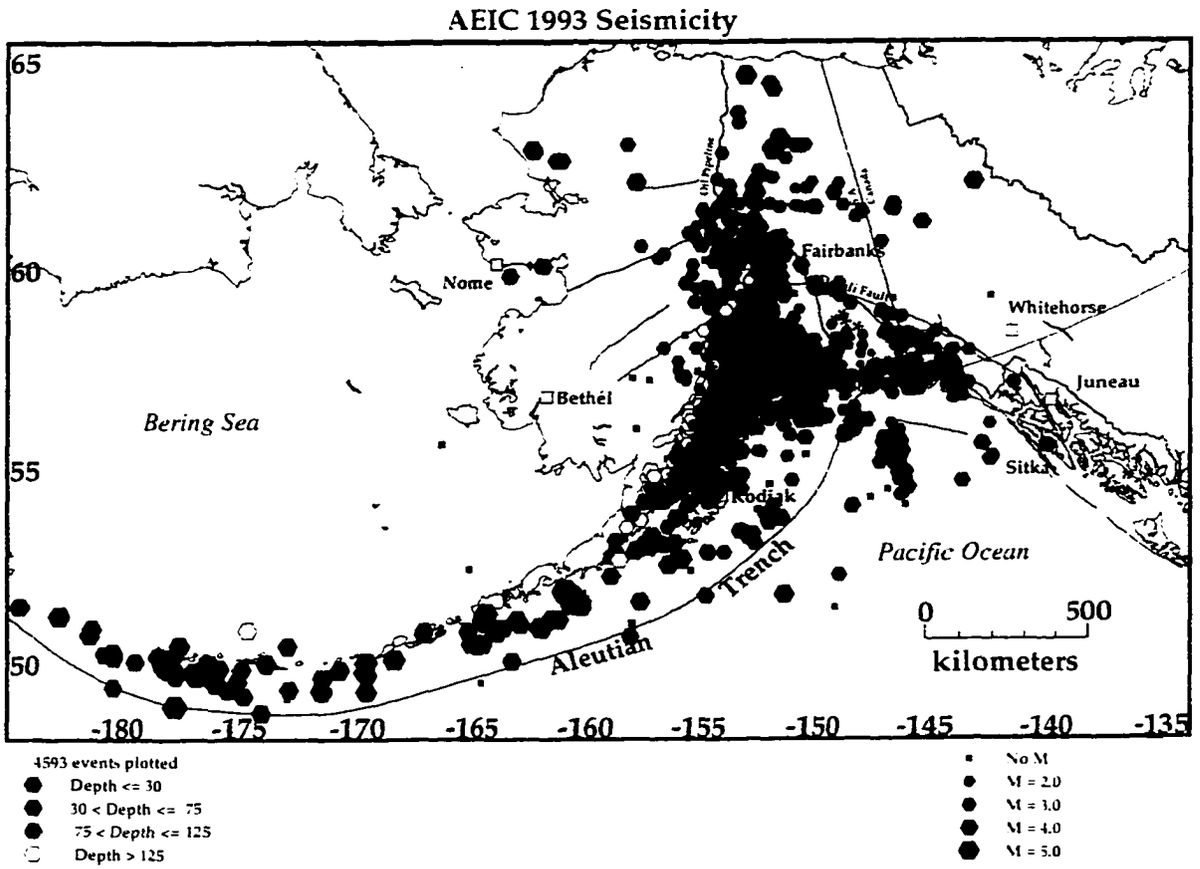

Figure 1.1

Map of seismicity detected by the Alaska Earthquake Information Center for 1993. Epicenters with magnitudes are shown as hexagons; epicenters without magnitudes are shown as squares. This map shows 4593 epicenters. Most of the epicentral locations in the Aleutians are taken from the National Earthquake Information Center.

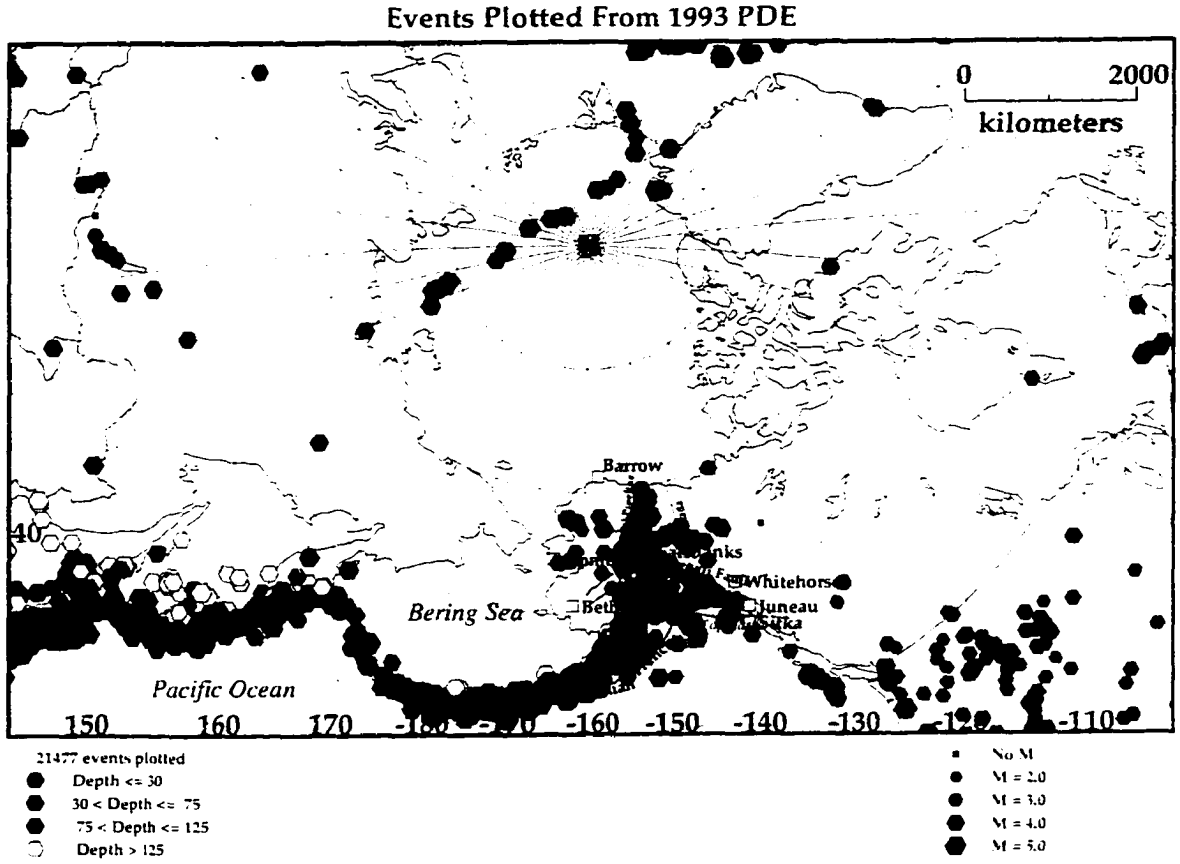

Figure 1.2

Map of seismicity in the USGS Preliminary Determination of Epicenters catalog for 1993. This map shows 21,477 earthquakes, with extensive seismicity along the Aleutian Islands; Arctic seismicity such as the northward extension of the mid-Atlantic ridge; and pronounced gaps in areas of known seismic activity, such as the Chukotsk peninsula.

contribute to this goal by turning several teleseismic arrays to the task of regional earthquake monitoring. Another large area for improvement is the integration of efforts and data flow to achieve unified monitoring at the lowest possible detection levels of the greater Alaskan region, including the Aleutian Islands, the Alaskan panhandle, and the Bering Sea. Automated seismic processing allows faster earthquake detection and location for hazard response, as well as more robust monitoring of active volcanoes. We have constructed an automated system to handle this processing, generalizable to allow the automated assembly of large data sets (tens of thousands of measurements) for scientific experiments. We demonstrate this with an attenuation study for Alaska that inverts for a regionalized local-magnitude scale. Characterizing attenuation (Q) and other propagation characteristics over the state of Alaska requires the integration and synthesized processing of large amounts of data from large areas, which requires a system such as the one developed in this work. To achieve these results we have implemented all of the automatic processing in the context of a Relational Database Management System, which smooths the integration of separate monitoring efforts for Arctic seismicity (for example monitoring by the Alaska Earthquake Information Center and Alaska Volcano Observatory; monitoring by the Pacific Geoscience Center of Western Canada; and global monitoring through the Preliminary Determination of Epicenters).

The software technology at many regional seismic networks is close to that in place for the Alaskan network at the onset of the current work, with 1971 seismic location software, ad-hoc data intake and archival software, and hand analysis of noisy, low-bandwidth,

analog seismic data. Individual experiments are often run within small sub-regions of a larger area, for example the network on Adak Island [Davies, 1985], but much work is then necessary to synthesize these results for a picture of the entire region's seismicity. Moreover, the database formats are often ad-hoc and either not very amenable to data-sharing, or not conducive to processing with the large numbers of tools available, or both. Earthquake catalogs produced come out weeks or months after the fact.

Alaska also has an extensive hardware deployment to study the earth processes described above, including a large, traditional-style regional seismic network, new array stations, and incoming new broadband stations. The computational infrastructure required to process such a large network (current Alaskan seismic data-flow rates are above 3.8 Gigabytes per day) becomes quite involved, however. This is a problem that is too large and specialized to be relegated to off-the shelf commercial packages, or to fragile, loosely constructed collections of computer scripts. In order to use the Alaskan seismic network to its maximum scientific potential, the software infrastructure must be tailored with the scientific and public safety goals in mind.

A number of issues are involved in the computational infrastructure necessary to run a seismic network, and to some extent we address them all in this work, dealing with some extensively. The needs of modern seismological networks are sufficiently involved that standard practice is to write multiple component parts that can communicate amongst one another. The first step, then, in assembling a real-time processing system is to establish a means of communicating amongst the different data-handling and processing modules.

We adopt two separate technologies for this, the Earthworm transport layer and the Datascope Object Ring-Buffer (ORB) software, and connect the two to create a flexible and powerful substrate for implementing real-time tasks.

Second, it is becoming more and more important for regional networks to communicate their data and processing results to the external community, not only after the fact but also in real-time. This aids scientific cooperation between networks; study of earth regions that lie between traditional regional networks; and response to large earthquakes, including those with tsunamigenic potential. We discuss our use of the Datascope ORB software for a variety of these intercommunication tasks, and note that in our relational database implementation we have chosen one of the most common relational-database schemas used for data exchange amongst seismic networks. The schema is the template for data storage in the database, discussed in more detail below.

None of this goes very far without an ability to acquire data into the processing system, of course. In this work we implement a strategy to receive data from a large variety of digitizers, instruments, and data-flow paths, such that all data can be handled by the same processing and storage tools.

Third is the necessity to provide data in useful form for real-time hazard response, as well as system-health monitoring. This includes display of incoming waveforms, display of the automated picks of incoming seismic energy, and hypocenter announcement and display. Through a combination of existing software integrated into our system and new software written by ourselves, we have addressed all these needs. Also, we have

adopted some software and written other software for quick email and pager notification of interesting activity.

Fourth, we have arranged to store all parametric and waveform data collected and generated by the system in non-volatile formats. In part because of computational limitations, many systems in the past have thrown away almost all of the incoming seismic data, saving only the most essential, and then often only the derived information, not the raw data. There are several problems with this, however. If all the input data are not present, it is hard to review critically the output of the automatic processing system. Also, the automatic system may miss things that are of interest, or that were not of interest during system setup and tuning. This requires archival of the input data for later review. While it may be true that much of the seismic time-series is not extremely helpful in learning about the earth, it is valuable to archive it nevertheless for the possibility that it will be helpful later. A prime example of this is the recent work by Song and Richards [1996], who have gone back to data 28 years old to look for core phases indicative of differential inner-core rotation. This type of study would not be possible without thorough data archival.

Finally, there is a need for a number of processing tasks for the seismic network, some of them standard and some relating to specific tasks at a given network or to individual scientific experiments being run on the real-time data stream. First among the standard tasks, of course, is the detection of incoming seismic energy, or automatic picking. Second is the sorting of incoming energy by source, namely phase association. Third is the extraction of source parameters such as the location and magnitude. The in-

frastructure we have in place will allow us also to take advantage of developments elsewhere with near-real-time moment-tensor estimation.

In order to handle arbitrary processing tasks on real-time seismic data streams, we have constructed a template for applying generic processing algorithms to a suite of data streams. It is with this template that we have implemented the automatic phase picking (using a modification of the Allen [1980] picking algorithm, as discussed below). In principle, any recursive or continuous time-series algorithm can be easily implemented to be applied to one or more seismic data streams. This includes a digital equivalent of the Earthquake and Volcano Alarm (EVA) that we have installed for quick, pager-based alerts about large earthquakes and active volcanoes.

Chapter two describes the Iceworm system, the entire software infrastructure we have assembled for complete seismic data handling, processing, and archiving in Alaska. While we have incorporated several large, existing packages in their entirety (including the USGS Earthworm package and Datascope from the University of Colorado), a great deal of original development has taken place to make the complete system. In subsequent chapters we describe specific applications of this system and/or developments that will contribute to it for several purposes of benefit both to the scientific community and the community at large.

By integrating Earthworm and Datascope so seamlessly we have set up the ability to do all routine processing based on automatic processing from Earthworm. This ability in large part comes from the power of the Datascope Seismic Application Package [Quinlan,

1994], which includes all the analyst review tools needed for the final production of seismicity catalogs. The relational database context makes it easy to handle the large amounts of data needed for catalog generation.

Chapter three describes a regionalized inversion for a local-magnitude scale for Alaska, one of the first steps towards quantifying the attenuation characteristics of the Alaskan crust. We present a complete automation of the local-magnitude calculation task, together with prospects for conducting the pilot study again with the newer, higher-quality data. We consider this an excellent example of a nearly-automated science project. Automating large-scale scientific measurements on the earth, thus handling repetitive tasks and freeing researchers for more sophisticated analysis, is one of the benefits of the work presented here.

Chapter four discusses our initial work with the Alaskan seismic arrays for monitoring of seismicity not only in the interior of the state, but also extending out towards the Aleutian Islands. We present empirical studies of the predicted magnitude-threshold improvement in the Aleutians and in fact over the entire Arctic with the Alaskan arrays, and in cooperation with other Nordic networks and arrays. We discuss progress towards bringing the array processing as well into the fully automated system for seismic monitoring in Alaska.

Finally, we conclude with a discussion of some of the many avenues for further development of the Iceworm system, and of near-real-time processing in Alaska for volcano monitoring, earthquake monitoring, better understanding of the complexities of

Alaskan seismic wave propagation, and public hazard response.

1.1 References for Chapter 1

Allen, R. V. (1978). Automatic Earthquake Recognition and Timing from Single Traces. *Bull. Seis. Soc. Am.* **68**, 1521-1532.

Biswas, N.N., L. Gedney, and J. Agnew (1980). Seismicity of Western Alaska. *Bull. Seis. Soc. Am.* **70**, pp. 873-883.

Davies, J. (1985). "Alaska Regional Seismographic Networks: Operational History and Principal Scientific Results", in *Symposium and Workshop: Regional Seismographic Workshops, Past-Present-Future*; from Eastern Section, Seismological Society of America, October 18-19, 1985, Knoxville, Tennessee.

Gedney, L. D. (1980). "Seismology in Alaska", Geophysical Institute Biennial Report, 1979-1980.

Johnson, C. E. (1979). I. CEDAR--An Approach to the Computer Automation of Short-Period Local Seismic Networks. II. Seismotectonics of the Imperial Valley of Southern California. *Ph.D. Thesis, California Institute of Technology.*

Monastersky, R. (1996). "Nations consent to ban all nuclear tests". *Science News* **150**, 183.

Page, R. A., N. N. Biswas, J. C. Lahr, and H. Pulpan (1991). "Seismicity of continental Alaska". *in* Slemmonds, D.B., Engdahl, E.R., Zoback, M.D., and Blackwell, D.D., eds., Neotectonics of North America: Boulder, Colorado, Geological Society of America, Decade Map Volume I.

Quinlan, D. M. (1994). Datascope: A Relational Database System for Scientists. *Eos Trans. Amer. Geophys. U.* **75**, No. 44, 431-432.

Song, X. and P.G. Richards (1996). Seismological evidence for differential rotation of the Earth's inner core. *Nature* **382**, 221-224.

Taber, J.J., S. Billington, and E.R. Engdahl (1991). "Seismicity of the Aleutian Arc." *in* Slemmonds, D.B., Engdahl, E.R., Zoback, M.D., and Blackwell, D.D., eds., Neotectonics of North America: Boulder, Colorado, Geological Society of America, Decade Map Volume I.

Chapter 2

Relational Database Implementation of Near-Real-Time Seismology with the Iceworm System

2.1 Abstract

Near-real-time seismology has undergone a number of advances recently, with a proliferation of systems to handle automatic processing at various networks and through cooperations amongst networks. Starting from existing software packages, including Datascope and the Datascope Seismic Application Package from the University of Colorado and Earthworm from the U.S. Geological Survey, we have assembled a near-real-time system with several new advances. First and foremost, all parametric information, segmented waveforms, and continuous waveforms are stored in a relational database. Second, we have built an architecture around a demultiplexed waveform-data format that allows the incorporation of analog and digital data from diverse sources into the same processing stream. Third, we have created a framework in which to run arbitrary algorithms on real-time data streams. This has already been applied not only to automatic phase picking but also to several volcano-monitoring tasks. Finally, we have prepared the way for better monitoring of Aleutian seismicity through joint network and array-processing techniques, since the new framework will allow real-time beamforming of data streams. Expansion of

the generalized beam-forming phase association techniques will allow, through international cooperation and exchange of real-time parametric information, the study of seismicity of the entire Arctic region.

2.2 Introduction and Overview

Near-real-time seismology has become a common goal now that computers are available with the power to make it possible. By "near-real-time," we mean the time frame several seconds to minutes after the onset of a seismic event and after the arrival of the elastic waves at the recording stations [Malone, 1996]. Above all, hazard mitigation and disaster response drive the need for fast information about large earthquakes and erupting volcanoes. For scientific purposes, the ability to run experiments on real-time data streams allows efficient study of earth processes. Also, the traditional role of regional networks in producing seismicity catalogs is vastly simplified by automatic processing.

In Alaska, one of the main tasks of the Alaska Earthquake Information Center (AEIC; see Appendix A for a glossary of acronyms) is the production of catalogs of regional seismicity. These catalogs contain approximately 6000 events annually, with a total catalog of 60,000 events overall since 1898 (e.g. Rowe *et al.*, 1996). Due to the station distribution (Figure 2.1), these catalogs have concentrated on the interior of the state. From 1989 until 1997, earthquake analysis at the AEIC has been done with JADE, or "Just An-

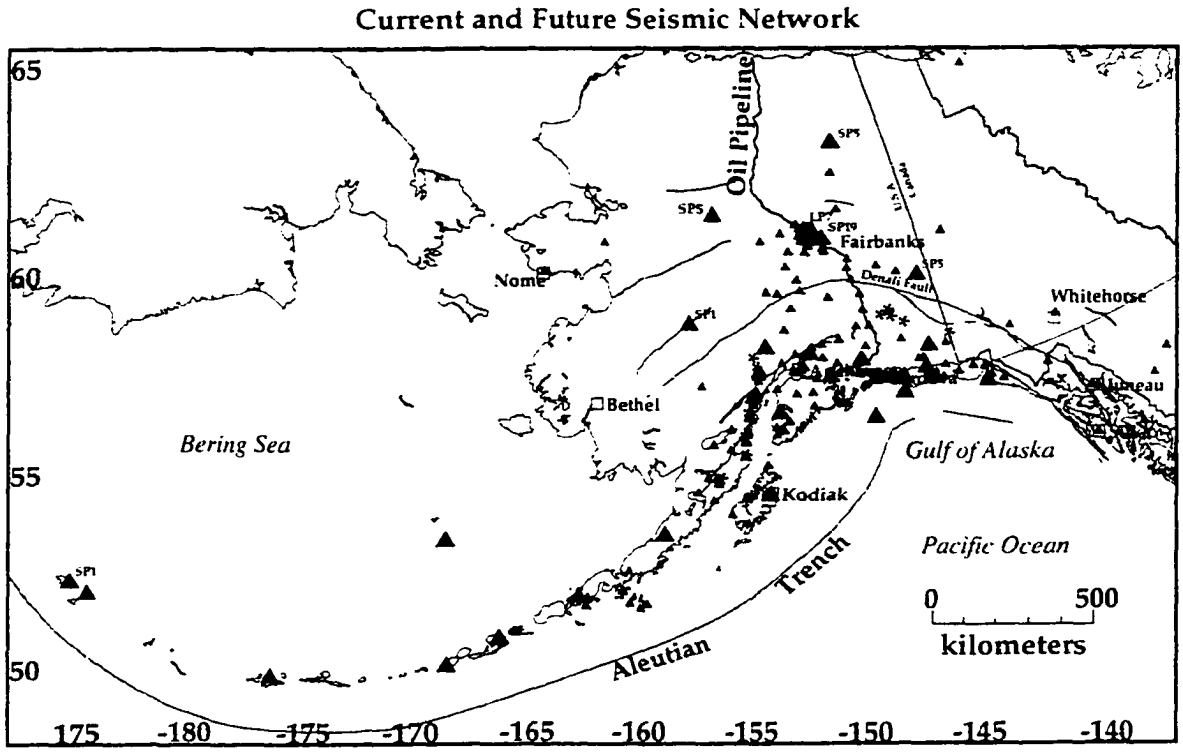

Figure 2.1

This map shows currently existing seismic stations in the Alaskan network, along with several proposed new sites. Triangles indicate station locations; squares show the locations of principal cities. Small triangles indicate short-period, analog-telemetered instruments. Large triangles indicate digital telemetry, array stations, and/or broadband installations. The black lines are traces of the major Alaskan faults. The Alyeska oil pipeline is shown running from North to South through the state.

other Detector of Events," an event trigger that saves segmented data for candidate earthquakes without any further processing [Sonafrank *et al.*, 1991]. All picking of arrival times and determining the locations of earthquakes has been done interactively [Rowe *et al.*, 1991] with the computer programs *Xpick* [Robinson *et al.*, 1991] and *Hypoellipse* [Lahr, 1989].

While many regional networks have constructed systems that do real-time processing to some degree, the state of the technology is that each networks' system is a custom installation. Different networks have different computer resources, station types, digitizer types, and telemetry strategies. At some point, the software required to run these may be commercially provided, as most digitizers are now, but at this time the engineering of an acquisition system still requires close involvement by the scientists, especially with a network as large and diverse as that in Alaska. Examples from the published literature of data collection and processing systems that have evolved to suit the needs of a variety of networks include the South Iceland Lowlands (SIL) system [Böðvarsson *et al.*, 1996; Stefansson *et al.*, 1993]; The CalTech-USGS Seismic Processing (CUSP) system of the U.S. Geological Survey [Dollar *et al.*, 1995] and the ISAIAH system based on it [Given, 1994]; the Earthworm replacement for the Real-Time-Picker at the USGS [Dietz *et al.*, 1994, 1995]; the Rapid Earthquake Data Integration (REDI) project and real-time seismology at Berkeley [Neuhauser *et al.*, 1995; Gee *et al.*, 1994, 1995, 1996]; the International Deployment of Accelerometers (IDA) by the Incorporated Research Institutions for Seismology (IRIS) [Berger *et al.*, 1997]; the Intelligent Monitoring System for globally-deployed ar-

rays [Bache *et al.*, 1990, Bratt *et al.*, 1990]; the Northern Norway seismic network [Havskov *et al.*, 1992]; real-time earthquake monitoring with Terrascope [Hauksson et al., 1994]; automatic processing of data from Scandinavian arrays [Kvaerna, 1994]; Sunworm at the University of Washington [Malone, 1995]; the Japanese Urgent Earthquake Detection and Alarm System (UrEDAS) [Nakamura, 1994]; real-time processing of ANZA data [Glushko *et al.*, 1994]; and previous work at the Alaska Earthquake Information Center [Lindquist *et al.*, 1995, 1996; Hansen *et al.*, 1996]. Due to the extent of previous work on automatic processing systems, an overview of all their features is beyond the scope of this presentation. We mention one more system of interest, the Caltech Earthquake Detection and Recording (CEDAR) system [Johnson, 1979]. The Earthworm system, which forms an important part of the current work, traces its history in part to CEDAR. The underlying philosophy in CEDAR was to throw away almost all data as quickly and efficiently as possible, saving only the most essential for earthquake detection. In the words of Carl Johnson [Johnson, 1979], the goal was to become a "clever dustman" to recover the data of value. This is one of the key elements that has been updated in the current work. Many elements of our system will share implementation strategies with a number of these systems.

We have constructed a near-real-time system, called *Iceworm*, that goes completely from data collection through automatic processing to final catalog production, with several new advances. To do this we have integrated two large software packages, plus developed new infrastructural software, processing software, and user-interface software, amounting

to over 20,000 lines of new source code, to make a complete system. The two major starting components of Iceworm are the Earthworm automatic processing system from the U.S. Geological Survey in Menlo Park [Bittenbinder, 1994; Johnson *et al.*, 1995], and the Datascope package [Quinlan, 1994] from the University of Colorado. We will describe both of these in more detail below.

First and foremost among the advances, all parametric information for located hypocenters, segmented waveforms corresponding to those events, continuous waveforms from the entire network, and quasi-static information about network configuration and system setup are stored automatically in relational databases. The use of relational databases in seismology is not new (e.g. Berger, 1984). For years they have been applied to global processing by the Air Force Technical Applications Center (AFTAC), the Norwegian Seismic Array (NORSAR), and the International Data Center (IDC) of the Center for Monitoring Research (CMR). However, to our knowledge the use of relational databases in real-time regional network processing is just now emerging [see also Kjartansson, 1996, as well as the preliminary work in Anderson *et al.*, 1994].

The second advance is that we have enhanced the near-real-time waveform handling in the system by designing a generic format for processing of digital data internal to the system. This allows the straightforward input of mixed analog and digital data from diverse sources. Notable examples include IRIS data from stations COLA and KDAK, coming from Quanterra and Reftek digitizers; import from Hokkaido University of Japanese data, sent via User Datagram Protocol (UDP) packets over internet in the Japanese

Win format; import of data from Guralp digitizers; and import of data from the University of Alaska seismic arrays, in addition to the analog data from the bulk of the Alaskan regional network. We have also already incorporated, automatically processed, and archived data from several infrasonic stations deployed on Alaskan volcanoes, in the context of Aleutian volcano monitoring.

Finally, the data-flow infrastructure in the Iceworm system allows the easy incorporation of new processing modules that ride the real-time data stream, processing single station-channels or combinations of station-channels simultaneously to produce near-real-time calculations for monitoring and research purposes. To achieve this we rely heavily on a type of programming relatively new to UNIX systems, called "multithreading." Within a single computer program, multiple, independent sequences of executed commands can run, access resources, and be scheduled simultaneously [Kleinman *et al.*, 1996]. This allows straightforward programming of asynchronous processes, for example application of the same algorithm to a number of different streams of data that are all coming in at once. The Iceworm system has multithreaded templates that allow arbitrary processing algorithms to be implemented quickly. One can specify an algorithm to apply to each data stream, plus the startup data for each stream, and run one thread for each stream. So far this has formed the basis for the Iceworm automatic picker, and has allowed some customized alarms to be built, such as the Earthquake-Volcano Alarm (EVA) described below. This has been applied to several volcano seismic networks, including those at Mt. Redoubt, Mt. Spurr, and Iliamna volcanoes. Ultimately this infrastructure will support near-real-time

beam-forming and generalized beam-forming of combined network and array data, as described in Chapter 4.

In addition to the availability of waveform data in near-real-time streams, continuous waveforms are buffered for several hours and made accessible via internet socket connections to various processing modules. This addition to data-distribution in Iceworm allows great flexibility for slightly delayed processing (seconds to several hours) and for data exchange, such as magnitude calculations for located earthquakes. Internet-based access to waveform data in near-real-time allows distribution of the Iceworm system's tasks amongst several computers, creating a robust system with multiple backup options. The waveform buffering capabilities have also made possible the construction of archive databases of continuous data, with up to 7 days online given current data-flow rates and disk space. Both the archive and the waveform-buffering utilities have also allowed us to run a variety of volcano-monitoring tasks on near-real-time data streams [Lindquist *et al.*, 1996].

The most recent addition to the Iceworm system is the O-Ring Buffer (ORB) capability of the University of Colorado's Datascope package. This communications software provides an alternative to the Earthworm communication utilities with which Iceworm was originally written. The ORB software provides communications of both parametric and waveform data between processing and display modules. The connection protocol is identical whether the connection is local within the computer, on the local lab ethernet, or across the world via internet. Integration of the ORB software with Iceworm has allowed, among other things, real-time, develocorder-style display of scrolling wave-

form data, and the import of worldwide seismic data from the IDA network in near-real-time. This latter ability is important for current proposals to monitor the entire Arctic region internationally through the Cooperative Arctic Seismology Program (COASP). In the future, ORB software will be used for much of the data communication from various parts of the state to the central lab in Fairbanks, as well as for the data communication with Hokkaido, given the success of our initial experiments.

2.3 Hardware, Instrumentation, and Setting

The stations used in this project are those maintained by the AEIC [Figure 2.1]. The AEIC monitors earthquakes in Alaska, provides rapid information on felt earthquakes, and disseminates information about earthquakes and seismic hazards to government officials, the media, the public, and the earth-science community worldwide. Established in 1988, the AEIC is operated by the Geophysical Institute of the University of Alaska, cooperatively with the United States Geological Survey. The main center of operations is located at the Geophysical Institute in Fairbanks, with the office of the Alaska State Seismologist. Most of the earthquakes located by the AEIC originate in a "core" area in central and southern Alaska, between latitudes 57°N and 67°N and longitudes 135°W to 170°E. We must emphasize the great extent of this region compared to most single regional networks in the world. This makes necessary a large, hybrid network and favors the use of joint

network and array processing to cover the entire region.

Since 1990, the AEIC has located approximately 30,000 earthquakes in Alaska and western Canada, or about 6,000 per year. The AEIC normally analyzes data from the University of Alaska-Fairbanks Geophysical Institute (UAFGI) seismograph network, which currently incorporates more than 200 stations, including 15 stations operated by the Alaska Tsunami Warning Center (ATWC) in Palmer, Alaska. Most of the stations are located in central and southern Alaska (Figure 2.1). The majority of the channels of data recorded at the AEIC are from short-period, vertical-component, analog stations. Eight of these short-period analog stations are three-component stations. Analog-to-digital conversion of the short-period analog stations in the Alaskan network is done by an IBM-compatible 486 personal computer controlling a National AT-MIO-16F-5 digital data acquisition board. Four AMUX-64T multiplexers offer 64 channels each, for a total of 256 channels attached to the digitizing board. The sample rate is currently set at 100 samples per second.

As mentioned above, there are also several high-dynamic-range, broadband stations operating in Alaska. The stations in Fairbanks (COLA), at Adak Island (ADK) and the station on Kodiak Island installed in June 1997 (KDAK) are all IRIS stations with the Kodiak station contributing to the auxiliary network of the GSETT3 ("Group of Scientific Experts Technical Test"). The COLA site is considered to be among the quietest sites in the world [Townshend, 1996]. The Data Processor (DP) unit for this station is located directly in the UAF Seismology lab, allowing convenient near-real-time access to the data streams over lab ethernet. The IRIS COLA station provides several channels each from a Kinem-

etrics KS-54000 instrument in a 425-foot borehole and from a Streckeisen STS-2 seismometer in a vault [Townsend, 1996]. The fourth existing broadband station is an STS2 seismometer with a Quanterra datalogger operated by the ATWC in Palmer.

Several proposed broadband sites are to be installed by the recently funded tsunami-hazard mitigation initiative. New funding from the Senate appropriations committee through NOAA and the USGS will be establishing communication links and high dynamic range broadband stations over the next few years. The remaining stations are borehole arrays run by UAF. There are three short-period 5-element arrays, one short-period 19-element array, one 7-element long-period array, and two single-element borehole stations. Finally, there are 15 closely spaced digital strong-motion seismographs recently installed in Anchorage. Work is underway to bring continuous data from these stations into the Iceworm processing system in Fairbanks.

Our computer hardware consists of dual-processor SUN SPARC workstations with several hundred megabytes of onboard RAM. A 63-Gigabyte RAID box provides approximately one week of on-line archived continuous data, plus space for about one month of segmented data for located earthquakes. A concurrently-running system with a smaller set of disk drives provides complete backup in the event of main system failure.

2.4 Software Architecture and Modules

In order to run a regional network and process the information in near-real-time for scientific and public-safety purposes, one needs to perform a number of functions. Below we discuss these problems as we have solved them, by taking functional parts from different systems or by writing new software. We precede this with a discussion of several processing-system issues that transcend individual modules.

2.4.1 Infrastructural Needs

2.4.1.1 Data Intake

The first need of a seismic network, of course, is to acquire data from the seismic instruments. For modern networks, this requires digitizing the analog signals from the seismometers. With a hybrid network as large as that of Alaska, the digitization is done in a number of different ways, which will be discussed below. The point of this is that many different types of data- intake are involved. To achieve integrated processing of all data for the entire region, one has two groups of choices: conversion of all data to a common format for handling, or maintaining parallel software capabilities for multiple formats. We have

chosen the strategy of converting all incoming data to a common, demultiplexed format. This allows processing utilities to be written only once, with the ability to trivially bring new types of data streams into the real-time processing with the construction of only the appropriate reformatting code.

The original Earthworm system took in analog data via a multiplexed digitizer, producing packets of multiplexed waveform data. This meant that utilities processing the real-time data stream, such as the picker, needed to be hard-wired to handle the multiplexed data format. Also, any data coming from other sources would need to be forced into the same multiplexed data format designed for analog data, or one would have to train all processing utilities to handle multiple data formats. To overcome this, we defined a new format for waveform data. All incoming data are immediately repackaged into a common format, called "trace-packets" in the Iceworm system. By the time these data become available to processing and archiving modules within Iceworm, all the complexity of differing data intake formats has been removed.

Each trace-packet of waveform data consists of a trace-packet header followed by the block of waveform data. This packet format contains everything a seismologist wants to know about incoming data (presuming that quasi-static information about that data stream, for example calibration information and station location, are stored elsewhere), and omits everything possible about the details of data delivery. This allowed the construction of a system that can be modularized such that the data-intake strategies can be modified for years to come, without having to rewrite any of the processing software because of it.

Different storage classes have been allowed for the raw data in these packets, however, to maintain efficient use of disk space and computer memory from data intake through to continuous-data archival. For example, there's no point in using four-byte words to store data that came in as two-byte integers. The trace-packet header contains station name, channel name, network name, starting time of the data packet in epoch seconds, number of samples, sample rate, and the two-character code for data storage format defined by the Center for Seismic Studies CSS3.0 database schema. An additional field, data-quality, has been added to record transient problems with data sources. The Earthworm pin-number, a "social-security number" for each data stream within the Earthworm system, is redundant with station and channel names, but is convenient for internal administrative tasks. The endtime of the data-packet, i.e. the time of the last sample in epoch seconds, could be computed from starting time, nsamp, and samprate, but since this is such a common task we precomputed and included the value. Note that this trace-packet format is optimized for data processing, not data exchange. Data exchange between systems and over large distances has been accomplished by exporting data from the Iceworm trace-ring to a Datascope ORB server, described below.

We have discovered that with today's workstations, even with a network as large as the Alaska network, reformatting issues are computationally inexpensive. We can easily demultiplex approximately 200 channels of two-byte, 100 sample-per-second data in near-real-time with a very small fraction of available CPU power even on a Sun SPARC IPX. Data come into the Iceworm system from a variety of sources [Figure 2.2]. In general, each

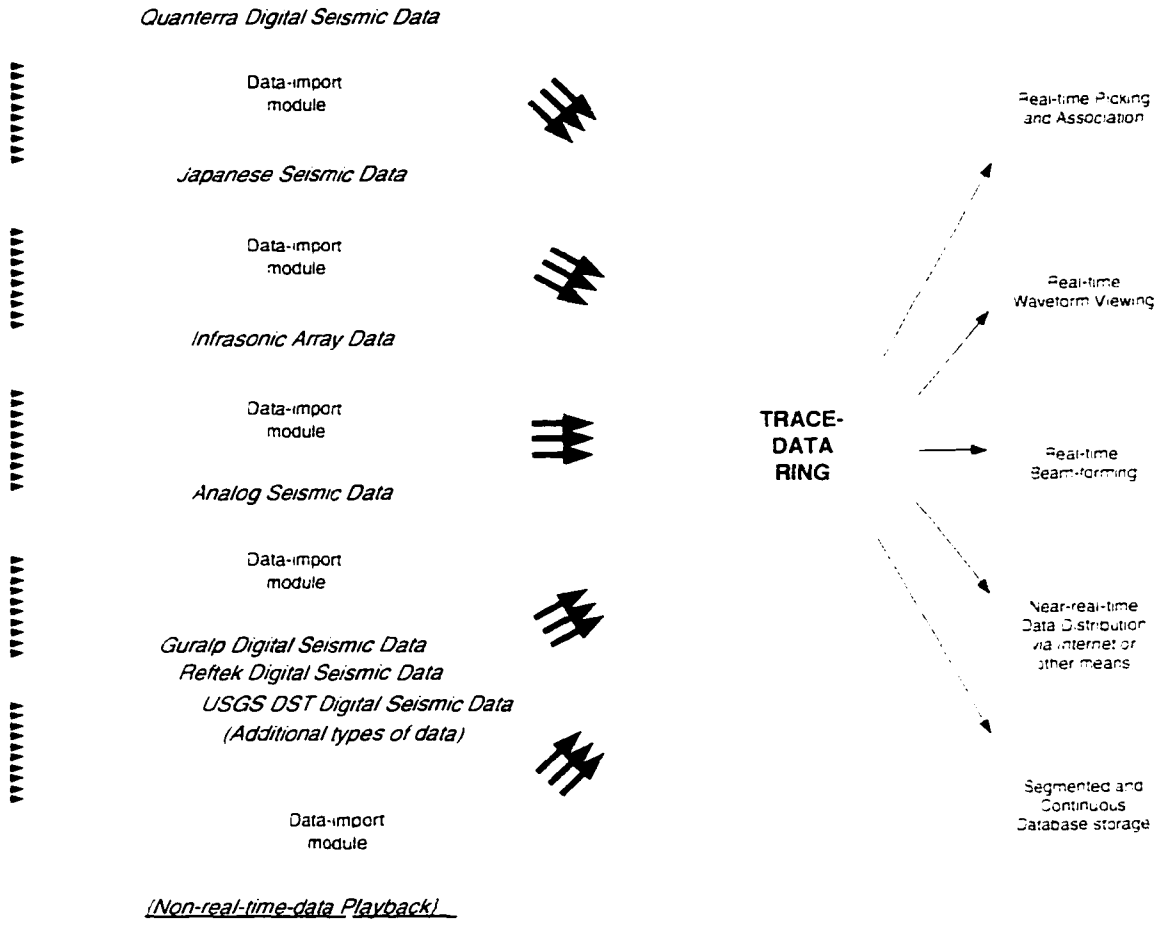

Figure 2.2

The Iceworm system allows data intake from a multitude of different types of sources. Data are converted to a common, demultiplexed format; packetized; and sent to the trace-ring for communication to various processing, buffering, archiving, and display software modules. Conversion to a common format allows the easy incorporation of new data sources without modification to existing data-handling and processing modules. For more detail, see the discussion in section 2.4.1.1 of the text.

type of source is handled by a different, custom data-intake module. As data arrive and are repackaged into trace-packets, they are put on the "trace-ring." The trace-ring is a shared-memory ring in the Iceworm system that makes demultiplexed data from a variety of sources available to seismological processing programs. Details about the data flow and reformatting issues are hidden from the users of the data. The only requirement on the trace-ring are that the data be packetized, correctly time-stamped (i.e. corrected for any communication delays), and that they appear in the right format, i.e. a trace-packet header followed by a block of data. In the current system, data packets are from 1 to about 30 seconds in length. The principal tasks of the import modules are to convert the data to trace-packet format, and to apply any time corrections to the timestamps to correct for communications delays.

The bulk of our data come from analog stations, which are digitized by the Earthworm digitizer and cast into the original Earthworm multiplexed packet format. They come from the personal computer doing the digitizing into our Sun Workstation via an Earthworm-custom UDP packet format. A demultiplexing module called *ad_demux* converts the multiplexed data to the demultiplexed format of the trace-ring.

For data from the IRIS COLA stations, we bring digital data in over lab ethernet from the IRIS Data Processing (DP) unit, which is located in our seismology lab. A TCP socket connection from the Iceworm computer to the DP provides 512-byte SEED data to a module which unpacks it, Steim-decompresses the data, repackages it into trace-packets, and puts them on the trace-ring (documentation of SEED format and the Steim compres-

sion algorithm may be found in Ahern *et al.* [1993]). . Because of the data compression and the multiplexing of several channels into each miniSEED volume, the incoming data are in packets with variable numbers of samples. We repackage the data into equal-length packets. While in principle the trace-ring can support data packets of variable length for the same station-channel, much of our code has been written to handle only fixed-length packets for each station, which sacrifices a small amount of generality and flexibility for programmer time. Note that it is no problem right now for the standard packet length for one station-channel to be different from that of another station-channel, as long as each station-channel's packet length does not change with time.

In recent experiments we have incorporated Reftek digital data into the Iceworm system, in cooperation with David Chavez and personnel at the University of Nevada, Reno; and incorporated Guralp digital data in cooperation with Digital Technology Associates and with Remote Possibilities, Inc. This will facilitate the Anchorage Digital Network, to be installed during the summer of 1998. This will also allow the real-time acquisition of the Anchorage strong-motion network of accelerometers.

2.4.1.2 Communication Between Modules; Communication Between Networks

As waveform and parametric data are collected, they must in some way be passed between software components of the processing system. Most all modern processing systems are modularized in some way, since the jobs they take on are large enough to make a

single program unwieldy. There are currently two parallel sets of software for message-passing within Iceworm. The first is the one around which Iceworm was initially designed, the message-passing implementation called the transport layer from the Earthworm software. Based on the shared-memory model for inter-process communication [Haviland *et al.*, 1987], the Earthworm transport layer allows many modules to observe and write to a ring buffer that is stored in the Random-Access Memory (RAM) of a workstation or personal computer. A ring-buffer is a temporary storage structure in which a predetermined amount of space is set aside for messages. Each incoming message overwrites the oldest message still in the ring. This Earthworm transport-layer allows independence of modules, although it does not directly allow different modules to run on different computers, without intervening communication utilities. The Earthworm shared-memory regions are intended merely as communications nodes, not as buffering areas that save old data and results. The lifetime of information in these shared-memory rings is short, ranging from seconds to just a few minutes, depending on the size of the messages and on the size of the ring. One weakness of this structure is that since the shared-memory mechanism requires multiple processes to access accounting information for the same memory region, it is possible for one module to corrupt the shared-memory region for all the others.

Recently a new option has become available, the O-Ring Buffer or ORB software from the Datascope package [D. Quinlan, *writt. comm.*]. Combining a disk-buffer with a socket-based interface for multiple read-write connections, the ORB software provides communications of parametric and waveform data over any distance, given an internet

connection. Connections are established by Transmission-Control Protocol (TCP) sockets [*e.g.* Comer, 1995] over any internet. The ORB sofware has built-in capability to reconnect broken connections; is non-volatile in the event of system failure because the ring buffer is memory-mapped from disk; and works regardless of native byte order of the host machine [D. Quinlan and D. Harvey, *pers. comm.*]. Optional data-compression is built into this interface, which is important for medium- and long-haul waveform data communications. Iceworm presently uses the ORB software in conjunction with the Earthworm transport layer to bring in some of the Alaskan waveform data, and to announce some of the derived parametric data. Interface modules allow the passage of all types of information between the Earthworm shared-memory rings and the Datascope ORB servers. In the future, we envision the ORB software playing a large part in our network communications and in our communication between modules in our automatic processing system.

The applications of data-communication between modules are implicit in the discussion of processing tasks below, and will not be discussed further here. Related to data intake to the Iceworm system is communication between networks. We have conducted several experiments to demonstrate the capabilities of the combined Datascope/Earthworm system in this work. In cooperation with Dr. Kei Katsumata of the Research Center for Earthquake Prediction, Hokkaido University, and personnel of the Seismology lab at the Geophysical Institute, we have developed software and performed several weeks of experiments resulting in the exchange of seismic data in near-real-time with Japan. We have taken multiple channels of seismic data from Iceworm, converted them to the Japanese

"win" data format, and transmitted them directly to other computers via TCP/IP sockets over public internet. We have also taken up to 180 channels of high-quality, Japanese seismic data from Hokkaido and brought them continuously into Alaskan computers. In addition, we have exchanged information on station and network configurations [Figure 2.3] that will allow these data to be used in earthquake locations. By exchanging seismic data in near-real-time, we improve our coverage of Aleutian Islands seismicity, especially in the far western Aleutians.

In conjunction with the installation of the KDAK station in Kodiak, Alaska, as part of the IRIS IDA network, with the help of David Chavez we have written software to bring IDA data into the Datascope ORB software, and therefore also into the Iceworm system. Most recently, we have written interfaces for the Datascope ORB software to Guralp digitizers. This will be used in many arenas, including possibly the exchange of data with high-schools in Alaska [Hansen *et al.*, 1997] that are participating in the Princeton Earth Physics Program (PEPP) [Nolet, 1995]. Successful data-exchange experiments have already been conducted between the University of Alaska and the University of Colorado; the University of Nevada, Reno; University of California, San Diego; and with Kinemetrics Corporation in Pasadena, California. We can exchange data seamlessly between Iceworm and the ORB ring buffers, which allows us to take advantage of the efficient communications implementation of the latter. In addition to long-haul communication of data, the Iceworm/ORB link has allowed us to exchange waveform data easily amongst different intake modules and between running Iceworm systems at the AEIC [Figure 2.4].

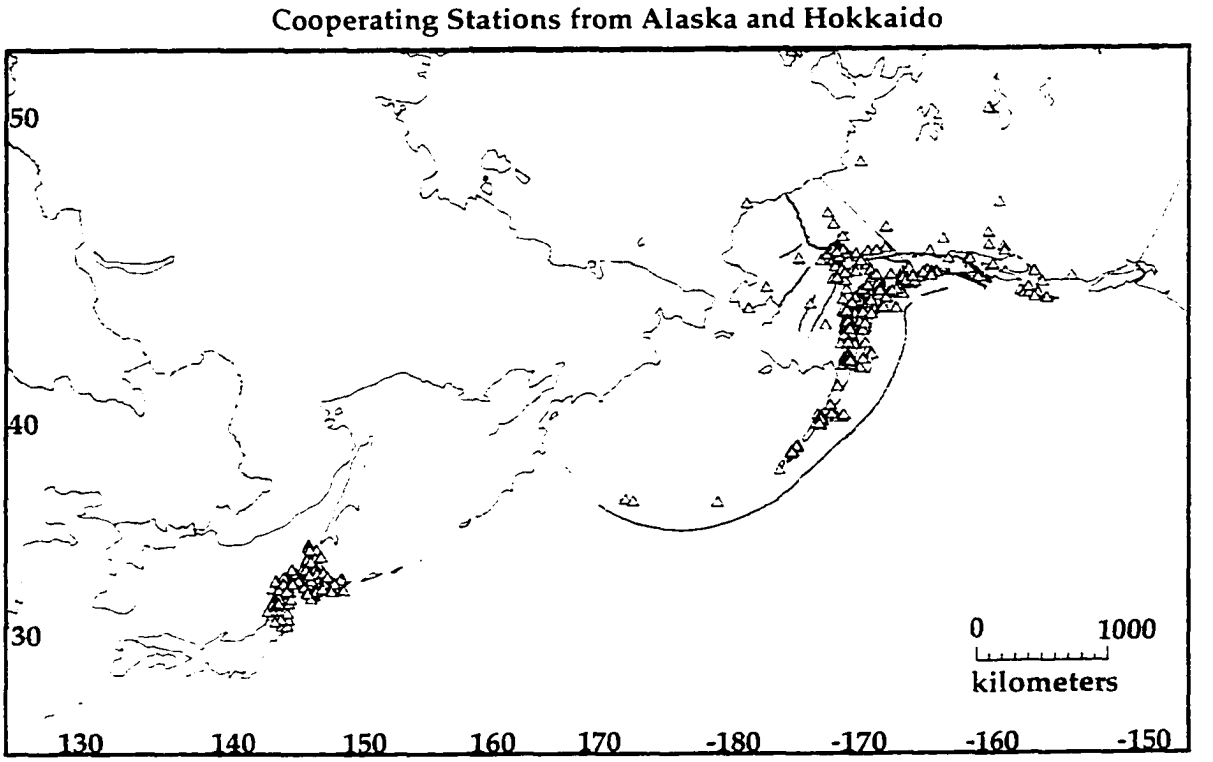

Figure 2.3

Map of seismic stations (triangles) used in an Internet data-exchange experiment between the Alaskan Iceworm system and Hokkaido, Japan. For more discussion, see section 2.4.1.2 of the text.

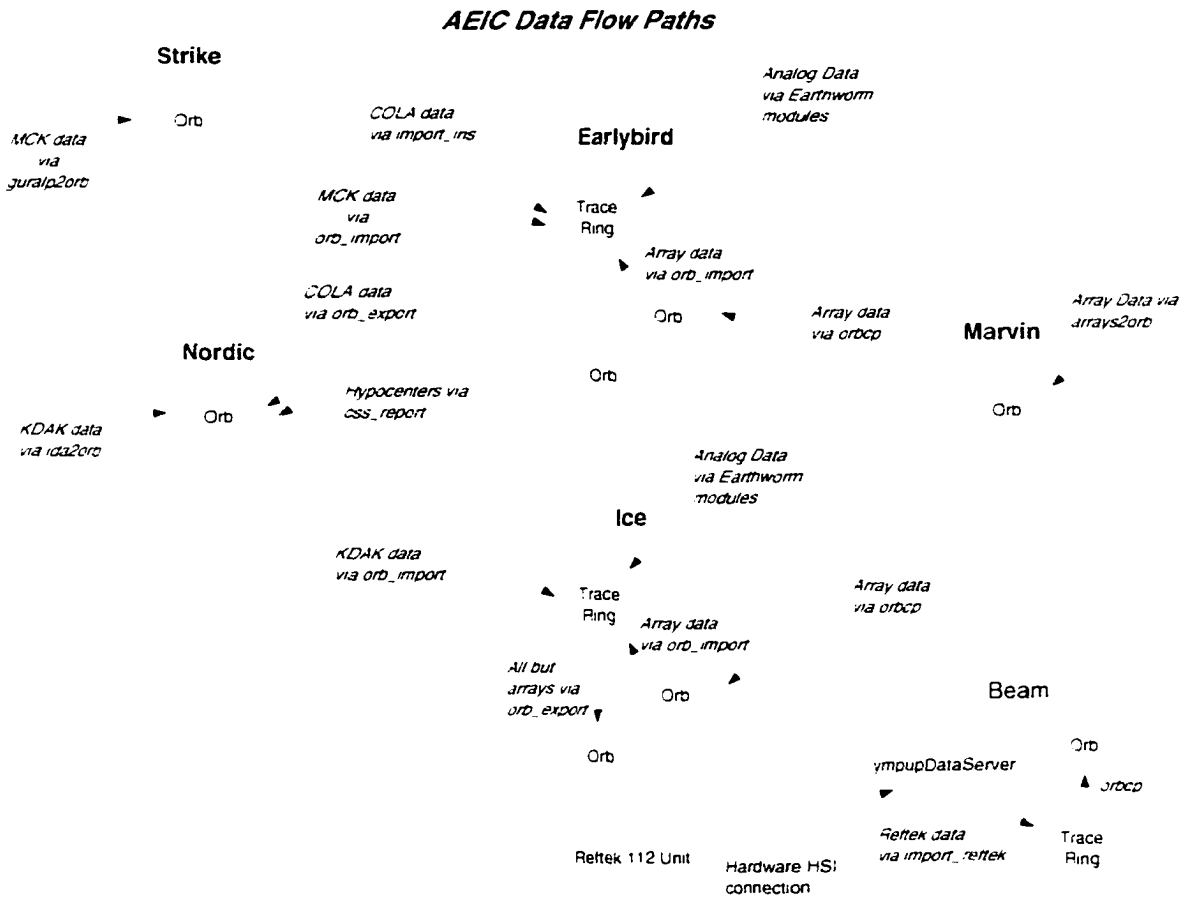

Figure 2.4

This diagram shows data-flow paths at the AEIC. Square boxes are individual Sun workstations, connected by internet. The names of the workstations are shown above the boxes. Doubled circles are Iceworm trace-rings for near-real-time data communication. Doubled ovals are Datascope Object-Ring Buffers (ORBs) for near-real-time data communication. Arrows indicate data-flow paths. This diagram illustrates the flexibility of the completely integrated combination of Earthworm and ORBs to provide data intake and processing from spatially separated sources of varying types, and to provide backup capability (on the machine *ice*) for a running acquisition system (on the machine *earlybird*).

2.4.1.3 Organization of Input and Output Data

While virtually any accumulation of data can be considered a "database" in some sense, a relational database is organized on the premise that each piece of information should be stored in only one place. Relational databases allow data normalization, a structuring of the database to avoid update anomalies. Single pieces of information such as station locations or earthquake hypocenters can be updated without affecting other parts of the database [Braithwaite, 1991]. Relationships between pieces of information are specified explicitly such that pieces of information can be grouped in multiple, sensible ways to suit the needs of the moment. For example, hypocenter locations at some times need to be associated with the phase-arrival information from which they are derived; at other times need to be associated with one or several computed magnitudes or moment tensors; and at some times need to be grouped into sets of competing hypotheses for the location of a single event. Similarly, seismic site information is associated at various times with information on the characteristics of deployed instruments as they change through time, associations of sites with different seismic networks, and groupings of different sites considered together for various processing tasks. The efficiency gained with relational database storage can drastically increase productivity for catalogs and scientific results, especially with hundreds of earthquakes per week and gigabytes of waveforms per day.

The output databases from the Iceworm system are in the standard CSS3.0 schema

distributed with the Datascope package (the CSS3.0 schema is described further in Anderson et al., 1990). In order to accommodate the storage of information internal to the Iceworm system, however, we have developed an expanded schema, based on CSS3.0, which is used for Iceworm processing. No modifications have been made to the original CSS3.0 tables; the changes are entirely additions and extensions. None of the added tables and fields are intended to appear in the final output databases.

Eight tables have been added to the CSS3.0 schema to form the Iceworm schema. The pins table associates an integer pin-number, a "social-security number" for each data stream, with each station and channel name. An additional field in this table, savechan, describes whether to save that data stream for processing (useful for turning off temporarily non-working stations). There is no historical tracking of pin numbers as their associations change or as station and channel names and characteristics change. They are simply a transient bookkeeping device.

The timecorr table gives the amount of communication delay (up to 0.27 seconds for a satellite hop) to be adjusted into the timestamps of the raw data before they reach the trace ring. The table contains station and channel names, the starting and ending times (epoch seconds) when those corrections were applied to the data, and the "commdelay" field for the size of the delay. Note that here, as elsewhere, we use the intuitively recognizable station and channel names as primary keys, rather than the arbitrary integer id's such as pin-number.

Four tables make possible the intake of data from various data sources. The ewan-

alog table specifies the wiring of the earthworm analog to digital converter. Since the Earthworm A/D is hard-wired into the discriminators that take analog signals off of phone lines in the Alaskan seismology lab, discriminator numbers are in this table along with station and channel name, and the details of A/D wiring. The "win" table supports the data exchange with Japan described in section 2.4.1.2, associating the Japanese code for each station from the win-format [K. Katsumata, *pers. comm.*] data with its station and channel name. The tables "reftekdas" and "reftekchan" associate Reftek datalogger serial numbers and channel numbers with the seismic station and channel names to which they correspond.

A picker table lists all the parameters needed to customize the phase picking for each station-channel. An additional field indicates whether that station-channel should be picked or ignored.

Finally, the "eva" table gives parameters for the Alaskan Earthquake/Volcano Alarm (EVA), described below. The EVA alarm is a rough measure of the energy content of a seismogram, used to set off alarms during potential large earthquakes and volcanic eruptions. The *eva* table specifies the stations and channels to watch, and the parameters for triggering the alarm for each station or combination of stations.

The power of relational-database management of input data shows itself in many ways. Perhaps the best example is in the handling of station subsetting with the network and affiliation tables of the schema. Relational Database Management is based on set theory [Braithwaite, 1991], such that all the rows in a table can be considered to form a set.

An example of this is the affiliation table, where each member of the set associates a station code with a given network. (See Appendix A for a discussion of subtleties of the "network" field.) A station can belong to several non-overlapping or partially overlapping networks. In processing data and/or archiving data, it is often useful to focus on only a subset of the stations in the entire network, for example, the six stations within 15 km of a volcano. One way to do this is to define a subnetwork for each possible combination of stations of interest. What we have done in Iceworm is to implement specification of the network to allow set-theoretic unions and differences of different seismic networks. Constructing an example for pedagogical purposes, one could define a network for each of six volcanoes, Spurr, Redoubt, Iliamna, Augustine, Shishaldin, and Makushin; and a network containing the first four networks called CIVolcanoes ("Cook Inlet Volcanoes"). The software would allow a choice of network to be "CIVolcanoes - Augustine + Makushin", which would pick the Spurr, Redoubt, Iliamna, and Makushin volcanoes. While this particular example is somewhat contrived, the power for handling data flow inherent in this capability is enticing.

An additional feature of Datascope in particular is dynamic schema recompilation. New fields can be temporarily added to a database table within a program. This is used to great effect in the *Wormwatch* utility described below. *Wormwatch* provides a powerful set of near-real-time response capabilities, all driven from the relational-database output of Iceworm. Dynamic schema recompilation internal to *wormwatch* allows a clean way to provide complex functionality for the scientists with relatively small development effort.

2.4.1.4 Accessibility of Recent Waveform Data

The final infrastructural problem to overcome was to archive the raw waveform data. Because the Earthworm system was designed as a replacement for the Real-Time Picker at the Menlo Park seismic installation, the need to archive waveform data was already taken care of by other means. The trace-ring, intended only as a communications node for data and not a storage ring of any sort, does not serve this need. To accommodate the need to access data from the recent past, a rudimentary "wave-server" was constructed [by Will Kohler] to support our initial efforts to integrate Datascope into Earthworm. This wave-server took in only multiplexed data from the Earthworm analog-to-digital converter, however, and the wave-server would simply return short packets of multiplexed waveform data as they came into the system. Data as the seismologist use them, extended time-series from individual station-channels, would have to be reconstructed individually by each processing application. We completely overhauled the original Earthworm wave-server. By taking the demultiplexed trace data as described above, we constructed an array of miniature disk-loops for each station (all in one large file), and set up the wave-server to deliver the packets on a station-by-station basis in extended segments. Most of the details of this are handled by a wave-client library. This library allows users to establish socket connections to the wave-server over the internet. The first available operation is to request a menu of the available stations and time periods in the wave-server. One can then post

requests to the wave-server for data in a given time range for any specified station and channel in the network (there is an alternative interface that supports specification of station-channels by the Earthworm pin-number, a kind of "social-security number" for an Earthworm data stream). Gaps in the data can be handled in one of several ways. Gaps can cause a failure to return any data; gaps can be filled in with zero values; or they can be filled in with the maximum value of the storage class. This is useful to support different operations which may or may not be possible, or desirable, to perform with gaps in the data; and to prevent data gaps from causing larger problems, for example in archiving. The frequency of data gaps varies widely, depending on the acquisition hardware in question. One critique of the Iceworm wave-server is that while in principle, in the Iceworm system, the packets from a given station-channel can vary in length with time, the wave-server does its accounting based on the length of packets from each station-channel, requiring that for a given station channel, as soon as the first packet comes in, the rest of the packets for that station-channel have to be the same length. This difficulty is overcome by the ORB software described above.

2.4.2 Processing Tasks

After the infrastructure is in place for data intake and communication between modules, a number of processing tasks are necessary for seismicity studies and other more complex measurements on the earth. In Figure 2.5, we show an overview of the current

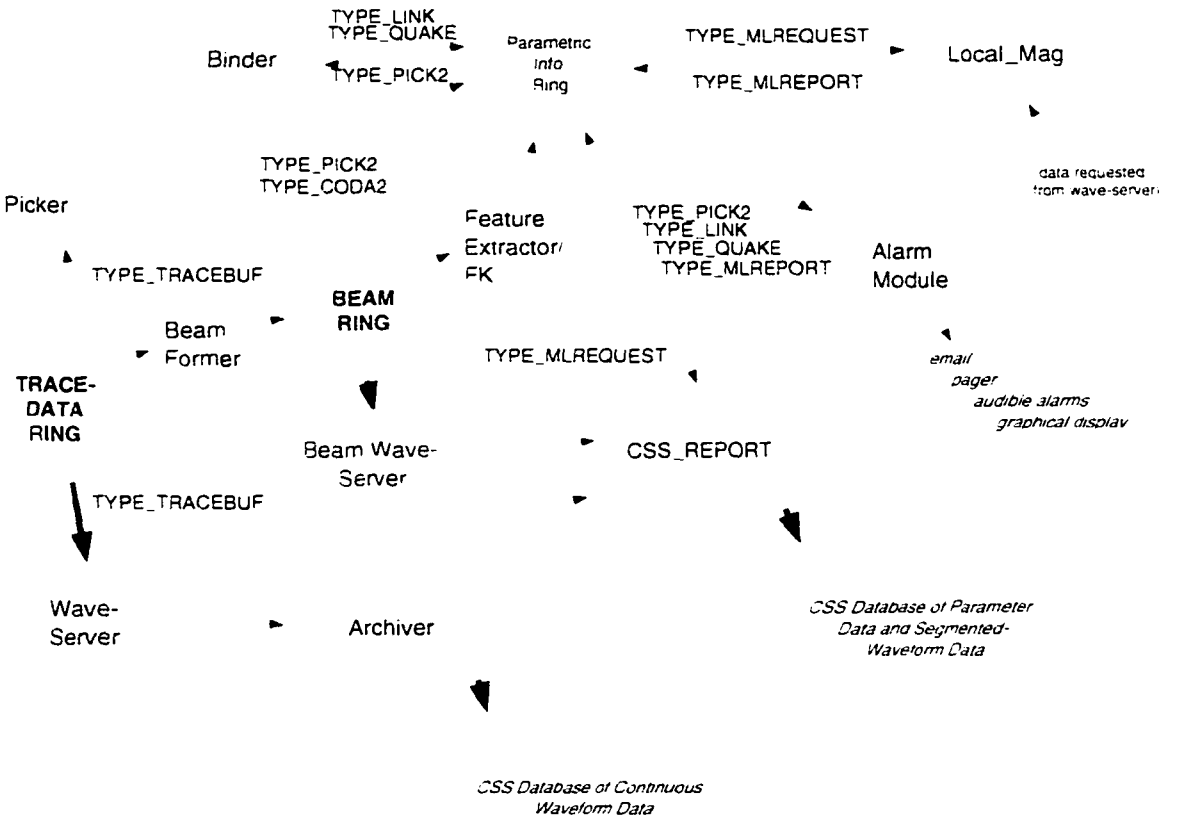

Figure 2.5

This figure shows the core processing and data storage modules of the Iceworm system. The doubled circles are Earthworm transport-layer shared-memory rings for communication between modules. The rectangular boxes show individual software programs, described in Section 2.4 of the text. Arrows indicate data-flow paths, with message types that flow along the paths labelled where appropriate. The beam-ring, beam-former, and beam-wave-server shown have not been implemented in this software release. They are shown to illustrate the potential for real-time implementation of the processing described in Chapter four of this thesis.

processing modules and the message-types they use to communicate amongst one another. The "parametric information ring" is an Earthworm transport-layer shared-memory ring used for much of the message passing between processing modules. Below, we describe the individual processes running in the current system.

2.4.2.1 Automatic Processing of Incoming Time-series, e.g. Automatic Picking

To accompany the trace-ring of waveform data we have written a template module, called a ring-rider, that can ride the near-real-time data streams and apply an arbitrary algorithm to any one or a number of station-channels of seismic data. The ring-rider architecture takes advantage of multithreaded programming to simplify the creation of new processing modules [Kleinman *et al.*, 1996], as well as to take advantage of multiprocessor machines. Multithreading allows several paths of control to execute simultaneously within a single computer program. In the ring-rider template, one thread watches the trace-ring, taking off packets from all station-channels of interest. For every station-channel to be processed, the main thread launches a handler thread with a copy of the processing subroutine and all the start-up data for that particular station. The main thread then acts as a railroad-yard switch, directing each incoming packet of interest to a data queue for the appropriate thread. The most important application of this template in Iceworm has been to algorithms for detecting incoming energy on seismograms, often called phase-picking.

For automatic processing of regional earthquakes, the first task is to apply some kind of detector for bursts of coherent energy to the incoming waveform data. In the system that preceded Iceworm in Alaska, the energy detector was simply a trigger for segmentation of continuous waveform data for a possible earthquake. This triggering system was called JADE, for Just Another Detector of Events [Sonafrank *et al.*, 1991]. One of the core features of the Earthworm system, which was initially developed as a replacement for the Real-Time Picker at the USGS Menlo Park installation, was its implementation of the Rex Allen picking algorithm [Allen, 1978, 82; Dietz *et al.*, 1993]. The algorithm compares Short-Term to Long-Term Averages (STA/LTA) of the continuous waveform data. Incoming seismic energy creates a difference between these two averages. With the help of David Chavez, we have rewritten the Earthworm implementation of the Rex Allen Picker to handle our demultiplexed data format. Cast into the multithreaded ring-rider template described above and taking all of its startup information from a relational database, the Iceworm version of the Rex-Allen picker (*icepick*) provides a flexible, easily configurable way to detect possible phases in the incoming continuous waveform data. Rejection of noise picks (false phase detections caused by telemetry problems, other electronic problems, wind, etc.), where necessary, is handled at the phase-association stage of processing.

2.4.2.2 Phase Association and Earthquake Location

The second benefit of the Earthworm system has been its implementation of a

back-projection stacker for regional phase association [Johnson, 1993; Johnson *et al.* ,1993; Johnson, 1994]. This back-projection stacking technique is a derivative of the original Generalized Beam-forming method of Ringdal and Kvaerna [1989]. The difference is that rather than forming beams directly, Johnson's implementation uses a matrix formulation with a combinatoric technique to optimize the grouping of N hypocenters with M phases, instead of relying on information on arriving phases that one can derive from coherent array processing (time-domain slant-stack beam forming [Filson, 1975] or FK analysis [Capon, 1969]). Johnson's length-metric for the residual calculation necessary to test optimal fit has a weighting factor that favors large events over small ones. Phases that group into large sets are favored over those that group into small sets. This helps prevent large events from being split into multiple, neighboring small events. A second addition by Dietz *et al.* [1997] to the Earthworm back-projection stacker, is a type of jackknife technique that employs Inglada's method [Bullen *et al.*, 1985] for earthquake location. This addition significantly hinders the association of spurious noise picks on distant stations from skewing the location of small events, although such problems still do exist. Though we have not done formal studies of the improvement gained by this jackknife method, we have noticed clear, qualitative improvement in spurious locations in the automatic output for the Alaska network. Since the AEIC and the Alaska Volcano Observatory (AVO) are co-located and share seismic data-collection infrastructure, our data stream is a mix of regional stations, seismic arrays, and tight clusters of seismic stations on volcanoes, used primarily for volcano monitoring but contributing also to regional earthquake detection.

These clusters of volcano stations will often produce several automatic picks for a small volcanic event, which will associate with noise picks from stations hundreds of kilometers away. The jackknife technique has cleared out many of these events.

2.4.2.3 Storage of Parametric Data and Detected Events with Segmented Waveforms

To run a regional network, one needs more than automatic picks and locations. The Earthworm system as we received it provided a report module that created flat-files of picks and hypocenters, in a format that could be fed to the downstream processing system at the USGS. No attempt was made to store the waveforms on which the picks were based. To address this principal failing of running the original Earthworm system divorced from waveform-data storage, we created a module (called *css_report*) that would store detected picks and hypocenters, together with segmented waveform data, in a relational database using the CSS3.0 schema and the Datascope software from the University of Colorado. This allowed easy integration of the Analyst Review software such as *dbloc2* and *dbpick* developed at the University of Colorado, which was a great improvement over reviewing individual ASCII files of detection information for events.

With near-real-time event location, there is a set of overlapping goals from which to decide in choosing how to report events and save them to the database. Often one wants the earliest information possible, the best information at any given time, and the best information that the automatic system can provide. It is not possible to provide a single

hypocentral estimate and satisfy all these goals perfectly. We have chosen the original strategies of the Earthworm reporting software. An event is reported after the hypocentral estimate from the associator has been stable for 60 seconds (actually a user-specifiable parameter). Also, if the event has more than 25 picks at any point before it has stabilized, a "quick-pick" solution is reported. The CSS3.0 database and the reporting strategies will naturally facilitate the addition of moment-tensor information and strong-motion parameters as well, when these features are implemented.

To provide data segments that correspond to detected events, we used the wave-server we have described in section 2.4.1.4. When the *css_report* module decides to report an event, it calculates an appropriate time-window of waveform data to request for each station; requests these segments of data from the wave-server; and stores the results in the CASS database of detected events. Optionally, *css_report* can also send the database row created to an *observer*, which in addition to handling waveform data can directly accept and deliver raw database rows from any database table. Several algorithms are available for segmenting the data. Currently we calculate the start time of each data segment as the expected P arrival time minus a small amount of time (currently 60 seconds) for padding. The end of each data segment is calculated based on the difference between S and P-phase travel times:

$$t_{start} = t_{origin} + ptime(\Delta, depth) - dt_{pre}$$
$$t_{end} = t_{start} + 2 * (stime(\Delta, depth) - ptime(\Delta, depth)) + dt_{post}$$

where t_{start} and t_{end} are the start and end times of the saved data segment: dt_{pre} and dt_{post} are padding terms; and the functions ptime and stime indicate the travel-times for waves from a seismic source at a specified range (Δ) and depth in a spherically-symmetric earth model. For close-in events on small networks, it is often simpler to make a straight cut of the continuous waveform data around the origin time.

In addition to the picks which correspond to specific earthquakes, which are stored in the main output database of detected events, we can save all the picks made at several subnetworks, with one database per subnetwork. The module providing this function is called *savepicks*. This is quite useful at volcano networks, where the small source region makes it very difficult to tune the Earthworm associator accurately. By saving every pick from these volcano networks, one can easily go back and analyze the events. The Datascope Seismic Application Package includes software that can cull out picks that do not appear associated with an event (the program looks for groups of picks that occur within a specified time interval). We have also used the *savepicks* utility to collect all the picks from aftershocks of a regional event. We defined a subnetwork appropriate to study the event and collected all the picks made at those stations into a database.

2.4.2.4 Local-magnitude Calculation

One of the primary uses of the wave-server for near-real-time processing is in the

calculation of automatic local-magnitudes. When the *css_report* module saves an event to the database, it makes a request on the parametric information ring for a local-magnitude calculation, passing in the message all the information about the relevant phase picks, event location, and origin time. The local magnitude module requests waveform information for the picked stations, computes synthetic Wood-Anderson recordings for those waveform segments that are not clipped, measures the maximum amplitude, and reports the detected station and network magnitudes. These are put back on the parametric information ring for storage by *css_report* in the relational database. Also, information on the raw measurement of waveform amplitude is included.

2.4.2.5 Archival of Continuous Waveform Data

With data buffered in the wave-server, we were able to support more of the necessary functions for regional-network data-handling. One of the most important, of course, was archiving of the continuous data stream. We wrote an archiver module to call up the wave-server at regular intervals, ask for all available data, and store these data in a CSS3.0 relational database. Those familiar with the CSS3.0 database format will recognize that the underlying format for the waveform data files is only minimally constrained. The archiver module we have written allows storage of the data files in AH, SAC, or raw-data (no header) forms. Writing the archiver module involved several traps, one of which was to follow very carefully the maxim, for asynchronous processing, that one should rely on data

synchronization rather than process synchronization [Kleinman *et al.*, 1996]. Our archiver has the very desirable feature that it archives whatever it sees in the wave-server menu, and if new data streams show up in the wave-server the archiver will automatically begin archiving them, without having to have any prior knowledge about what it should expect to be archiving. The one difficulty with this is that there is no inherent difference between segmented data and continuous data with large gaps, seen from the perspective of the archiver. This means that some data segments can remain for a long time in the wave-server before being written to the database by the archiver (usually triggered by the next incoming segment). One solution to this, which we have not yet implemented, is to introduce a latency timeout [D. Quinlan, *pers. comm.*, 1997]. The difference between the end-time of available data for a station is compared to the time of the latest data received for all stations. If this difference exceeds a preset threshold, data for the station are stored in the archive without waiting to complete the whole segment.

2.4.2.6 Volcano and Earthquake Alarm Triggering

For the past several years, alarms at the Alaska Earthquake Information Center and Alaska Volcano Observatory have been handled with an analog circuit called EVA. This circuit AC-couples the signals from 8 analog stations into op-amp integrators with one-second time constants, then monitors the envelopes to see if any signal stays above a preset threshold for a specified amount of time. Single stations on volcanoes can trigger the alarm

if their envelopes stay above the threshold for a specified amount of time (usually five minutes). For regional earthquakes, three or more stations must simultaneously stay above threshold for approximately 30 seconds. One of the problems with this alarm has been the arbitrariness of the gain settings for the stations, and the inability to study the envelope functions or to improve the algorithm easily.

We have made a digital equivalent of the EVA circuit to run in the Iceworm system. Incoming data streams are demeaned, L1-normed, tracked against specifiable thresholds, and saved for later review. As mentioned above, the timespans and threshold amplitudes for the EVA triggers are specified in a database, allowing them to be easily configured. Being able to review the envelope functions allows quantitative setting of the trigger levels, as opposed to the purely qualitative control on the analog EVA circuit.

2.4.2.7 Notification About Automatic Processing Results

The Iceworm system has the capability to notify duty personnel via pager and email of important events, both seismic events and system-operation conditions. We have taken part of the software for this from the original Earthworm [Oppenheimer *et al.*, 1994], though we have had to modify much of it to match our paging services.

2.4.2.8 Display Utilities for Incoming Data and Output Derived Information; Maintenance Utilities for the System

The final, user-level software that the Iceworm system makes possible is of course one of the main reasons for the current work. Automated results are made available for rapid review by human analysts, facilitating hazard response. Many of the analyst-review tools come directly from the Datascope Seismic Application Package of the University of Colorado.

To display located events as they occur and to provide the first level of review capability, we have written a utility called *wormwatch*. *Wormwatch* shows a digital-elevation map or satellite image of the state of Alaska portrayed on an X-Window display. This program watches a Datascope ORB for output database rows of automatically detected events, displaying the most recent hypocenters. The cursor can be used to probe for the hypocentral parameters of each event, and an interactive menu allows one to create a subset database of the parametric information for a given event. From this, one can look at the waveforms, the automatic picks, and perform one's own re-analysis of the event location and hand-refinement of the picks. A screen-dump of the main window of the wormwatch utility is shown in Figure 2.6.

With a real-time system as involved as Iceworm, it is also necessary to have an easy-to-use utility to monitor system performance and quickly evaluate error conditions. To address this we have written *logwatch*, a graphical user interface for system monitoring

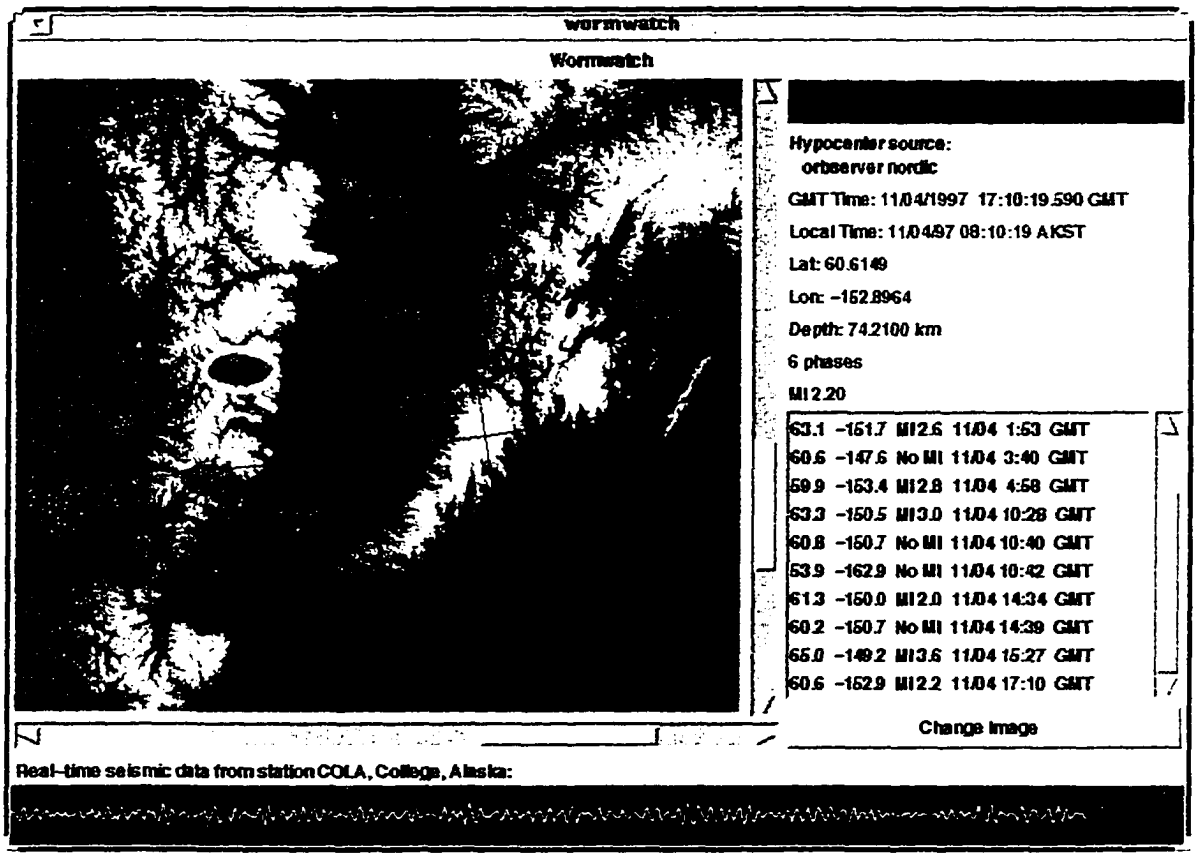

Figure 2.6

This figure shows a screen-dump of the *wormwatch* utility, described in Section 2.4.2.8 of the text. A visible-band satellite image of Alaska (cropped in this figure, but scrollable to other parts of the image) provides a map view on which automatically-determined earthquake epicenters are plotted as ovals. The automatic magnitude is written in the center of the oval when possible. *Wormwatch* is interactive, allowing the user to subset the Iceworm output database for a given event, view the results, and relocate the earthquake. The bottom of this figure shows scrolling, near-real-time seismic data from station COLA at College, Alaska. Wormwatch runs off an ORB (as shown here) or a database.

and maintenance. *Logwatch* allows access to all of the most recent log files from the individual modules running in the system. In addition, it has buttons to launch database and waveform-viewer programs on the segmented and continuous output database, plus a variety of the utilities described here. A screen dump of the graphical user interface for logwatch is shown in Figure 2.7.

A pick-display utility has proven quite useful for system tuning. This software takes each pick from the pick-ring as the pick is made, then requests a small window of data around it. This is yet another unique and valuable use of the wave-server. A graphical display of the automatic pick and its associated waveforms allows one to very quickly see which stations are contributing many noise picks. One can also watch earthquakes as their waves propagate across the state.

Finally, the *interwave* utility provides a Graphical User-Interface (GUI) directly to the wave-server. One can choose any available station and request a section of recent data from that station for display. Another highly useful display utility for recent, continuous waveform data is the *orbmonrtd* program from the University of Colorado. This utility provides a computerized, develocorder-style output of one or more continuous seismic traces as the data arrive. The advantages of this utility include system health monitoring, public-information display, and visual monitoring of earth motion for stations and areas of interest.

The rest of the software we describe here comes directly from the Datascope Seismic Application Package (DSAP). The DSAP package is far too extensive to describe here

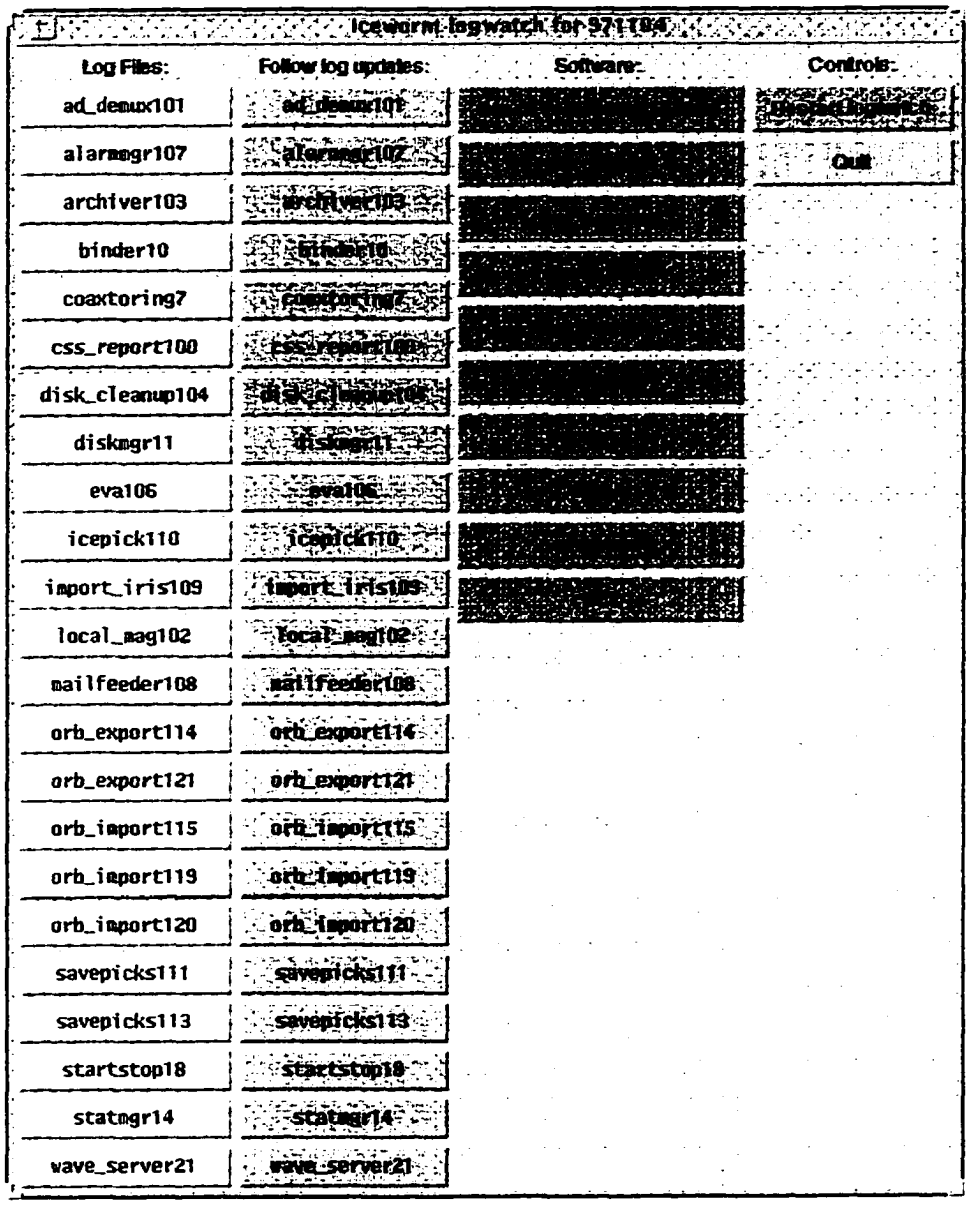

Figure 2.7

This is a screen-dump of the *logwatch* utility, a graphical-user-interface for Iceworm to monitor system performance. *Logwatch* allows access to all the most recent log files from individual modules running in the system. Logwatch also has a variety of buttons to launch database and waveform-viewer programs on the Iceworm output databases.

in full, although it is necessary to describe a few of the highlights. The *dbheli* program allows one to make helicorder-style plots of data from the archive of continuous waveform data. *Dbpick* allows interactive review and picking of waveforms, as well as review of automatic picks already made. *Dbloc2* is a GUI driver script for location programs of choice. The most common are *locsat* and Gary Pavlis' *genloc*, both of which come with DSAP. Together, *dbloc2* and *dbpick* form an analyst review software station that can be used to process the automatic detection databases of Iceworm into final, reviewed catalogs of detected earthquakes.

2.5 System Performance

One could discuss at great length the tuning of regional network associators, and of automatic phase-picking routines. We limit the presentation here to a discussion of system performance for recently detected alarm events at the AEIC.

Between March 1, 1997 and August 1, 1997 there were 329 events located both by the automatic system and by the AEIC analysts, correlating catalogs of the AEIC locations with the Iceworm automatic locations. Of these, 203 events had location residuals of less than 0.2 degrees, or 22 kilometers. Sixty-five events had location residuals between 0.2 and 1.0 degrees, still quite useful for hazard response. Another sixty-one events had location residuals greater than 1.0 degree, many because they occurred outside the core of the

Alaskan regional network. Maps of these mislocation vectors are shown in the attached Figures 2.8a-c. Depth, azimuth, and distance residuals for all events together are shown in Figure 2.9.

For the same time period, March 1, 1997 to August 1, 1997, there were 70 earthquakes for which the AEIC published alarm-notification releases. Of these, 42 were located by the Iceworm system. The 28 information-release events that were missed by Iceworm are shown in Figure 2.10. Of these, the four that one would not expect Iceworm to have missed, the four events north of Prince William Sound and the event near Katmai, occurred during times when the Iceworm system was down. The rest are all outside the core network of stations, where the performance of the Earthworm associator (binder) degrades markedly; or outside the Earthworm associator grid entirely. For the 42 automatically located information-release events, location residuals between Iceworm and the AEIC analysts are shown in Figure 2.11. With one exception, an event northeast of the core network with a residual of 2.8 degrees, the agreement between automatic and analyst solutions is excellent. The mean residual for these 42 events is 0.20 degrees (excluding the 2.8 degree outlier drops this to 0.14 degrees). The median is 0.05 degrees. A histogram of these residuals is shown in Figure 2.12.

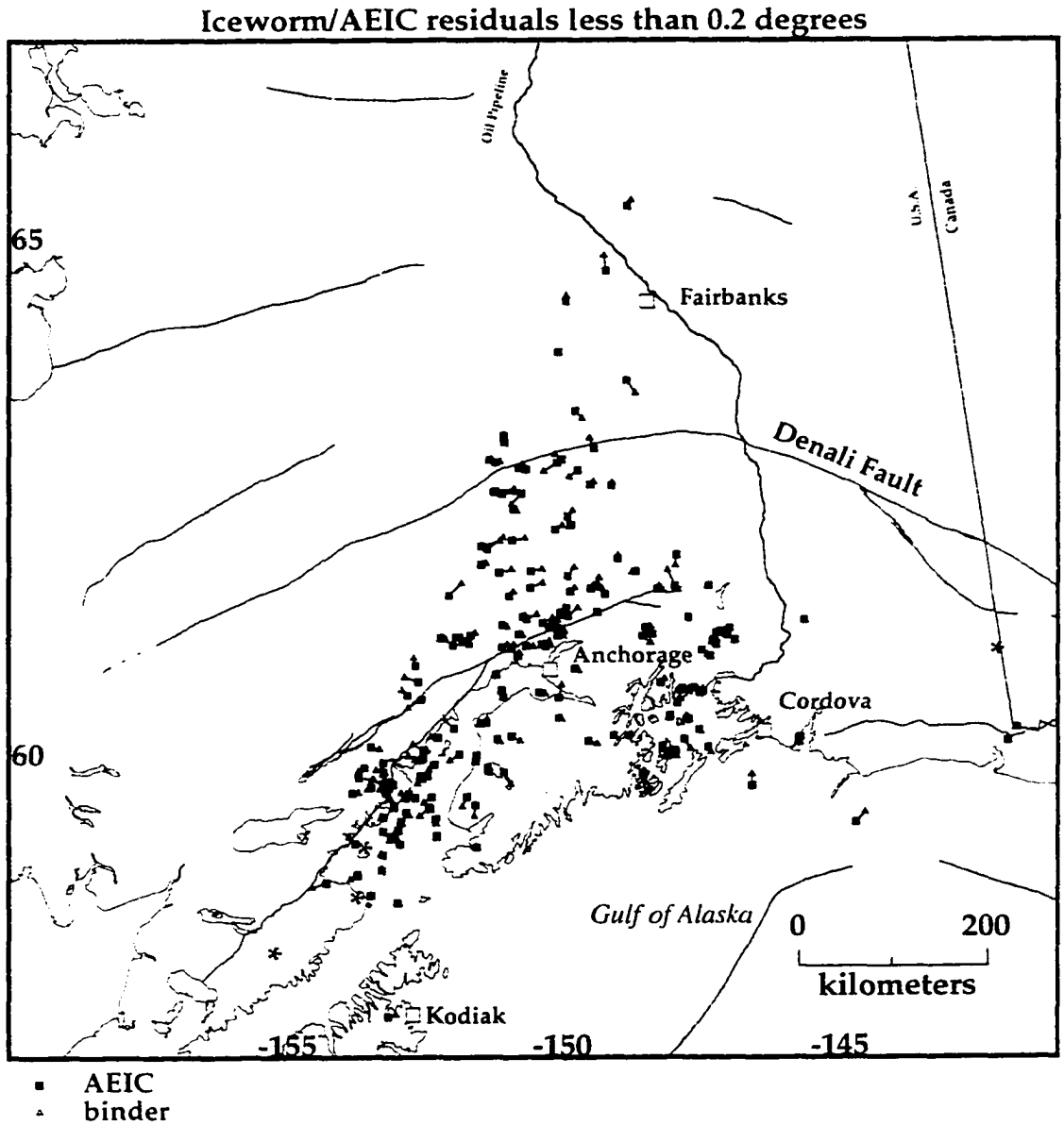

Figure 2.8 a

Mislocation vectors between epicentral solutions from the Iceworm system (binder: triangles) and the AEIC analysts (small squares). Of the 329 earthquakes located by both systems between March 1st and August 1st, 1997, the 203 events shown above (62% of the total) had location residuals less than 0.2 degrees, about 22 km.

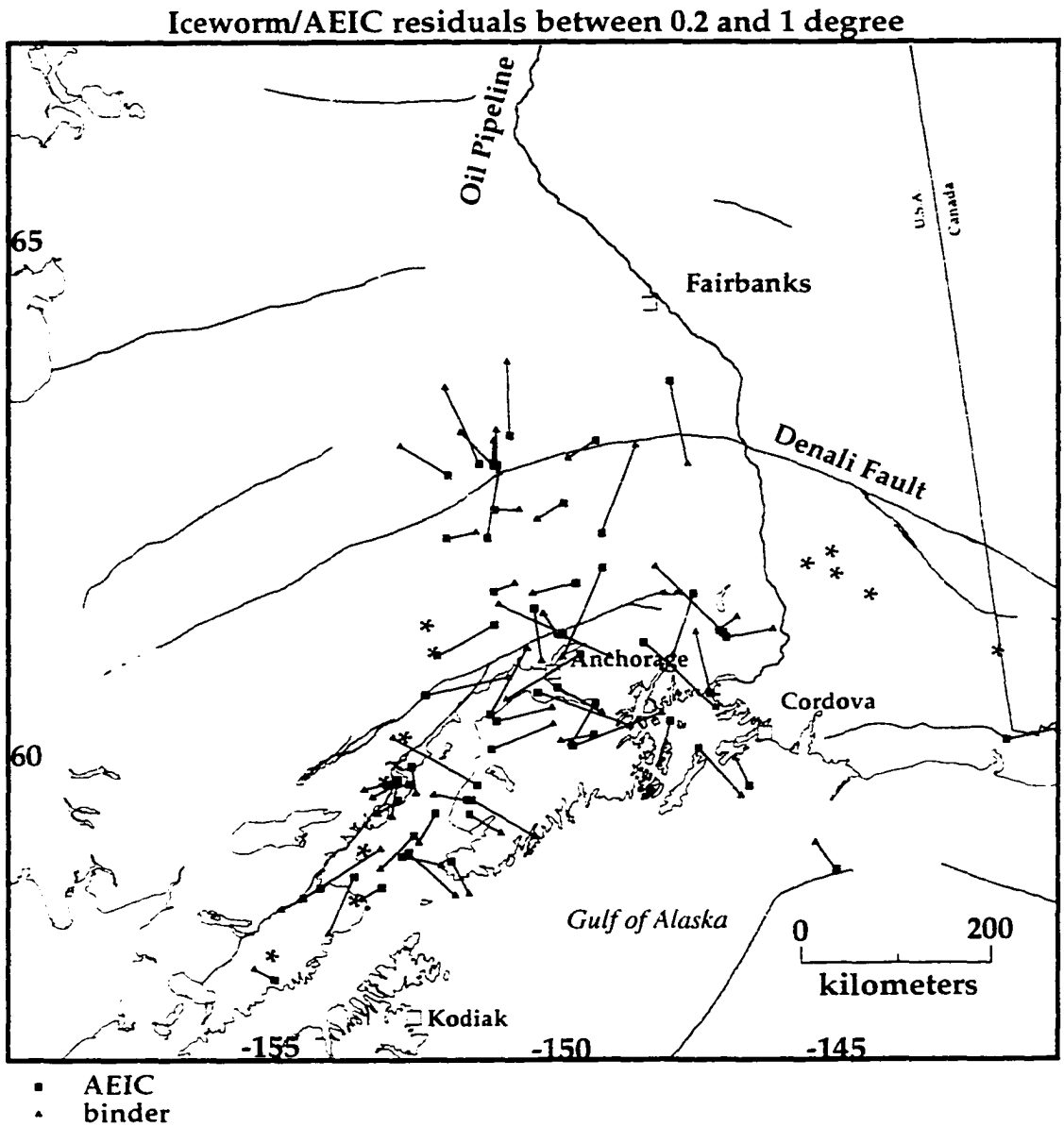

Figure 2.8 b

Mislocation vectors between epicentral solutions from the Iceworm system (binder: triangles) and the AEIC analysts (small squares). Of the 329 earthquakes located by both systems between March 1st and August 1st, 1997, the 65 events shown above (20% of the total) had location residuals between 0.2 and 1.0 degrees, (22 km to 111 km).

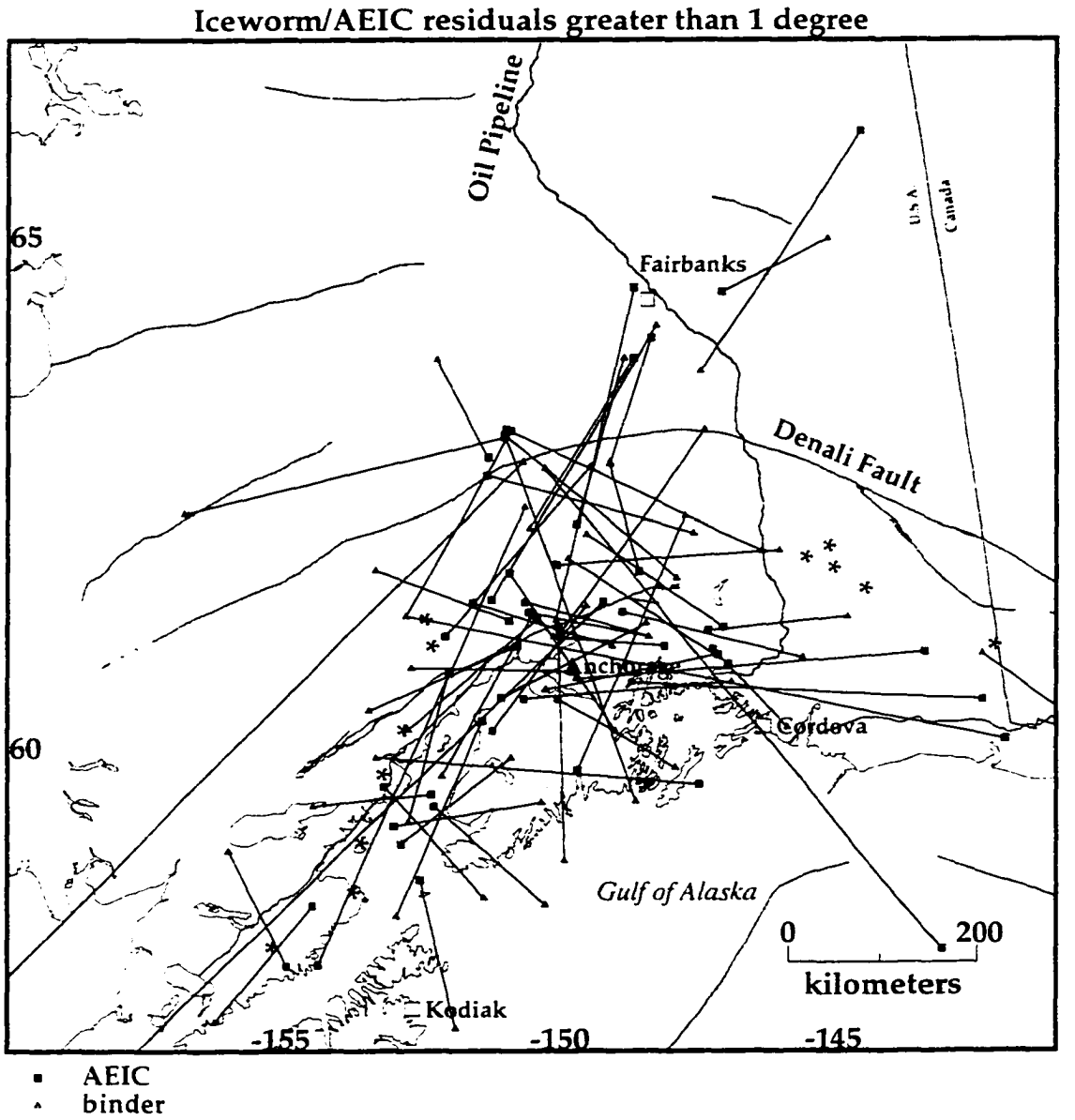

Figure 2.8 c

Mislocation vectors between epicentral solutions from the Iceworm system (binder: triangles) and the AEIC analysts (small squares). Of the 329 earthquakes located by both systems between March 1st and August 1st, 1997, the 61 events shown above (18% of the total) had location residuals greater than 1.0 degree (111 km). Because of the long lines, the visual impact of this figure is strong; however, only approximately one in five events assembled by the Earthworm associator produces a seriously mistaken location.

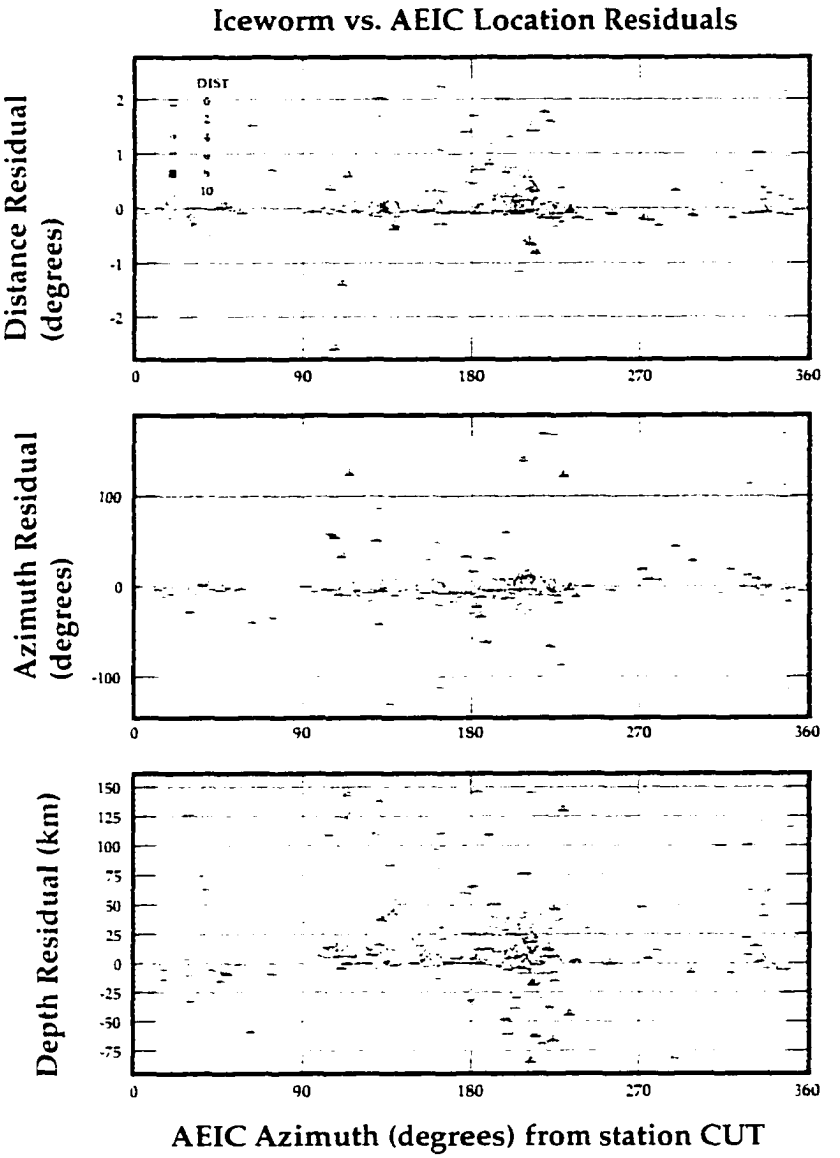

Figure 2.9

Location residuals between Iceworm and AEIC as a function of azimuth of the event from station Chulitna, CUT, which is at 62.4047° North, 150.2694° West. Chulitna is chosen as a reference station because of its central location. Each triangle represents a single earthquake.

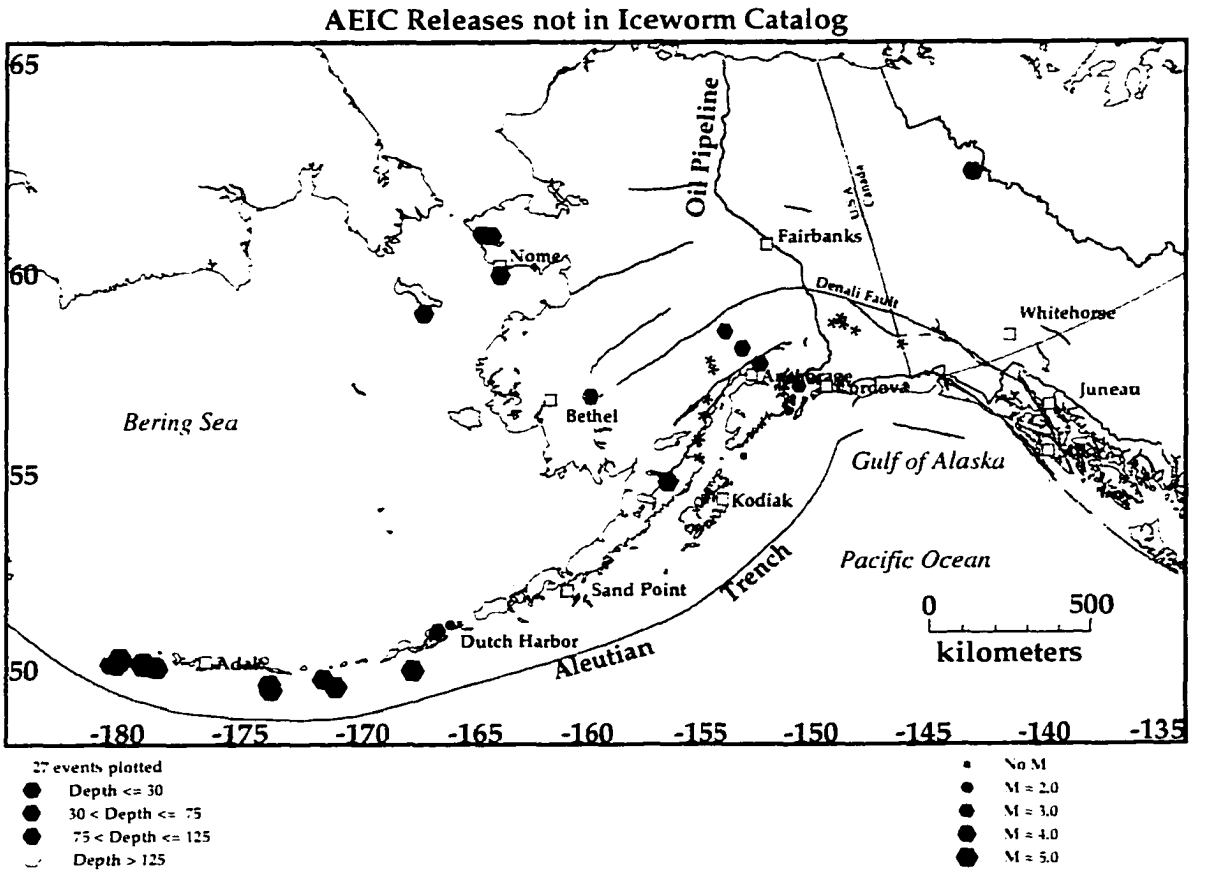

Figure 2.10

This map shows the earthquakes (hexagons) for which AEIC distributed information releases and which Iceworm missed, taking a time period between March 1st, 1997 and August 1st, 1997. A discussion of these missed earthquakes is presented in Section 2.5 of the text.

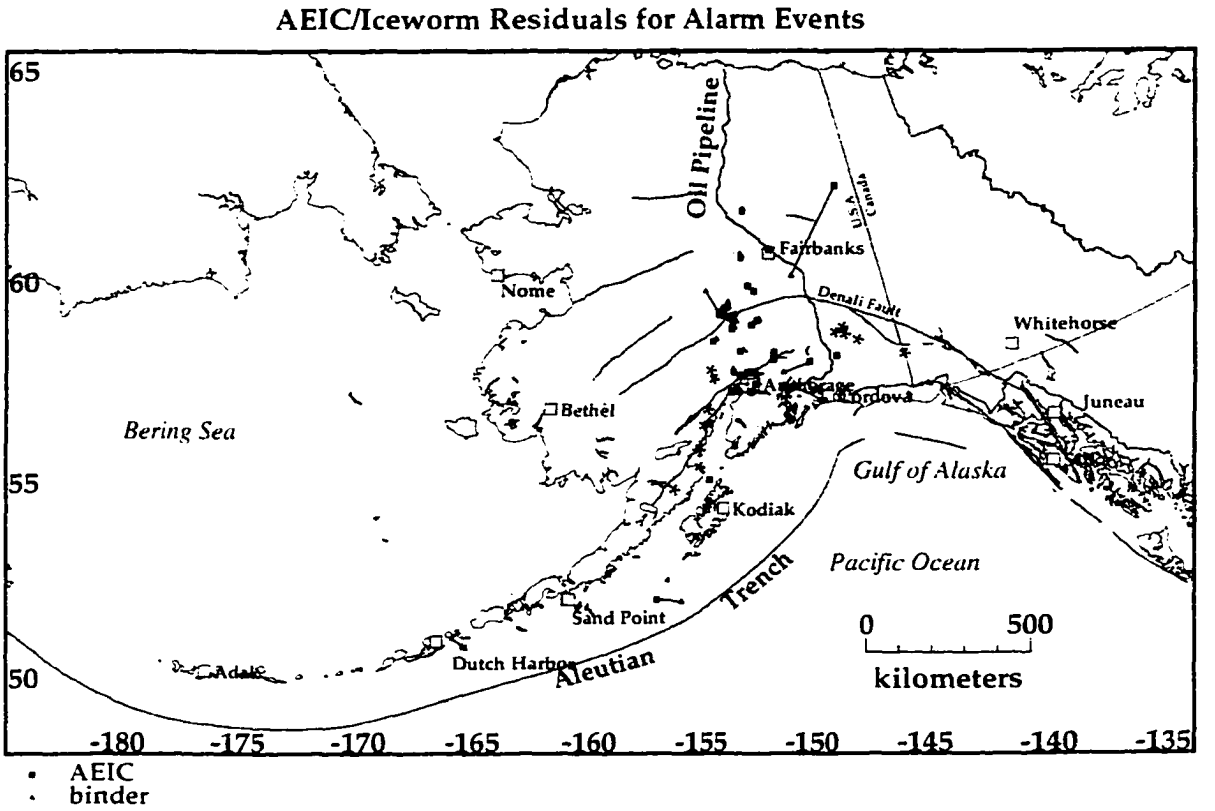

Figure 2.11

There were 70 information-release earthquakes announced by the AEIC for March 1st through August 1st, 1997. The 42 of these that were located by the Iceworm system are shown in the above map, along with mislocation vectors between the automatic and human-analyst solutions. The agreement between Iceworm and reviewed epicentral solutions is excellent, with a mean residual of 0.20 degrees. Excluding the 2.8 degree outlier reduces this mean to 0.14 degrees distance, or slightly over 15 km. The median is 0.05 degrees, or 5.5 km.

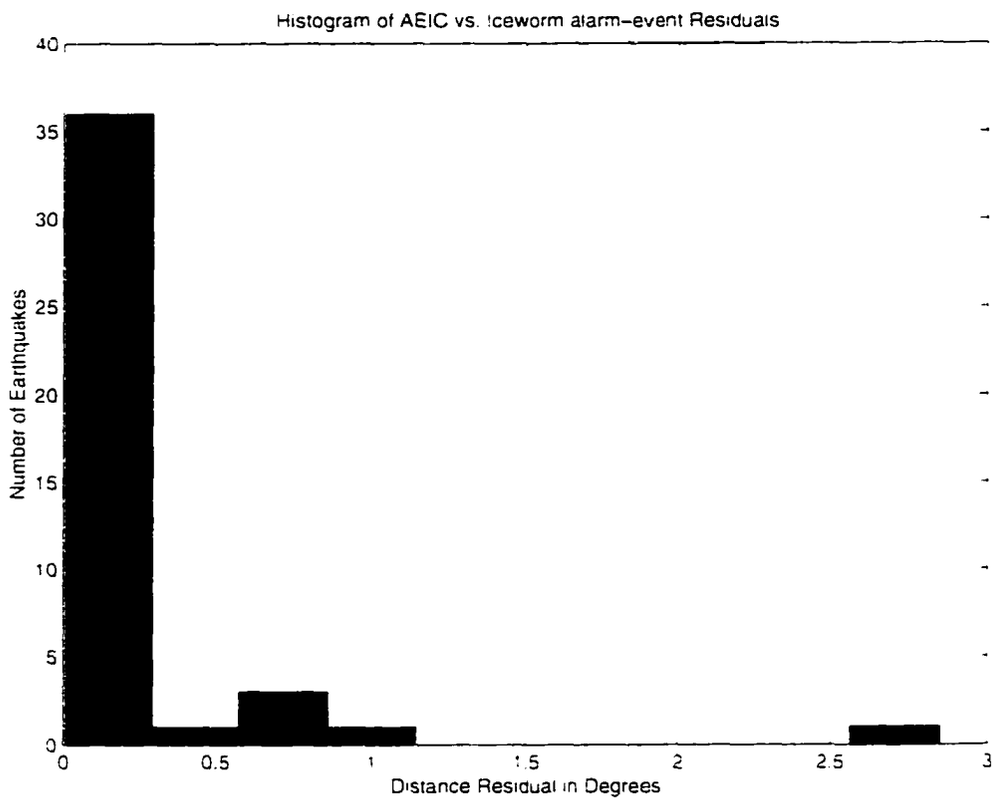

Figure 2.12

This figure shows a histogram of distance residuals between AEIC and Iceworm epicentral locations for 42 information-release earthquakes covering March 1st through August 1st, 1997.

2.6 Conclusion

The Iceworm system has been running since March. 1997 as the principal data-acquisition and triggering system for the Alaska seismic network. Qualitative results indicate quite good performance compared to the predecessor system. especially with the larger data set made possible by the waveform handling infrastructure. We see great potential for the system not only through the traditional network-based earthquake detection. but also through the addition of beam-forming and other array-processing results to the network analysis. Comparison of the Iceworm performance on alarm events to the list of alarm releases by the AEIC demonstrates the importance of expanding the geographic coverage of the automatic system with array-based techniques. Because of the high seismicity of Alaska and the surrounding regions. the contributions to real-time seismic experiments and to the improvement of public-safety through volcano monitoring. rapid evaluation of. and rapid notification about large earthquakes proves valuable.

2.7 Acknowledgments

We would like to thank Danny Harvey and Dan Quinlan of the IRIS Joint Seismic Program Center for their development and free distribution of the Datascope RDBMS and Datascope seismic application package; we would also like to thank Dan Quinlan for dis-

cussions and advice during a one-week visit in the summer of 1995. David Chavez and Ken Smith of the University of Nevada, Reno provided subroutines that were instrumental in writing icepick, the Rex-Allen picker with flexibility to handle all types of input data. Sue McLafferty and Bob Hutt at USGS Albuquerque provided software to connect to the IRIS DP unit for the COLA-station data, software which we then modified to bring the data directly into our system. Kevin Engle and Mitch Robinson of the University of Alaska Seismology Lab provided valuable programming and system support. We thank Dave Oppenheimer of the USGS for providing an initial PC-based Earthworm system to get us started. We thank the Earthworm team of the USGS for providing us a copy of their software, and Alex Bittenbinder, Barbara Bogaert, Lynn Dietz, and Will Kohler of the USGS Earthworm team for valuable discussions and visits. Funding for this work was provided by the State of Alaska, NSF grant number EAR93-16337, and IRIS sub-award number 218. Implementation of the automatic local-magnitude routines was aided by Suzanne Floyd, working under the Research Experience for Undergraduates program, NSF grant number EAR95-31601.

2.8 References for Chapter 2

Ahern, T.K., R. Buland, and S. Halbert (1993). Standard for the Exchange of Earthquake Data: Reference Manual, SEED Format Version 2.3, February, 1993. Seattle: Incorporated Research Institutions for Seismology, 203 pp.

Allen, R. V. (1978). Automatic Earthquake Recognition and Timing from Single Traces. *Bull. Seis. Soc. Am.* **68**, 1521-1532.

Allen, R. (1982). Automatic Phase Pickers: Their Present Use and Future Prospects. *Bull. Seis. Soc. Am.* **72**, S225-S242.

Anderson, J., W.E. Farrell, K. Garcia, J. Given, and H. Swanger (1990). Center for Seismic Studies Version 3 Database: Schema Reference Manual, Science Applications International Corporation, Arlington, Virginia, Technical Report C90-01, 61 pp.

Anderson, M.P., M.R. Robinson, T.M. Jiang, G.H.C. Sonafrank, and P.L. Ward (1994). Alaska Seismic Network Database Management and Analysis Software at the University of Alaska Geophysical Institute, *Seis. Res. Lett.* **65**, 51.

Bache, T.C., S.R. Bratt, J. Wang, R.M. Fung, C. Kobryn, and J. Given (1990). The Intelligent Monitoring System, *Bull. Seis. Soc. Am.* **80**, 1833-1851.

Berger, J. and D. Chavez (1997). The IDA Near-Real-Time System, *Seis. Res. Lett.* **68**, 223-227.

Berger, J., R.G. North, R.C. Goff, and M.A. Tiberio (1984). A Seismological Data Base Management System, *Bull. Seis. Soc. Am.* **74**, 1849-1862.

Bittenbinder, A. (1994). Earthworm: A Modular Distributed Processing Approach to Seismic Network Processing, *Eos Trans. Amer. Geophys. U.* **75**, No. 44, 430.

Böðvarsson, R., S. Th. Rögnvaldsson, S. S. Jakobsdóttir, R. Slunga, and R. Stefánsson (1996). The SIL Data Acquisition and Monitoring System, *Seis. Res Lett.* **67**, 35-46.

Braithwaite, K. S. (1991). "Relational Theory: Concepts and Application," San Diego: Academic Press, Inc., 261 pp.

Bratt, S.R., H.J. Swanger, R.J. Stead, F. Ryall, and T.C. Bache (1990). Initial results from

the Intelligent Monitoring System. *Bull. Seis. Soc. Am.* **80**, 1852-1873.

Bullen, K.E. and Bruce A. Bolt (1985). "An introduction to the theory of seismology, fourth edition." Cambridge: Cambridge University Press, 499 pp.

Capon, J. (1969). "High-resolution frequency-wavenumber spectrum analysis." *Proc. IEEE* **57**, 1408-1418.

Comer, D. E. (1995). "Internetworking with TCP/IP: Volume I: Principles, Protocols, and Architecture." Englewood Cliffs: Prentice-Hall, 613 pp.

Dietz, L. D., W. Kohler, and W.L. Ellsworth (1993). A Real-time P-wave Picker (RTP) for a Fast Earthquake Response System (Earthworm). *Eos Trans. Amer. Geophys. U.* **74**, No. 43, 429.

Dietz, L., W. Kohler, A. Bittenbinder, B. Bogaert, and B. Hirshhorn (1994). Larva: an Implementation of Earthworm on the USGS Northern California Seismic Network. *Eos Trans. Amer. Geophys. U.* **75**, No. 44, 430.

Dietz, L., A. Bittenbinder, B. Bogaert, W. Kohler, and C. Johnson (1995). Automatic

Seismic Network Processing with Earthworm. *Eos Trans. Amer. Geophys. U.* **76.** No. 46. F395.

Dietz. L.D.. C.E. Johnson. W.L. Ellsworth. B.M. Bogaert. A. N Bittenbinder. and W.M. Kohler (1997). Recent improvements to Earthworm: The Associator. *Seis. Res. Lett.* **68.** 331-332.

Dollar. R.S. and A.W. Walter (1995). Hybrid Analog and Digital Realtime Earthquake Analysis Using CUSP_RT in a High Speed Network. *Eos Trans. Amer. Geophys. U.* **76.** No. 46. F395.

Filson. J. (1975). "Array Seismology." *Ann. Rev. Earth Planet Sci.* **3.** 157-181.

Gee. Lind S.. D. S. Neuhauser. D. S. Dreger. M. E. Pasyanos. B. Romanowicz. and R. A. Urhammer (1994). Real-time Seismology at UC Berkeley. *Eos Trans. Amer. Geophys. U.* **75.** No. 44. 429.

Gee. L. S.. D. S. Neuhauser. D. S. Dreger. M. E. Pasyanos. M. H. Murray. R. A. Uhrhammer. and B. Romanowicz (1995). The REDI Project - Current Status and Future Development. *Eos Trans. Amer. Geophys. U.* **76.** No. 46. F395.

Gee, L.S., D. S. Neuhauser, D. S. Dreger, M. E. Pasyanos, R. A. Urhammer, and B. Romanowicz (1996). Real-Time Seismology at UC Berkeley: The Rapid Earthquake Data Integration Project, *Bull. Seis. Soc. Am.* **86**, 936-945.

Given, D. D. (1994). ISAIAH: Information on Seismic Activity in a Hurry, *Seis. Res. Lett.* **65**, No.1, 47.

Glushko, M., F.L. Vernon, A. Edelman, and B. McManus (1994). Array Studies in the Joint Seismic Program, *Eos Trans. Amer. Geophys. U.* **75**, No. 44, 432.

Hansen, R. A. and K. G. Lindquist (1996). Array Processing for a Cooperative Arctic Seismology Program, *Abstracts from the XXV General Assembly of the European Seismological Commission*, Sept. 9-14, 1996, Reykjavik, Iceland.

Hansen, R. A., K. G. Lindquist, and M. Bifelt (1997). Near-real-time seismic data exchange for education and research, *Abstracts from the Ninth Annual IRIS Workshop*, June 8-12, The IRIS Consortium.

Hauksson, E., P. Maechling, and H. Kanamori (1994). Real-Time Earthquake Monitoring

Using Terrascope, *Seis. Res. Lett.* **65**, No. 1, 47.

Haviland, K. and B. Salama (1987). "Unix System Programming", Workingham: Addison Wesley Publishing Company, 339 pp.

Havskov, J., L.B. Kvamme, R.A. Hansen, H. Bungum, and C.D. Lindholm (1992). The Northern Norway Seismic Network: Design, Operation, and Results, *Bull. Seis. Soc. Am.* **82**, 481-496.

Johnson, C. E. (1979). I. CEDAR--An Approach to the Computer Automation of Short-Period Local Seismic Networks. II. Seismotectonics of the Imperial Valley of Southern California, *Ph.D. Thesis, California Institute of Technology*, 332 pp.

Johnson, C.E., A. Bittenbinder, and B. Hirshorn (1993). Auryn: A Stacking Method for the Rapid Association of Multiple Earthquake Phases, *Eos Trans. Amer. Geophys. U.* **74**, No. 43, 394.

Johnson, C. E. (1994). Rapid Association of Regional Network Phases, *Eos Trans. Amer. Geophys. U.* **75**, No. 44, 430.

Johnson, C.E. (1993). "Phase Associator: Programmer's notes." Technical report 93-001. Koa'e Systems, Volcano, HI, 52pp.

Johnson, C.E., A. Bittenbinder, B. Bogaert, L. Dietz, and W. Kohler (1995). Earthworm: A Flexible Approach to Seismic Network Processing, *IRIS Newsletter* XIV, Number 2, 1-4.

Kjartansson, E. (1996). Database for SIL Earthquake Data, *Abstracts from the XXV General Assembly of the European Seismological Commission*, Sept. 9-14, 1996, Reykjavik, Iceland.

Kleiman, S., D. Shah, and B. Smaalders (1996). Programming with Threads, Mountain View: SunSoft Press, 534 pp.

Kvaerna, T. (1994). Automatic Processing of Data from Small-aperture Arrays and Seismograph Networks in the Context of Seismic Verification, *Ph.D. Thesis, University of Oslo*, 125 pp.

Lahr, J.C. (1989). HYPOELLIPSE/Version2.0: A computer program for determining local earthquakes hypocentral parameters, magnitude, and first motion pattern, *U.S. Geological Survey Open File Report* **89-116**, 92 p.

Lindquist, K. G., J.P. Benoit, and R. A. Hansen (1996). Advances to Near-real-time Spectral Monitoring at Volcanoes with an Iceworm-based Implementation. *Eos Trans. Amer. Geophys. U.* **77**, No. 46, F451.

Lindquist, K. G., R. A. Hansen, and M. Garcés (1996). Progress towards Iceworm-based Monitoring of Aleutian Seismicity, *Abstracts from the Eighth Annual IRIS Workshop*, June 19-23, 1996, the IRIS Consortium.

Lindquist, K. G. and R. A. Hansen (1995). Relational Database Implementation for Near-real-time Earthquake Monitoring," *Eos Trans. Amer. Geophys. U.* **76**, No. 46, F395.

Malone, S. (1995). SUNWORM: The Pacific Northwest Seismograph Network Real-time Seismic Recording and Processing System, *Eos Trans. Amer. Geophys. U.* **76**, No. 46, F395.

Malone, S. (1996). The Electronic Seismologist: "Near" Realtime Seismology, *Seis. Res. Lett.* **67**, No. 6, 52.

Nakamura, Y. (1994). Urgent Earthquake Detection and Alarm System (UrEDAS), *Seis.*

Res. Lett. **65**, No. 1, 47.

Neuhauser, D., B. Romanowicz, T. McEvilly, F. Morrison, W. Karavas, J. Friday, D. Rapkin, R. Clymer, R. Uhrhammer, L. Gee, and M. Murray (1995). Digital Telemetry and Recording Enhancements for the Berkeley Digital Seismic Network, *Eos Trans. Amer. Geophys. U.* **76**, No. 46, F394.

Nolet, G. (1995). PEPP - Princeton Earth Physics Project, *IRIS 2000: Section II, Scientific Contributions*, from the Proposal *A Science Facility for Studying the Dynamics of the Solid Earth*, submitted to the National Science Foundation, The IRIS Consortium.

Oppenheimer, D., B. Bogaert, A. Michael, and A. Jones (1994). Rapid Reporting of Hypocentral Information via Nationwide Pagers, *Eos Trans. Amer. Geophys. U.* **75**, No. 44, 430.

Quinlan, D. M. (1994). Datascope: A Relational Database System for Scientists, *Eos Trans. Amer. Geophys. U.* **75**, No. 44, 431-432.

Ringdal, F. and T. Kvaerna (1989). A multi-channel processing approach to real time network detection, phase association, and threshold monitoring,, *Bull. Seis. Soc. Am.* **79**,

1927-1940.

Robinson, M.R., C.A. Rowe, G.H.C. Sonafrank, and J.D. Davies (1991). Xpick demonstration: seismic analysis software system at the University of Alaska Geophysical Institute, *Seis. Res. Lett.* **62**, p.23.

Rowe, C.A., G.H.C. Sonafrank, and J.D. Davies (1991). Data Analysis at the University of Alaska Geophysical Institute seismology laboratory, *Seis. Res. Lett.* **62**, p.23.

Rowe, C.A. and R. Hansen (1996). Earthquakes in Alaska--January, March, 1995, Alaska State Seismologist's Reports 95-01-01 and 95-01-03.

Sonafrank, C., J. Power, G. March, and J. Davies (1991). Acquisition and automatic processing of seismic data at the Geophysical Institute, *Seis. Res. Lett.* **62**, p.23.

Stefansson, R., R. Böðvarsson, R. Slunga, P. Einarsson, S. Jakobsdóttir, H. Bungum, S. Gregersen, J. Havskov, J. Hjelme, and H. Korhonen (1993). Earthquake Prediction Research in the South Iceland Seismic Zone and the SIL Project, *Bull. Seis. Soc. Am.* **83**, 696-716.

Townshend, J. (1996). Unique Borehole for Seismic Instrumentation. *Abstracts from the 8th Annual IRIS Workshop*. Semi-ah-moo, Washington.

Chapter 3

A Local-Magnitude Inversion for Alaska

3.1 Introduction

With the accumulation in the literature of more precise estimates of slip and rupture properties for individual earthquakes, it is natural to review the consistency of traditional, empirical earthquake parameters such as local magnitudes and their relationship to more physical ones, such as seismic moment, stress drop, and energy release. Despite the relatively recent introduction of magnitude scales more sophisticated and better grounded in physical theory, such as the moment magnitude, the local magnitude scale retains its value for many applications. Traditional local magnitude scales have retained their importance for seismic hazard analysis, historical comparison, and studies of small events. To be useful in catalogs of seismicity, these magnitudes must give a measure of earthquake size that is consistent over both time and space. Also, often for small events or numerous events, the volume and types of processing necessary to compute a moment magnitude for each one are not practical or sometimes even possible. This is often true at volcanoes, where many small events must nevertheless be categorized by size for b-value studies and other measures of volcanic seismicity.

The original local magnitude scale was tailored by Richter for southern California

[Richter, 1935]. As such, it is not directly applicable to other regions of the world, especially volcanoes, where the elastic and anelastic attenuation characteristics may be much different than those in southern California. It is desirable, therefore, to establish a separate magnitude scale for each different region of the world, taking care to relate the new scales to the original to preserve in the scale some meaning that transcends the area in which it is defined. Previous inversions for local magnitude scales in Norway [Alsaker *et al.*, 1991] emphasize the importance of allowing for variations in attenuation created by local geology and tectonics. Errors in magnitude estimates in such shield areas can be as great as one full magnitude unit if California attenuation values are used [Alsaker *et al.*, 1991].

In this study we follow the method of Alsaker *et al.* (1991), which fits a curve of the form expected for local magnitude to a suite of amplitude measurements made for a set of earthquakes at known distances. The technique is a regression analysis of synthesized Wood-Anderson amplitude measurements. The problem is posed such that a linear matrix equation can be formed and solved by standard inversion techniques. The model space consists of the earthquake magnitudes, the station corrections, and the a and b coefficients in the M_L formula (see below). We invert for attenuation parameters appropriate for computing local magnitudes in Alaska. We are using data selected from five years of digital recordings of local earthquakes from approximately 150 seismic stations (mostly vertical-component) distributed throughout Alaska. Approximations to equivalent Wood-Anderson amplitudes have been computed. Details of the approximation technique, including the use of vertical component stations in place of the horizontal-component Wood-Anderson in-

struments, are discussed in the Data section (Section 3.3) below.

3.2 Theory

The basic formula for local magnitude, from the original definition [Richter, 1935], is

$$M_L = \log A - \log A_0 + S$$

where A is maximum trace amplitude (zero to peak) in millimeters as measured on a horizontal component Wood-Anderson seismometer recording, S is a station correction term, and $-\log A_0$ is a distance correction term. This latter term can be expressed in a form slightly more general than the original Richter definition as follows [Alsaker *et al.*, 1991]:

$$-logA_0 = a \cdot \log(R/R_{ref}) + b(R - R_{ref}) + K(R_{ref})$$

where R is the hypocentral distance and R_{ref} is a reference distance at which the magnitude scale is pinned to the California scale. The constant *a* is a measure of geometric spreading, and the constant *b* is a measure of attenuation. For the Californian scale, a is 1.110 and b is 0.00189. The function K gives the reference magnitude, and comes from the original Richter scale. K can be expressed

$$K(R_{ref}) = 1.110\log(R_{ref}/100) + 0.00189(R_{ref} - 100) + 3.0$$

which gives a value of 3.0 at a reference distance of 100 km. We have chosen a reference distance of 17 km, as suggested by Hutton and Boore (1987), giving a reference magnitude of 2.0.

To establish the new magnitude scale, we can combine the first two equations to yield [Alsaker *et al.*, 1991]

$$\log A_{ij} = -a\log(R_{ij}/R_{ref}) - b(R_{ij} - R_{ref}) - \sum_{k=1}^{N_e} M_k\delta_{ik} + \sum_{l=1}^{N_s} S_l\delta_{lj} - K(R_{ref})$$

Here A_{ij} is the maximum zero-to-peak amplitude of earthquake i at station j, R_{ij} is the hypocentral distance for earthquake i at station j, M_k and S_l give the magnitudes and station corrections for the earthquakes and stations used in the study, and δ_{ij} is the Kroenecker delta function. N_e and N_s are the number of earthquakes and stations used, respectively.

To make this useful for a computation, we need to put it in the form

$$\mathbf{Ax} = \mathbf{y}$$

which we can do [Alsaker *et al.*, 1991] by writing

$$\begin{Bmatrix} 1 & 0 & \cdots & 0 & 1 & \cdots & 0 & r_{11} & u_{11} \\ 1 & 0 & \cdots & 0 & 0 & \cdots & 0 & r_{12} & u_{12} \\ \vdots & \vdots & \ddots & \vdots & \vdots & \ddots & \vdots & \vdots & \vdots \\ 1 & 0 & \cdots & 0 & 0 & \cdots & 1 & r_{1N_s} & u_{1N_s} \\ 0 & 1 & \cdots & 0 & 1 & \cdots & 0 & r_{21} & u_{21} \\ 0 & 1 & \cdots & 0 & 0 & \cdots & 0 & r_{22} & u_{22} \\ \vdots & \vdots & \ddots & \vdots & \vdots & \ddots & \vdots & \vdots & \vdots \\ 0 & 0 & \cdots & 1 & 0 & \cdots & 1 & r_{N_e N_s} & u_{N_e N_s} \end{Bmatrix} \bullet \begin{Bmatrix} M_1 \\ \vdots \\ M_{N_e} \\ S_1 \\ \vdots \\ S_{N_s} \\ -a \\ -b \end{Bmatrix} = \begin{Bmatrix} y_{11} \\ y_{12} \\ \vdots \\ y_{1N_s} \\ y_{21} \\ y_{22} \\ \vdots \\ y_{N_e N_s} \end{Bmatrix}$$

This is a system of at least N_e+N_s+2 linearly independent equations. We have assigned $r_{ij}=\log(R_{ij}/R_{ref})$, $u_{ij}=(R_{ij}-R_{ref})$, and $y_{ij}=\log A_{ij}+K(R_{ref})$. The sum of the station corrections has been constrained to be zero for this inversion. The large number of stations (over 100) in a diversity of siting environments justifies this choice of the value zero for the average station correction.

Fortran code has been written by the authors of the Alsaker *et al.* (1991) paper to set up and invert the above equation with a Singular Value Decomposition technique. The code, *maggt*, provided by one of its authors [R. Hansen, *writt. comm.*, 1994], has been used in this study.

The attenuation coefficient b may be formally related to an attenuation quality-factor Q by recognizing that the attenuation term in the magnitude formula is of the form

$$A \sim 10^{-br}$$

where A is the amplitude and r is the propagation distance. From Lay *et al.* [1995] we can write amplitude as a function of time t as

$$A \sim e^{\frac{-\pi f t}{Q}}$$

where f is the frequency of the propagating wave. Converting the propagation time t to a propagation distance r through a velocity β (taken to be an average shear-wave velocity of 3.6 km/sec), we can write

$$A \sim e^{\frac{-\pi f r}{3Q}}$$

Equating this with the attenuation expression in terms of b, we derive

$$Q = \frac{\log(e)\pi f}{3b}$$

Great care must be taken in interpreting Q values obtained through this method, however. The point of this inversion is to obtain an empirical fit for the a and b coefficients. Q values interpreted from b are subject to bias resulting from trade-off between the a and b coefficients in the inversion.

3.3 Data

Because full phase and amplitude response information was not readily available for the stations used in the study, the ideal method of constructing the synthesized Wood-Anderson amplitude measurements was impractical. One would prefer to take the original waveforms, deconvolve the instrument response, convolve in a Wood-Anderson response function and then re-measure the amplitudes on the horizontal components. This would require three-component instruments, of which less than thirty exist in continental Alaska.

Historically, Wood-Anderson synthetics at the Alaska Earthquake Information Center (AEIC) have not been calculated in this way. Amplitude measurements have been made from the vertical-component analog, short-period stations that form the bulk of the Alaskan seismic network. These are velocity seismograms, unlike the displacement seismograms of the original Wood-Anderson instrument. The AEIC analysts have been trained to avoid high-frequency components of the seismograms while making the amplitude measurements, in effect performing, by inspection, a qualitative low-pass filtering on the data.

The use of vertical-component measurements in place of horizontal components requires some justification. Alsaker *et al.* [1991] analyzed 126 three-component recordings from 100 earthquakes at four stations, comparing the mean log maximum trace amplitudes from the two horizontal components with the vertical component. They found a mean value of the ratio to be 1.008 with a correlation coefficient of 0.99, an insignificant difference that allows vertical amplitudes to be used in the study as if they were horizontal.

Furthermore, catalog data have not been stored as raw amplitude measurements. Only the resulting station magnitude has been stored, in the *xmag* field of the Hypoellipse pickfiles containing the parametric data for events. The formula for obtaining the *xmag* value in the pickfiles from the amplitude measurement was [Lahr, 1994]:

$$XMAG = \log(A/2) + \left[-B1 + B2\log\left(D^2 + Z^2\right)\right] + G$$

where B1=0.15, B2=0.80 for epicentral distance D< 200 km and B1=3.38, B2=1.50 for 200 km <= D <= 600 km. *G* is a station correction. *A* in the above formula is the maximum peak-to-peak amplitude in millimeters and Z is the focal depth in kilometers. We solved the *xmag* formula above for A, in order to obtain amplitude readings from the event pickfiles for the regression analysis.

The regional earthquake inversions in this study were done with data from 1994. Since several different inversions were done, we summarize the data input along with the results in Table 3.1, to be discussed at greater length below.

The data used for the volcano portion of this study have been taken from the Alaskan catalogs of volcanic events from 1991 through 1993 [Jolly *et al.*, 1996]. Recovery of 99% of the Hypoellipse pickfiles [Lahr, 1994] from this database yields 13,779 pickfiles, only some of which contain usable data. Extraction of the pickfiles was accomplished with Unix utilities on the command line, described in Appendix B section B.1. The pickfiles were converted to the format needed for the inversion program, *maggt*, with a Tcl script

Table 3.1
Summary of Input Data and Results for Regionalized M_L Inversions

Data Set	Number of Earthquakes	Number of Stations	Number of Amplitudes	Reference Distance (km)	Reference Magnitude	Geometric Spreading (a)	Attenuation (b)	Comparison (M_L units) to California	Comparison Distance (km)
Norway	195	21	741	60	2.7	1.037±0.092	0.0007810.000090	1.0	870
Alaska 4/94	155	48	1248	17	2.0	1.111±0.07	0.001110.0002	0.5 to 0.6	650
Northern Alaska	187	43	1906	17	2.0	0.960±0.07	0.001910.0002	0.2	400
South Central Alaska	237	45	1861	17	2.0	1.21±0.07	0.000451±0.0003	0.4	400
North of Cook Inlet	159	31	1073	17	2.0	1.141±0.13	0.0008110.0007	0.4	400
Deep events	158	58	1854	17	2.0	1.0 (fixed)	0.00136	0.6	650
Spur	129	5	485	5	1.38	0.825±0.27	0.023310.012	0.2	25

listed in Appendix B section B.2. The station correction G in the *xmag* formula was set to zero for calculations of *xmag* in the Spurr event catalog [J. Lahr, *pers. comm.*, 1995] and therefore can be omitted from our current reformatting considerations.

The above reformatting steps yield 4111 amplitude measurements for 1991, 6463 for 1992, and 1896 for 1993. We have winnowed these to select observations made at Spurr stations only; observations of earthquakes with epicentral depths of less than 20 km; and observations made within 25 km of the volcano. The winnowing procedure is described in Appendix B Section B.3. These limits have been set in order to assure that the results will be characteristic of the volcano itself, not the surrounding region. The resulting data set contains 6967 usable amplitude measurements. Since the inversion code can take a maximum of 1000 input observations, this data set is larger than we can use all at once. Clearly there is room for improvement here: when the automated data-sets discussed below are inverted, there will be justification to expand the inversion code to handle larger data sets. For the current work, independent, 1000-data-point inversions each produce consistent results which serve well enough to establish the regionalized properties we demonstrate here. Our principle inversion has been done with the first 1000 records in the data set, extending from day 008 of 1991 to day 362 of 1991.

There is a further subsetting of the data done by the inversion program itself, in order to assure that each event has a minimum of three observations, and that each station has a minimum of ten observations. These parameters are adjustable, but we have found in the past that these minima are sufficient. After this subsetting, the final data set comprises

485 observations at five stations, corresponding to 129 earthquakes in the distance and depth ranges listed above.

3.4 Discussion

3.4.1. Regional Earthquakes

We observe attenuation values close to and slightly less than those seen in California, and much higher than those seen in previous studies of a shield area such as Norway. This is consistent with what one would expect for a tectonically active area such as Alaska. Tectonically active areas typically have relatively high heat flow compared to colder regions, making them more attenuating since many intrinsic attenuation mechanisms are thermally activated [Lay *et al.*, 1995]. A summary of our inversion inputs and results for the various M_L regressions, along with the Norwegian results of Alsaker *et al.* [1991], is presented in Table 3.1. Our values for the geometric spreading and attenuation constants in the $-\log A_0$ term show some variation from month to month and from region to region for shallow earthquakes, as shown in the later inversions, some of which is undoubtedly due to trade off between these parameters in the inversion. Experiments have also been done with changing the selection of input data, shifting the reference distance at which the Alaskan $\log A_0$ curve is anchored to the Californian curve, shifting the source depth used in the calculations, and omitting stations with consistently high magnitude corrections before

inverting. One set of spreading and attenuation parameters will probably not be sufficient for shallow seismicity in the entire state of Alaska. We conclude this due to the measured differences between regions of more than several tenths of a magnitude unit at hundreds of kilometers distance (see Table 3.1). A separate inversion suggests parameters that may be used with caution for deep events at sufficient distance (discussed below). The regional parameters will not be appropriate for volcanic events, as shown by our preliminary result for Mount Spurr Volcano, Alaska discussed below. The latter point is significant for the volcano monitoring efforts led by the Alaska Volcano Observatory.

Figure 3.1 shows the results of a local-magnitude inversion for Norway by Alsaker *et al.* (1991). Circles show the attenuation ($-\log A_0$) values vs. epicentral distance for 741 short-period recordings of 195 earthquakes at 21 Norwegian seismic stations. The solid line is the simultaneously-determined $-\log A_0$ calibration curve for an M_L scale for Norway. The dashed line shows, for comparison, the Southern Californian curve using values from Hutton and Boore (1987). The offset of over a full magnitude unit at large distances shows that attenuation in Norway, as parameterized by this simple frequency-independent relation, is much lower than in Southern California. This result in large part motivated the current study.

Figures 3.2a-e show an inversion using earthquakes in northern Alaska, all north of the Denali Fault. The maps illustrate the epicenters used in this inversion (Figure 3.2a) and the ray path coverage (Figure 3.2b) between the stations (triangles) and the 187 earthquakes (squares). Figures 3.2c-e give the results of this inversion. Figure 3.2c shows the

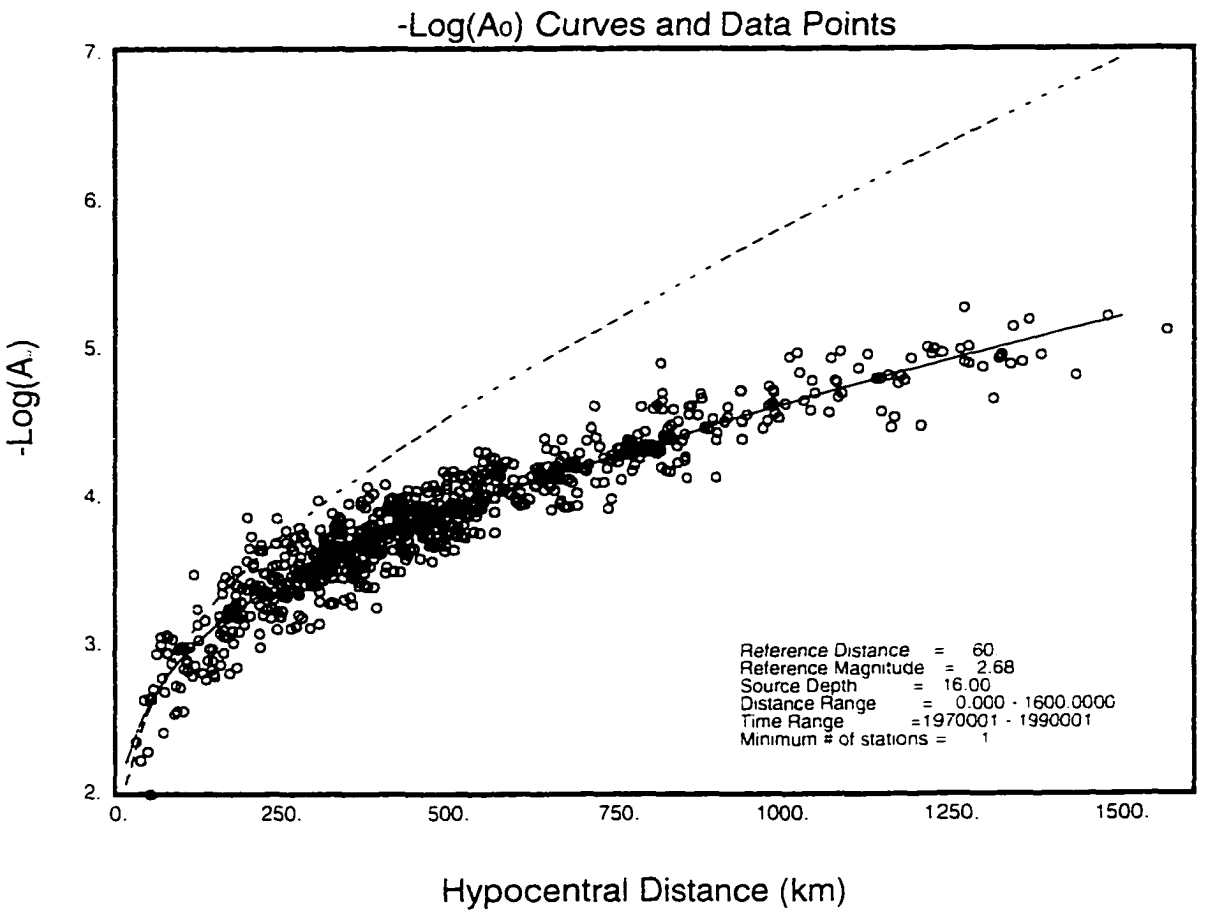

Figure 3.1

This figure shows the $LogA_0$ results for Norway, reproducing the results of Alsaker et al. [1991]. The $-LogA_0$ curve indicates the magnitude of an earthquake at a given distance that will produce 1 mm of motion on a Wood-Anderson instrument. For details, see Section 3.2 of the text. The dashed line is the original Richter-magnitude definition for California. The solid line is the regressed fit to data for Norway, as presented in Alsaker *et al.* [1991]. The difference between the two curves is one full magnitude unit at 870 km, with Norwegian attenuation being less than that of California.

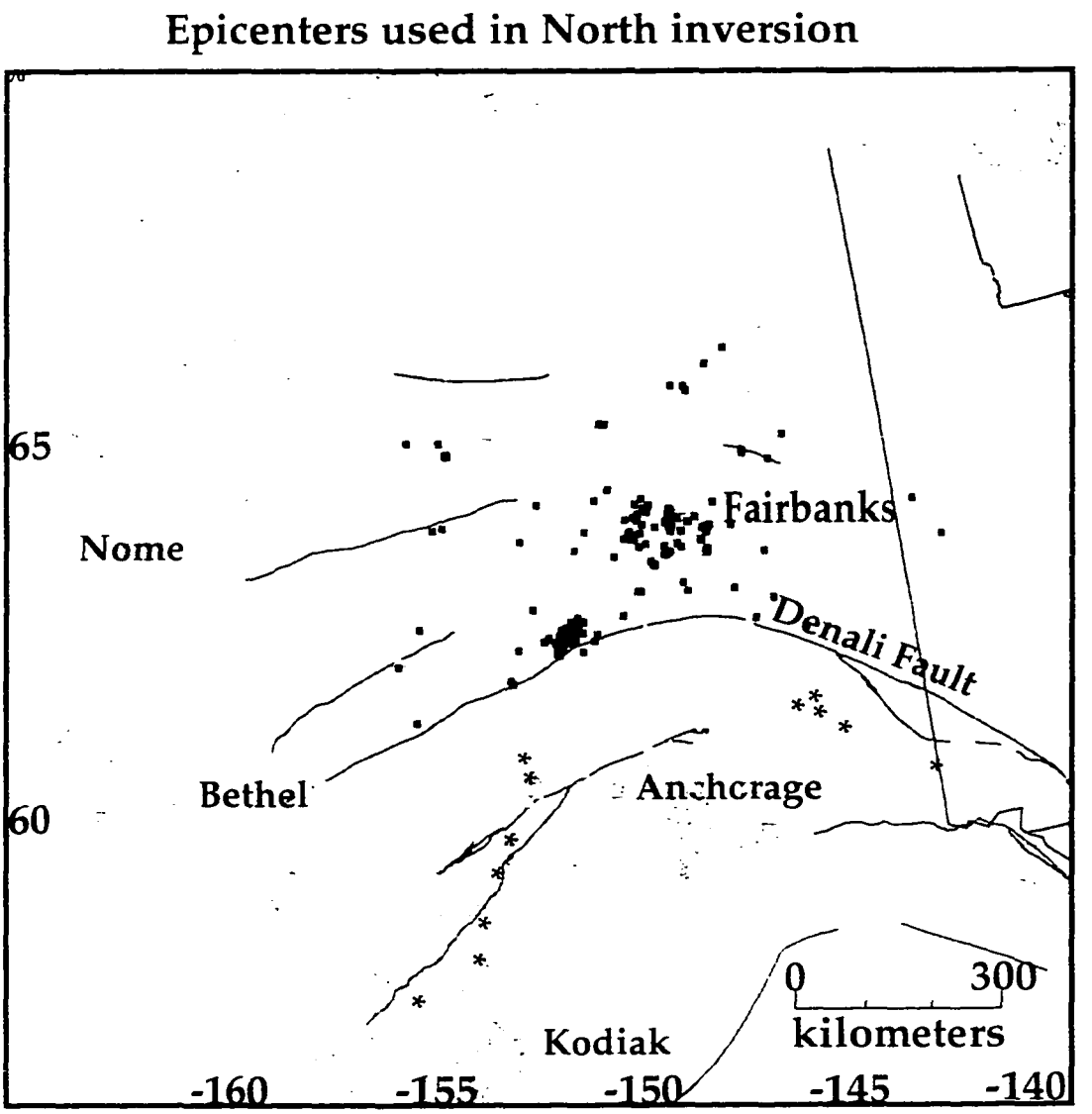

Figure 3.2 a

This map of Alaska shows epicenters used in an inversion for local magnitude for earthquakes north of the Denali Fault. Squares represent the earthquakes, and triangles show the locations of stations at which amplitude measurements were made. There are 198 earthquakes plotted and used in this inversion. Traces of the major faults are shown as solid lines.

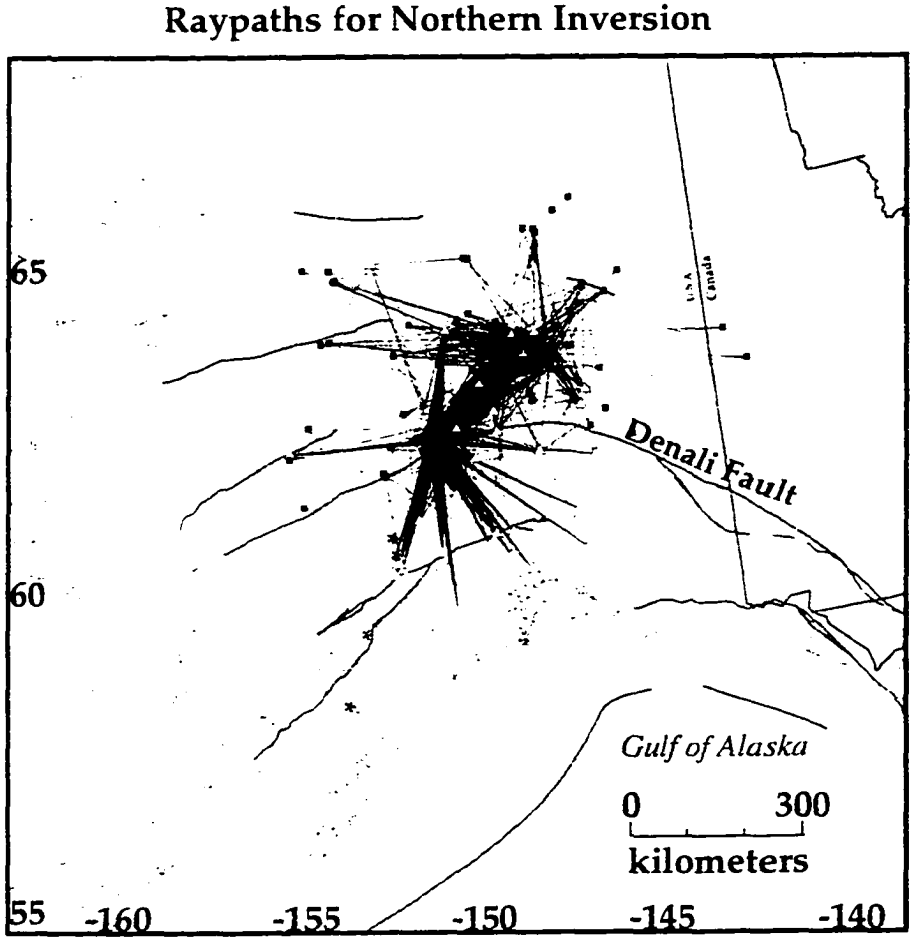

Figure 3.2 b

This map of Alaska shows the raypaths used for the inversion of data for a magnitude scale north of the Denali fault. Squares represent earthquakes, and triangles show the stations at which they were recorded. There is one station-to-event raypath line for each amplitude measurement used in the inversion. Traces of the major faults are shown as solid lines.

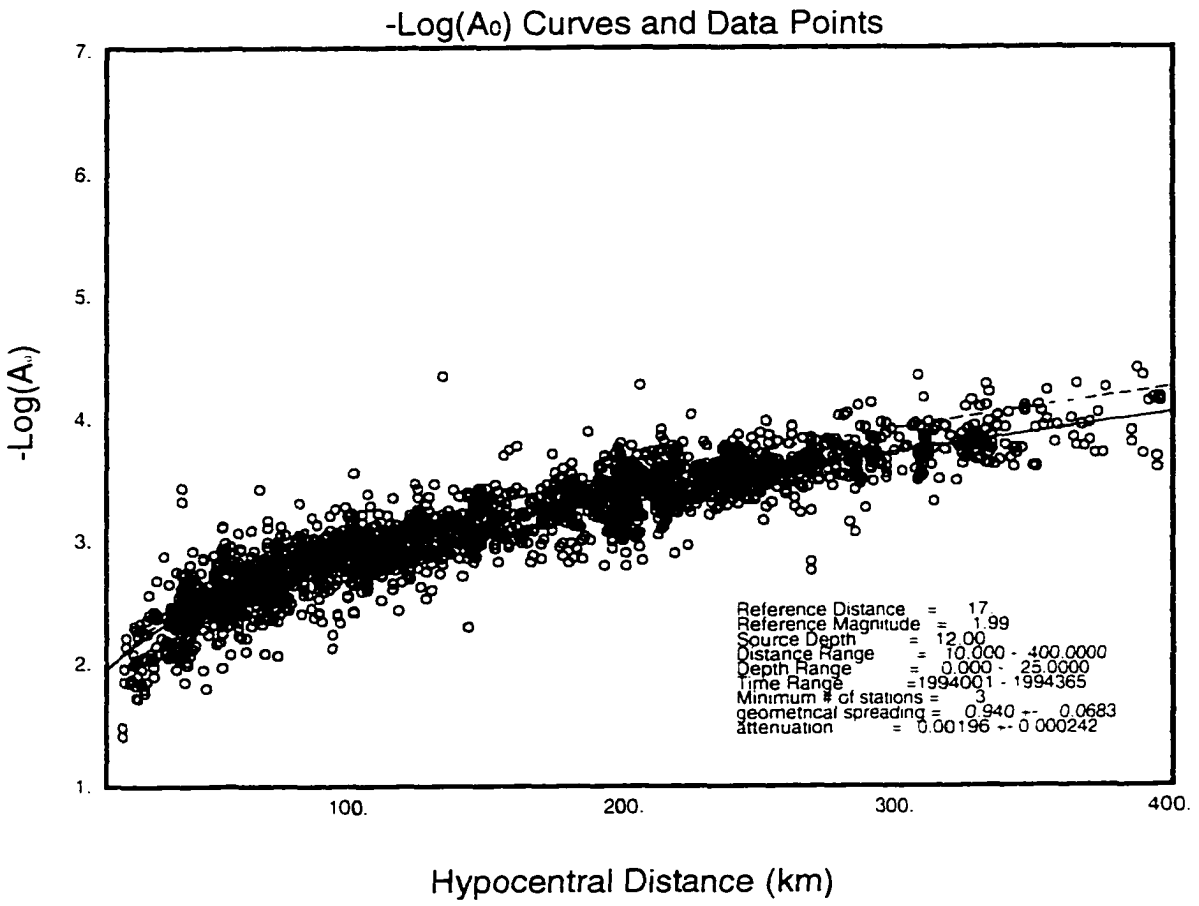

Figure 3.2 c

This figure shows the results of the M_L inversion for earthquakes north of the Denali fault. The symbols, lines, and axes are as described in the caption to Figure 3.1. For discussion, see Section 3.4 of the text.

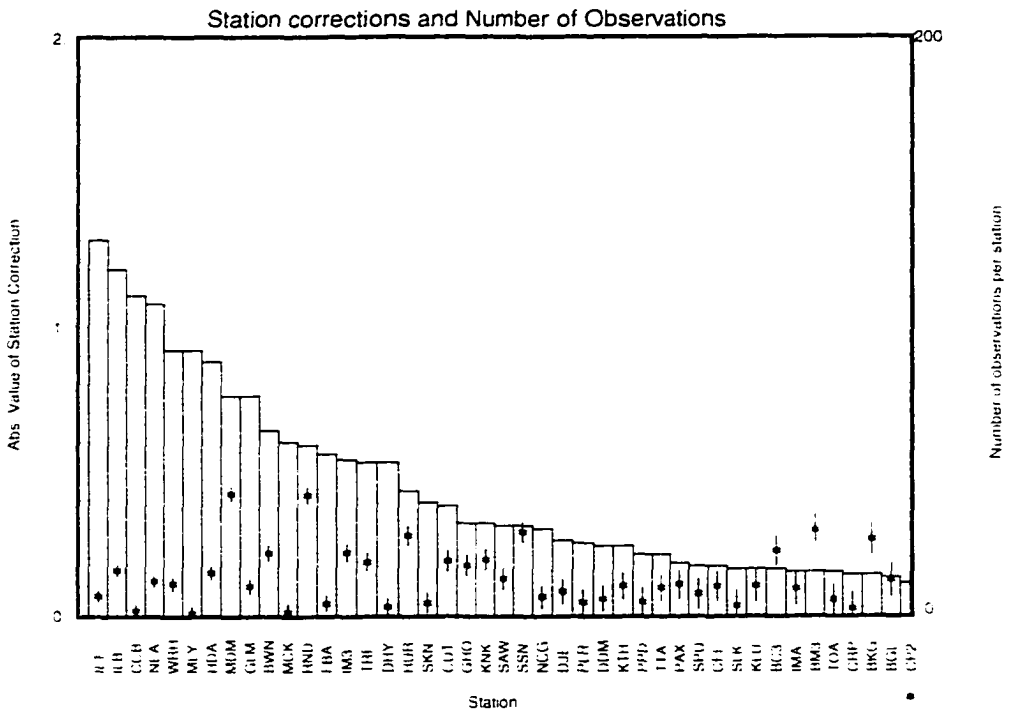

Figure 3.2 d

This figure shows the absolute values (asterisks) of station corrections obtained from the inversion for earthquakes north of the Denali fault. One-standard-deviation error bars are included with the data points. The axis on the left indicates the size of the station correction in magnitude units. The boxes, referenced to the axis on the right, show the number of amplitude measurements used at each station for this inversion. The station names are shown along the horizontal axis.

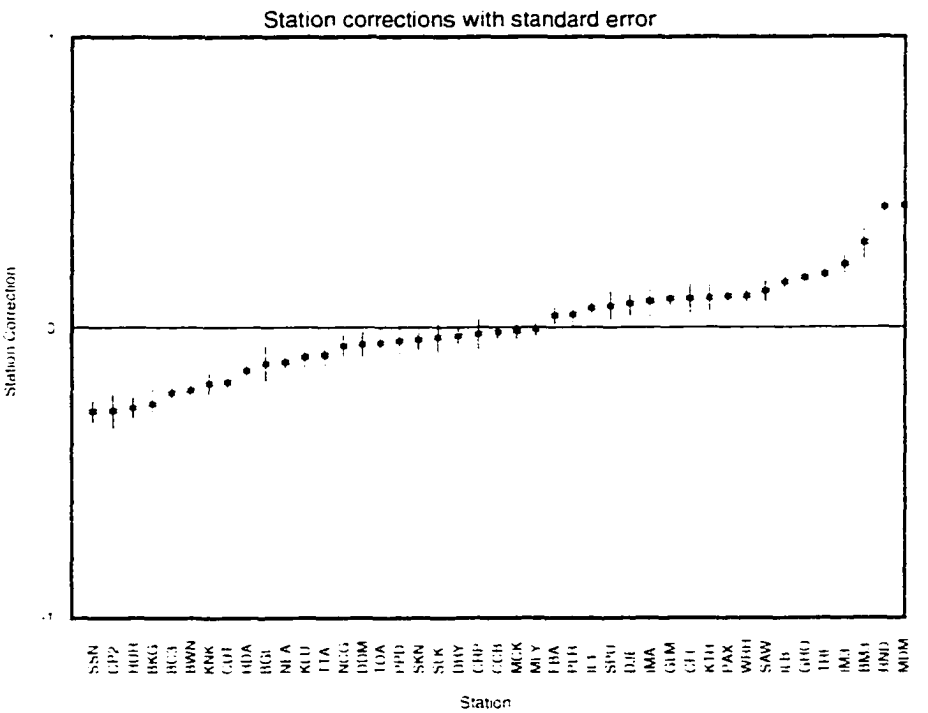

Figure 3.2 e

This figure shows the station corrections with standard error for the inversion of data from earthquakes north of the Denali fault. The vertical axis is in units of local magnitude. Station names are shown along the horizontal axis.

attenuation values ($-\log A_0$) for the 1906 ray paths. Figure 3.2d and e give magnitude corrections for each of the 43 stations used, including the number of observations per station. The solid line on Figure 3.2c is the calibration curve for local magnitude obtained from this inversion, showing an attenuation constant of 0.00191 ± 0.0002 and a geometric spreading value of 0.960 ± 0.07. The resulting magnitude difference of 0.2 magnitude units between the Alaskan (solid line) and Californian (dashed line) $-\log A_0$ curves at 400 km is slightly smaller than that seen in curves for Southern Alaska, shown below.

Figures 3.3a-e show an inversion using earthquakes from a region north of Cook Inlet, Alaska. The maps, Figures 3.3 a and b, illustrate epicenters used and ray-path coverage between the stations (triangles) and the 159 earthquakes (squares). The ray paths shown cover Anchorage. The next three plots give the results of this inversion. The first shows the attenuation values ($-\log A_0$) for the 1073 ray paths; the second and third show magnitude corrections for each of the 31 stations used. The solid line on Figure 3.3c is the calibration curve for local magnitude obtained from this inversion, showing an attenuation constant of 0.00081 ± 0.0007 and a geometric spreading constant of 1.14 ± 0.13. Comparison with the plot for the entire state, shown below, suggests that a trade-off has occurred here in the inversion between the geometric spreading factor and the attenuation constant, although the end result is similar: there is a magnitude difference of about 0.4 magnitude units between the inversion result (solid line) and the Californian curve (dashed line) at 400 km distance. A separate inversion (not shown) with the geometric spreading constant fixed at the theoretically expected value of 1.0 confirms this. The results of this inversion are also

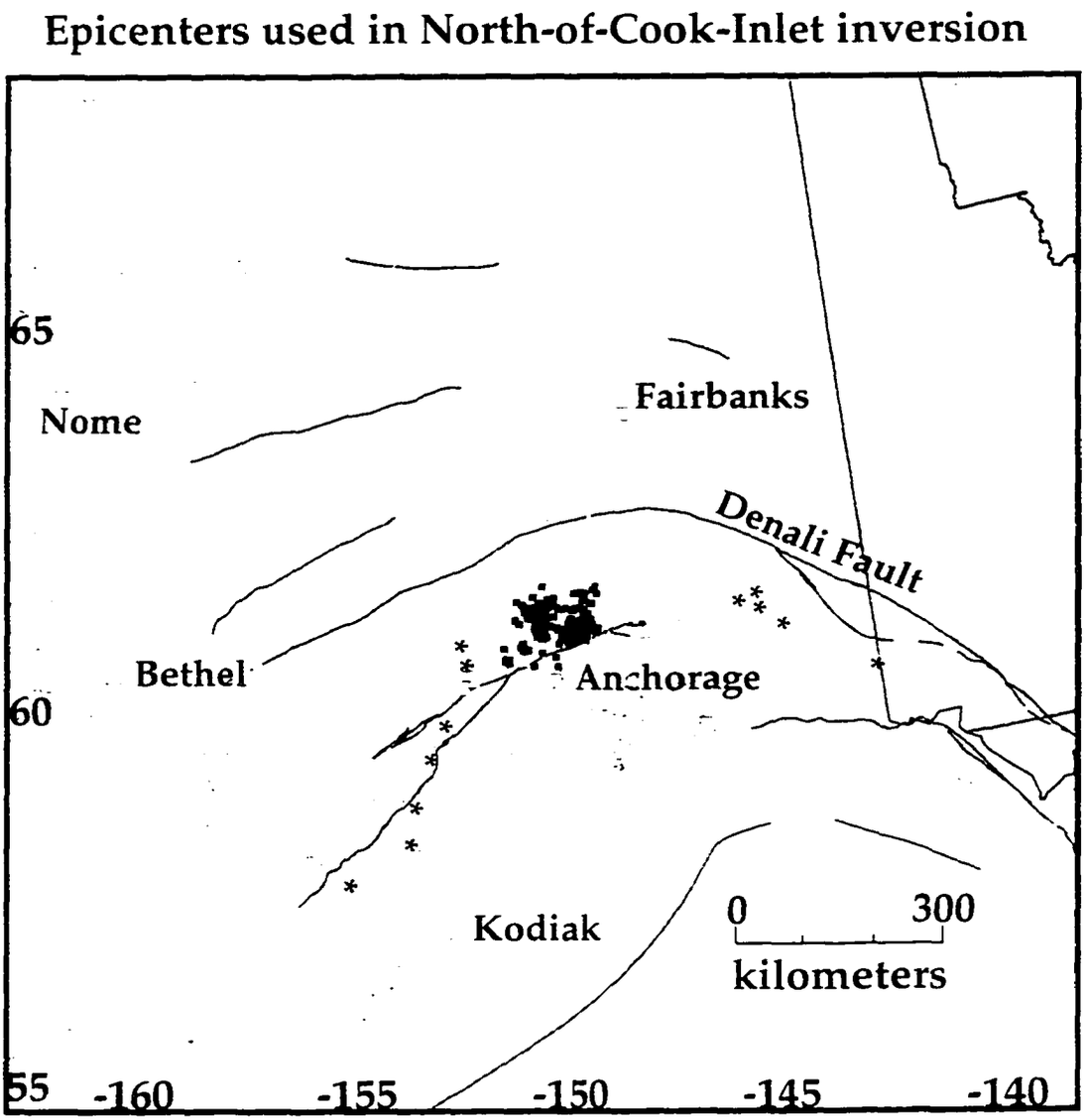

Figure 3.3 a

This map of Alaska shows epicenters used in an inversion for local magnitude for earthquakes north of Cook Inlet. Squares represent the earthquakes, and triangles show the locations of stations at which amplitude measurements were made. There are 163 earthquakes plotted and used in this inversion. Traces of the major faults are shown as solid lines.

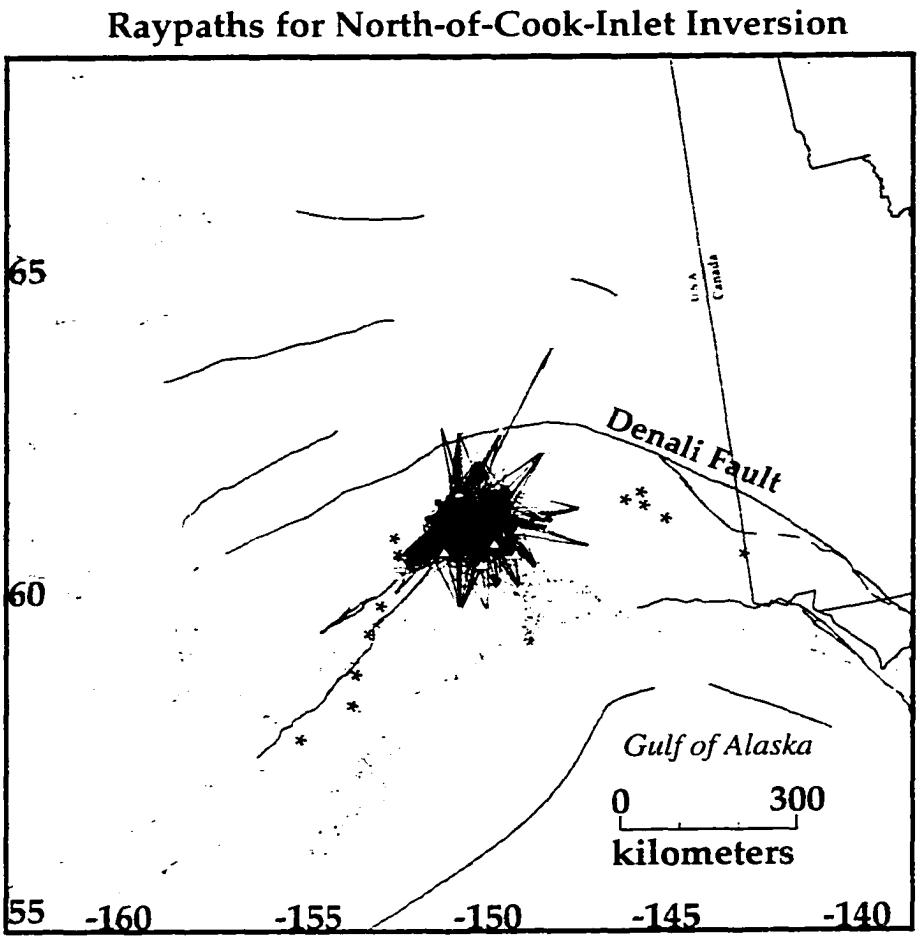

Figure 3.3 b

This map of Alaska shows the raypaths used for the inversion of data for a magnitude scale north of Cook Inlet. Squares represent earthquakes, and triangles show the stations at which they were recorded. There is one station-to-event raypath line for each amplitude measurement used in the inversion. Traces of the major faults are shown as solid lines.

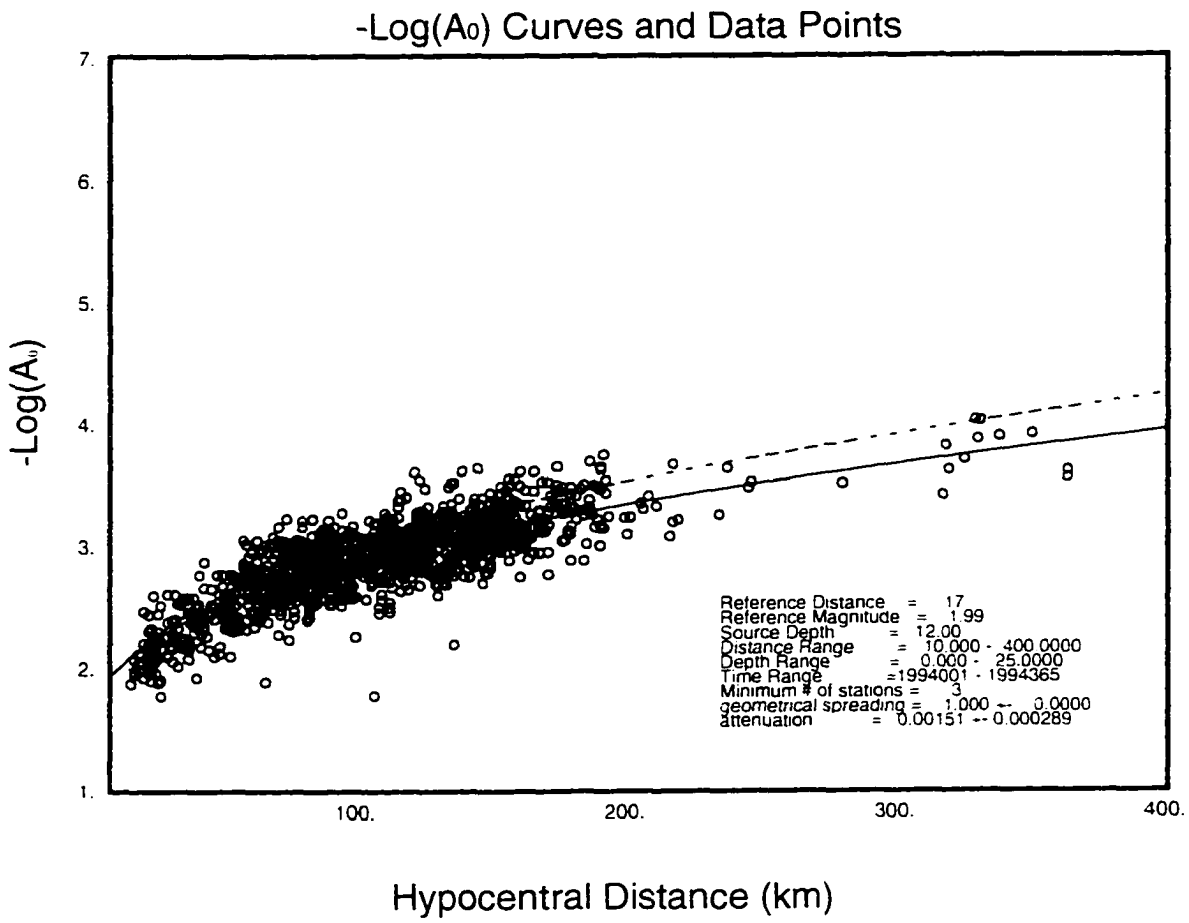

Figure 3.3 c

This figure shows the results of the M_L inversion for earthquakes north of Cook Inlet. The symbols, lines, and axes are as described in the caption to Figure 3.1. For discussion, see Section 3.4 of the text.

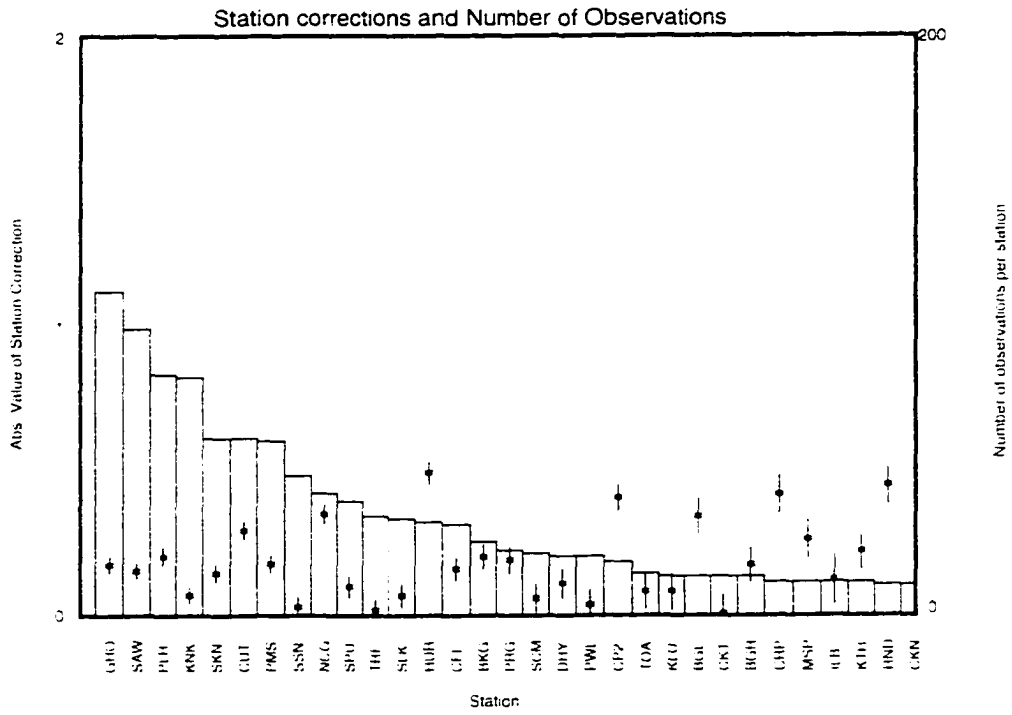

Figure 3.3 d

This figure shows the absolute values (asterisks) of station corrections obtained from the inversion for earthquakes north of Cook Inlet. One-standard-deviation error bars are included with the data points. The axis on the left indicates the size of the station correction in magnitude units. The boxes, referenced to the axis on the right, show the number of amplitude measurements used at each station for this inversion. The station names are shown along the horizontal axis.

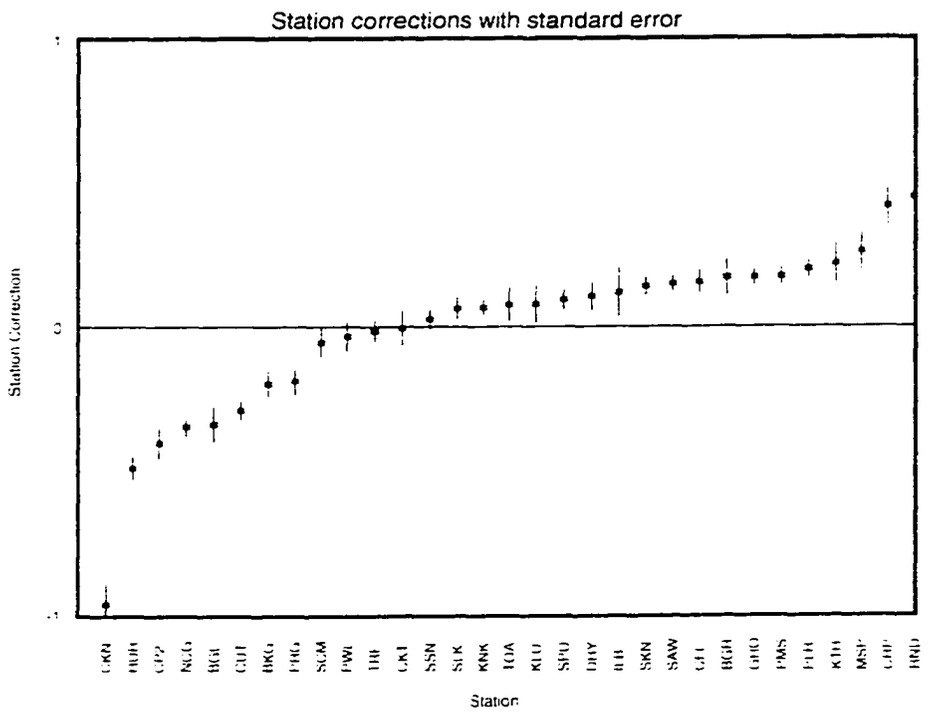

Figure 3.3 e

This figure shows the station corrections with standard error for the inversion of data from earthquakes north of Cook Inlet. The vertical axis is in units of local magnitude. Station names are shown along the horizontal axis.

consistent with those for the larger, South-Central Alaskan region which includes this region, shown below.

In the next set of figures, 3.4a-e, we show an inversion using earthquakes in South-Central Alaska, all south of the Denali Fault. The maps in Figures 3.4a and b illustrate the epicenters used and the ray path coverage between the stations (triangles) and the 237 earthquakes (squares). The next three plots give the results of this inversion. First are the attenuation values ($-\log A_0$) for the 1861 ray paths. The magnitude corrections follow in Figures 3.4 d ad e for each of the 45 stations used. The solid line on Figure 3.4c is the calibration curve for local magnitude obtained from this inversion, showing a rather low attenuation constant of 0.00045 ± 0.0003, compensated by a slightly high geometric spreading value of 1.21 ± 0.07. As with the inversion for the region North of Cook Inlet, the magnitude differences between South-Central Alaska and Central California (dashed line) are still approximately 0.4 magnitude units at 400 km.

Figures 3.5a-e show an inversion for Alaskan catalog data for the entire state for the month of April, 1994. The maps illustrate the epicenters and the ray-path coverage between the stations (triangles) and the 155 earthquakes (squares) used in this inversion. Figures 3.5c through e show the results of this inversion. Figure 3.5c shows the attenuation values ($-\log A_0$) for the 1248 ray paths. Figures 3.5d and e are the magnitude corrections for each of the 48 stations used. The solid line on Figure 3.5c is the calibration curve for local magnitude obtained from the April 1994 data, showing a characteristic attenuation constant of 0.0011 ± 0.0002 and a geometric spreading constant of 1.11 ± 0.07. Comparison

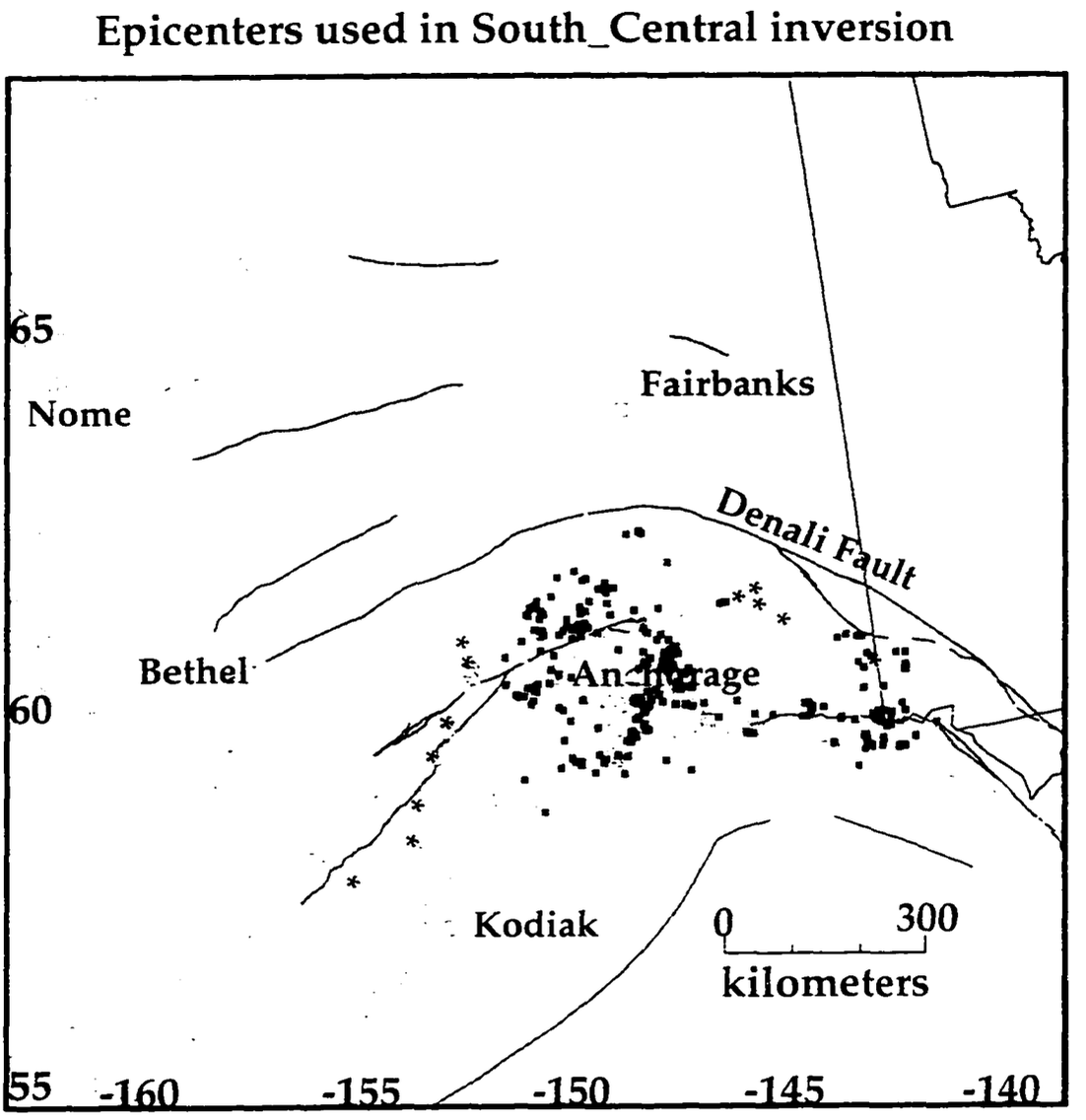

Figure 3.4 a

This map of Alaska shows epicenters used in an inversion for local magnitude for earthquakes south of the Denali Fault. Squares represent the earthquakes, and triangles show the locations of stations at which amplitude measurements were made. There are 255 earthquakes plotted and used in this inversion. Traces of the major faults are shown as solid lines.

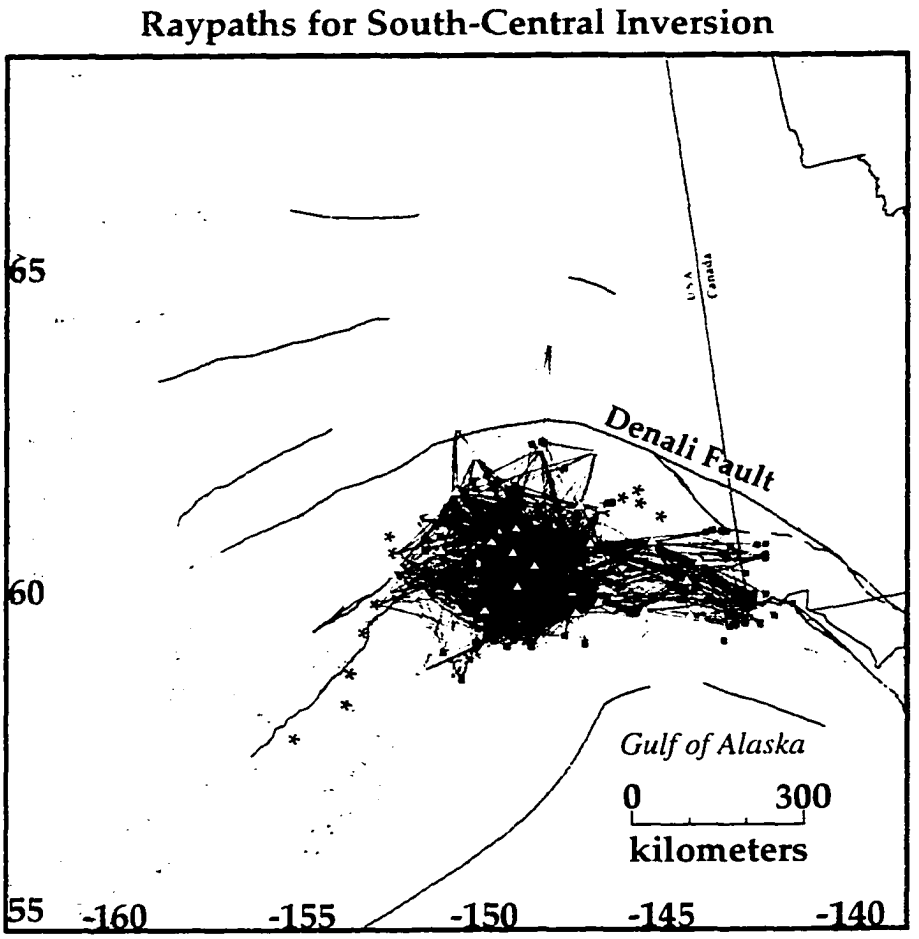

Figure 3.4 b

This map of Alaska shows the raypaths used for the inversion of data for a magnitude scale south of the Denali fault. Squares represent earthquakes, and triangles show the stations at which they were recorded. There is one station-to-event raypath line for each amplitude measurement used in the inversion. Traces of the major faults are shown as solid lines.

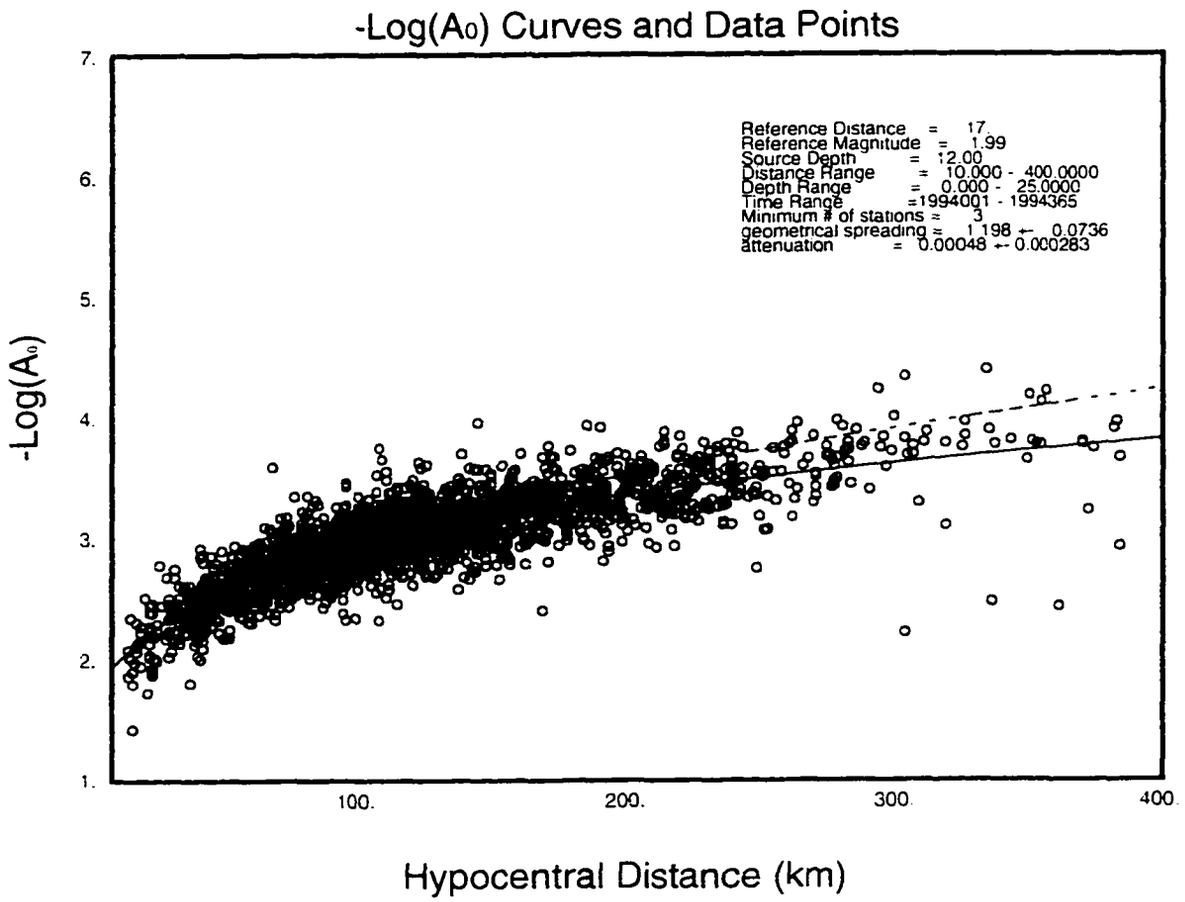

Figure 3.4 c

This figure shows the results of the M_L inversion for earthquakes south of the Denali fault. The symbols, lines, and axes are as described in the caption to Figure 3.1. For discussion, see Section 3.4 of the text.

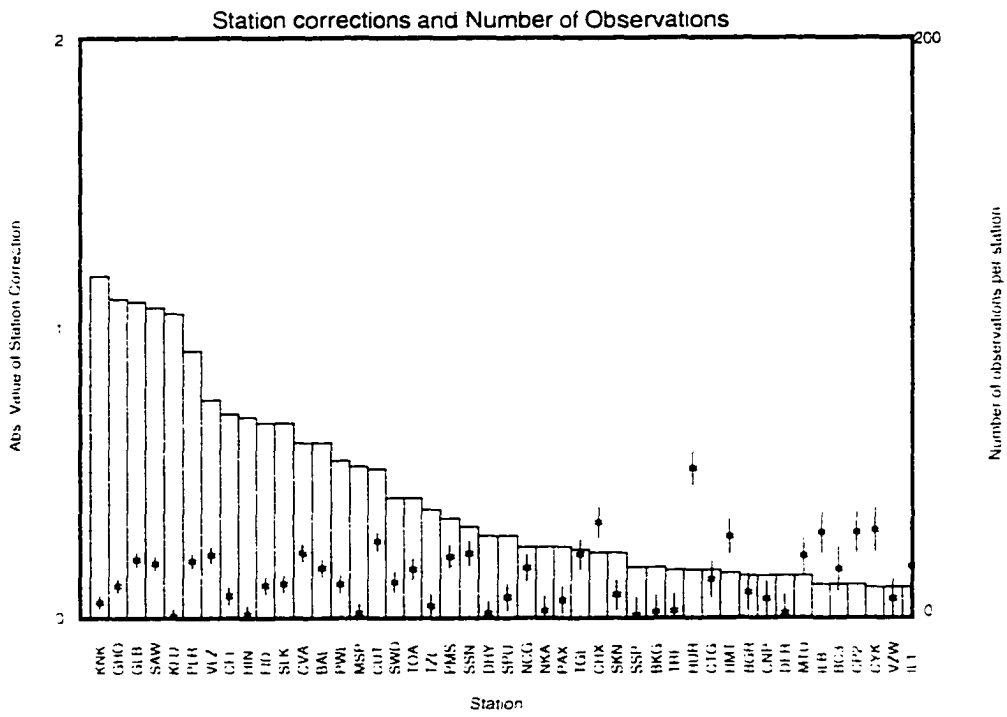

Figure 3.4 d

This figure shows the absolute values (asterisks) of station corrections obtained from the inversion for earthquakes south of the Denali fault. One-standard-deviation error bars are included with the data points. The axis on the left indicates the size of the station correction in magnitude units. The boxes, referenced to the axis on the right, show the number of amplitude measurements used at each station for this inversion. The station names are shown along the horizontal axis.

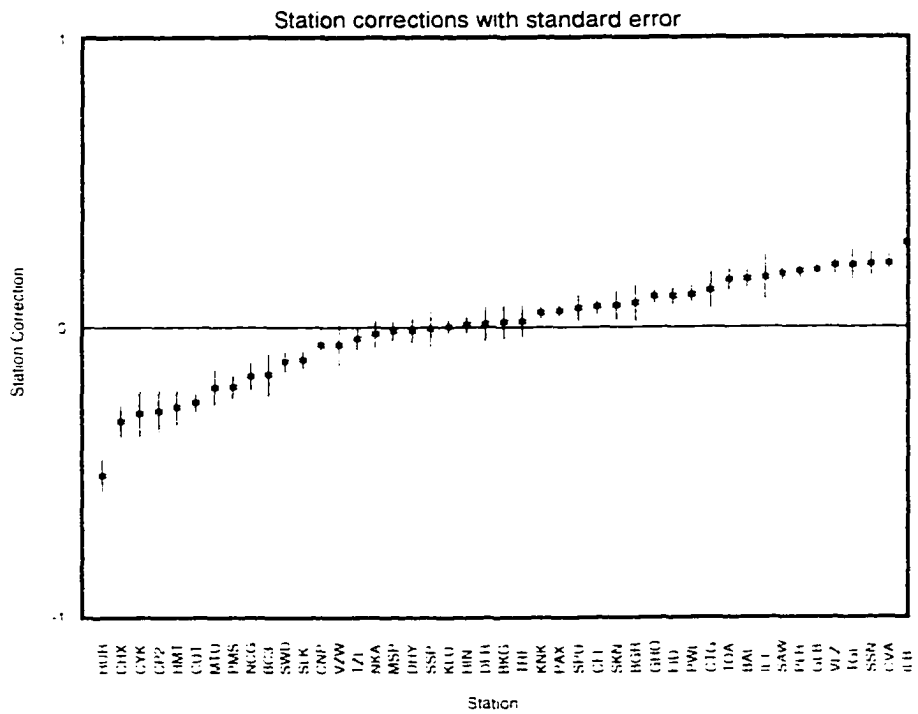

Figure 3.4 e

This figure shows the station corrections with standard error for the inversion of data from earthquakes south of the Denali fault. The vertical axis is in units of local magnitude. Station names are shown along the horizontal axis.

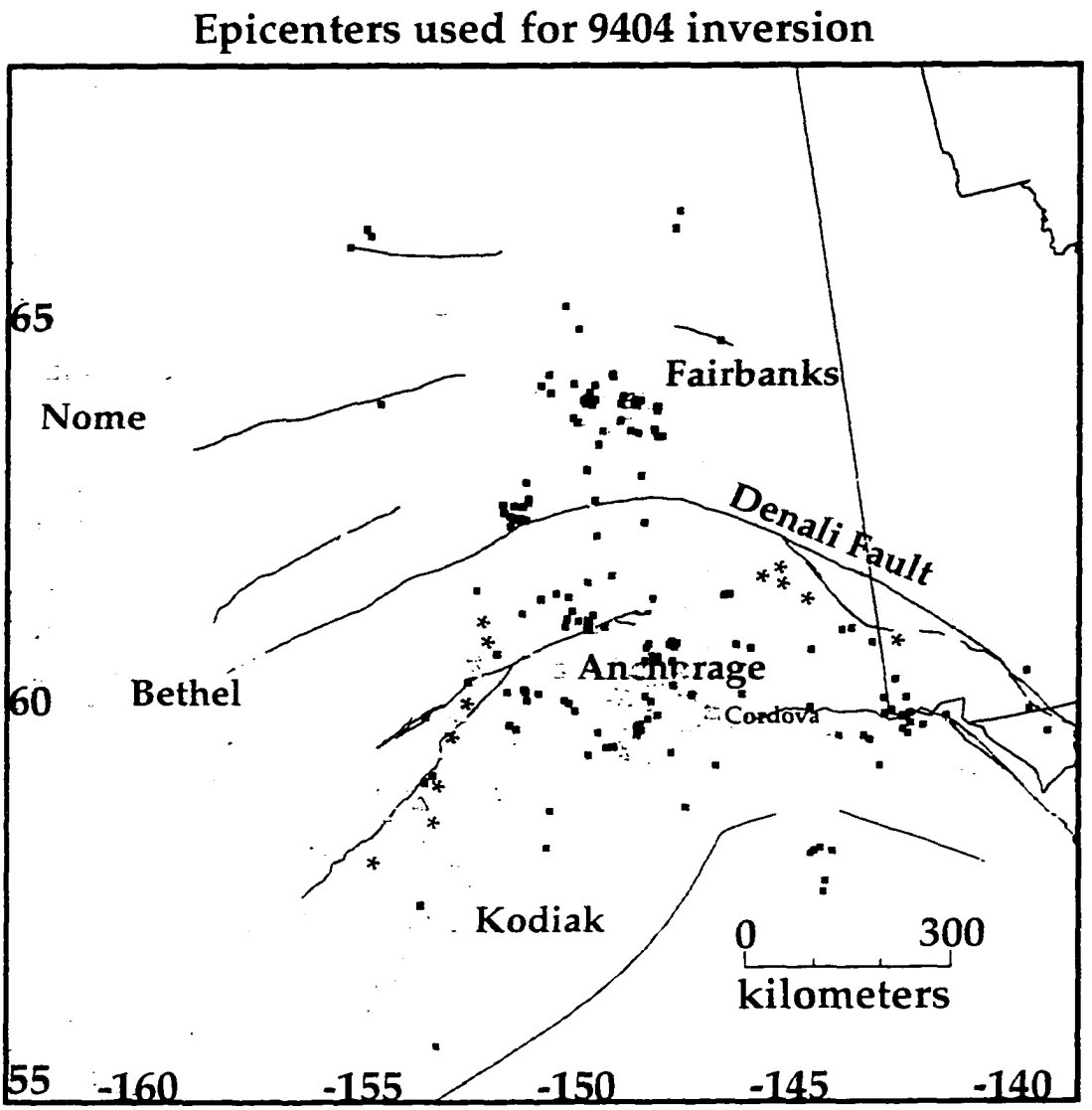

Figure 3.5 a

This map of Alaska shows epicenters used in an inversion for local magnitude for earthquakes recorded by the AEIC in April of 1994. Squares represent the earthquakes, and triangles show the locations of stations at which amplitude measurements were made. There are 177 earthquakes plotted and used in this inversion. Traces of the major faults are shown as solid lines.

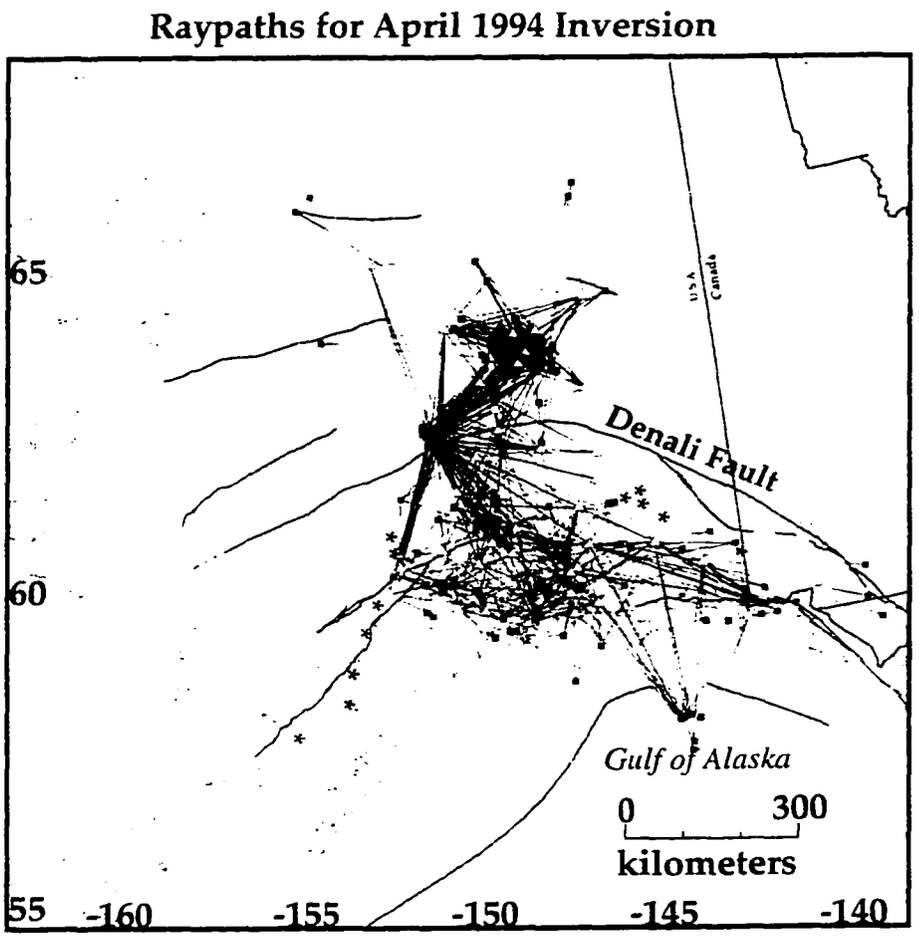

Figure 3.5 b

This map of Alaska shows the raypaths used for the inversion of data for a magnitude scale from April, 1994 earthquakes. Squares represent earthquakes, and triangles show the stations at which they were recorded. There is one station-to-event raypath line for each amplitude measurement used in the inversion. Traces of the major faults are shown as solid lines.

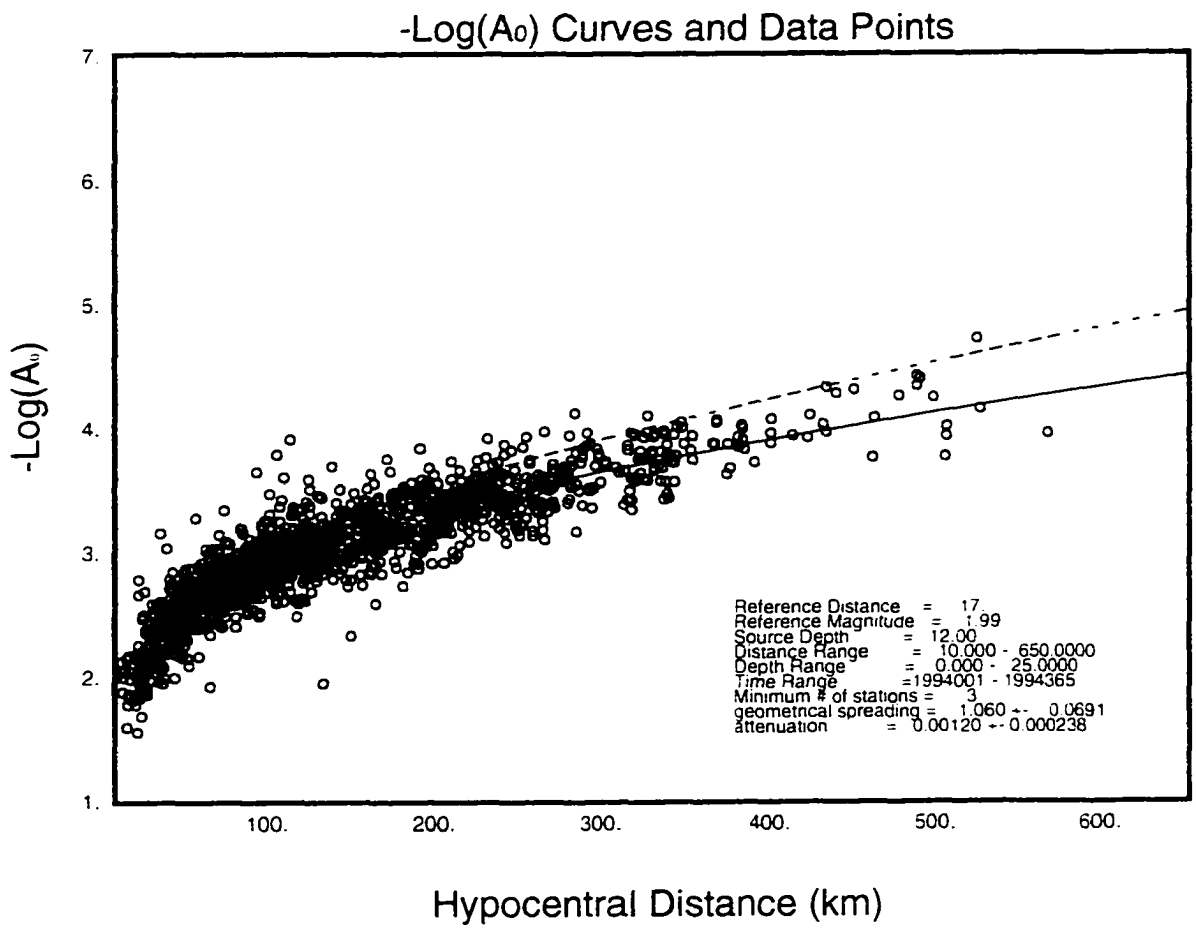

Figure 3.5 c

This figure shows the results of the M_L inversion for earthquakes in April of 1994. The symbols, lines, and axes are as described in the caption to Figure 3.1. For discussion, see Section 3.4 of the text.

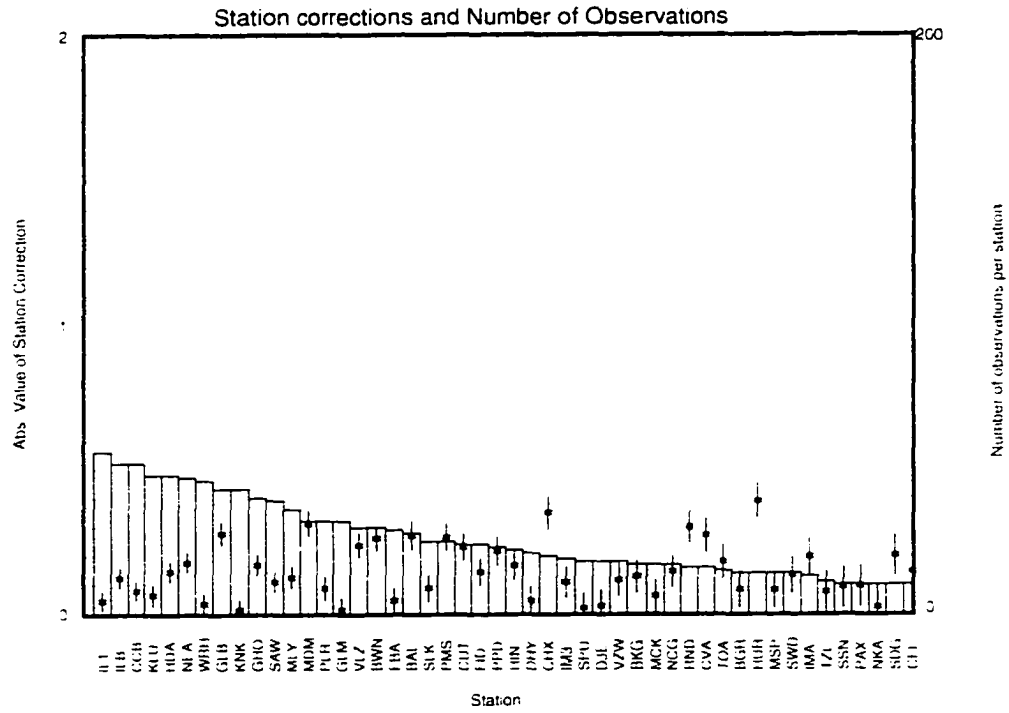

Figure 3.5 d

This figure shows the absolute values (asterisks) of station corrections obtained from the inversion for April, 1994 earthquakes. One-standard-deviation error bars are included with the data points. The axis on the left indicates the size of the station correction in magnitude units. The boxes, referenced to the axis on the right, show the number of amplitude measurements used at each station for this inversion. The station names are shown along the horizontal axis.

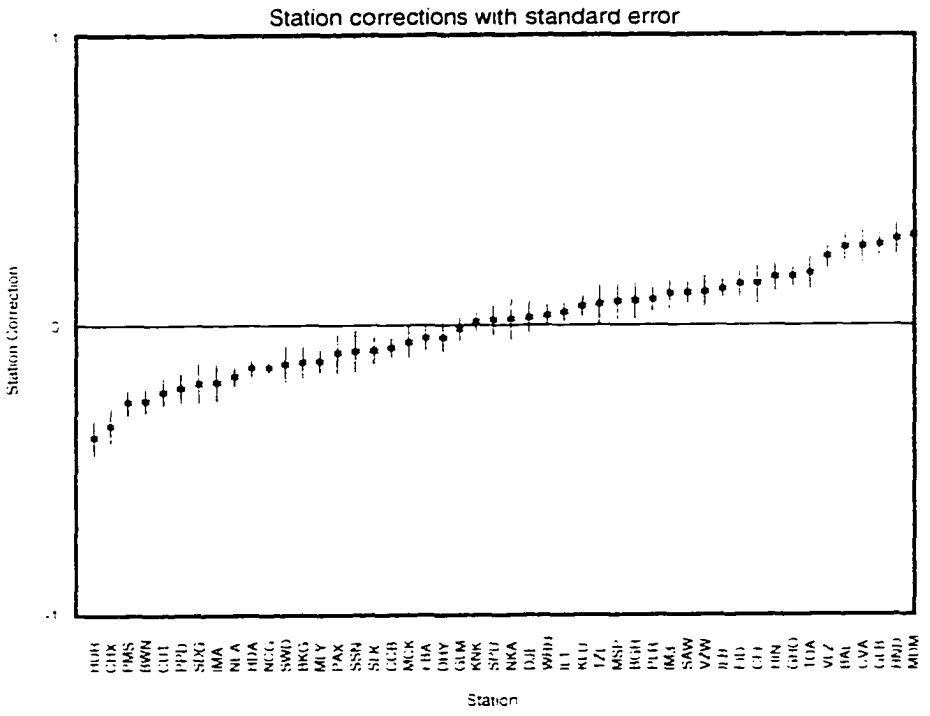

Figure 3.5 e

This figure shows the station corrections with standard error for the inversion of data from April, 1994 earthquakes. The vertical axis is in units of local magnitude. Station names are shown along the horizontal axis.

with the Californian curve (dashed line) shows a magnitude difference of between 0.5 and 0.6 magnitude units at a distance of 650 km. Use of the California curve for Alaskan earthquakes would result in an overestimate of earthquake magnitude by this amount. Inversions for other months of data have shown similar results, with some variation in the attenuation and spreading constants due to the trade-off between the two in the inversion.

Next we show the results of an inversion with deep earthquakes. 158 events were selected with depths between 30 and 100 km, providing 1854 raypaths covering primarily the region near the slab subducting under continental Alaska. Note that these events are concentrated in and around the subducting slab of the Pacific plate. With the geometric spreading value fixed at 1.0 (necessary to get reasonable convergence for this inversion), the attenuation constant obtained is 0.00136, comparable to the values obtained for shallow events shown in the regionalized inversions in this study. Figures 3.6a-e show the results. The solid line is the $-\log A_0$ curve corresponding to the attenuation and spreading coefficients obtained in this inversion. The dashed line is the Californian curve. At 650 km distance the curves differ by 0.6 magnitude units, comparable to the result from the shallow-depth inversions. The curves have been calculated assuming a source depth of 67 km, the average depth of the events used. Note how this has changed the shape of the curve for short epicentral distances compared to the shallow-earthquake curves.

Finally, for the regional earthquake studies, we show a summary of our inversions for shallow earthquakes using 1994 data. Each curve in Figure 3.7 shows a local-magnitude calibration line, $-\log A_0$, for one month of data. The green, dot-dashed lines were

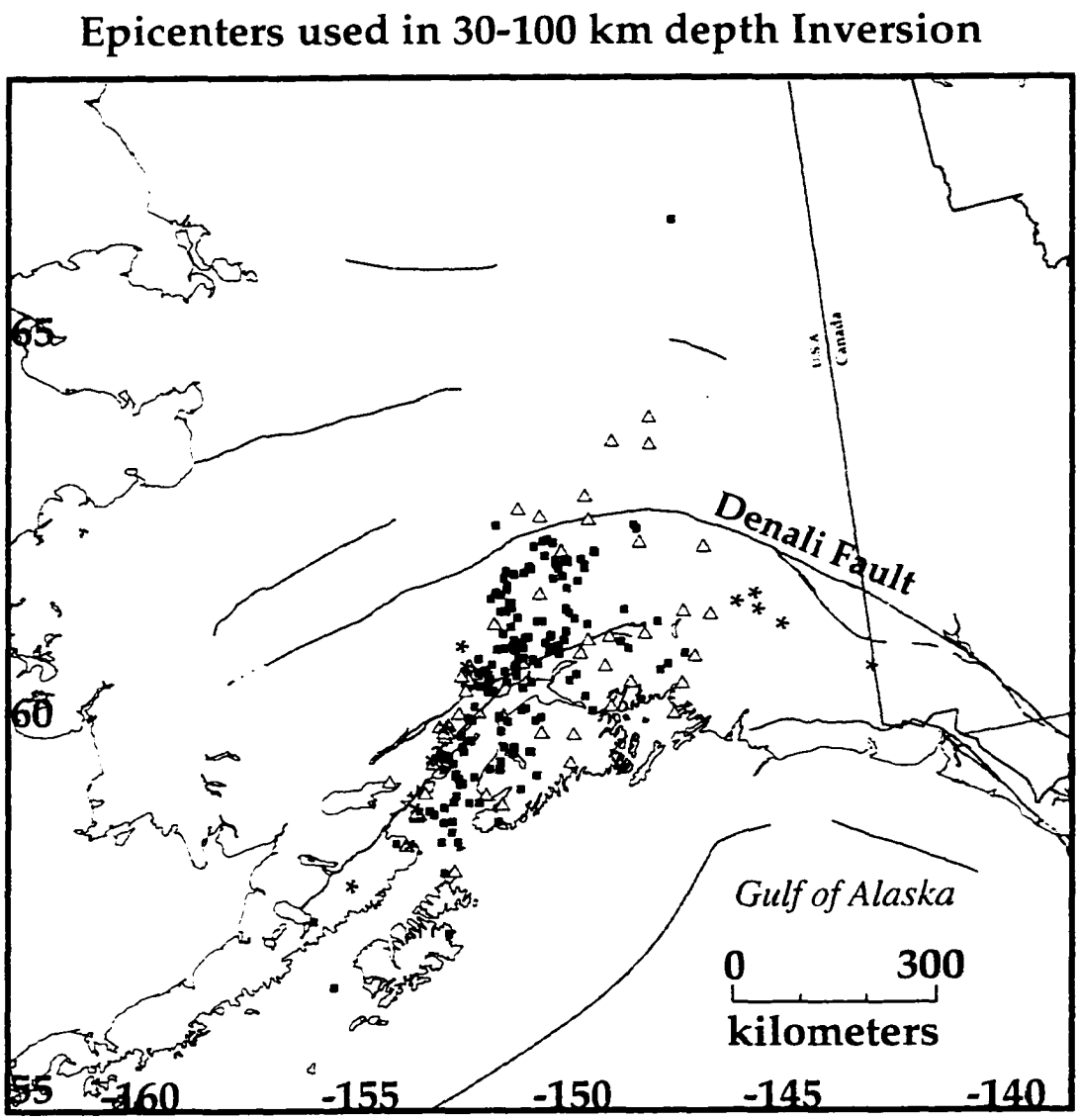

Figure 3.6 a

This map of Alaska shows epicenters used in an inversion for local magnitude for subduction-zone earthquakes between 30 and 100 km depth. Squares represent the earthquakes, and triangles show the locations of stations at which amplitude measurements were made. There are 158 earthquakes plotted and used in this inversion. Traces of the major faults are shown as solid lines.

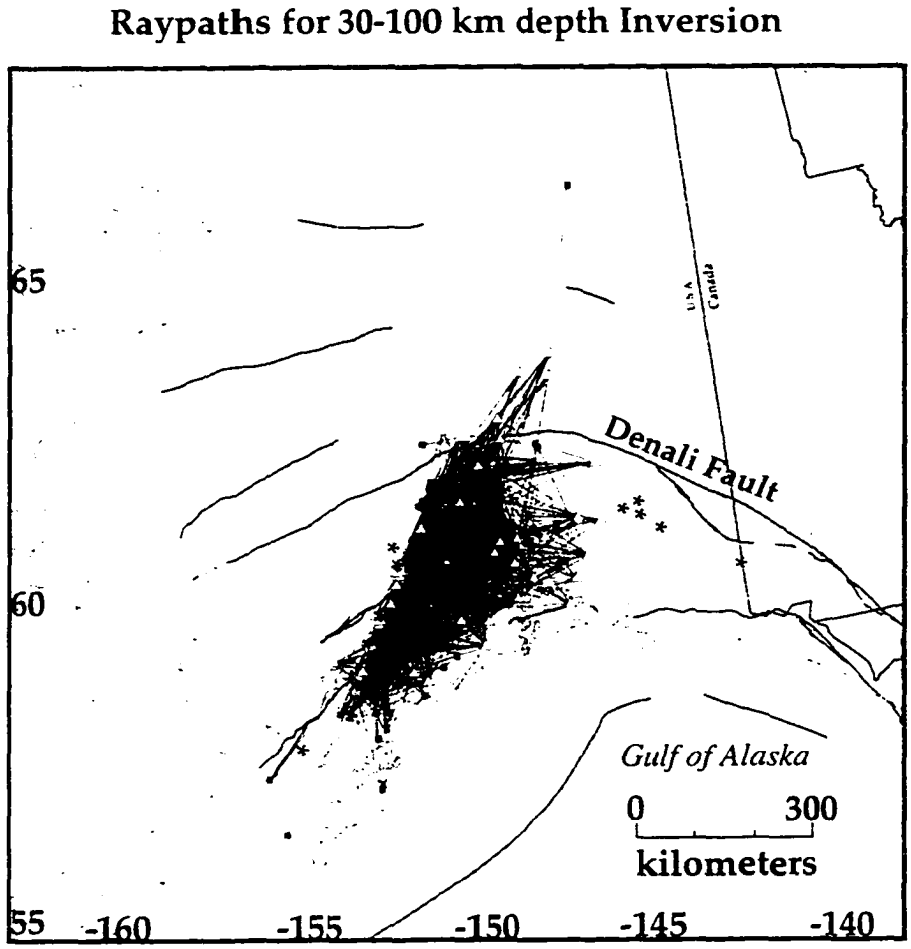

Figure 3.6 b

This map of Alaska shows the raypaths used for the inversion of data for a magnitude scale from subduction-zone events. Squares represent earthquakes, and triangles show the stations at which they were recorded. There is one station-to-event raypath line for each amplitude measurement used in the inversion. Traces of the major faults are shown as solid lines.

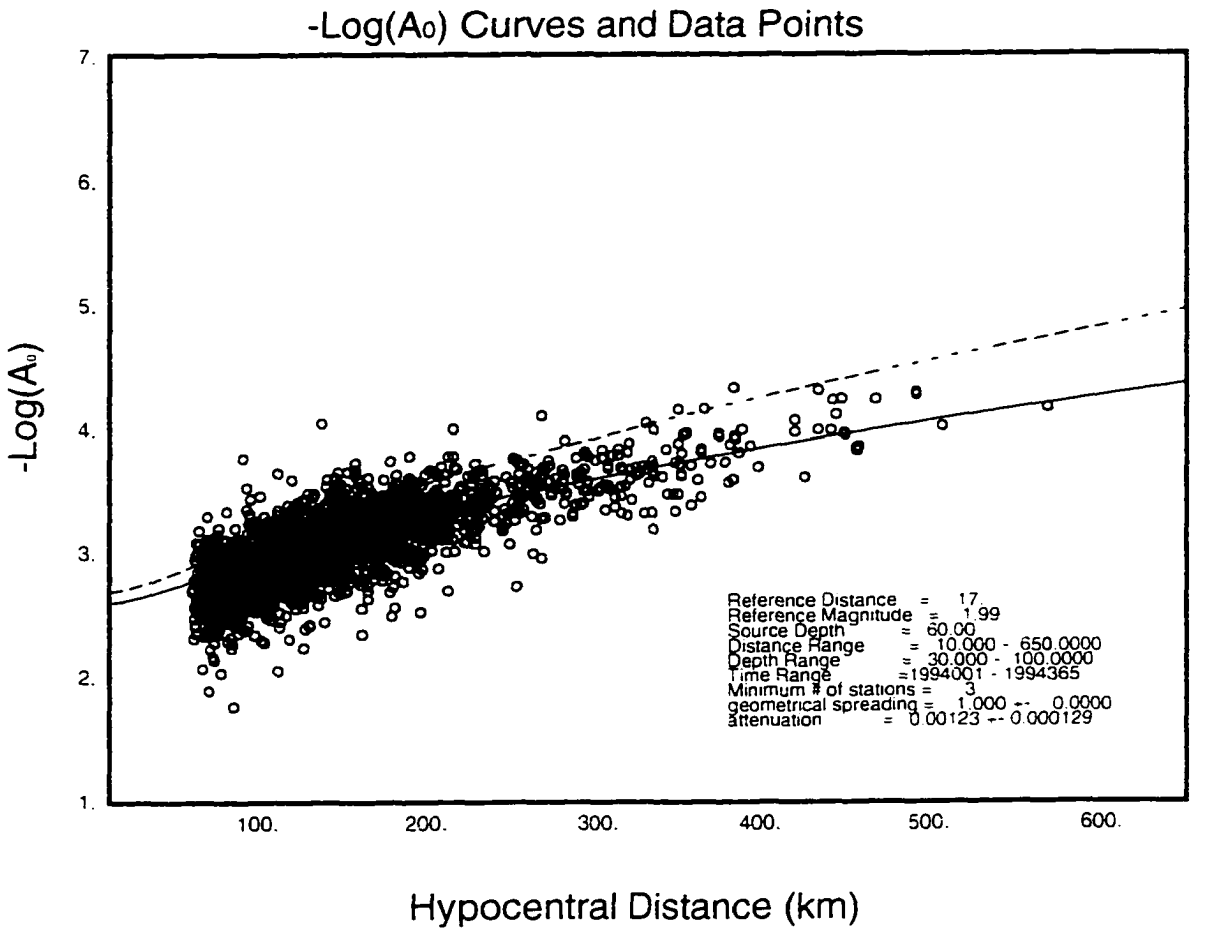

Figure 3.6 c

This figure shows the results of the M_L inversion for earthquakes between 30 and 100 km depth. The symbols, lines, and axes are as described in the caption to Figure 3.1. For discussion, see Section 3.4 of the text.

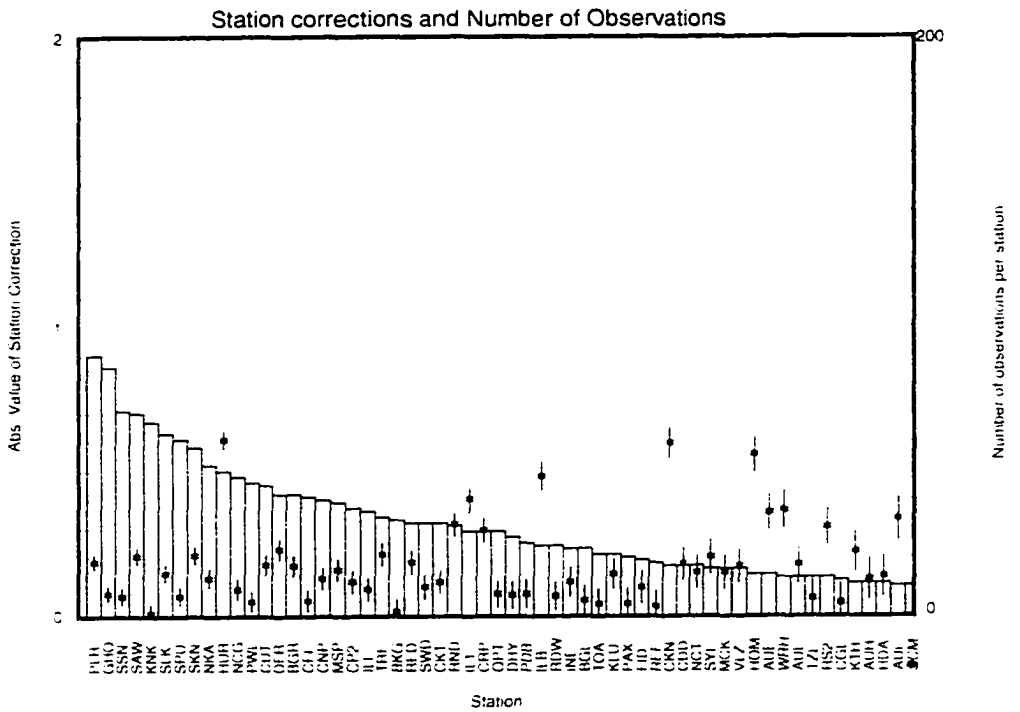

Figure 3.6 d

This figure shows the absolute values (asterisks) of station corrections obtained from the inversion for subduction-zone earthquakes. One-standard-deviation error bars are included with the data points. The axis on the left indicates the size of the station correction in magnitude units. The boxes, referenced to the axis on the right, show the number of amplitude measurements used at each station for this inversion. The station names are shown along the horizontal axis.

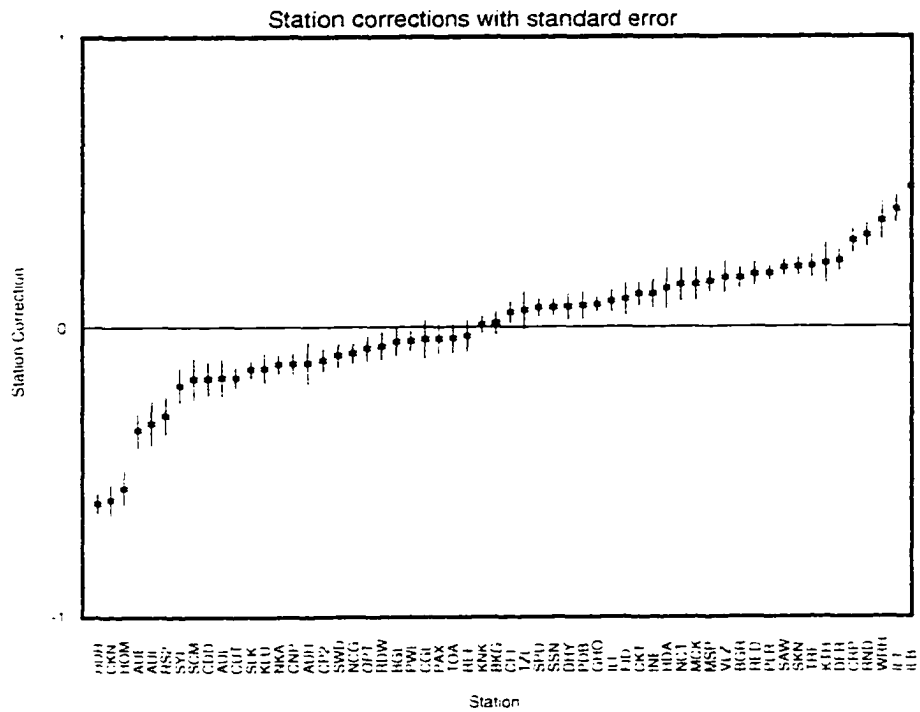

Figure 3.6 e

This figure shows the station corrections with standard error for the inversion of data from subduction-zone earthquakes. The vertical axis is in units of local magnitude. Station names are shown along the horizontal axis.

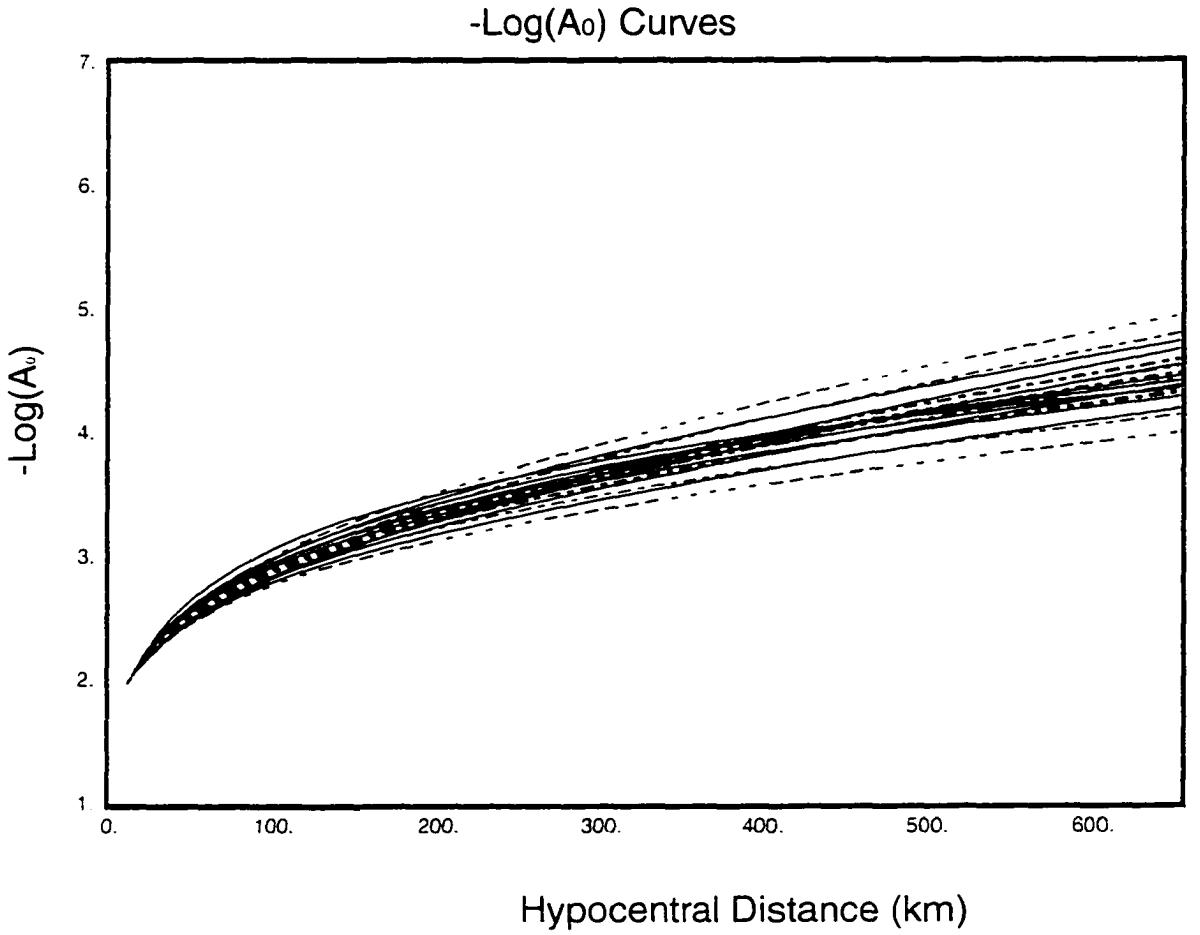

Figure 3.7

This figure shows a summary of inversion results for all shallow 1994 earthquakes. Each curve shows a $-\log A_0$ curve for one month of data. The green, dot-dashed curves were computed with the geometric spreading constant fixed at 1.0. The blue, solid curves were computed with all coefficients constrained only by the data. The red, dashed curve above all the others is the original result for California. The black, dashed curve below all the other curves is Alsaker *et al.*'s [1991] result for Norway.

run with the geometric spreading constant fixed at 1.0, and the blue, solid lines were run with both the geometric spreading and the attenuation constants free. The dashed, red line above all of our curves shows the $-\log A_0$ curve for Southern California, calculated with the parameters given by Hutton and Boore (1987) . The dashed, black line below all of our curves shows the attenuation obtained in a previous study by Alsaker et al. (1991) for the Norwegian shield. All of the curves have been computed assuming a source depth of 12 km. From this figure we conclude that even accounting for some variations in our inversion results, the measures of attenuation used in this study yield values in Alaska in between the values for Southern California and Norway.

Our preliminary inversions for a local magnitude scale for Alaska indicate attenuation properties similar to those in California, justifying the use of a slight modification of the Richter magnitude scale for shallow events.

3.4.2 Mt. Spurr Volcano Earthquakes

Figures 3.8a-c show our preliminary results for an Alaskan volcano. The solid line in Figure 3.8a shows the local-magnitude calibration curve we obtained for events near Mt. Spurr volcano, Alaska. The small circles are the $-\log A_0$ values obtained for the 129 earthquakes in this inversion. The solid line is the regressed fit to the data. The 485 amplitude measurements for this inversion were made at five seismic stations on the volcano. We required the corresponding hypocenters to be within 25 km of the station and shallower than 20 km. The earthquake magnitudes in this inversion ranged from -0.2 to 1.2. The

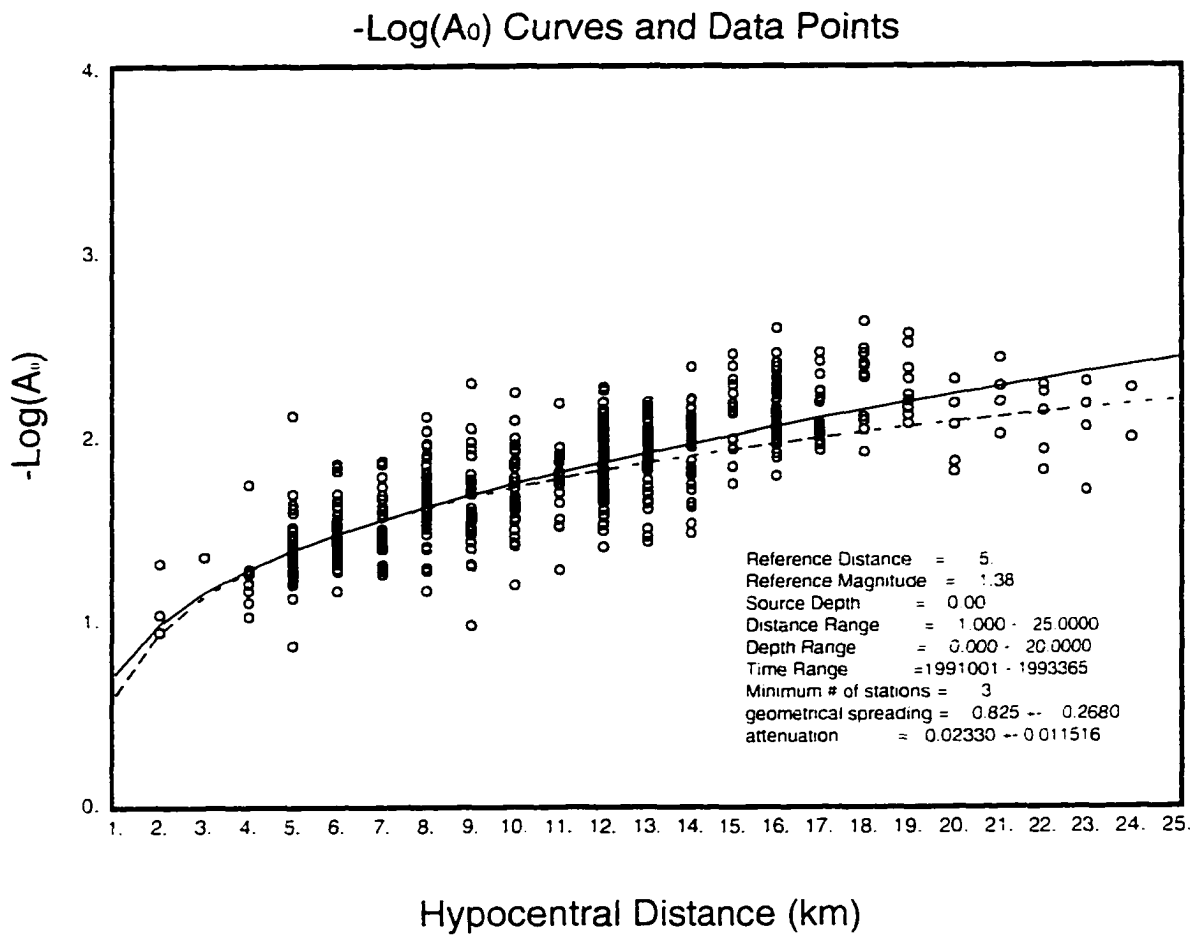

Figure 3.8 a

This figure shows the results of the M_L inversion for earthquakes at Mount Spurr volcano, Alaska. The symbols, lines, and axes are as described in the caption to Figure 3.1. For discussion, see Section 3.4.2 of the text.

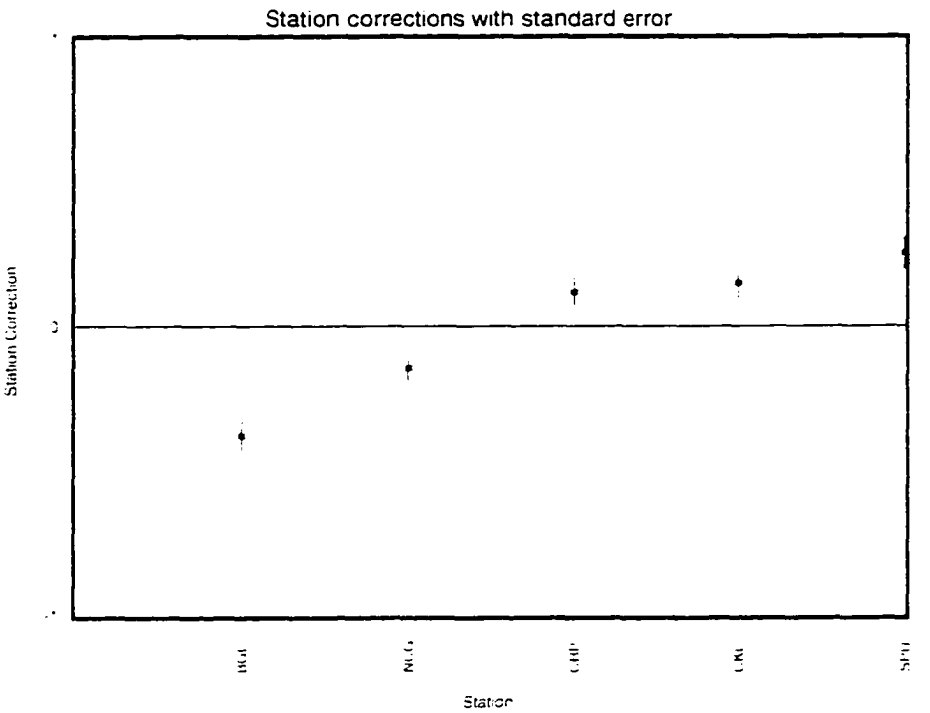

Figure 3.8 b

This figure shows the station corrections with standard error for the inversion of data from Mt. Spurr earthquakes. The vertical axis is in units of local magnitude. Station names are shown along the horizontal axis.

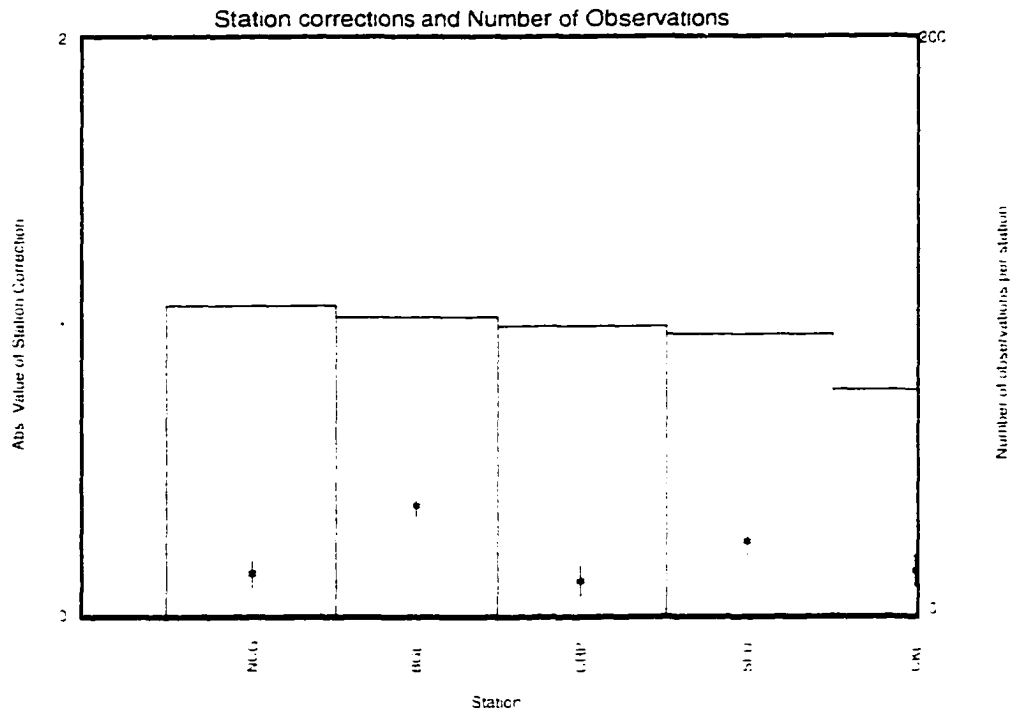

Figure 3.8 c

This figure shows the absolute values (asterisks) of station corrections obtained from the inversion for Mt. Spurr earthquakes. One-standard-deviation error bars are included with the data points. The axis on the left indicates the size of the station correction in magnitude units. The boxes, referenced to the axis on the right, show the number of amplitude measurements used at each station for this inversion. The station names are shown along the horizontal axis.

$-\log A_0$ curve was anchored to the Californian curve (dashed line) at 5 km distance, the closest point where we had a reasonable amount of data. This reference distance gives a reference magnitude of 1.38. A close anchor point is desirable in cases like this, where the attenuation value is potentially much different than the California value. Inversion of the Mt. Spurr data set has yielded a geometric spreading value of 0.825 +- 0.27 and an attenuation value of 0.0233 +- 0.012, implying a preliminary Q of 223 +- 70 at 13.7 +- 4 Hz. An example of the complete program input and output of *maggt* is provided in Appendix C.

One of the encouraging results of this study is the agreement of our measured Q value with the preliminary value of Q obtained by Power (*pers. comm.*, 1995) by a completely different method. Power initially obtained a Q of 94 by Frankel's (1982) spectral ratio method. This was obtained for frequencies between 5 and 20 Hz. Later revisions have brought this nearer to 150 [J. Power, *pers. comm.*, 1995], consistent with our value. Despite the preliminary nature of Q by Power's method and the rough estimate from our inversion, the agreement of the two numbers from completely different techniques suggests that attenuation is indeed high at Mt. Spurr.

The strong difference between volcanic and continental attenuation values shown by this inversion suggest that the volcanic M_L scale should be anchored to the California scale at as close a reference distance as possible. It may be reasonable to move our reference distance in even closer, perhaps 1 km. The strong difference between the volcano results and other continental results suggests that volcanic earthquakes should be removed

from inversions for regional-earthquake M_L to avoid bias.

Station corrections obtained for the five Mt. Spurr stations NCG, BGL, CRP, SPU, and CKL are shown with uncertainties in Figure 3.8b. A plot of the absolute values of the station corrections is plotted in Figure 3.8c, along with the number of observations per station. We had between 78 and 109 observations per station, with station corrections (in magnitude units) ranging from -0.38 at BGL to +0.25 at SPU.

A comparison of our station corrections with those obtained from previous results will also be desirable. Steve Estes [*pers. comm.*, 1995] has pointed out that we have station (magnitude) corrections available for some of the stations used in this study (determined from average station-magnitude residuals for events processed by AEIC), but the time periods do not match the current runs. This will be simple to correct in future studies by appropriately subsetting the input data so the station corrections obtained are applicable to the time periods for which station corrections have already been computed by other methods.

A comparison of magnitudes obtained from the inversion with those currently in the database would be straightforward, though not supported by current code, and may shed light on past studies which have used cataloged local magnitudes from the Alaskan volcanic event catalogs.

The inversion for a local magnitude scale for Mt. Spurr has produced results significantly different from the scales for continental regions. Given the frequency with which local magnitude estimates are used in studies of volcanic seismicity, this study suggests the

importance of computing local magnitude scales for each monitored volcano, and shows the ease with which this can be done.

3.5 Automation

We have taken several steps to improve magnitude calculations, in an ongoing effort to automate the magnitude calculation process and improve the data set for future inversions. The two main steps we have taken are to enhance the calculation of synthetic Wood-Anderson traces, coming probably as close as possible with the Alaskan short-period analog network to realistic Wood-Anderson equivalents; and to implement the magnitude measurement into the Iceworm processing system and save both the raw measurements and the derived magnitudes in a relational database. This latter step has involved the design and implementation of a new database table for the CSS3.0 schema [Anderson *et al.*, 1990], plus the development of new software for the Iceworm system.

3.5.1 Synthetic Wood-Anderson Seismograms

Proper measurement of M_L requires that the measurement be made as if the seismogram were collected by a Wood-Anderson seismometer. This preserves the meaning of the empirically derived parameters in the Richter magnitude formula, allowing comparison of measured magnitudes with historic data. A different instrument, because of different

frequency response, might produce a trace with the maximum amplitude in a different part of the wave train than the Wood-Anderson instrument. Also, different instrument types may have gains different than that of the Wood-Anderson instrument, making trace-amplitude measurements inconsistent with the $\log A_0$ curve fitted to Wood-Anderson amplitudes for the local magnitude scale.

For the analog stations of the Alaskan network, full compliance with this is often not possible since the Wood-Anderson seismometer had horizontal components and most of the Alaskan analog stations are vertical-component instruments. Nevertheless, the frequency responses can be addressed if not the orientation of the motion. Figure 3.9 illustrates the instrument response for the Wood-Anderson seismograph; and, as a characteristic example of the Alaskan network stations, the response for the short-period (1-second period) analog instrument installed at station CUT (Chulitna) in Alaska. Note that at the outset of this study, only the amplitude responses were available for the Alaskan stations. The phase response for the CUT station, as well as for many of the other Alaskan analog stations, was obtained from the amplitude response through the assumption of minimum-phase, using computer codes constructed following the methods of Bolduc and Ellis (1972). Measurement of the synthetic Wood-Anderson amplitude is a matter of removing, or deconvolving the instrument response of the actual instrument used and convolving in the response of the original Wood-Anderson seismometer.

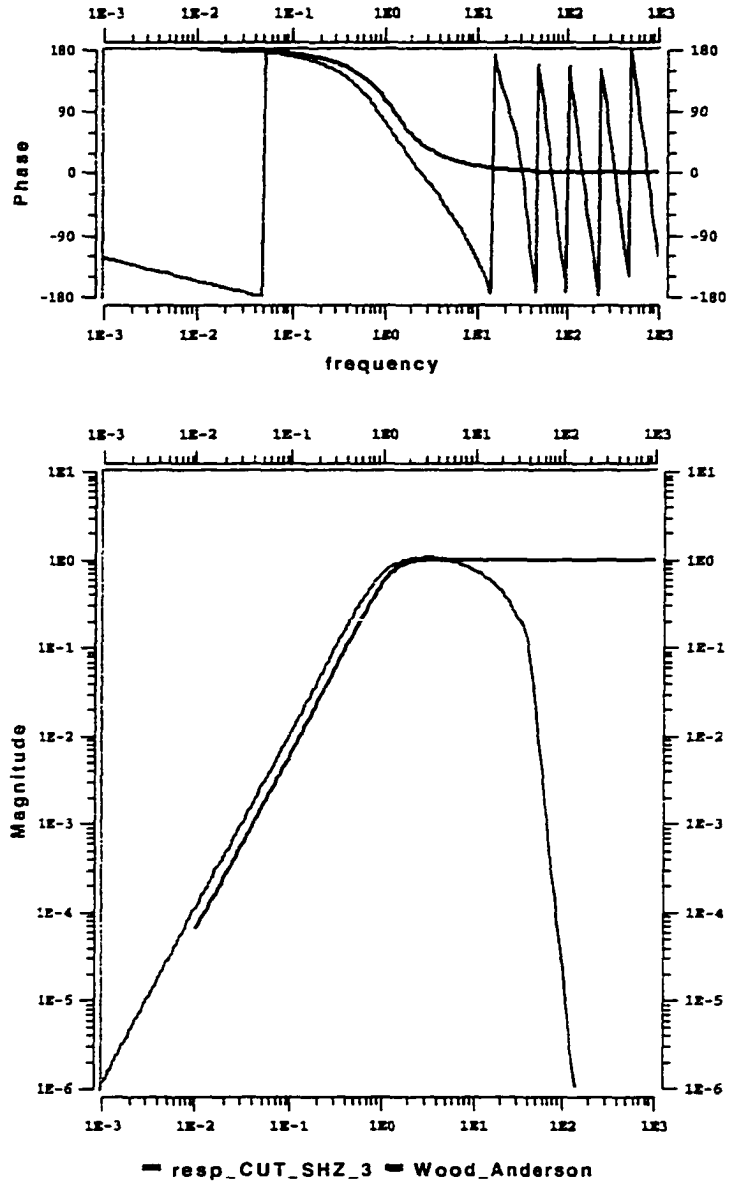

Figure 3.9

This figure shows the normalized phase and amplitude response for the Wood-Anderson seismometer (darker curves), and for a representative short-period station (Chulitna, CUT) of the Alaskan seismic network (lighter curves). The horizontal axis is frequency in Hertz.

3.5.2. Automatic M_L Calculation and Database Storage

Automation of the amplitude measurement on Wood-Anderson synthetic seismograms has been achieved with the *local_mag* module of the Iceworm system. The *local_mag* module receives data on the phase arrival times and location of each earthquake through the PICK_RING of the Iceworm system, as described in Chapter two. Data from each station with an automatic phase arrival are requested from the wave-server. The time series requested for each station begins three seconds before the first arrival and lasts twice the difference between the predicted P and S travel times from the hypocenter. For each time-series, the first step is to apply the calibration value for the instrument, since the instrument-response curves themselves are stored, normalized to unity gain, at a reference frequency of 5 Hz. The trace is then demeaned, cosine-tapered, and Fourier-transformed into the frequency domain. A deconvolution is performed by complex division in the frequency-domain of each seismogram-spectrum data-point by the complex instrument response at that frequency. The trace is then integrated in the frequency domain (dividing each point in the seismogram spectrum by $i\omega$, where ω is the angular frequency and i is $(-1)^{1/2}$), since the analog stations being discussed are velocity-response instruments and the Wood-Anderson instrument measures displacement. A bandpass filter from 0.5 to 10 Hz is applied, followed by frequency-domain convolution of the Wood-Anderson response curve with the seismogram. Finally, the seismogram is brought back to the time domain with an inverse Fourier transform. Actual measurement of the synthetic Wood-Anderson amplitude is done by scanning through the seismogram for the largest difference between

a consecutive peak and trough (or trough and peak). Dividing this in half, we get a zero-to-peak amplitude which is used in the local-magnitude formula presented in the theory section above. The geometric spreading and attenuation coefficients used by the *local_mag* module are specified in the setup file for the program. The currently running Iceworm system is still using the original Californian values. Once the individual station-magnitudes are measured, the network magnitude for the event is obtained by averaging the station-magnitudes. All of the information computed by the *local_mag* module is put back on the PICK_RING of the Iceworm system, where it is distributed appropriately to the output databases. It is the magnitude from the *local_mag* module that appears in the display of the *Wormwatch* utility, discussed in chapter two.

In order to store the results for the local-magnitude measurement, we have designed a new table, called *wfmeas* for "waveform measurements," to incorporate into the CSS3.0 relational-database schema. This table is intended to store arbitrary measurements on waveforms. A screen-dump of the Datascope *dbhelp* utility displaying the characteristics and a description of the *wfmeas* table is shown in Figure 3.10.

Two difficulties we had to overcome in the automatic measurement of amplitudes for local-magnitude calculation were clipping of the analog signal and gain-range pulses from the A1 VCO gain-ranging oscillators used in the analog telemetry. The clipping problem was overcome simply by adding parameters in the *local_mag* module to throw out all measurements on seismograms that came within a certain threshold of some maximum, currently set at 90% of 2048 counts for the analog stations. Gain ranging was more

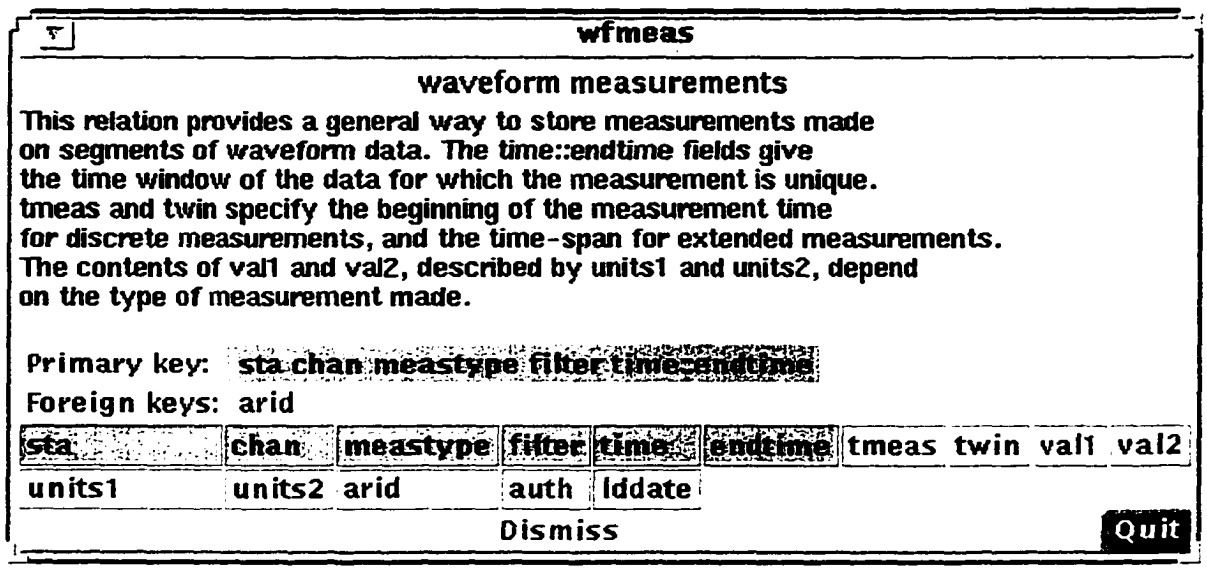

Figure 3.10

This figure shows a screen-dump of the *dbhelp* utility from the Datascope Seismic Application Package, showing the field names and description of the *wfmeas* table in the expanded CSS3.0 Schema. The *wfmeas* table, which was implemented to support the work in this chapter, is designed to store arbitrary measurements on waveform data. This eases the implementation of future, customized automatic measurements in the Iceworm system.

difficult. Some of the Voltage-Controlled Oscillators (VCOs) used in telemetry for the Alaskan analog network will change gains automatically if signal amplitudes become too large [Rogers *et al.*, 1980]. These VCOs will scale down the telemetered signal amplitude by a factor of 10 or 500 to avoid clipping. The VCOs signal this change with a gain-ranging pulse (see Figure 3.11), a short swing to the negative and then positive that follows the gain change by 3.0 seconds for 10x gain ranging, and a series of six pulses delayed 30 seconds for 500x gain ranging. This pulse is recognizable to a human analyst but hard to identify as such automatically. Nevertheless these gain range pulses are occasionally picked by the automatic picker. Also, the return to normal gain often resembles an S-phase, and often requires an analysis of the event to distinguish it from the true S-phase. These returns to normal gain are also often picked by the automatic picker. For large earthquakes, several false events can be built by the associator out of these gain-ranging "phases." In terms of magnitude measurements, the gain-range pulses are disastrous, since the true gain of the instrument and telemetry system is not known by the *local_mag* module when it computes the amplitude. To overcome this we exclude gain-ranging stations from automatic magnitude measurement. We have made a network (specified in the CSS3.0 affiliation table) called "mag" and included in it all stations which may be used for automatic magnitude calculation. None of the gain-ranging stations are allowed in this mag network.

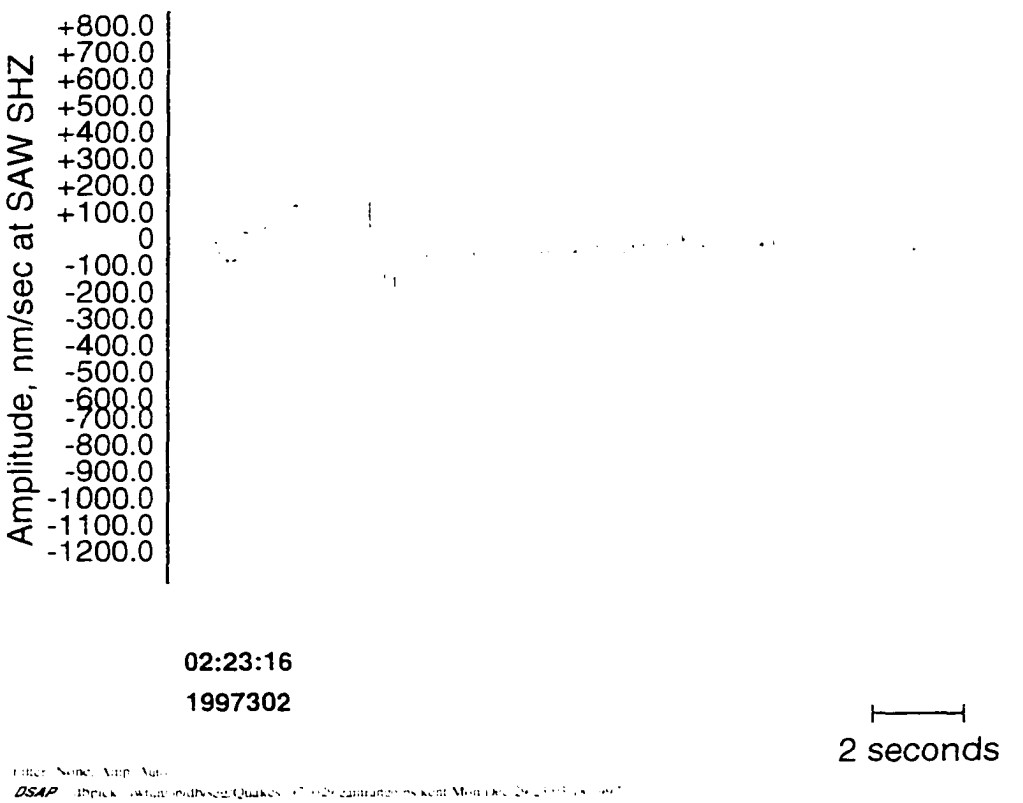

Figure 3.11

This figure shows a characteristic gain-ranging pulse (described in Section 3.5.2 of the text) on the Alaskan short-period station SAW. The gain-ranging pulse in this figure is the narrow, highest feature on the waveform shown. Gain-ranging pulses interfere with the automatic measurement of earthquake magnitudes.

3.5.3. Magnitude Review and Future Work

While the automation of the local-magnitude measurement has allowed the collection of a large data set for future inversions, it is still necessary to review these measurements by hand to throw out the occasional bad measurement. These newly-collected data have not yet been used in an inversion since the automatic amplitude measurements have not been reviewed. Software development is under way to allow review of synthetic Wood-Anderson amplitude measurements. The principle issue is the generation, on demand, of synthetic Wood-Anderson seismograms and measurement and review software that integrates with existing, day-to-day analysis packages for regional seismicity. Packages such as SAC [Tapley *et al.*, 1990] allow the development of this type of code for research purposes, but such script-driven approaches do not integrate well with existing processing software.

We have begun developing a generic time-domain, recursive filtering implementation for seismic data that will integrate into our processing software such that analyst review of automatic magnitude measurements will be possible. This recursive filtering software will be able to handle frequency-domain filtering tasks based on arbitrary groups of poles and zeros (constrained by stability requirements, of course) such as deconvolving and convolving instrument responses. While this development effort will be relevant to a reanalysis of the current inversion work when complete, we relegate discussion of the theory involved to Appendix D since the time-domain recursion filters do not appear di-

rectly in the processing of the data presented in this thesis.

The fact that further progress on the magnitude-scale inversion project will require a significant development effort emphasizes the expense and complexity of software infrastructure in a near-real-time environment, and the necessity for close involvement of scientists in order to guarantee that measurements being made as part of regional network processing are as close as possible to the original intent. This also illustrates, however, that once that complexity is handled up front in the software infrastructure itself, the automated generation and collection of large data sets can be a powerful tool for progress in regional seismology.

3.6 Acknowledgments

This research was greatly aided by Roger Hansen, who, in addition to useful discussions and explanations, kindly provided the code from the Alsaker *et al.* (1991) BSSA paper. Thanks also to John Power for providing preliminary results on Spurr attenuation, for useful discussion that spurred me to continue this project, and for helping me get the parameter data for Spurr events from the catalog of Alaskan volcanic events. Suzanne Floyd, working under the NSF REU program, grant number EAR 95-31601, helped in the initial stages of the development of the automatic local-magnitude calculation routine.

3.7 References for Chapter 3

Alsaker, A., L. B. Kvamme, R. A. Hansen, A. Dahle, and H. Bungum (1991). The M_L Scale in Norway, *Bull. Seis. Soc. Am.* **81**, 379-398.

Anderson, J., W.E. Farrell, K. Garcia, J. Given, and H. Swanger (1990). Center for Seismic Studies Version 3 Database: Schema Reference Manual, Science Applications International Corporation, Arlington, Virginia, Technical Report C90-01, 61 pp.

Bakun, W. H. and W. B. Joyner (1984). The M_L scale in Central California, *Bull. Seis. Soc. Am.* **74**, 1827-1843.

Bolduc, P.M., R.M. Ellis, and R.D. Russell (1972). Determination of the seismograph phase response from the amplitude response, *Bull. Seis. Soc. Am.* **62**, 1665-1672.

Hutton, L. K. and D. M. Boore (1987). The M_L scale in Southern California, *Bull. Seis. Soc. Am.* **77**, 2074-2094.

Bullen, K.E. and B. A. Bolt (1985). An introduction to the theory of seismology, fourth

edition. Cambridge University Press, Cambridge, 499 pp.

Frankel, A. (1982). The effects of attenuation and site response on the spectra of microearthquakes in the northeastern Caribbean. *Bull. Seis. Soc. Am.* **72**, 1379-1402.

Jolly, A. D., R. A. Page, and J. A. Power (1994). Seismicity and Stress in the vicinity of Mount Spurr volcano, south central Alaska. *J. Geophys. Res.* **99**, 15,305-15,318.

Jolly, A.D., J.A. Power, S.D. Stihler, L.N. Rao, G. Davidson, J. Paskievitch, S. Estes, and J.C. Lahr (1996). Catalog of earthquake hypocenters for Augustine, Redoubt, Iliamna, and Mount Spurr volcanoes, Alaska. U.S. Geological Survey Open-File Report 96-70, 90 pp.

Lahr, J. (1994). Hypoellipse/Version 3.0: A computer program for determining local earthquake hypocentral parameters, magnitude, and first-motion pattern. *USGS Open-file Report*, revision 6/9/94.

Lay, T. and T.C. Wallace (1995). Modern Global Seismology. San Diego: Academic Press, 521 pp.

Richter, C.F. (1935). An instrumental earthquake magnitude scale. *Bull. Seis. Soc. Am.* **25**, 1-32.

Rogers, J.A., S. Maslak, and J.C. Lahr (1980). A seismic electronic system with automatic calibration and crystal reference. U.S. Geological Survey Open-File Report 80-324, 130 pp.

Tapley, W.C. and J.E. Tull (1990). SAC--seismic analysis code, command reference manual, Lawrence Livermore National Laboratory, informal report, 260 pp.

Chapter 4

Array processing for Regional Seismic Monitoring in Alaska

4.1 Introduction

Earthquake processing at the Alaska Earthquake Information Center has traditionally been limited to earthquakes in the interior of the state. The automatic regional associator described in Chapter 2 is also limited to the interior of the state, although the extensive seismicity in the Aleutian chain [Taber *et al.*, 1991] merits close seismic monitoring, as much as the continental Alaskan earthquakes. We have begun processing several seismic arrays to improve interior Alaskan earthquake monitoring and to extend event detection and location into the Aleutians. In this work the word "array" is used as it is in the nuclear-test-ban verification community, to mean not just a collection of seismometers, but a spatially tight group of similar instruments with the same sample rates, deployed to take advantage of any coherence of the incoming wavefield across the collection of stations [Ringdal *et al.*, 1982]. The station spacing must be narrow enough that signal waveforms are correlated between adjacent seismographs, a distance which depends on the frequency of interest [Aki *et al.*, 1980]. There are several problems on which our array-processing work has made progress, which we present as part of this thesis. First, with few stations in

the Aleutian Islands, earthquake location is a difficult problem since the events occur outside the bulk of the Alaskan network. Arrays address this [Bratt *et al.*, 1988] by providing information about the incoming wavefront which helps identify the arrival azimuth, distance range and type of incoming phases. Second, signal strength is a problem for many of the smaller Aleutian events. Arrays provide improved detection thresholds due to the signal-to-noise improvement of multichannel filtering [Ringdal *et al.*, 1982], which we describe in more detail below. Third, the Earthworm regional associator has been repeatedly fooled into building multiple, nonexistent interior-Alaskan events out of the phases from large teleseisms [Lindquist *et al.*, 1997]. The arrays will improve hazard response because of their ability to discriminate between teleseisms and large, local earthquakes. Finally, the high quality of the array stations has already allowed reliable magnitudes for earthquakes throughout Alaska, plus the detection of more small events near the arrays, including felt events, that were missed by the regional associator. Empirical studies to determine the potential of the array stations for earthquake monitoring around the entire Arctic suggest the benefit of collaborative array processing amongst the entire Arctic seismic community [Hansen *et al.*, 1996]. We end by outlining, through an example, the procedures for fully automated monitoring of Alaska and the Aleutians with the array stations.

4.2 Theory

Array processing improves signal detection by suppressing noise relative to the incoming signals through a process called "beamforming," also known as stacking in the seismic exploration literature. In describing beamforming we follow roughly the presentation of Fyen [1996]. Standard coherent beamforming assumes the same seismic signal arrives at each station in the array, while the noise at each station is incoherent with the noise at the other stations. The arrival times of the seismic signals at each station are delayed according to the relative geometry of the station layout and the incoming wave. The waveforms, after being shifted to line up the seismic signals, are summed in order to enhance the signal at the expense of incoherent noise. The seismic signals that are coherent across the array interfere constructively, while the incoherent noise interferes destructively.

In order to compute the time delays to apply to each station to align the incoming seismic signals, it is assumed that the incoming wavefront is a plane wave. In this case, two angles are necessary to specify the orientation of the wavefront relative to the array. These angles are measured from the normal-vector for the wavefront. In the horizontal plane, the wave approaches the array at an angle from north called "backazimuth" or just "azimuth." In the vertical plane, the wave approaches at an angle called the angle of incidence, measured between the normal to the earth's surface and the normal to the wavefront. The angle of incidence along with the wave-propagation velocity under the array uniquely determine the apparent propagation speed of the wavefront horizontally across the array. Because of

this, the incoming wavefront is often described in terms of azimuth and apparent velocity rather than in terms of the two angles azimuth and angle of incidence. A third, alternate quantity used in this work is the vector horizontal slowness of the wavefield, the magnitude of which is the inverse of the apparent horizontal velocity. Often we plot horizontal slowness in terms of its two components s_x and s_y, the horizontal slownesses in the East-West and North-South directions.

Calculating the appropriate delays starts with assigning zero delay to one station, usually the center element of the array. The positions of the other elements of the array are taken to be $r_i=(x,y,z)$, where x, y, and z are Cartesian coordinates in kilometers East, North, and upwards of station i relative to the center element. Taking the angle of incidence Φ between the wavefront-normal and vertical, and the crustal seismic-wave velocity v_C, the apparent horizontal velocity v_{app} of the wavefront across the array is

$$v_{app} = \frac{v_C}{\sin \Phi}$$

The time delay τ for a given station relative to the center element depends on the horizontal distance between the center element and the station, along the propagation direction of the wave. If we call ρ the backazimuth and **k** the horizontal component of the direction of propagation of the wave, then

$$\tau = \frac{\mathbf{k} \cdot \mathbf{r}}{v_{app}} = \frac{-x \sin\rho - y \cos\rho}{v_{app}}$$

The negative sign comes from the fact that **k** points approximately from the event to the station, where backazimuth is measured from the station to the event. The trigonometric functions arise through the difference between backazimuth, which is measured clockwise from North; and the polar-coordinate azimuthal angle, which is measured counterclockwise from the Eastward-pointing x-axis. Applying these time delays to each waveform, we can delay the signals into alignment and add the delayed waveforms to emphasize the signal. Let y($\mathbf{r}_i$,t) be the time-series from site i at time t. Then the beam is

$$b(t) = \frac{1}{N}\sum_{i=1}^{N} y(\mathbf{r}_i, t + \mathbf{r}_i \cdot \mathbf{u})$$

$$y(\mathbf{r}_i,t) =$$

where N is the number of stations in the array. Assuming that the incoming signal is a harmonic plane-wave of frequency f

$$y(\mathbf{r}_i,t) = Ae^{j2\pi(ft-\mathbf{k}\cdot\mathbf{r})}$$

$$y(\mathbf{r}_i,t) = Ae^{j2\pi(ft-\mathbf{k}\cdot\mathbf{r})}$$

we obtain, through substitution (taking **k=fu,** where **u** is the vector slowness).

$$b(t) = \frac{1}{N}\sum_{i=1}^{N} Ae^{j\omega[t+\mathbf{r}_i\cdot\mathbf{u}-\mathbf{r}_i\cdot\mathbf{u}]} = \frac{1}{N}\sum_{i=1}^{N} Ae^{j\omega t} = Ae^{j\omega t}$$

Note that we have substituted ω for 2πf. This beamforming operation "aims" the array at location **u** in inverse apparent velocity space. To realize the utility of the arrays for superior signal detection, we need to examine the effect of the beamforming on incoherent noise relative to the harmonic signal. The observed signal is the sum of background noise plus the seismic arrival of interest:

$$y(t) = S(t) + n(t)$$

Taking S as the harmonic plane wave as above, we need only to examine the effect of the beam-forming on the noise n(t). The beamed noise is

$$b_n(t) = \frac{1}{N}\sum_{i=1}^{N} n(\mathbf{r}_i, t + \mathbf{r}_i \cdot \mathbf{u})$$

If n(t) has normal amplitude distribution, zero mean value, and zero correlation between sensors, the beamforming process will reduce the noise variance [Mykkeltveit *et al.*, 1990] by

$$\langle b_n(t) \rangle = \frac{\langle n(t) \rangle}{\sqrt{N}}$$

Arrays provide not only noise reduction, but also direct observation of wavefront velocity and direction of approach [Fyen, 1996]. The wavefield incident on an array at a given time can be decomposed into a suite of plane-waves [Aki *et al.*, 1980]

$$f(x, y, t) = \iiint_{-\infty}^{\infty} f(k_x, k_y, \omega) \exp(ik_x x + ik_y y - i\omega t) \frac{d\omega dk_x dk_y}{8\pi^3}$$

Estimation of $f(k_x, k_y, \omega)$, so-called FK analysis for "frequency-wavenumber" analysis, yields the incoming direction of the seismic signal, taken as the peak of the function $f(k_x, k_y, \omega)$.

In this work we avoid the discrete, inverse spatial Fourier transform suggested by the above equation, instead applying a grid-search technique: we form a suite of beams directly that covers all parts of slowness space of interest, computing the power for each. This is done for a small time window of array data, usually 2-4 seconds, with a Butterworth bandpass filter applied to each trace beforehand to select a particular frequency window. The frequency band of interest varies on a case by case basis, but in this work the passband

generally lies between one and five Hertz. Examples from specific earthquakes will be presented in context below. Our slowness limits for FK processing are -0.4 to 0.4 sec/km in each direction (North-South and East-West), with a grid of 51 by 51 points for a total of 2601 power points. In this work, the FK spectra are actually plots of semblance: the values for power are normalized by taking a ratio of stacked trace energy to input energy [Neidell *et al.*, 1971]:

$$S = \frac{1}{2} + \frac{R_{12}(0)}{R_{11}(0) + R_{22}(0)}$$

Here R_{12} is the cross-correlation of an individual trace with the stack; R_{11} is the autocorrelation for the stack; and R_{22} is the autocorrelation for the individual trace. Semblance has a range of 0 to 1. The advantage of semblance is that it measures coherence independent of the joint power level of the traces [Kanasewitch, 1975].

4.3 Alaskan Arrays

There are five arrays in Alaska, four of which are used in this research. Tables 4.1 through 4.6 present names, center elements, and locations of the arrays. Figures 4.1a-f show the locations and geometries of the arrays. The Alaskan Long-Period Array, or AL-PA, consists of seven Teledyne-Geotech KS-54000 broadband instruments deployed in

Table 4.1: University of Alaska Seismic Arrays					
Array name	Array code	Number of Elements	Band	Components	Center Element
Eielson	IL	19	Short-period	Vertical	iLBB
Indian Mountain	IM	5	Short-period	Vertical	IM03
Burnt Mountain	BM	5	Short-period	Vertical	BM03
Beaver Creek	BC	5	Short-period	Vertical	BC03
Alaska Long-Period Array	ALPA	7	Long-period	Three-component	ALL1

Table 4.2: Eielson Array Coordinates					
Station Name	Latitude	Longitude	Elevation (km)	Distance North of center element (km)	Distance East of center element (km)
IL01	64.7716	-146.8861	0.4180	0.0213	0.0208
IL02	64.7847	-146.8643	0.2610	1.4720	1.0541
IL03	64.7714	-146.8512	0.4400	-0.0043	1.6747
IL04	64.7570	-146.8761	0.5280	-1.5996	0.4976
IL05	64.7731	-146.9229	0.3890	0.1832	-1.7192
IL06	64.7792	-146.9040	0.2620	0.8633	-0.8254
IL07	64.7993	-146.8393	0.4010	3.0991	2.2397
IL08	64.7903	-146.7969	0.5050	2.0972	4.2483
IL09	64.7681	-146.7832	0.4940	-0.3750	4.8991
IL10	64.7529	-146.8431	0.5860	-2.0583	2.0590
IL11	64.7415	-146.8974	0.4440	-3.3252	-0.5138
IL12	64.7447	-146.9436	0.3660	-2.9722	-2.7040
IL13	64.7479	-146.9865	0.3670	-2.6173	-4.7372
IL14	64.7750	-146.9794	0.2230	0.3929	-4.3998
IL15	64.7777	-146.9428	0.3360	0.6987	-2.6657
IL16	64.7933	-146.9215	0.3820	2.4295	-1.6543
IL17	64.8072	-146.8898	0.3570	3.9717	-0.1521
IL18	64.7575	-146.7768	0.5540	-1.5536	5.2048
IL19	64.7461	-146.7974	0.5490	-2.8156	4.2277
ILBB	64.7714	-146.8866	0.4190	0.0000	0.0000

Table 4.3: Indian Mountain Array Coordinates					
Station Name	Latitude	Longitude	Elevation (km)	Distance North of center element (km)	Distance East of center element (km)
IM01	65.9969	-153.7225	0.3602	1.4977	1.2026
IM02	66.0005	-153.7971	0.6451	1.8993	-2.1734
IM03	65.9835	-153.7491	0.3720	0.0000	0.0000
IM04	65.9745	-153.7828	0.5872	-0.9954	-1.5249
IM05	65.9751	-153.7253	0.4503	-0.9326	1.0777

Table 4.4: Burnt Mountain Array Coordinates					
Station Name	Latitude	Longitude	Elevation (km)	Distance North of center element (km)	Distance East of center element (km)
BM01	67.4507	-144.5273	0.4630	2.4270	2.2807
BM02	67.4297	-144.4915	0.5296	0.0887	3.8060
BM03	67.4192	-144.6071	0.8020	-1.0800	-1.1265
BM04	67.4181	-144.5584	0.5160	-1.2011	0.9498
BM05	67.4289	-144.5807	0.7560	0.0000	0.0000

Table 4.5: Beaver Creek Array Coordinates					
Station Name	Latitude	Longitude	Elevation (km)	Distance North of center element (km)	Distance East of center element (km)
BC01	63.0619	-141.8279	0.7466	-0.4117	-2.1565
BC02	63.0440	-141.8021	0.5637	-2.3931	-0.8571
BC03	63.0656	-141.7851	0.8469	0.0000	0.0000
BC04	63.0809	-141.7684	0.7908	1.7101	0.8399
BC05	63.0610	-141.7534	0.9087	-0.5063	1.5974

Table 4.6: Alaska Long-period Array Coordinates					
Station Name	Latitude	Longitude	Elevation (km)	Distance North of center element (km)	Distance East of center element (km)
ALL1	65.0653	-147.5639	0.6260	0.0000	0.0000
ALL2	65.1944	-147.3161	-999.0000	14.3622	11.6150
ALL3	65.0286	-147.1961	-999.0000	-4.0770	17.2401
ALL4	64.9100	-147.4464	-999.0000	-17.2655	5.5080
ALL5	64.9447	-147.8595	-999.0000	-13.4047	-13.8546
ALL6	65.0978	-148.0014	-999.0000	3.6137	-20.5085
ALL7	65.2333	-147.7433	-999.0000	18.6863	-8.4117

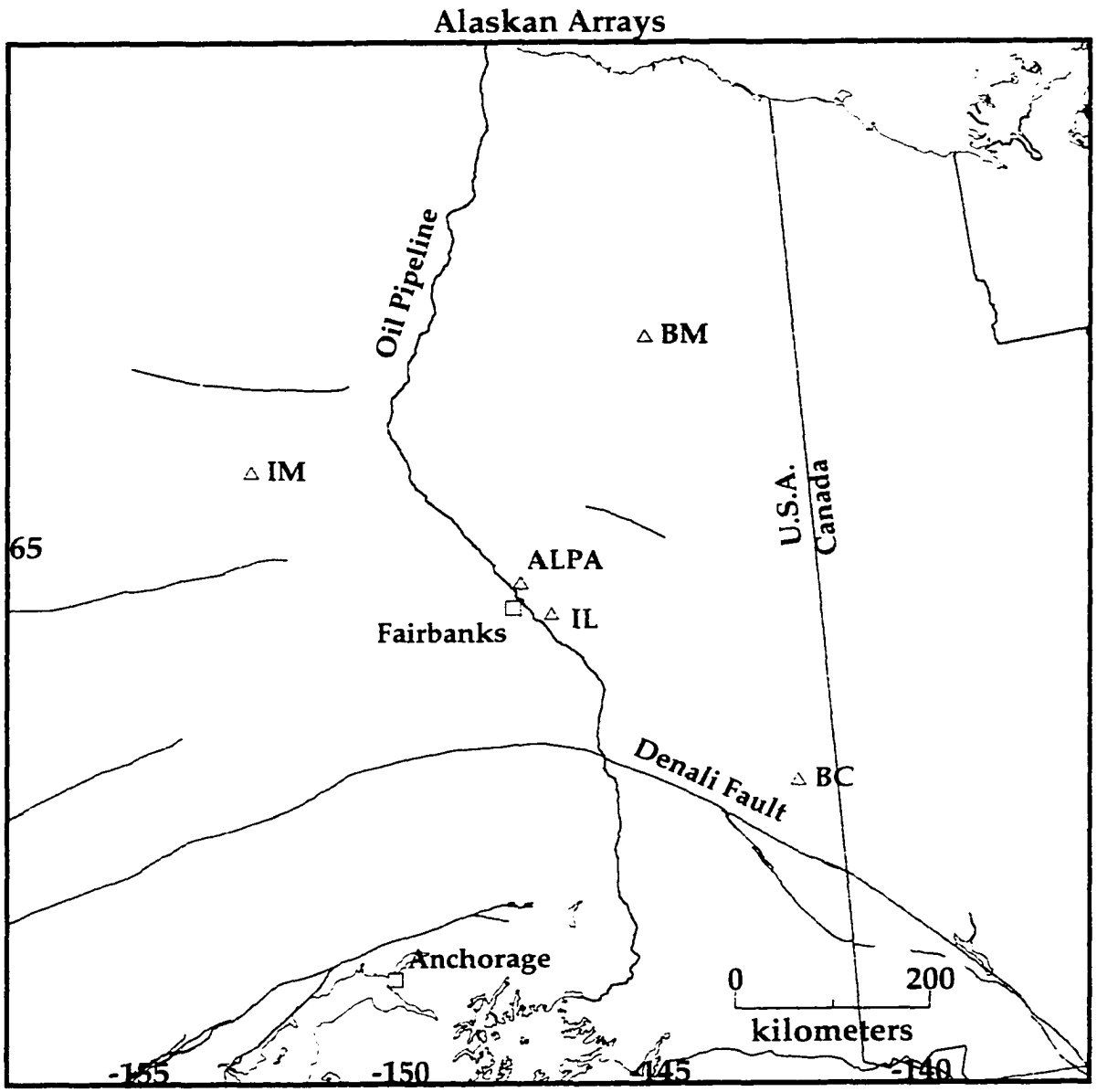

Figure 4.1a

Map of Alaskan Seismic Array locations. Triangles represent array locations. IM is the Indian Mountain array; BM is the Burnt Mountain array; BC is the Beaver Creek array; IL is the Eielson array; and ALPA is the Alaska Long-period array.

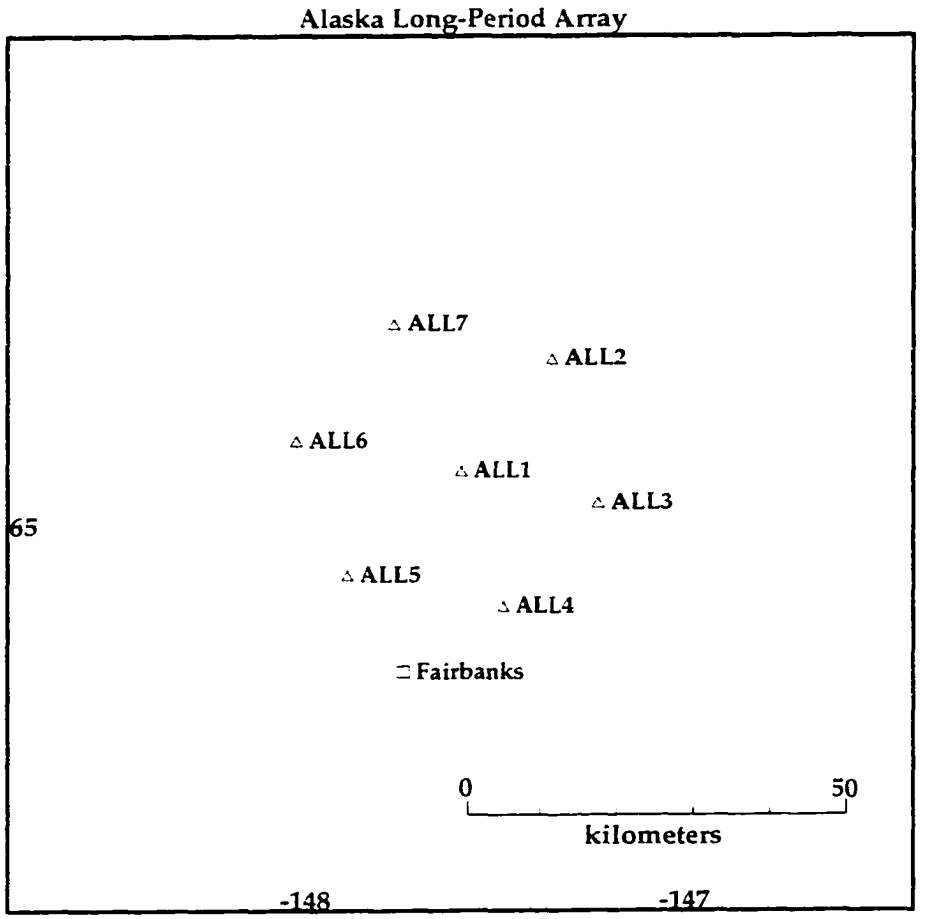

Figure 4.1 b

Geometry of the Alaska Long-Period Array (ALPA). Triangles indicate the locations of the seven individual stations in the array.

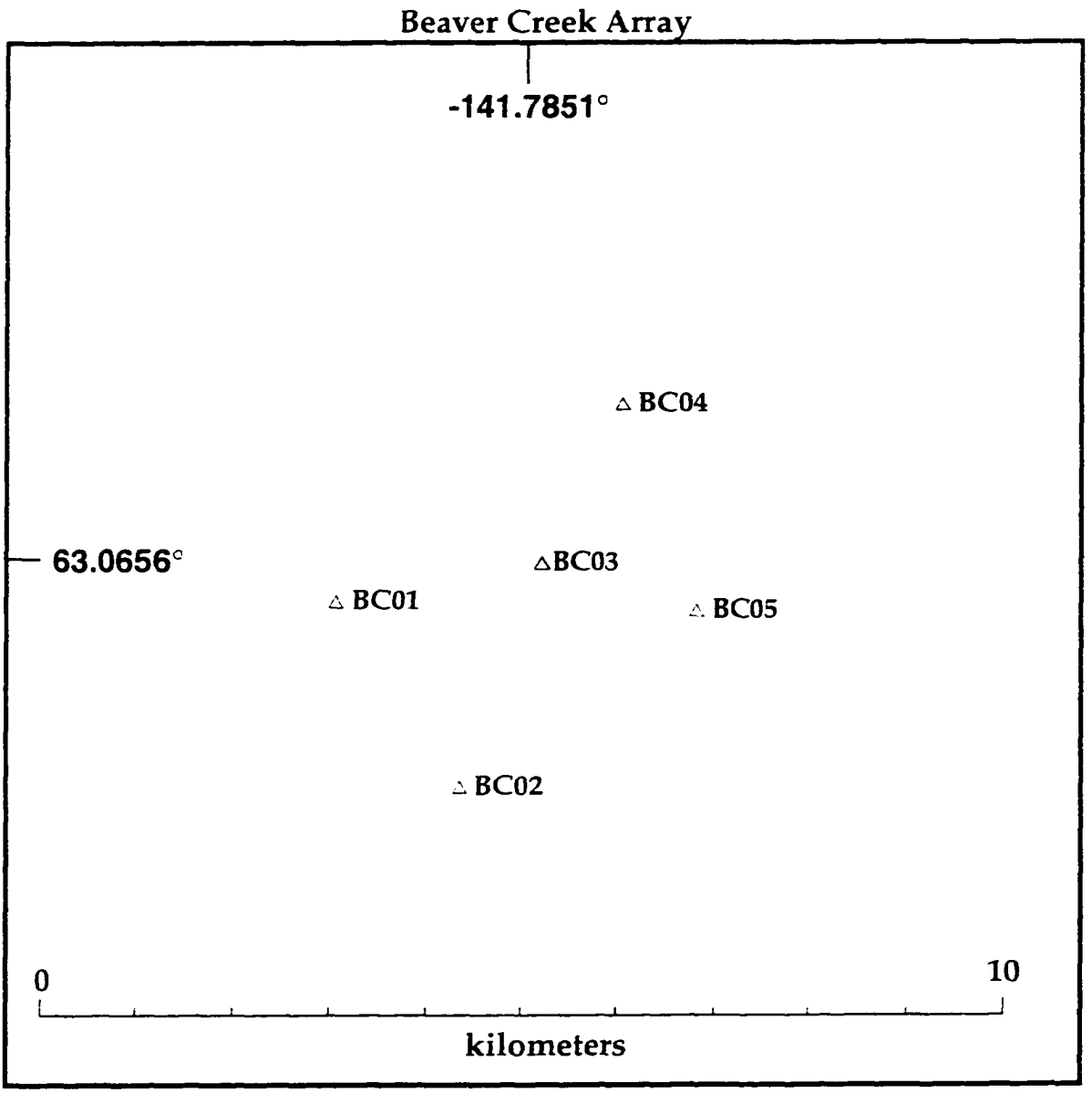

Figure 4.1 c

Geometry of the Beaver Creek five-element, short-period, borehole seismic array. Triangles indicate the locations of the individual stations in the array.

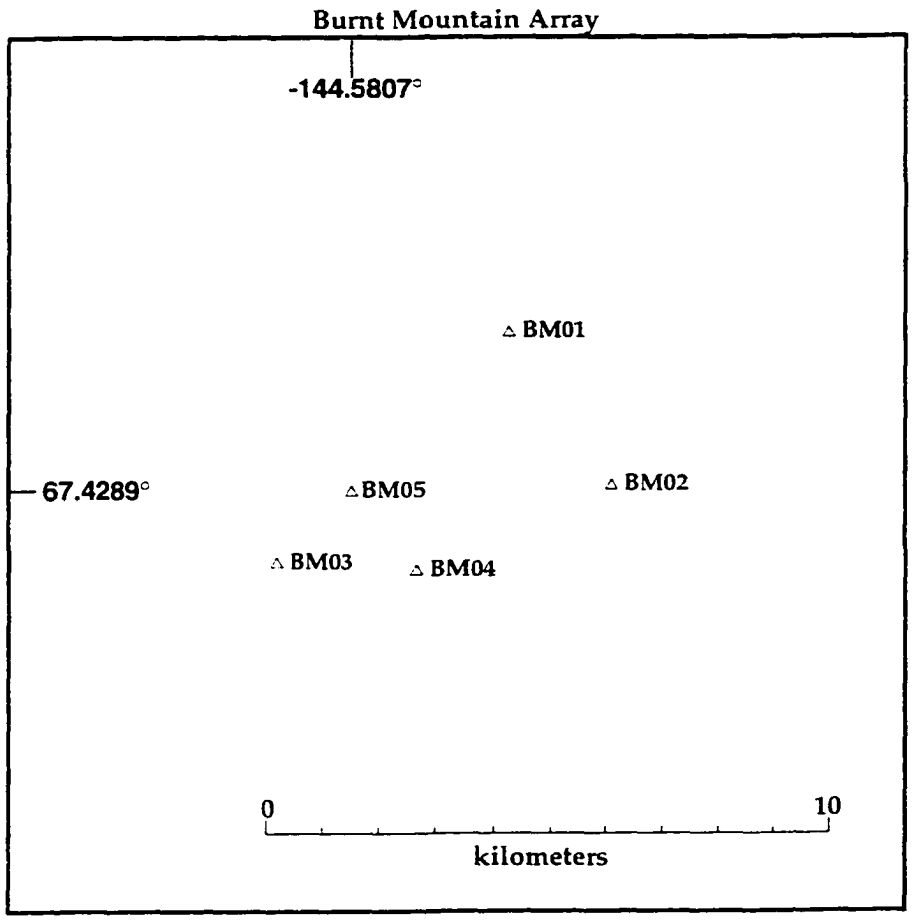

Figure 4.1 d

Geometry of the Burnt Mountain five-element, short-period, borehole seismic array. Triangles indicate the locations of the individual stations in the array.

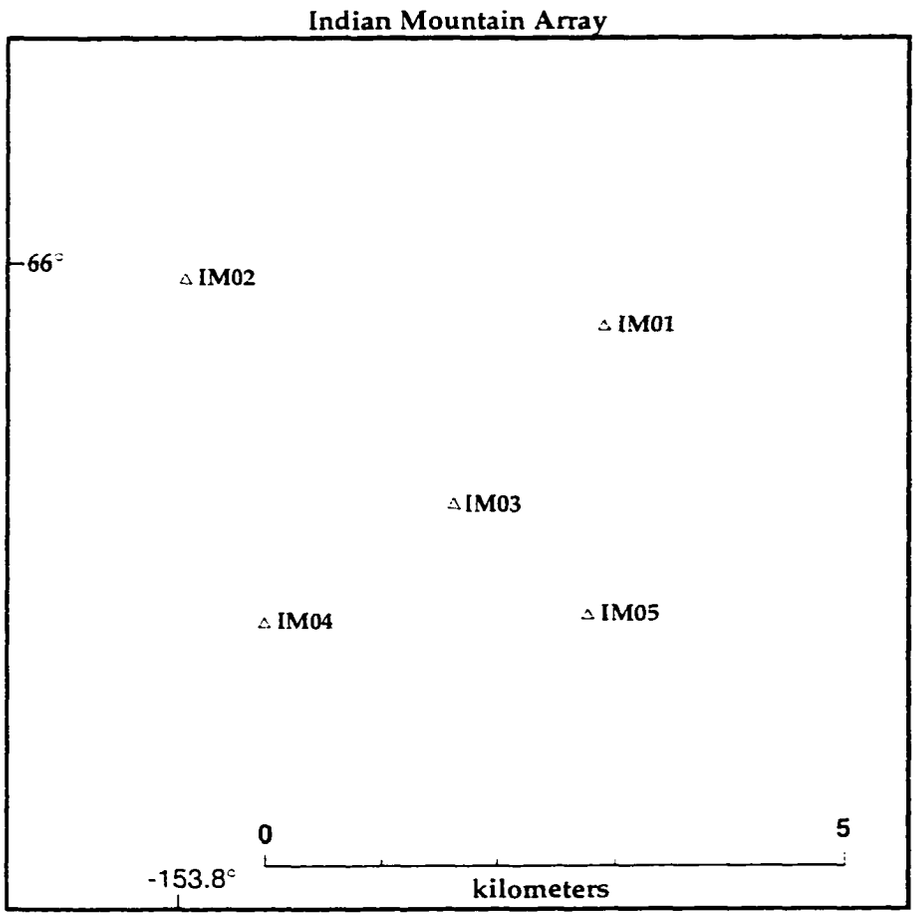

Figure 4.1 e

Geometry of the Indian Mountain five-element, short-period, borehole seismic array. Triangles indicate the locations of the individual stations in the array.

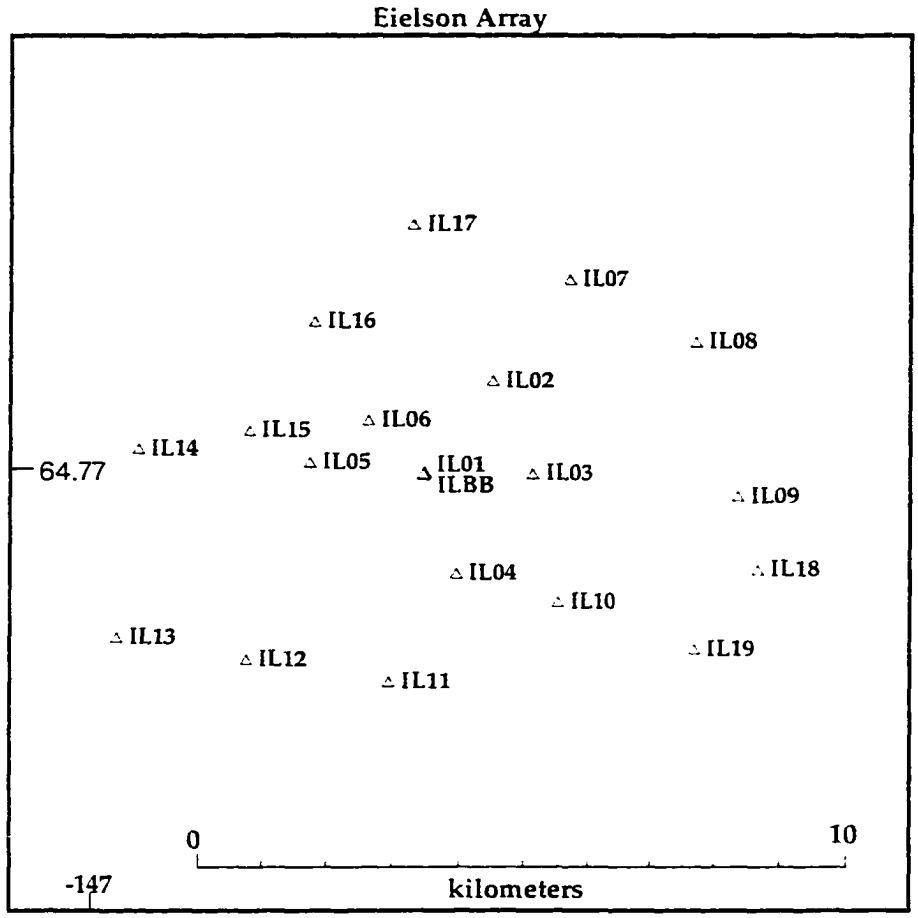

Figure 4.1 f

Geometry of the Eielson seismic array. Triangles indicate the locations of the individual stations in the array. There are 19 single-component, short-period, borehole stations and one three-component, broadband, borehole station in this array. Note that the short-period element IL01 is in almost the same place as the broadband instrument ILBB.

100-meter boreholes. These instruments are filtered to provide long-period data channels. We mention this array for completeness but do not use it for the array studies in the current work. In addition to ALPA, there are four short-period arrays consisting of Teledyne-Geotech model 23900 seismometers deployed in boreholes approximately 100 meters deep. The Burnt Mountain, Beaver Creek, and Indian Mountain arrays are all five-element, shotgun-pattern groups of stations with apertures of approximately four to five kilometers. The Eielson array consists of 19 short-period seismometers in a shotgun pattern, with a twentieth element provided by short-period filtering of a KS-54000 borehole broadband instrument in the center of the array. The aperture of the Eielson array is approximately 10 kilometers. Digital data from all these arrays are telemetered in near-real-time to the Fairbanks seismology lab, where they are incorporated into the Iceworm processing system described in Chapter 2. Continuous archives of the array data from July 14, 1997 to the time of writing have been saved to writable CDROM in CSS3.0 relational database format, providing highly convenient processing and review.

4.4 Magnitude-threshold Study

Before we began acquiring the array data, we conducted an empirical study to predict the detection and location magnitude-thresholds of the arrays for Alaskan, Aleutian, and Arctic monitoring. Although we now have the array data on-line, these predicted

location-sensitivity results are still of interest until we have built an extended catalog of seismicity located with the arrays to measure their sensitivity. This catalog will be relevant to monitoring of the entire Arctic through the COASP program [Hansen *et al.*, 1996], discussed in Chapter 5.

We have applied the empirical technique of Harvey and Hansen [1994], which relies on observed relationships between signal-to-noise observations and magnitude-distance curves to predict detection and location thresholds for various network configurations. We have predicted the location thresholds of various combinations of Arctic stations and arrays in order to establish the networks to be used for Arctic monitoring. The technique consists of measuring signal-to-noise ratios for located events, then extrapolating them to provide expected threshold magnitudes for detected events in a monitored region. We have made maps of our expected location threshold from the Alaskan regional network stations, the Alaskan array stations, and the Alaskan array stations combined with other stations in the Arctic. The center-element array stations were weighted by the expected $1/\sqrt{N}$ signal to noise improvement for the given number of elements in the array.

We took a catalog of 93,625 P-phase arrivals for 3,572 Alaskan events located between May 1, 1995 and July 22, 1996 at the AEIC. For each of these arrivals we took the root-mean-square (RMS) value of a five-second window of data before and after the P-wave. The ratio of the signal RMS to the noise RMS provided our Signal-to-Noise Ratio:

$$RMS = \sqrt{\frac{\sum_{i=1}^{M} x_i^2}{M}}$$

$$SNR = \frac{RMS_{signal}}{RMS_{noise}}$$

where x_i are the M data points in the window for the RMS measurement. We assume that the smallest signal we can detect with confidence has a signal-to-noise ratio (SNR_{min}) of two. From this ratio, we can take each observed arrival and predict from it the minimum magnitude earthquake that could have been seen at the same distance at that station:

$$SNR_{quake} = \frac{A_{quake}}{A_{noise}}$$

$$SNR_{min} = \frac{A_{min}}{A_{noise}}$$

$$\log\left(\frac{SNR_{quake}}{SNR_{min}}\right) = \log A_{quake} - \log A_{min}$$

Combining these with the Richter equation [Richter, 1935] for local magnitude:

$$M = \log A - \log A_0 + S$$

we determine the minimum detectable magnitude at the station by projecting the observed signal-to-noise ratio to the threshold signal-to-noise ratio for detection:

$$M_{min} = M_{quake} - \log\left(\frac{SNR_{quake}}{SNR_{min}}\right)$$

The threshold signal-to-noise ratio for detection is taken to be two in this thesis. Applying this calculation to every arrival observation yields a curve of minimum-detection-magnitude vs. distance for each station. An example is shown for the station Chulitna in Figure 4.2, which contains 2004 signal-to-noise measurements projected to the minimum detectable magnitude. This procedure was carried out for 151 separate seismic stations. To find the magnitude threshold for earthquake location, a grid was laid out over the region of interest. At each point, the minimum magnitude event that would be detected by at least four stations was plotted, based on the minimum-magnitude-vs.-distance curves computed for each station. A contour map of these values produces the predicted magnitude threshold for the network of stations used. Examples are shown and discussed below.

We applied this technique to a number of possible station combinations over the Arctic. Note that our data set of P arrivals contained phase picks for the center elements of the Alaskan arrays. In order to estimate the detection sensitivity of these arrays, we took the signal-to-noise measurements for the center-elements and improved them by the factor of $\sqrt{N}$ described in the theory section. The results of our study are shown in Figures 4.3a-d. We compute the magnitude thresholds for the Alaskan regional network (Figure 4.3 a); for

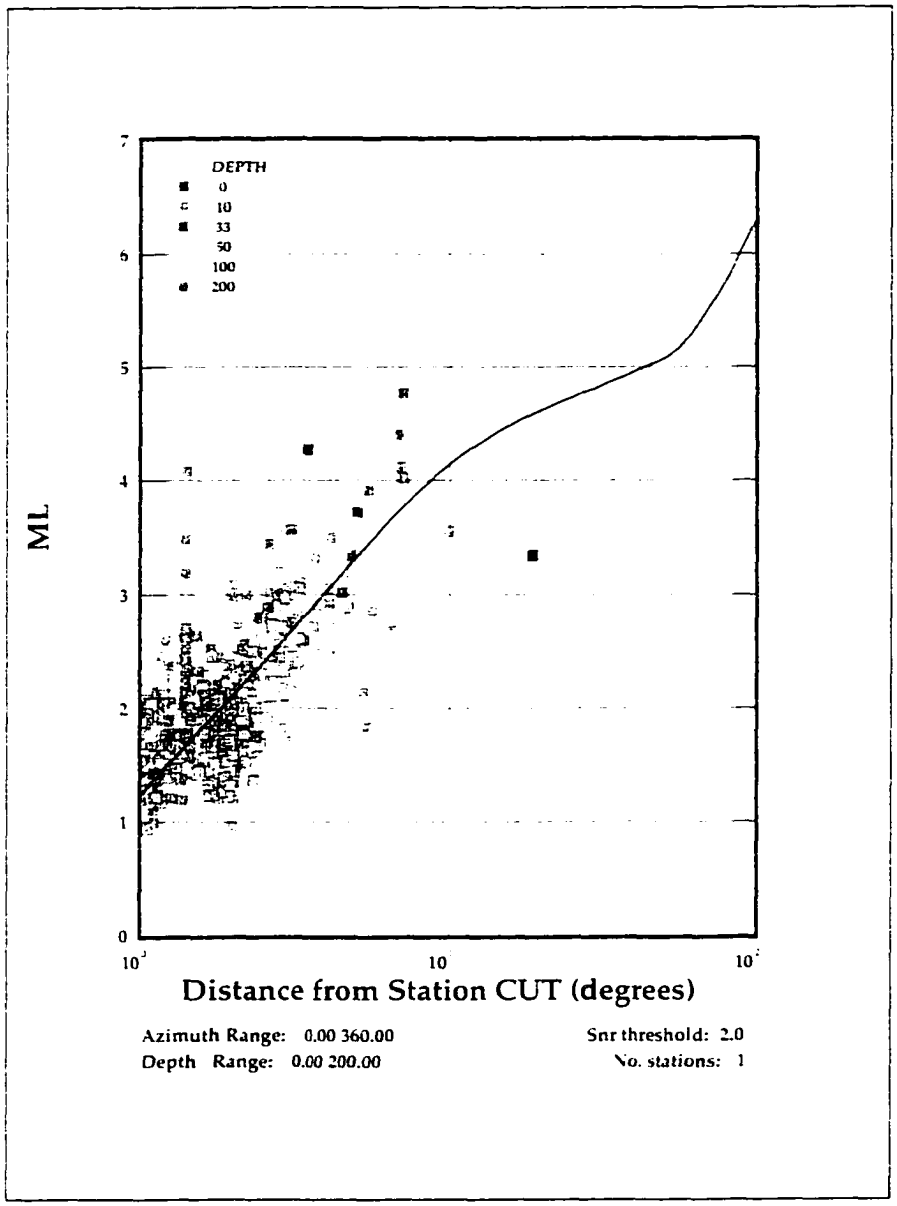

Figure 4.2

Two-thousand four earthquakes measured at seismic station Chulitna (62.4047° North, 150.2694° West) are plotted vs. station-to-event distance in degrees. Each square, shaded to show hypocentral depth, represents one earthquake. The vertical axis shows the measured local-magnitude of the earthquake, reduced by the log of the ratio of measured signal-to-noise for the P wave arrival to a threshold signal-to-noise ration of two, as discussed in Section 4.4 of the text. The curve is fit to the data interactively by inspection. This curve shows the empirical average detection sensitivity of the station as a function of distance.

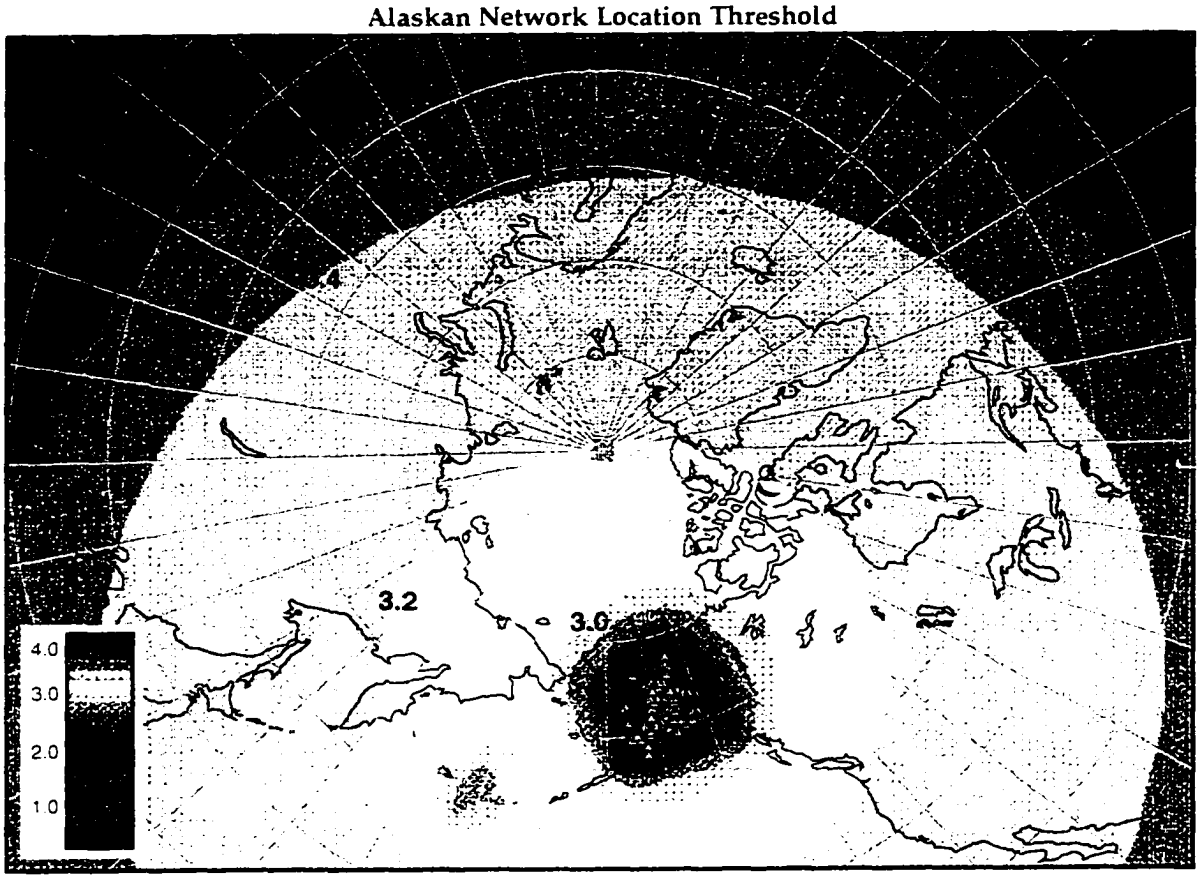

Figure 4.3 a

This map of the polar region shows the predicted magnitude threshold for earthquake location for the Alaskan regional seismic network, based on empirical measurements as discussed in Section 4.4.

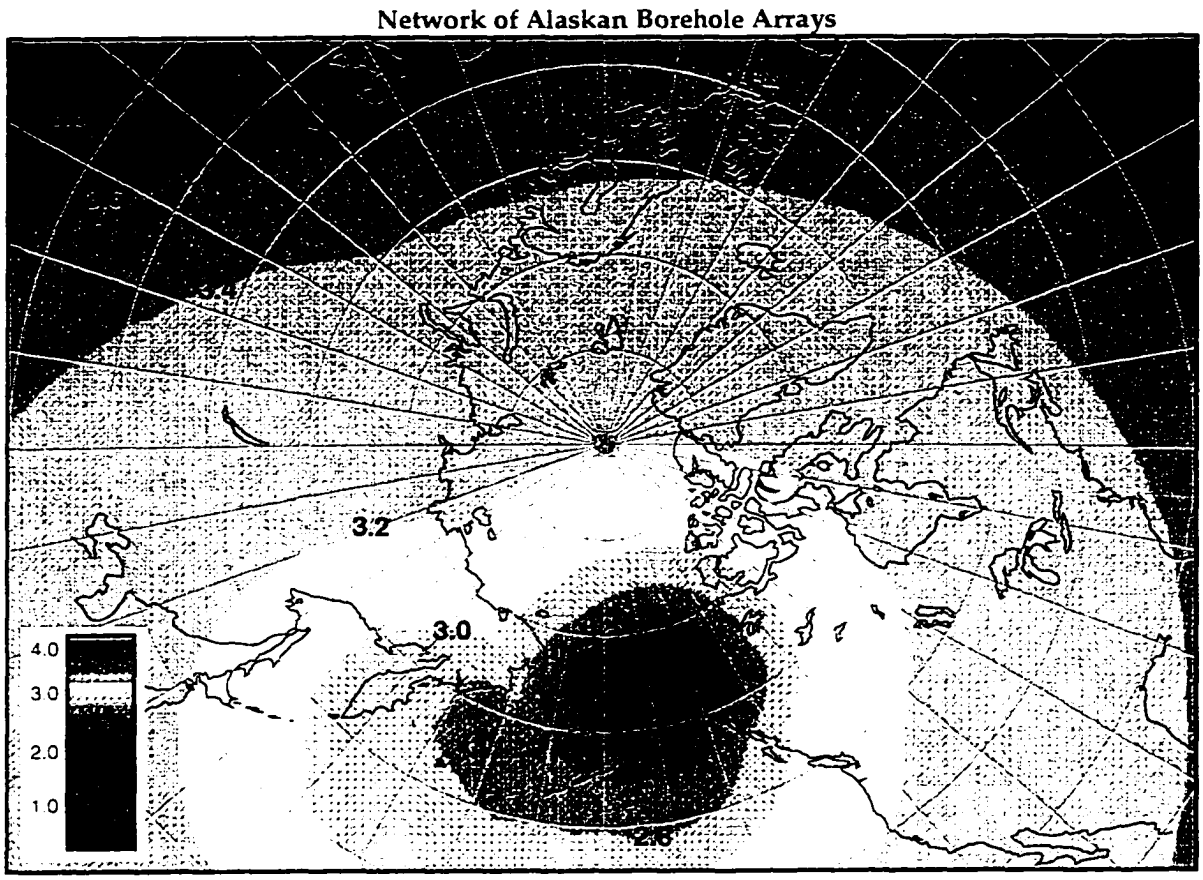

Figure 4.3 b

This map of the polar region shows the predicted magnitude threshold for earthquake location for the existing Alaskan borehole arrays, plus a new array near Anchorage that is currently under installation. Comparison with Figure 4.3a reveals the arrays should perform as well as if not better than the Alaskan regional network in all areas but Prince William Sound and Cook Inlet, which are most densely covered with Alaskan regional network stations.

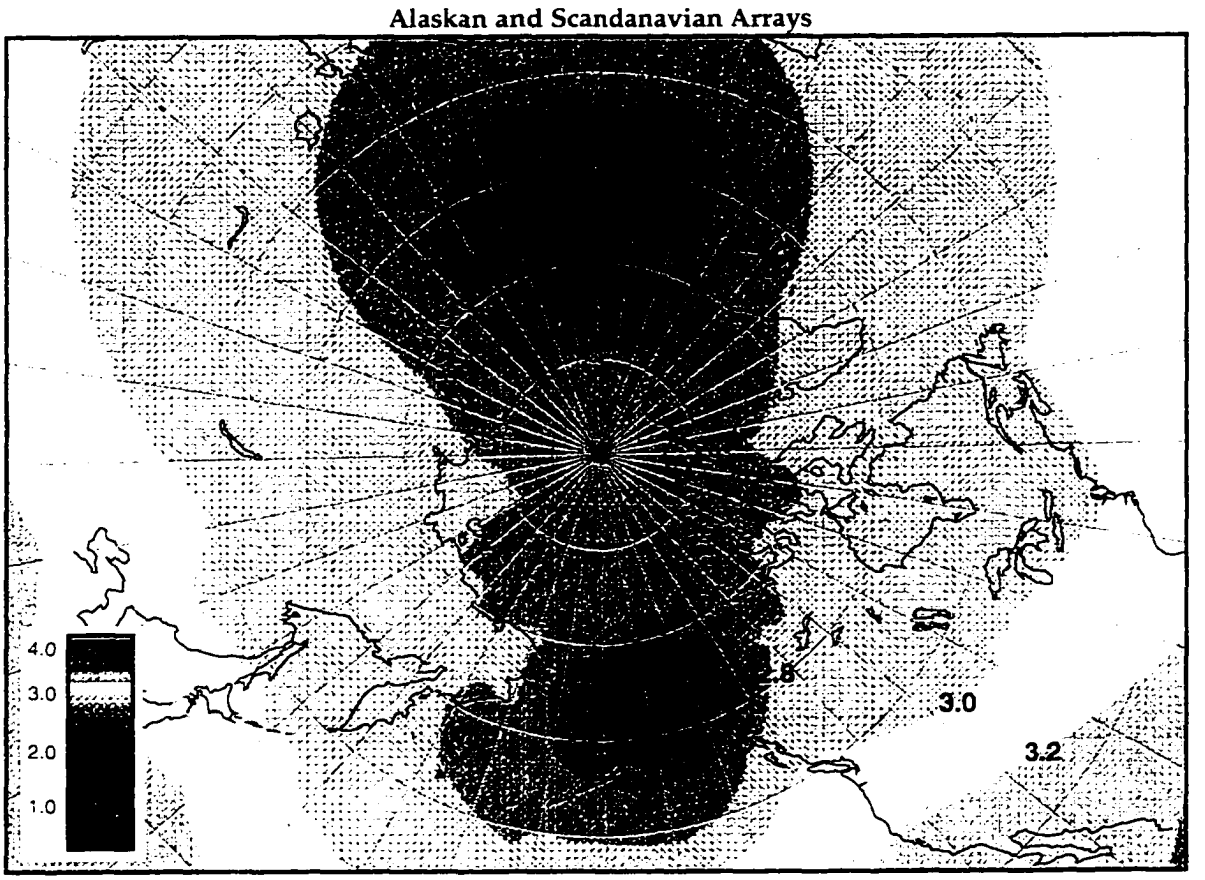

Figure 4.3 c

As in Figures 4.3a and b, this map shows the predicted magnitude threshold for earthquake location over the polar region. Here, however, we add several Scandinavian stations and arrays, investigating the proposed COASP collaboration discussed in Section 4.4 and Chapter 5 of the text. This joint processing of Alaskan and Scandinavian arrays promises to improve detection thresholds in the entire Arctic region.

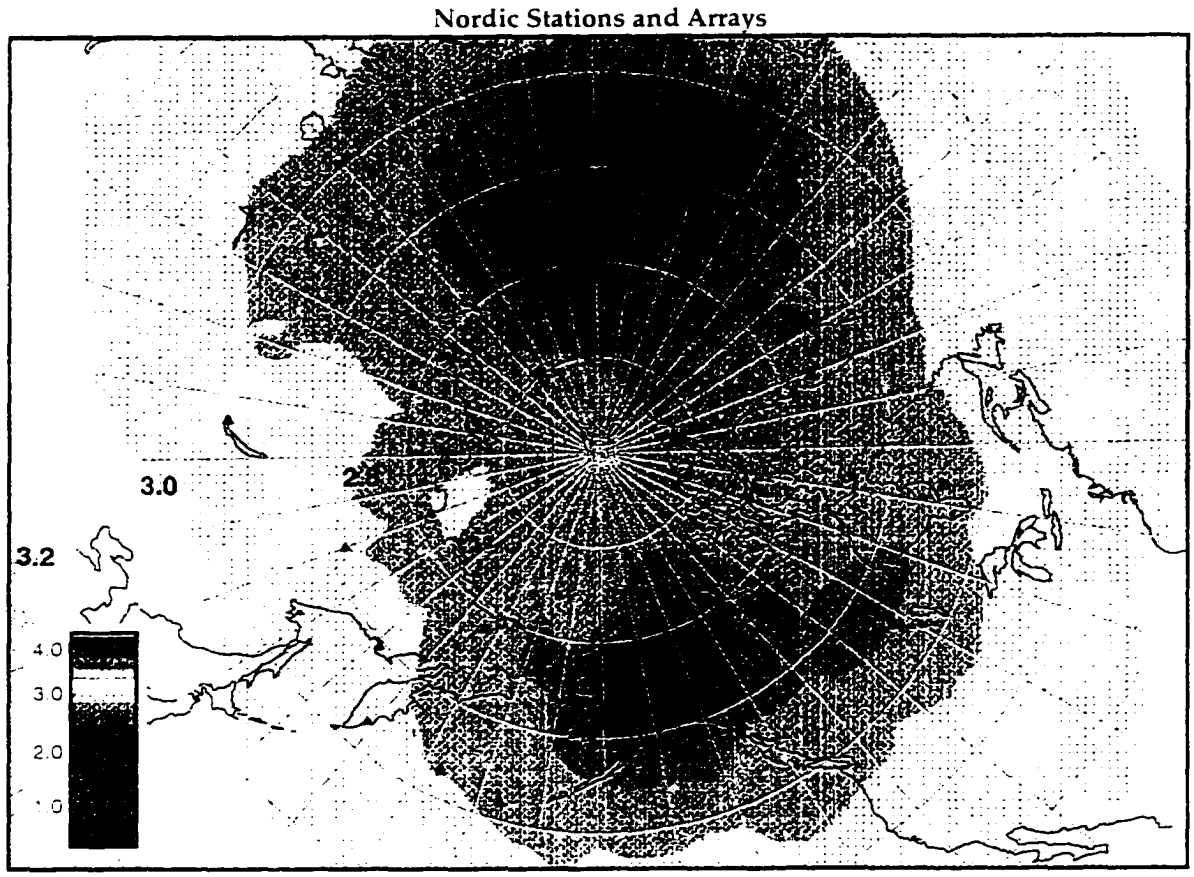

Figure 4.3 d

Combining Alaskan and Scandinavian arrays along with an assortment of Nordic stations improves the predicted magnitude thresholds of Figures 4.3a-c even further.

the Alaskan arrays (Figure 4.3b); for the Alaskan arrays combined with the Scandinavian arrays NORESS, Spitsbergen, FINESA, and ARCESS (Figure 4.3 c); and for a collection of Nordic stations and arrays around the entire Arctic (Figure 4.3 d). According to these predictions, the borehole arrays of the University of Alaska perform at least as well, if not better than the network of 200 short-period, regional stations of the Alaska network in all but the most dense parts of the Alaskan regional network. For this reason, plots 4.3b through 4.3d are computed with the Alaskan array stations only. The Alaskan arrays alone cover the interior of the state fairly well, especially with the addition of a proposed new array near Anchorage; but the coverage decreases over the polar cap, as expected. Addition of the NORSAR arrays substantially improves this, creating a "corridor" of high sensitivity directly over the North pole and across part of the region with the extended seismicity of the mid-Atlantic ridge. The addition of single IRIS stations in the Former Soviet Union improves the coverage in Eastern Siberia and the Laptev sea. The possible addition of Japanese stations could substantially improve our monitoring of Eastern Siberia and the junction between the Eurasian plate and North American plate, as well as the many microplate boundaries in the region of the Okhotsk sea. Finally, various other northern stations such as those in Canada, England, Scotland, and Greenland round out the coverage of the entire Arctic.

4.5 Detected Microseismicity: Station Quality

We begin our observations on the array data themselves with two microseismic events that show the high quality of the array instruments and installations compared to the rest of the Alaskan seismic network. These events were both missed in processing by the Iceworm system described in Chapter 2, and by the analysis at the AEIC.

The first earthquake is a local-magnitude 0.6 event which occurred July 16, 1997 approximately 40 km from the Indian Mountain array. This event was discovered in the data accidentally during other processing. Waveforms from the Indian Mountain array and from the nearby station IMA are shown for this event in Figure 4.4a. The clear superiority of the Indian-Mountain borehole array stations can be seen by comparing any one of them to IMA, a Teledyne-Geotech S13 instrument installed on the earth's surface. The P-wave is not even visible in the unfiltered seismogram from IMA. On the array stations, the P-wave signal-to-noise ratio varies between 3 and 7. Our location for this event (Figure 4.4b), obtained with the Datascope *dbloc2* software, comes from a standard travel-time inversion based on P and S picks at the array stations. The magnitude was computed with the automatic local-magnitude calculation program *dbml*, described in Chapter 3. This event appears to be part of the Indian Mountain cluster of seismicity, for which there are records of activity since the beginning of seismic recording by the Geophysical Institute [Estabrook *et al.*, 1988].

The second event was discovered only because it was felt near Fairbanks. A resi-

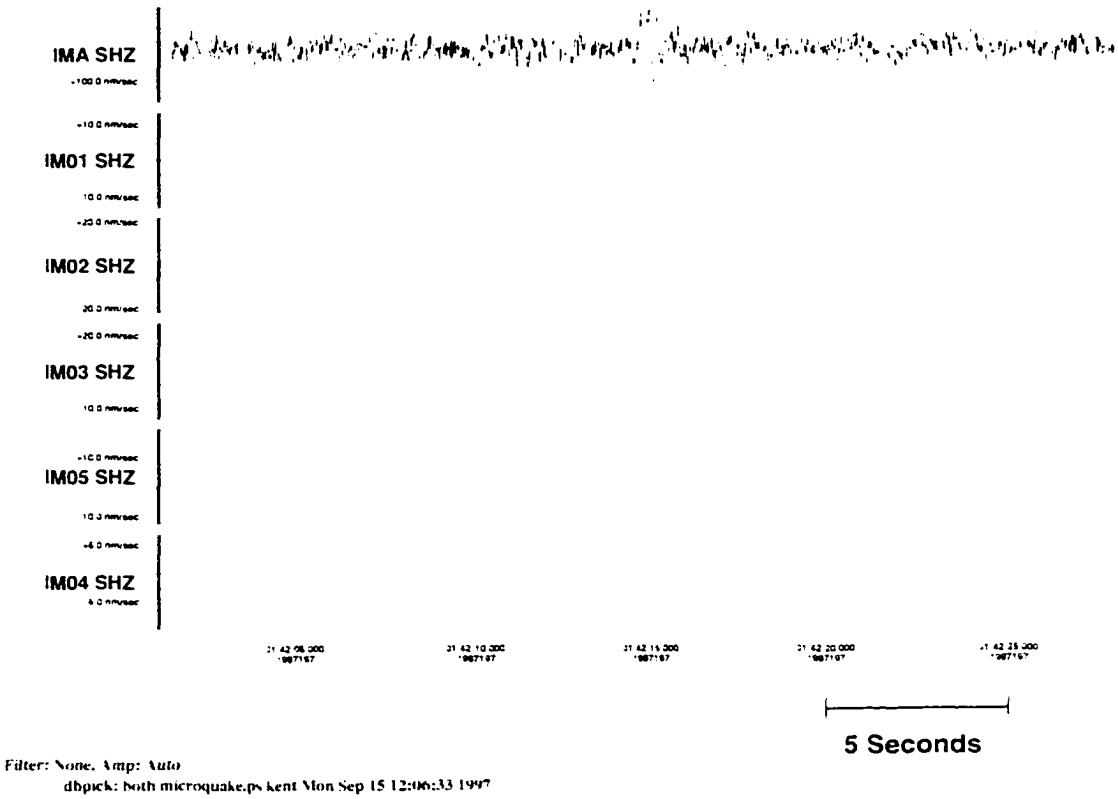

Figure 4.4 a

Waveforms for an M_L 0.6 event 40 km from the Indian Mountain array. Comparison of the IMA waveform to any of the Indian Mountain array stations shows the clear superiority of the borehole array installations to the surface installation of the IMA instrument.

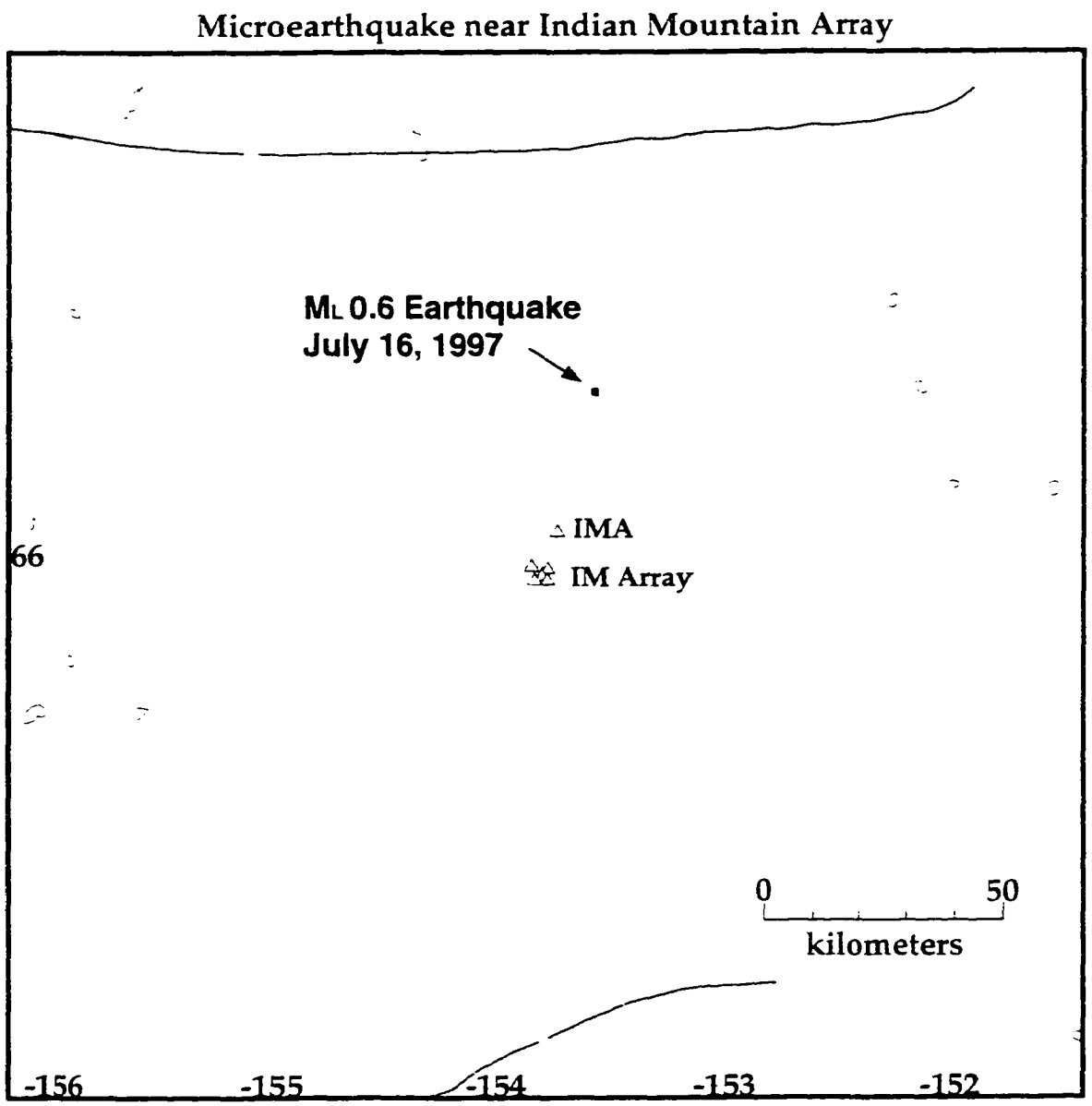

Figure 4.4 b

This map shows the location of the earthquake whose waveforms are displayed in Figure 4.4a. The triangles on the map indicate the locations of the station IMA and the five Indian Mountain array stations. Note the close spacing of the stations in the Indian Mountain array. This event appears to be part of the Indian Mountain cluster of microseismicity [Estabrook *et al.*, 1988].

dent called AEIC concerned that explosives were being used near his house. From the dilatational first motions of the waveforms in Figure 4.5a this is clearly a small earthquake, not an explosion. The location of the event is shown in Figure 4.5b. As with the Indian Mountain event, this location was determined with *dbloc2* from P and S arrivals on all of the array stations . The magnitude of this event computed from station IL02 with the *dbml* program is 1.8. One would hope to trigger on and detect an event of this size with the regional network. This event is clear evidence that there is room for improvement in Ice-worm event detection, and that the array stations themselves should be able to contribute to interior-Alaska seismicity monitoring even without the added benefits of array processing.

4.6 Array-processing to Expand Spatial Coverage of Event Detection Around Alaska: Chukchi Sea Event

One of the greatest benefits of the arrays is the ability to detect events outside the Alaskan regional network. For example, seismicity around the Bering sea will be important for analysis of the Bering Sea block model proposed by Mackey *et al.* [1997]. These authors suggest an independent Bering Sea block in motion with respect to the North American plate, driven by westward extrusion of southwestern Alaska due to compression in southern Alaska from Pacific-plate subduction and accretion of the Yakutat terrane. A large part of their argument rests on analysis of seismicity that outlines the Bering Sea block. Catalogs of this seismicity come from four sources: global catalogs; a Western

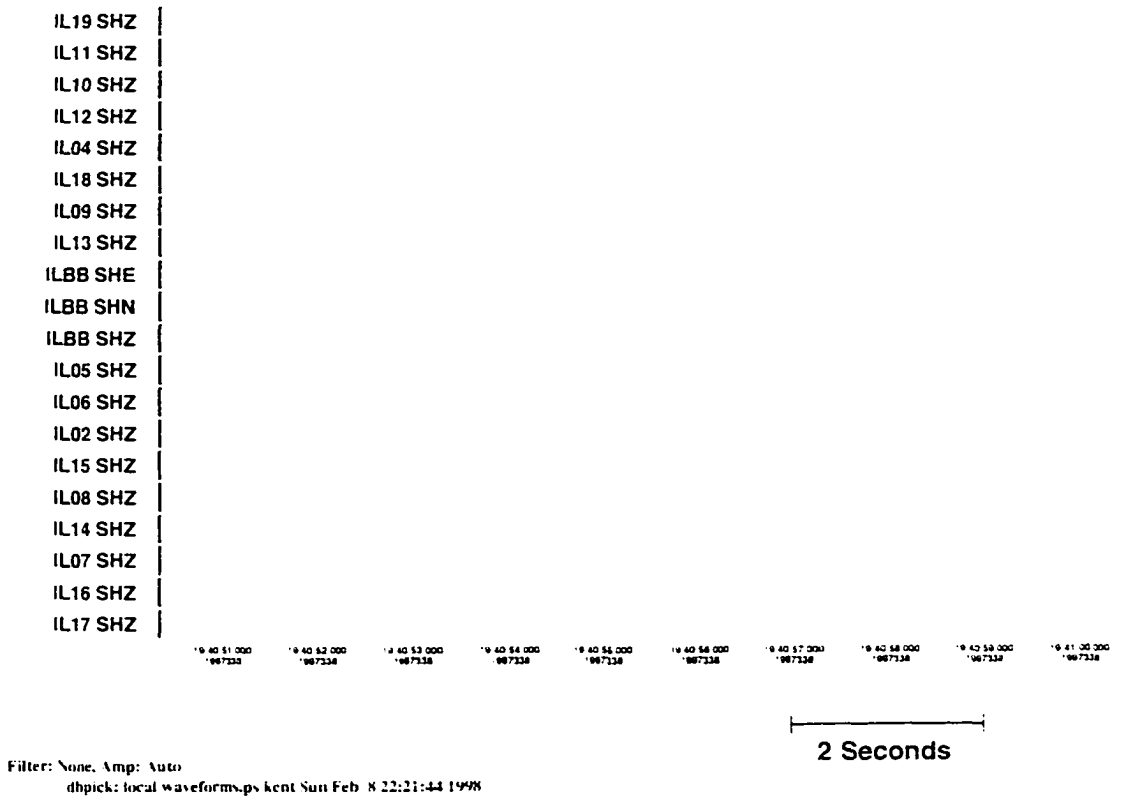

Figure 4.5 a

Waveforms from an M_L 1.8 event near the Eielson array. This earthquake was felt in North Pole, Alaska. The earthquake was not detected by the Iceworm system of Chapter 2, nor by the Alaska Earthquake Information Center.

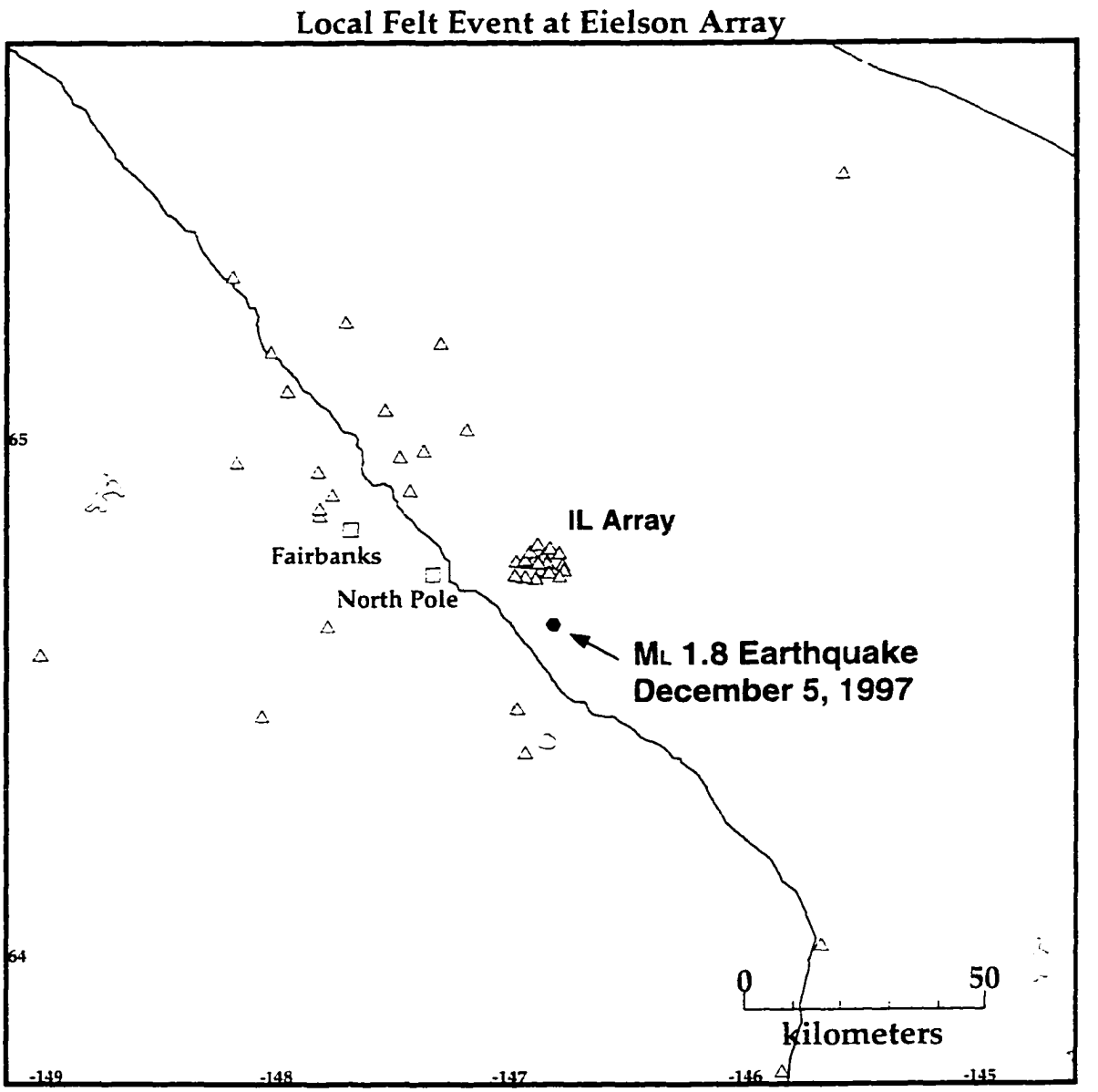

Figure 4.5 b

Location of the earthquake (hexagon) near the Eielson array, the waveforms from which are shown in Figure 4.5a. Triangles show nearby seismic stations. The dark, diagonal line through the center of the map is the Alaskan oil pipeline.

Alaska seismic network which is no longer running; a catalog of single-station locations from a seismometer in Chukotka, with clear problems in the locations [Mackey *et al.*, 1997]; and the Chukotka regional network, also no longer running.

With array processing, we can reopen study of the Bering block seismicity beyond the coverage of the global catalogs. To demonstrate this, we locate an event in the Chukchi sea that did not appear in any other catalog. Initial discovery of this Chukchi sea event was serendipitous. A temporary, broadband seismometer was deployed at Tin City on the tip of the Seward Peninsula for 24 hours on September 9th, 1997 for a site-survey. Review of the data from this station (Figure 4.6a, top 3 traces) revealed an event which did not associate with any event in available catalogs. FK analysis at the Indian Mountain array for this event yielded azimuth, slowness, and arrival-time information for the P and S phases. Figures 4.6 b and c show the results of the FK analysis. The top trace of Figure 4.6 b shows the P-wave from the Chukchi event, filtered with a two to four Hertz Butterworth bandpass filter. Two short vertical bars show the time window for the FK plot. At the lower left, an FK diagram reveals a peak power at a backazimuth of 290.1° and an apparent velocity of 8.2 km/sec. The beam formed at this slowness is shown in the second trace in Figure 4.6b. Note the reduction in noise level before the seismic arrival on the best beam, compared to the single-element trace. A similar plot for the S-wave is shown in Figure 4.6c, which yields an azimuth of 298.4° and an apparent velocity of 3.5 km/sec. When we combine these array measurements with the P and S arrival times for the temporary station, we can locate the event in the Chukchi sea as shown in Figure 4.6d. Adding P and S arrival times

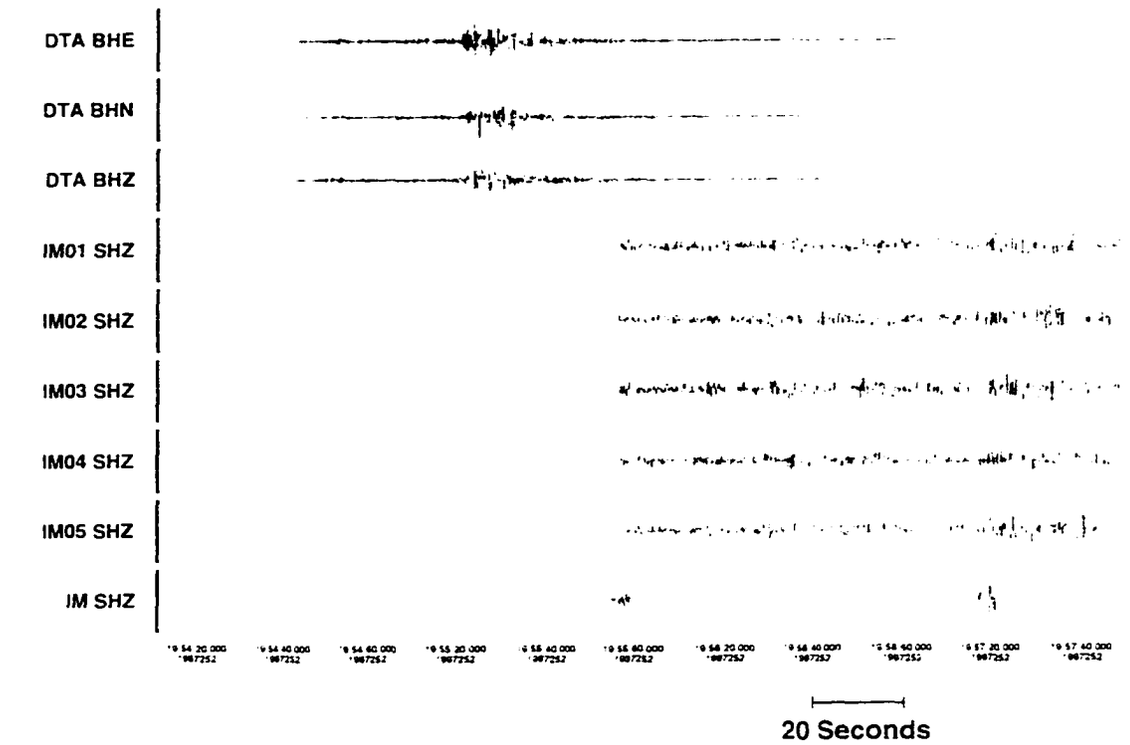

Figure 4.6 a

Waveforms from a Chukchi Sea event with M_L 4.0 detected on September 9, 1997. The top three traces are from a temporary broadband installation in Tin City, Alaska. The next five traces show the waveforms from this event at the Indian Mountain array. The last, segmented trace shows the computed best-beams for the Indian Mountain array for P and S arrivals from this event. Expanded plots of these best beams are shown in Figures 4.6b and c.

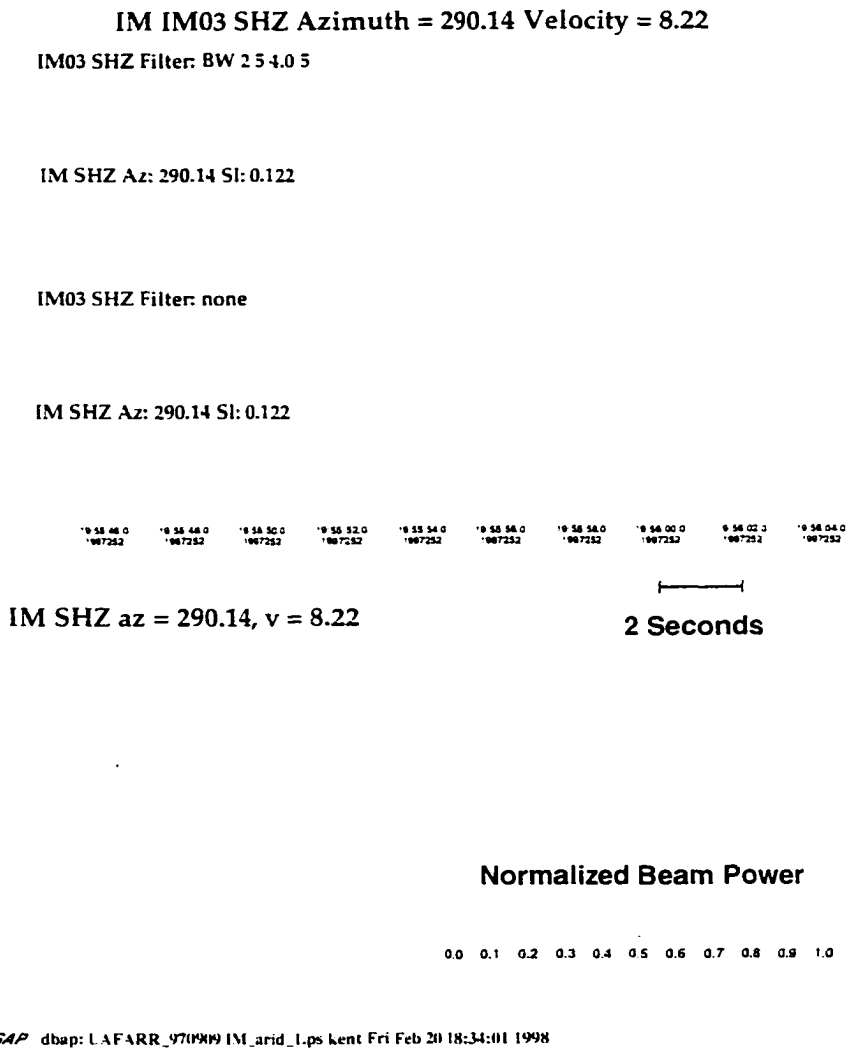

Figure 4.6 b

The top two traces show the center element of the Indian Mountain array, then the best beam for the P phase arrival (both filtered from 2 to 4 Hertz) for the Chukchi Sea event.. The bottom two traces show the same with no filtering. The contour plot at lower left, with scale bar at lower right, shows semblance vs. North-South slowness (vertical axis) and East-West slowness (horizontal axis). The slowness plot spans -0.4 sec/km to 0.4 sec/km in each dimension. The circles correspond to apparent velocities of 10, 5, and 3.3 km/sec. Further discussion of these results is presented in Section 4.6 of the text. The vertical ticks on the waveforms indicate the time window of data used in the FK processing.

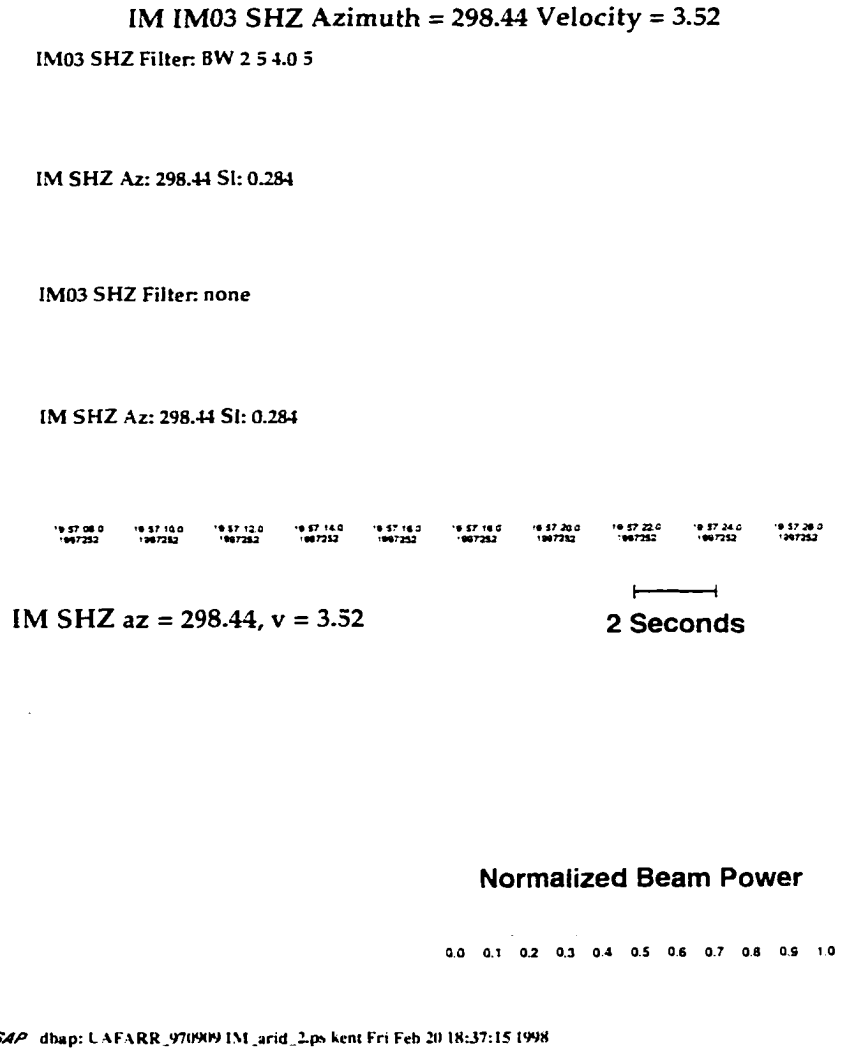

Figure 4.6 c

The top two traces show the center element of the Indian Mountain array, then the best beam for the S phase arrival (both filtered from 2 to 4 Hertz) for the Chukchi Sea event.. The bottom two traces show the same with no filtering. The contour plot at lower left, with scale bar at lower right, shows semblance vs. North-South slowness (vertical axis) and East-West slowness (horizontal axis). The slowness plot spans -0.4 sec/km to 0.4 sec/km in each dimension. The circles correspond to apparent velocities of 10, 5, and 3.3 km/sec. Further discussion of these results is presented in Section 4.6 of the text. The vertical ticks on the waveforms indicate the time window of data used in the FK processing.

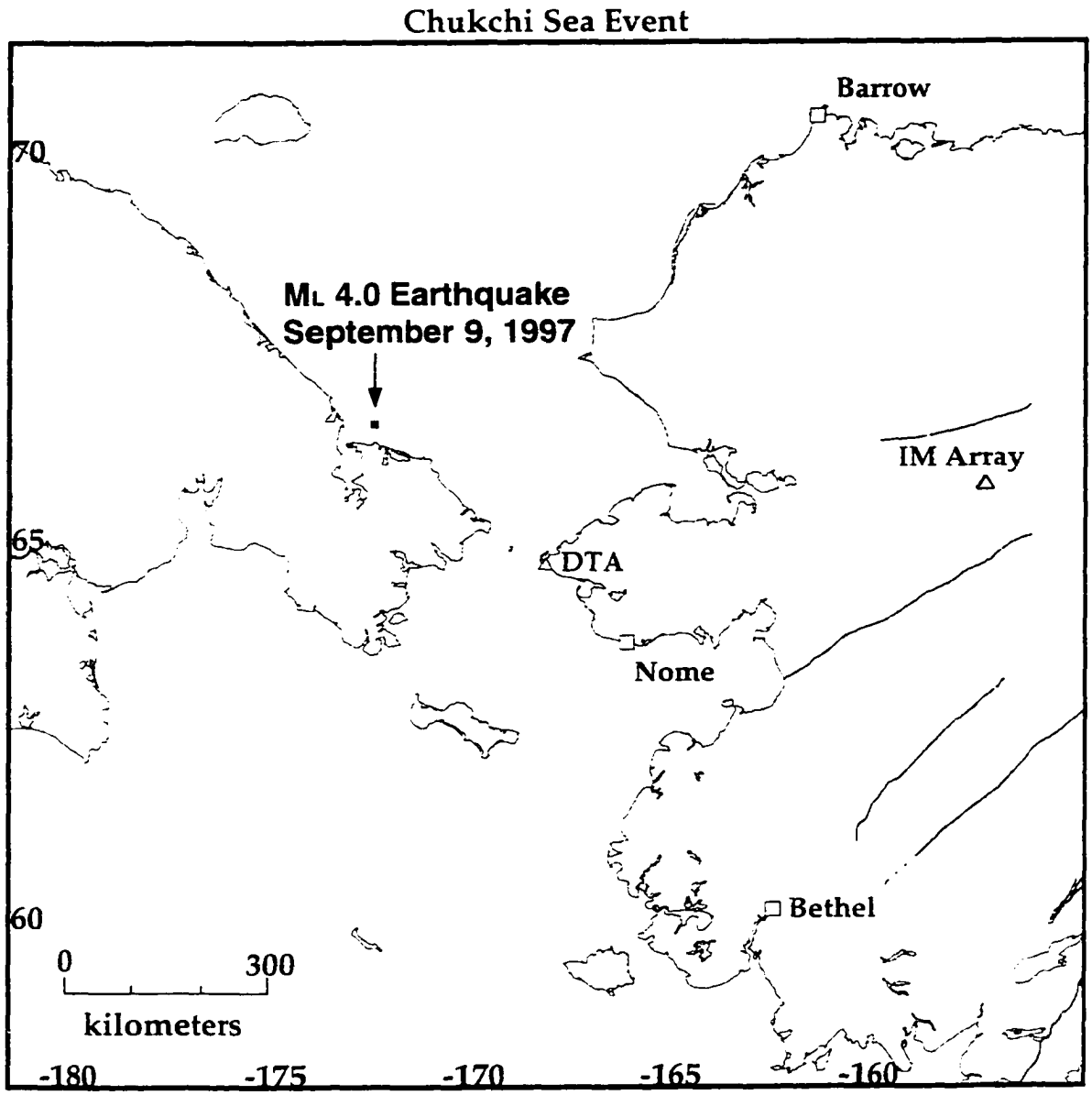

Figure 4.6 d

This is a map of the location computed for the Chukchi Sea event based on the temporary seismic station at Tin City, Alaska (shown by the triangle labelled DTA) and on the Indian Mountain array. This event lies in a cluster of seismicity outlining the Bering Sea block proposed by Mackey *et al.* [1997]. Addition of P and S arrival time data from a seismometer at Anadyr moves this location 76 km east, not shown.

from station Anadyr [Fujita, *pers. comm.*, 1997] at 64.735° North, 177.4955° East, our epicentral solution moves 76 km eastwards, still in the same cluster of seismicity as our original location. Single-station measurements from station IM03 give a local magnitude of 3.97 and a body-wave magnitude of 2.5. The disagreement may stem from the 8 degree station-to-event distance for this event, beyond the normal maximum distance for local magnitudes but short of the teleseismic distance for M_b.

4.7 Teleseismic Locations and the Resolution of Regional Associator Problems

The four arrays discussed here are actually capable of locating events not only slightly outside of continental Alaska, but also all across the globe. To demonstrate this we show a location for an M_b 4.6 (M_L 3.9) event in Iceland, 44 degrees away from the Eielson array. This earthquake occurred on July 22, 1997. We have determined the location based on P phases from the Eielson, Indian Mountain, and Beaver Creek arrays (Burnt Mountain data were not available at the time due to hardware problems), plus the single-component station FX01 on Attu Island. Our epicentral result is compared to the global catalogs in Figure 4.7. The location was computed with the *dblocsat2* software from the Datascope Seismic Application Package. *dblocsat2* is essentially an implementation of the TTA-ZLOC procedure outlined in Bratt and Bache [1988]. This procedure uses backazimuth and arrival-time measurements in a least-squares-inverse location algorithm. The array location for the Icelandic event agrees to within 50 km with the locations from PDE and REB global catalogs. This level of precision is quite reasonable, based on past work with array

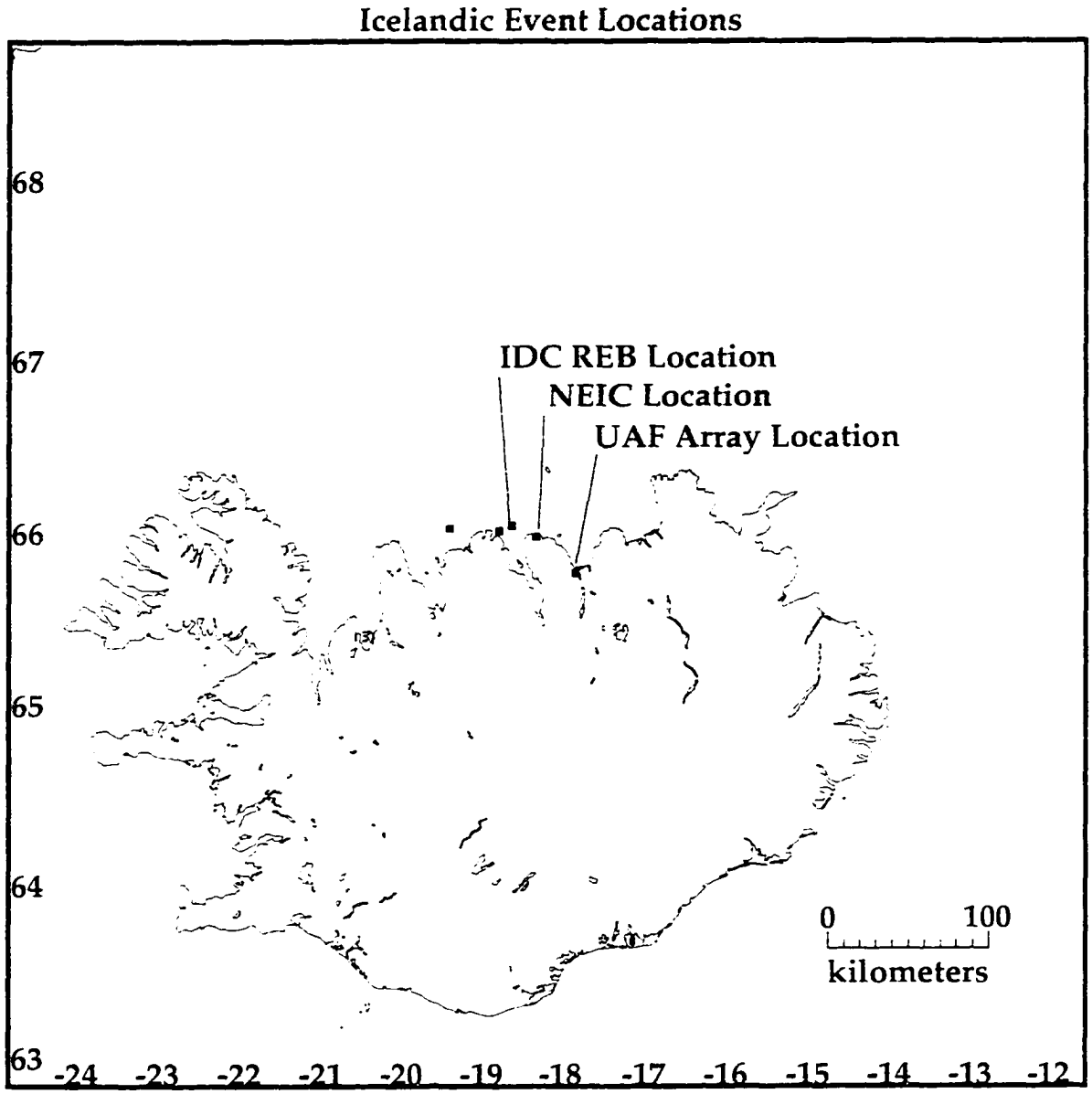

Figure 4.7

This map shows three locations (squares) for an M_b 4.6 teleseismic event in Iceland that occurred on July 22, 1997. The locations (labelled) are from the Reviewed Event Bulletin of the International Data Center; from the Preliminary Determination of Epicenters from the USGS; and from the Alaskan arrays, as discussed in Section 4.7 of the text. The two unlabeled epicenters are for an M_b 3.4 event preceding the main event by 15 minutes and an M_b 3.6 event following the main event by 20 minutes.

locations, as discussed in Ringdal and Husebye [1982]. In the case of this Icelandic event, convergence of the location with *dblocsat2* to the known location of the event was quite sensitive to the relative weighting of the input information into the inversion.

An M_b 5.7 event in Hokkaido that occurred on November 15, 1997 (see the map of Figure 4.8) illustrates the relevance of teleseismic location ability to regional seismological monitoring. The Earthworm regional associator built the phases arriving from this event into three false locations, shown in Figure 4.9. Automatic magnitude calculations for these false events reported M_L values of 3.5 in Cook Inlet, 4.4 Northeast of Prince William Sound, and 4.7 North of the Kobuk fault. All three of these meet alarm criteria for the AEIC. Two of the reported events lie near the Alaska oil pipeline. Clearly, a decrease of false-alarms will result from the incorporation of array processing into regional monitoring. In order to take full advantage of this, we will have to incorporate the array data into the near-real-time phase association and event location process.

In the case of the Hokkaido event, convergence on the correct location required increasing the slowness uncertainty from the *dblocsat2* default of 0.01 sec/km to 0.1 sec/km, vastly de-emphasizing slowness measurements in the inversion for location. With the default slowness uncertainty, the location for the Hokkaido event came out in the mid-Pacific at approximately 30° N 171° E, 25 degrees Southeast of the location computed by the National Earthquake Information Center (NEIC). De-emphasizing slowness in the inversion allowed the solution to converge 8 km away from the NEIC location, as shown in Figure 4.8. Inspecting the raw data for the Hokkaido event and using the IASP91 travel-

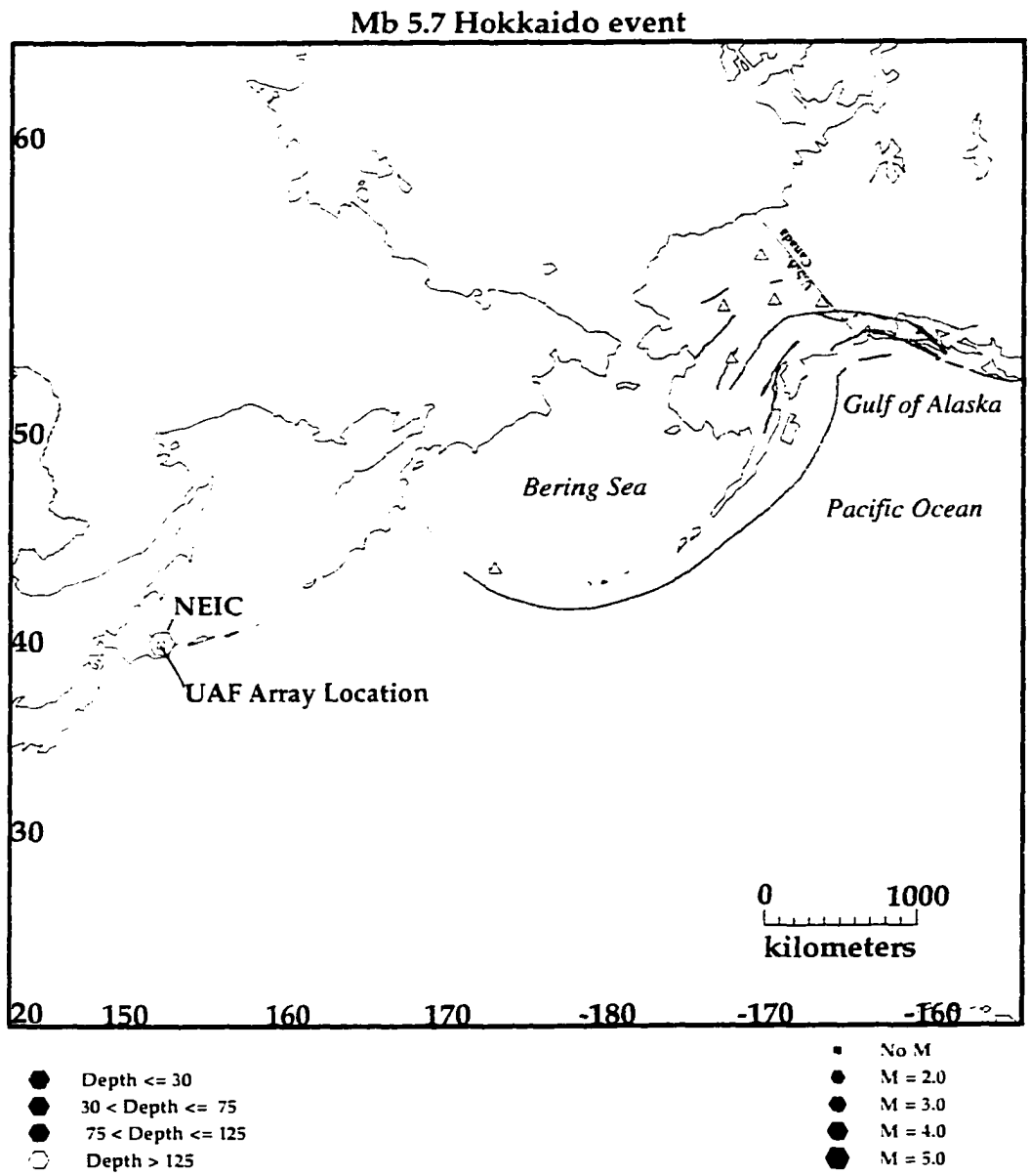

Figure 4.8

This map shows locations for an M_b 5.7 earthquake that occurred in Hokkaido, Japan on November 15, 1997. The epicentral estimate from the National Earthquake Information Center and the epicentral estimate from the Alaskan arrays and the stations TT01 and FX01 (triangles) agree to within 8 km.

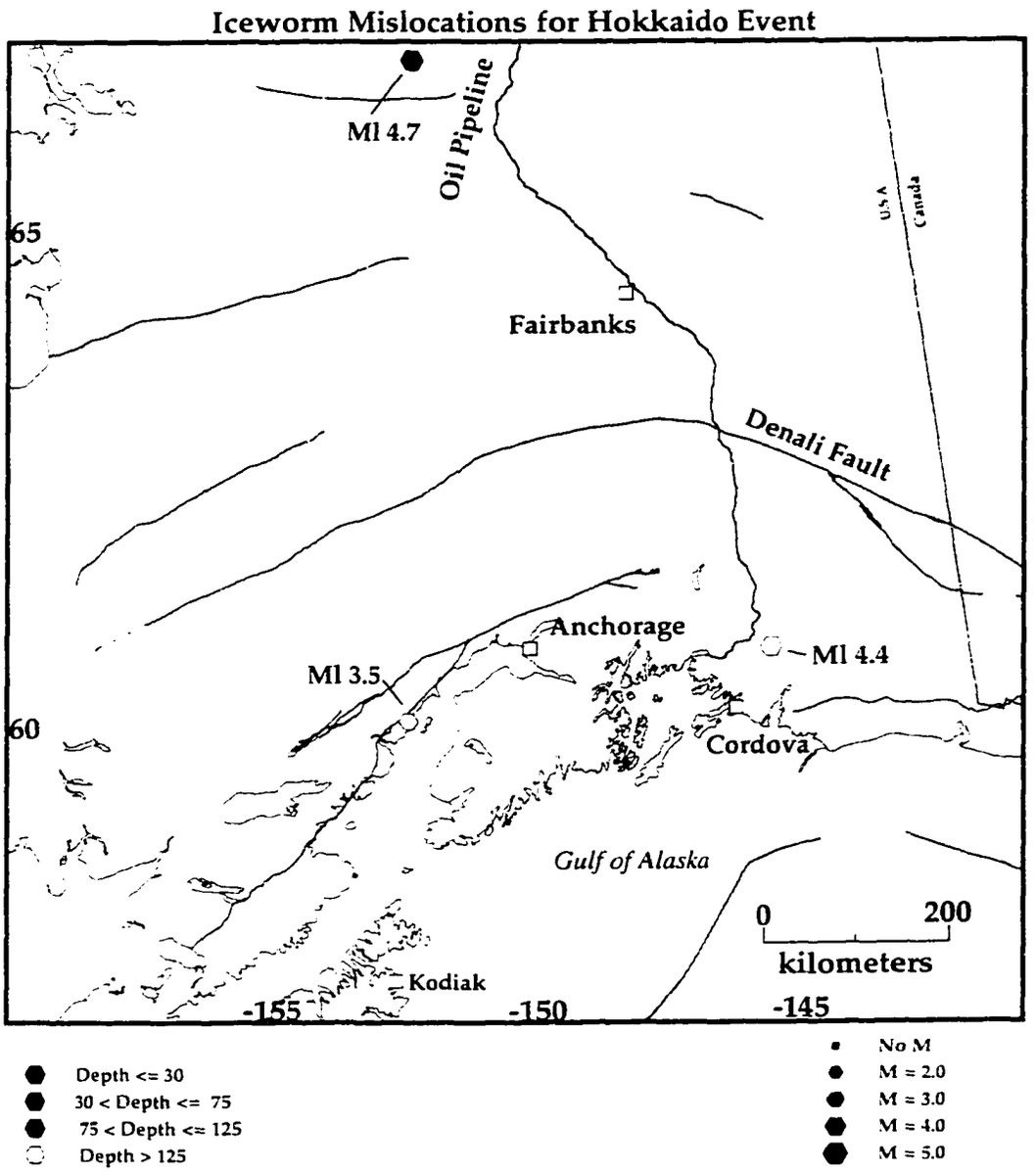

Figure 4.9

This map shows three mislocations announced by the Iceworm system of Chapter 2 for the Hokkaido earthquake shown in Figure 4.8. The magnitudes shown are those computed by the automatic *local_mag* module described in Chapter 2 for these fictitious local events.

time predictions for phases based on the NEIC location, we were able to identify P, S, PcP, and ScP arrivals at the array stations, all of which were used in the location. Azimuth residuals were computed by subtracting the observed azimuth of the wavefront obtained by FK analysis from the station-to-event azimuth pointing from the array to the event location. There are notable differences in the azimuth residuals between P phases and the ScP and PcP core-bounce phases at all the arrays, however with just one event it is hard to observe a clear pattern. At Eielson, we see a -18.6° residual for the P phase, with ScP 27 degrees clockwise at 9.1°. For the Indian Mountain array, the P phase has an azimuth residual of 5.5°, where the PcP phase is 6 degrees further clockwise at 11.4°, and the ScP phase at 18.9° is 12 degrees further clockwise than the P phase. Burnt Mountain shows the opposite offset: The P phase has an azimuth residual of -9.2°, with an ScP residual of -25.5°, 16 degrees counterclockwise of the P phase. Finaily, Beaver Creek has a P-phase azimuth residual of -3.5° and an ScP residual of -6.4°. Such residuals are not uncommon [Bame *et al.*, 1990]; though the difference between residuals at the same array for different travel paths suggests that effects of structural heterogeneity on the wavefield may become apparent with studies of regional-event azimuth residuals. The residuals for the S-phases are disturbingly high: 68 and 66 degrees at Eielson and Indian Mountain, respectively; 99 degrees at Burnt Mountain; and -13 degrees at Beaver Creek. Such large residuals immediately lead one to suspect misassociation of phases with the event; yet similar results for S-wave azimuth residuals appear for some Aleutian events in the REB catalog. We explore the detected azimuth residuals further in Section 4.9 of this chapter.

4.8 Detection and Location of Aleutian Earthquakes

We have studied a number of Aleutian events in order to establish the ability to detect and locate earthquakes in the Aleutians. We present several representative examples to illustrate our progress. First, to show the improved detection sensitivity of the array stations, we process a magnitude 3.2 (M_L) event that occurred January 28, 1998 near Unimak Island, Alaska. The AEIC location for this event is 53.8898° North latitude, 164.1678° West longitude at a depth of 10 km. We observed this event on the Indian Mountain array, a distance of 13.1 degrees or 1460 km from the epicenter. The P-wave signal-to-noise ratio on the center element IM03 was 2.74, measured on a trace filtered with a 5-pole Butterworth bandpass filter with a passband from 2 to 4 Hertz. The FK grid, raw and filtered data, and best beam are shown in Figure 4.10. FK processing yielded an azimuth of 218.7° for the incident wavefield from this earthquake, with an apparent velocity of 11.21 km/sec across the array. The best beam formed with these parameters is shown in Figure 4.10. Note the reduction in the noise level on the beam compared to the center element of the Indian Mountain array. The Signal-to-noise ratio measured on the best beam from this event is 10.0, a factor of 3.6 improvement over the center element. If we require a minimum signal-to-noise ratio of 2 in order to claim that we have successfully detected an event, the UnimakIsland event has a signal-to-noise ratio five times higher than the minimum. Given the observed M_L of 3.2, we can project a minimum detectable event

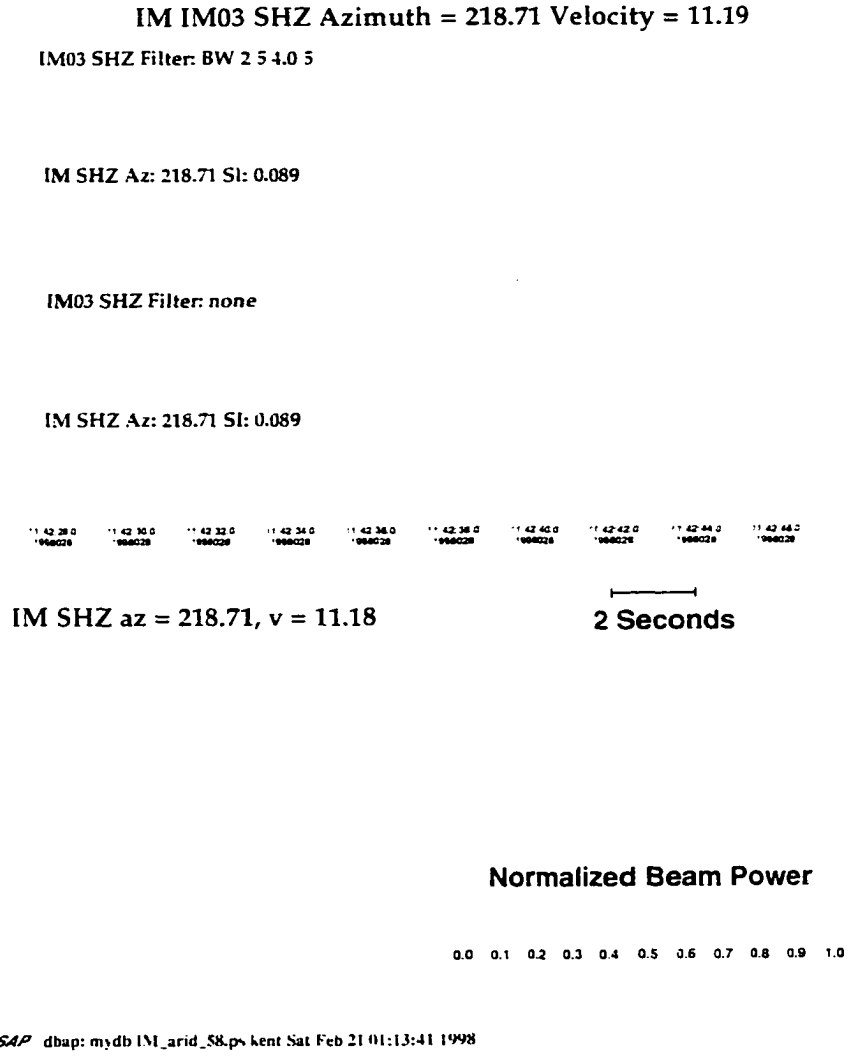

Figure 4.10

This figure shows array-processing results for an M_L 3.2 earthquake that occurred near Unimak Island, Alaska on January 28, 1998. The top two traces show the center element of the Indian Mountain array along with the best beam, filtered with a 2 to 4 Hertz Butterworth bandpass filter. The bottom two traces show the same, without the filter. Note the signal-to-noise improvement of the best beam over the center element. The contour plot at left, with axes as in Figure 4.6b, shows a peak power at an azimuth of 218.71 degrees with an apparent velocity across the array of 11.18 km/sec. The vertical ticks on the waveforms indicate the time span of data used in the FK analysis.

magnitude of 3.2 - log(5), or M_L 2.5. This is close to agreement with the magnitude-threshold predictions of section 4.4, which (referring to Figure 4.3b) gives M_{min} of 2.8 for the Unimak Island region. Note that that minimum-magnitude is for location of the event, not just detection. The factor of 3.6 improvement in signal-to-noise with beamforming is better than the theoretically expected factor of 2.24 ($\sqrt{N}$, for N=5) for the Indian Mountain array. This is reminiscent of the observations of Kvaerna [1989] for the NORESS array (see also Mykkeltveit *et al.* [1990] for further discussion). Kvaerna observed negative noise correlations in the 2-4 Hz band for some inter-station spacings at NORESS, indicating a possibility of noise suppression beyond $\sqrt{N}$.

As an example of our ability to locate events in the Aleutian Islands, we present an M_L 6.6 event that occurred near Adak Island on June 17, 1997 at latitude 51.347° North, longitude 179.332° West (taking the location from the USGS Preliminary Determination of Epicenters, which fixed the depth at 33 km). The location published by the International Data Center in the Reviewed Event Bulletin agrees with this to within 12 km. We have relocated the event based on P-phase, array-processed arrivals from the Indian Mountain, Eielson, and Beaver Creek arrays, plus P-phase arrival-time picks at the stations Tatalina (TT01) and Fox Broadband (FXBB) on Attu Island. With just this information, the location of the event from *dblocsat2* comes out 3.0 degrees south of the PDE location. The simple steps of adding one P and one S pick from a close-in station, FX01, plus a P-phase pick at station ADK on Adak Island, brings the hypocentral solution into close agreement with the REB and PDE catalog solutions. A map of these solutions, along with the hypocentral

coordinates announced by the Alaska Tsunami Warning Center, is shown in Figure 4.11. This shows that combined processing of the sensitive Alaskan seismic arrays with a few well-placed Aleutian stations will vastly improve our earthquake-location capabilities in the Aleutian Islands.

4.9 Measurement of Azimuth Residuals for Aleutian Earthquakes

Our initial attempts to locate events in the Aleutians, our objective in this work, were met with difficulty. This was apparently due to residuals in the FK azimuth measurements compared to the station-to-event backazimuths at the arrays. The slab is known to affect incoming phases with which it interacts, as demonstrated for example by Abers *et al.* [1996] with travel-time delays for phases dispersed through interaction with the slab.

As a first step in understanding these residuals, we imported a catalog of events from the Reviewed Event Bulletin (REB) of the International Data Center (IDC). We create a subset of earthquakes in the Aleutian Islands, covering latitudes 48° to 58° North and longitudes 170° East to 158° West. This yielded 204 earthquakes from July 2 through December 17, 1997, ranging in magnitude from M_b 2.7 to M_s 6.5. A map of these events is shown in Figure 4.12. The REB catalog comes with measured FK azimuths at the Eielson array, which, usually labelled ILAR, forms part of the alpha detection network for international test-ban treaty verification. Unfortunately the REB bulletin does not provide uncertainties for the azimuth measurements, however one can assume a standard uncertainty of 10° as an upper limit, as in Bratt and Bache [1988]. The 134 REB measurements

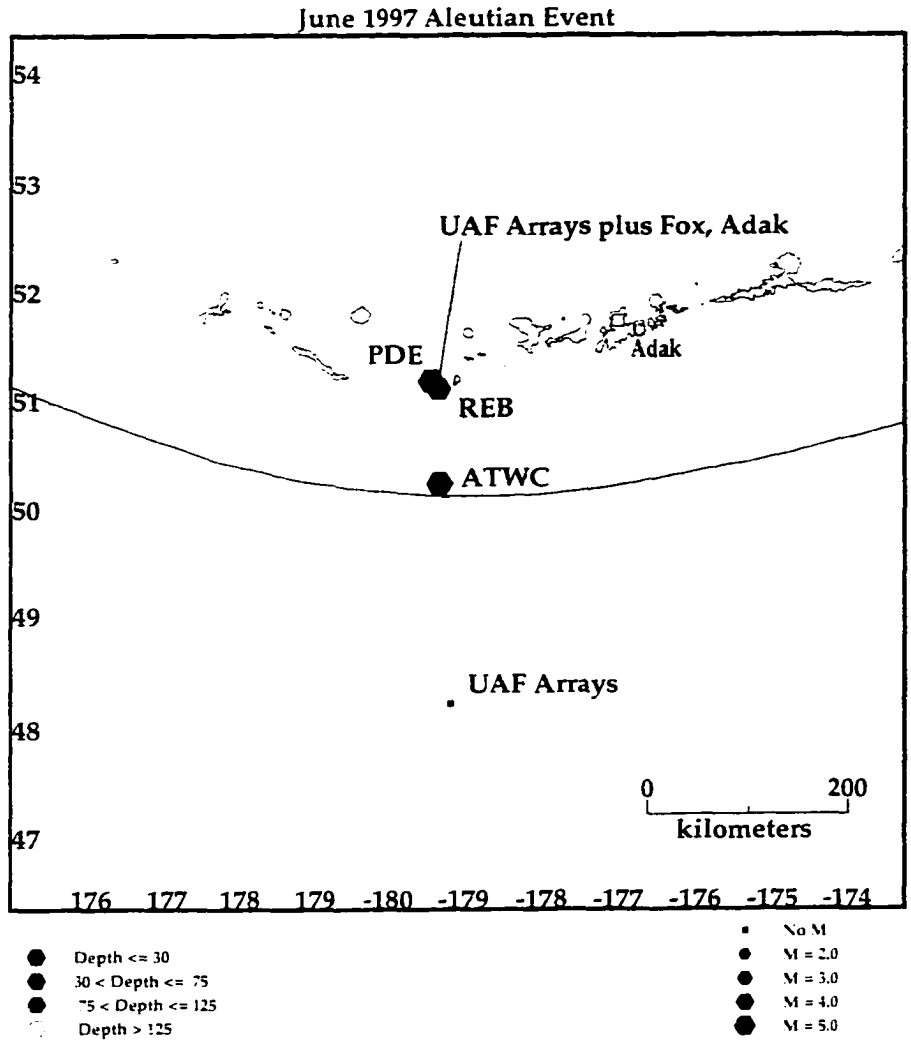

Figure 4.11

This map shows locations for an M_b 6.6 earthquake that occurred in the Aleutian Islands on June 17, 1997. The locations from the Preliminary Determination of Epicenters of the USGS, the Reviewed Event Bulletin, of the International Data Center, and the Alaska Tsunami Warning Center are shown along with two solutions based on the Alaskan arrays. In the southernmost epicentral estimate, only the arrays and the P phase from station FXBB were used. Adding P and S picks at the station FX01, plus a P pick from station ADK on Adak Island pulled the array-based location into near coincidence with the PDE and REB solutions.

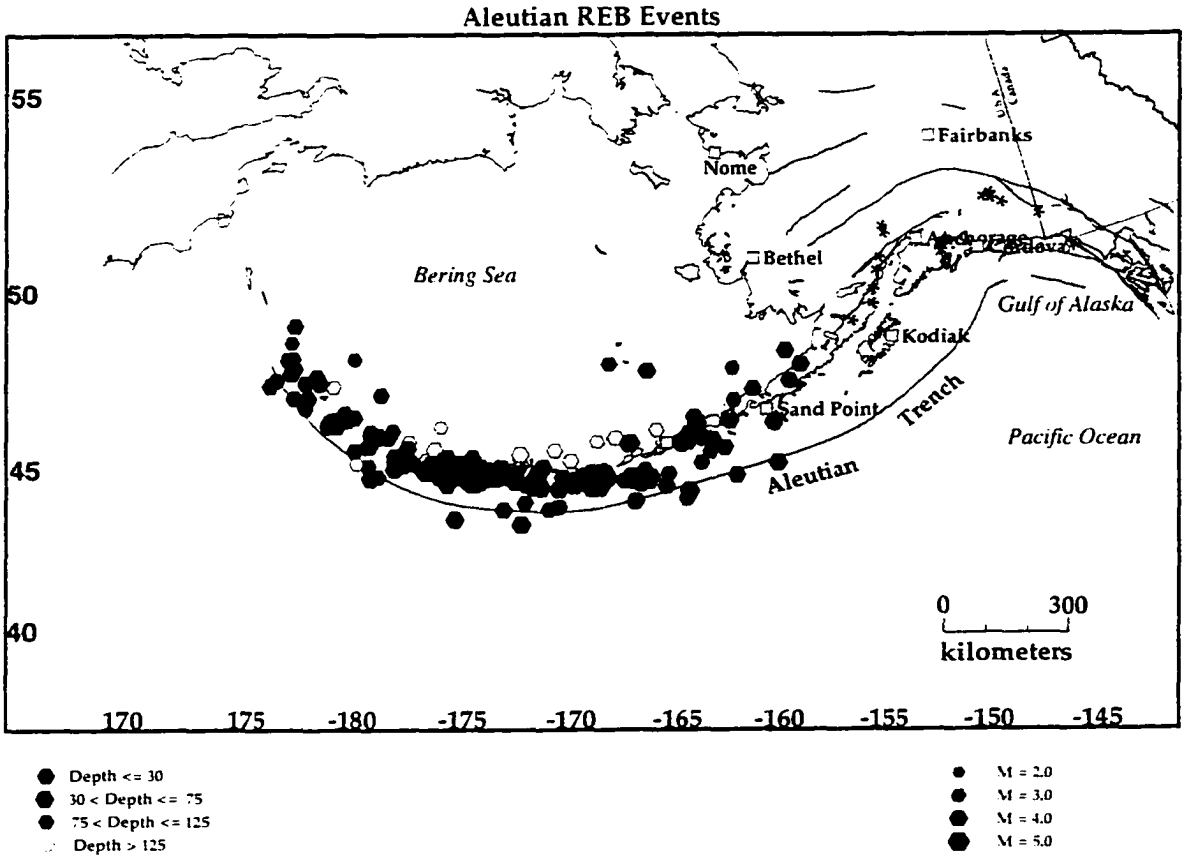

Figure 4.12

This map shows a catalog of Aleutian events from the Reviewed Event Bulletin, imported to study azimuth residuals observed for seismic arrivals from the Aleutian arc.

of P-phase azimuth residuals scatter between -20 and +15 degrees, as shown in Figure 4.13a. The median of these residuals is -6.9 degrees; the mean is -5.7 degrees. There does not appear to be any clear dependence of azimuth residual on the location of the earthquake along the chain; just a slight rotation counterclockwise of the incoming wavefield from the great-circle path from the station to the event. With the exception of a few outliers, the core-bounce phases PcP and ScP also show a constant azimuth residual for events along the Aleutian chain (Figures 4.13 b and c), though the magnitude of these residuals is much different than for the P-phase azimuth residuals. The azimuth residuals from PcP and ScP arrivals have a median of 35.8 degrees and a mean of 28.4 degrees. This includes two outliers with azimuth residuals of -160° and -54°. Omitting these raises the mean to 34.7 degrees. For the core-bounce phases, the observed backazimuth is (on average) clockwise from the great-circle direction from station to event. Finally, in Figure 4.13d we include a plot of the few available S-phase azimuth residuals from the REB phase bulletin, to show that there are two residuals with magnitudes a substantial fraction of 100 degrees, corroborating our observations of large S-phase azimuth residuals from the Hokkaido event discussed previously.

If these effects are indeed due to interaction of the wavefields with the slab, one should observe differences in the patterns of residuals amongst the four arrays. To test this, we measured FK azimuths at all four arrays for as many events and phases as possible from the catalog of REB earthquakes described above. We were rarely able to identify more than P phases, since the picking for these measurements was done on the raw data rather

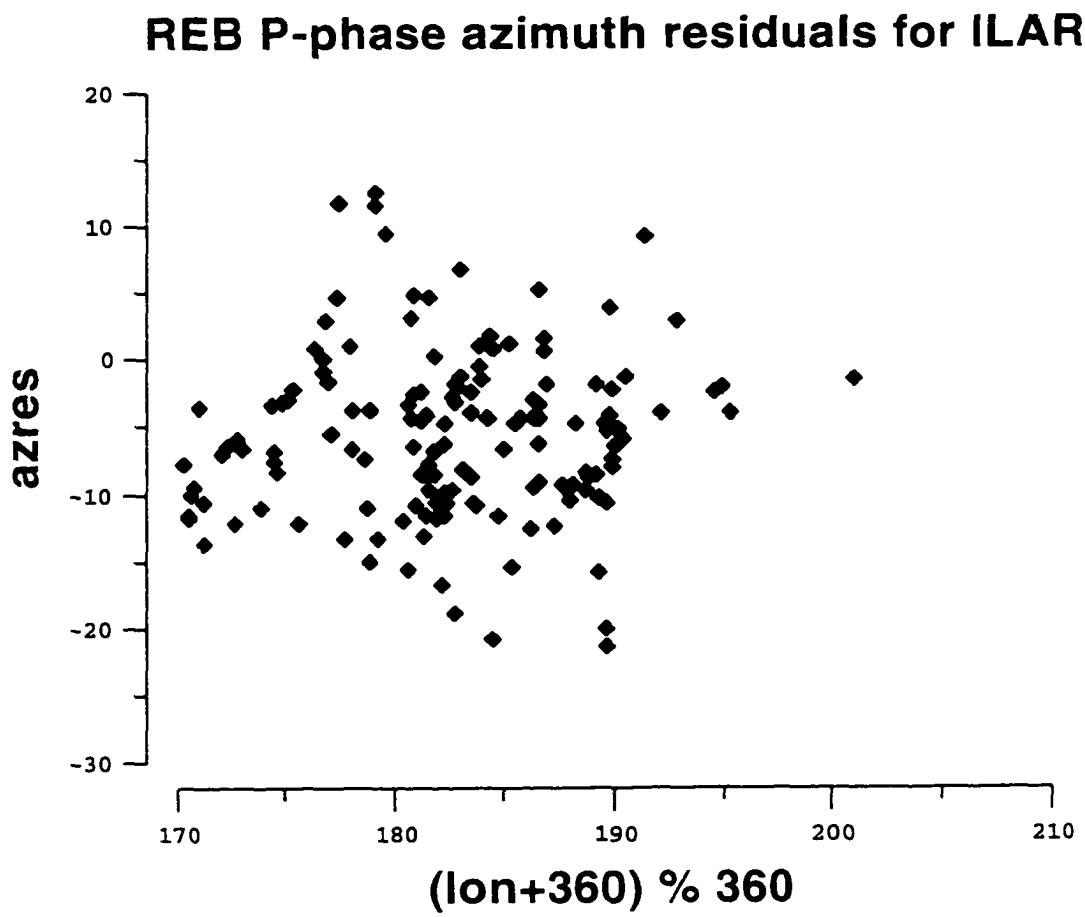

Figure 4.13 a

Reviewed-Event-Bulletin azimuth residuals observed at the Eielson array for P-phases incident from the earthquakes in Figure 4.12, plotted vs. longitudinal position of the epicenter along the Aleutian arc. For discussion, see Section 4.9 of the text.

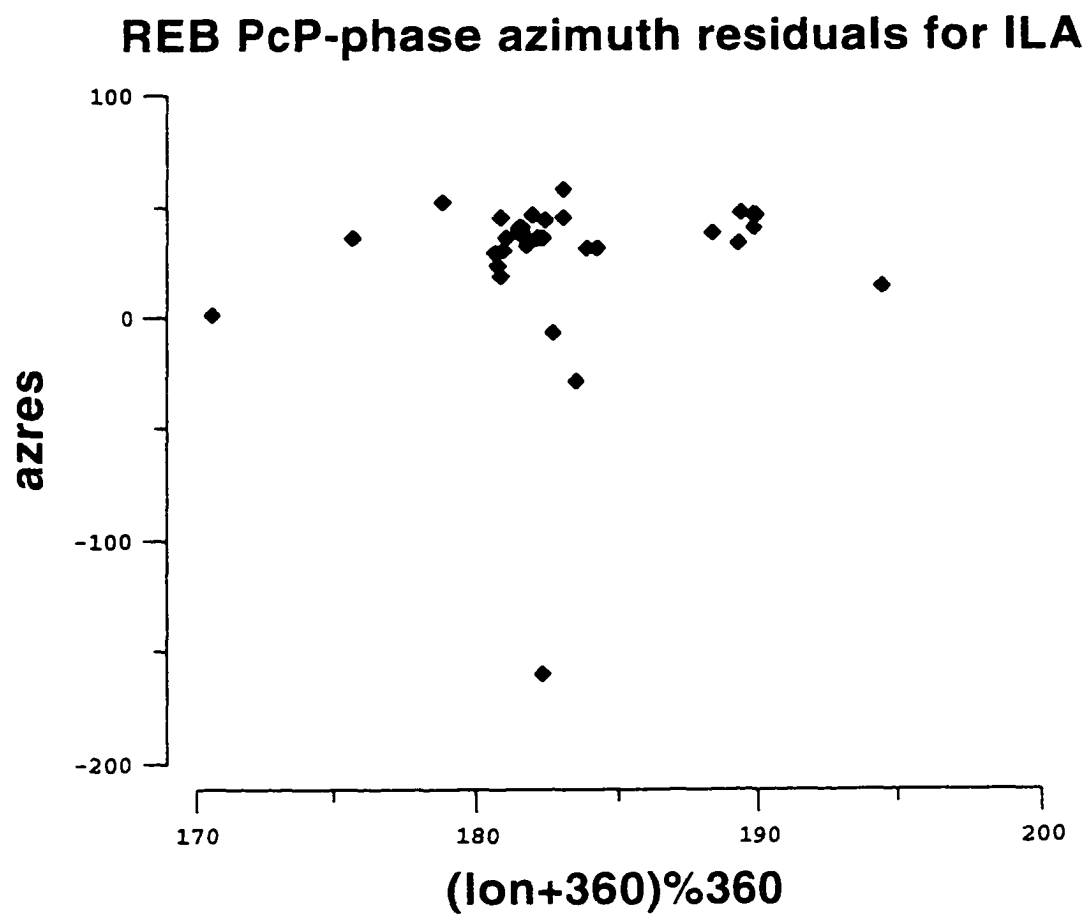

Figure 4.13 b

Reviewed-Event-Bulletin azimuth residuals observed at the Eielson array for PcP-phases incident from the earthquakes in Figure 4.12, plotted vs. longitudinal position of the epicenter along the Aleutian arc. For discussion, see Section 4.9 of the text.

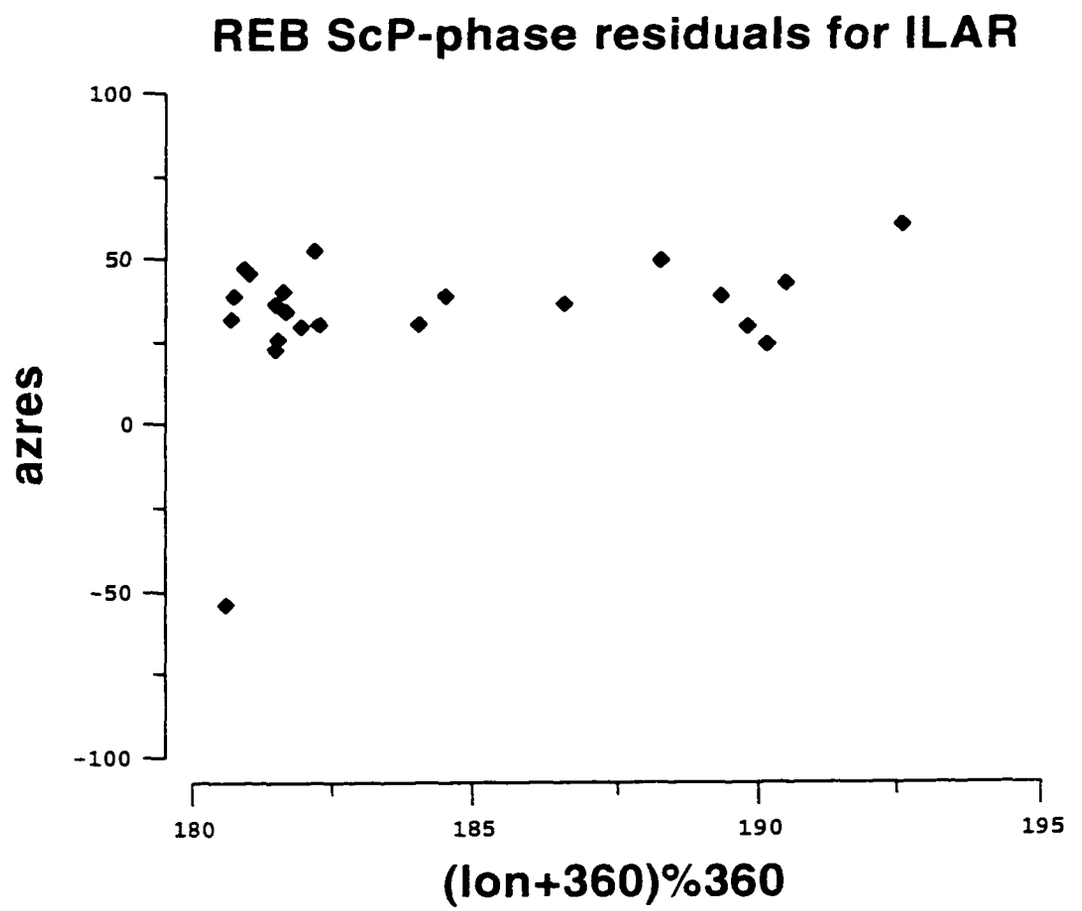

Figure 4.13 c

Reviewed-Event-Bulletin azimuth residuals observed at the Eielson array for ScP-phases incident from the earthquakes in Figure 4.12, plotted vs. longitudinal position of the epicenter along the Aleutian arc. For discussion, see Section 4.9 of the text.

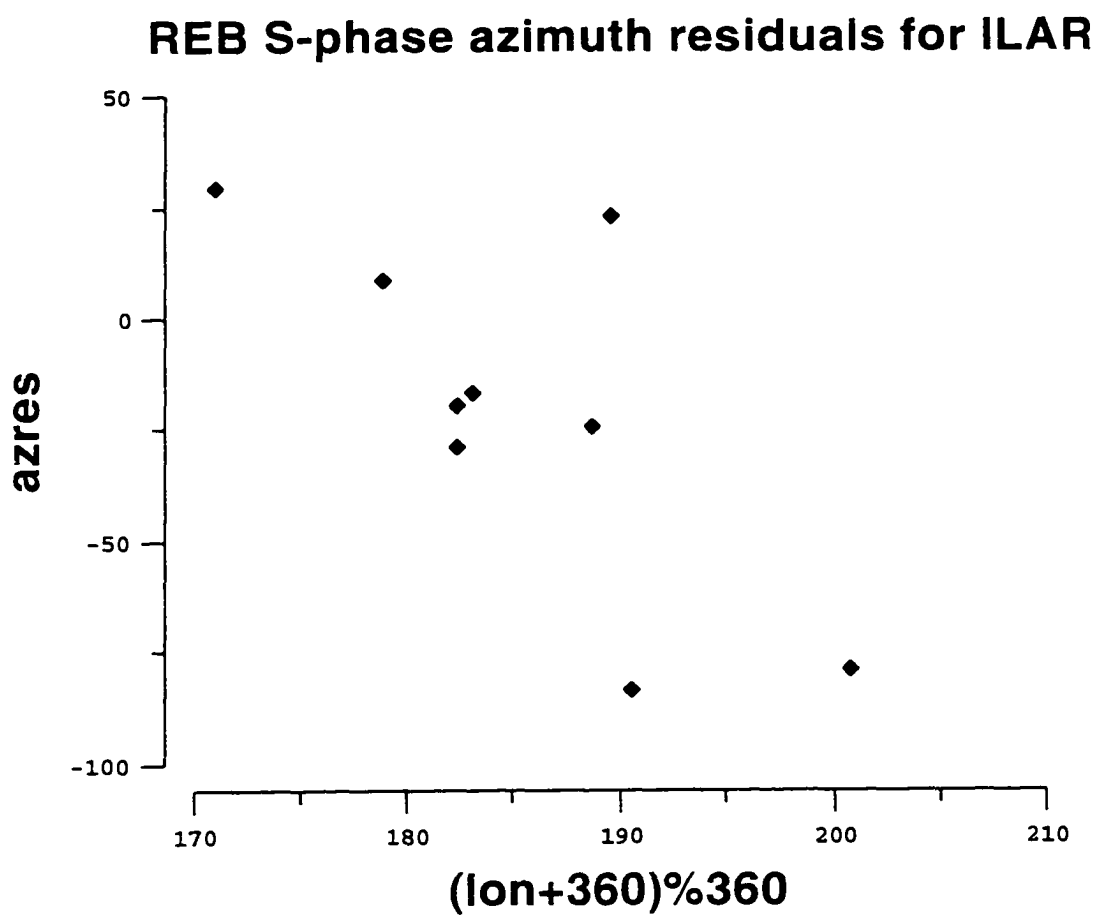

Figure 4.13 d

Reviewed-Event-Bulletin azimuth residuals observed at the Eielson array for S-phases incident from the earthquakes in Figure 4.12, plotted vs. longitudinal position of the epicenter along the Aleutian arc. For discussion, see Section 4.9 of the text.

than on steered beams. Nevertheless, there are some possible trends. The Eielson array once again shows no clear variation of azimuth residual with longitude along the arc, but there is a clear counterclockwise offset of the incoming wavefield from the great circle event to station path (Figure 4.14a). Quantitatively, the P-phase azimuth residuals at the Eielson array have a median of -6.0 degrees and a mean of -7.5 degrees (-5.7 degrees after removing one outlier). This agrees fairly well with the REB results described above for the same events and the same array. The Indian Mountain array shows a smaller average azimuth residual, with a median of -0.85° and a mean of -2.6°. A plot of these results is shown in Figure 4.14b. Both Burnt Mountain and Beaver Creek arrays show possible systematic dependence of the P-phase azimuth residuals with position along the Aleutian arc (Figures 4.14 c and d). The Burnt Mountain residuals have a median of -24 degrees and a mean of -27 degrees (-20.6 degrees if we remove the five outliers with more than 50 degrees residual). The Beaver Creek residuals have a median of -3.6 degrees and a mean of -8.6 degrees (-3.7 degrees without the five outliers with more than 50 degrees residual). Both of these arrays show hints of a trend in azimuth residuals vs. position along the arc. As a first exercise, we fit a straight line in a least-squares sense to the set of residuals from each array, as shown in Figures 4.14 c and d.

Much remains to be done with these measurements of azimuth residuals: corrections for the depth of the events; latitude offset of the events from the central axis of the Aleutian chain; full uncertainty analysis for each azimuth measurement based on the quality of the FK peak; and comparison of P vs. PcP residuals for individual events. Full

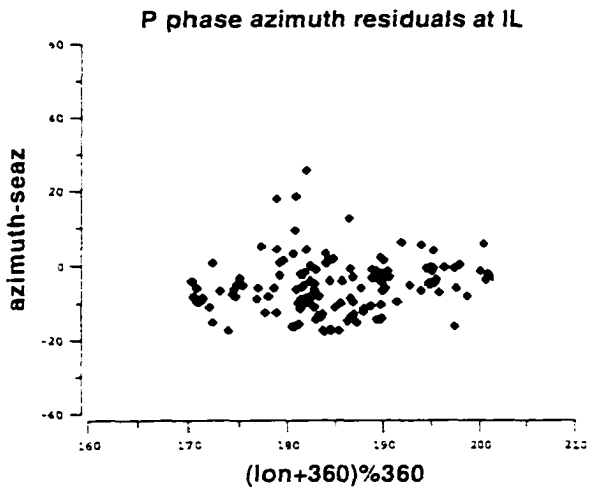

Figure 4.14 a

This figure shows recomputed azimuth residuals observed at the Eielson array for P-phases incident from the earthquakes in Figure 4.12, plotted vs. longitudinal position of the epicenter along the Aleutian arc. For discussion, see Section 4.9 of the text.

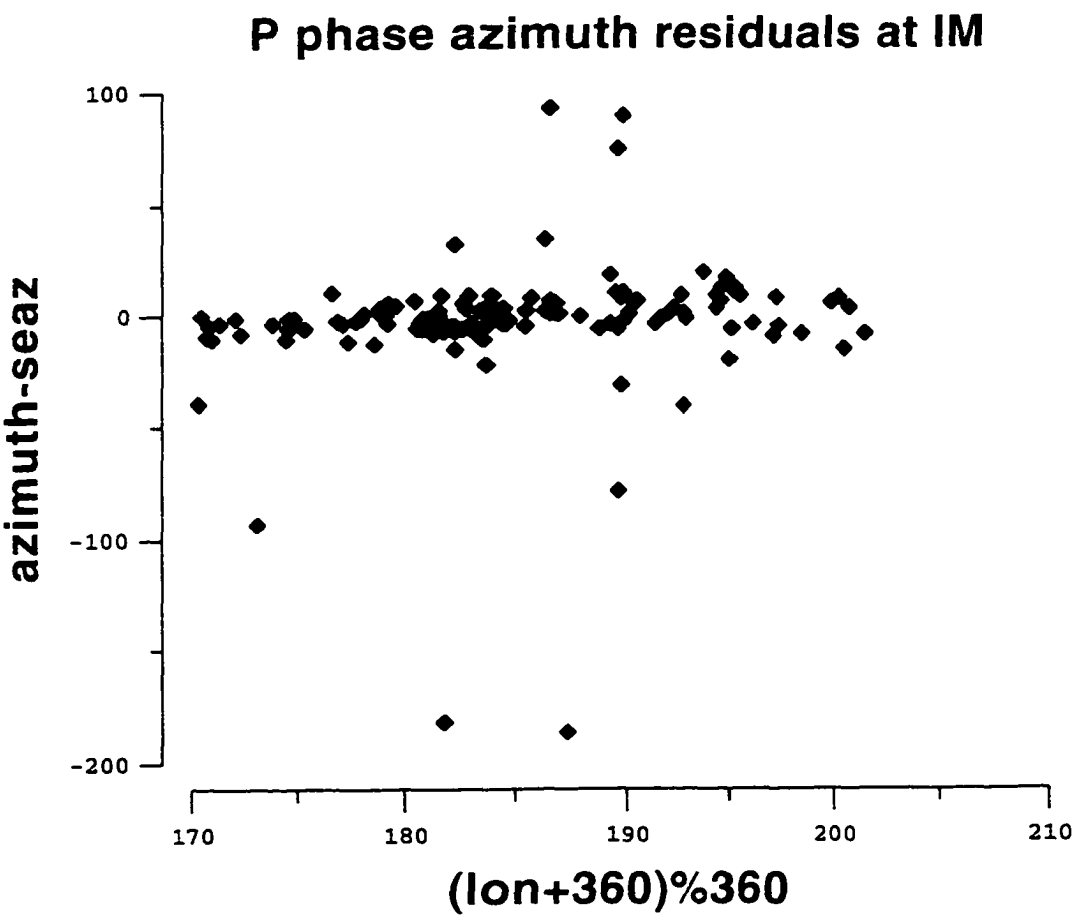

Figure 4.14 b

This figure shows azimuth residuals observed at the Indian Mountain array for P-phases incident from the earthquakes in Figure 4.12, plotted vs. longitudinal position of the epicenter along the Aleutian arc. For discussion, see Section 4.9 of the text.

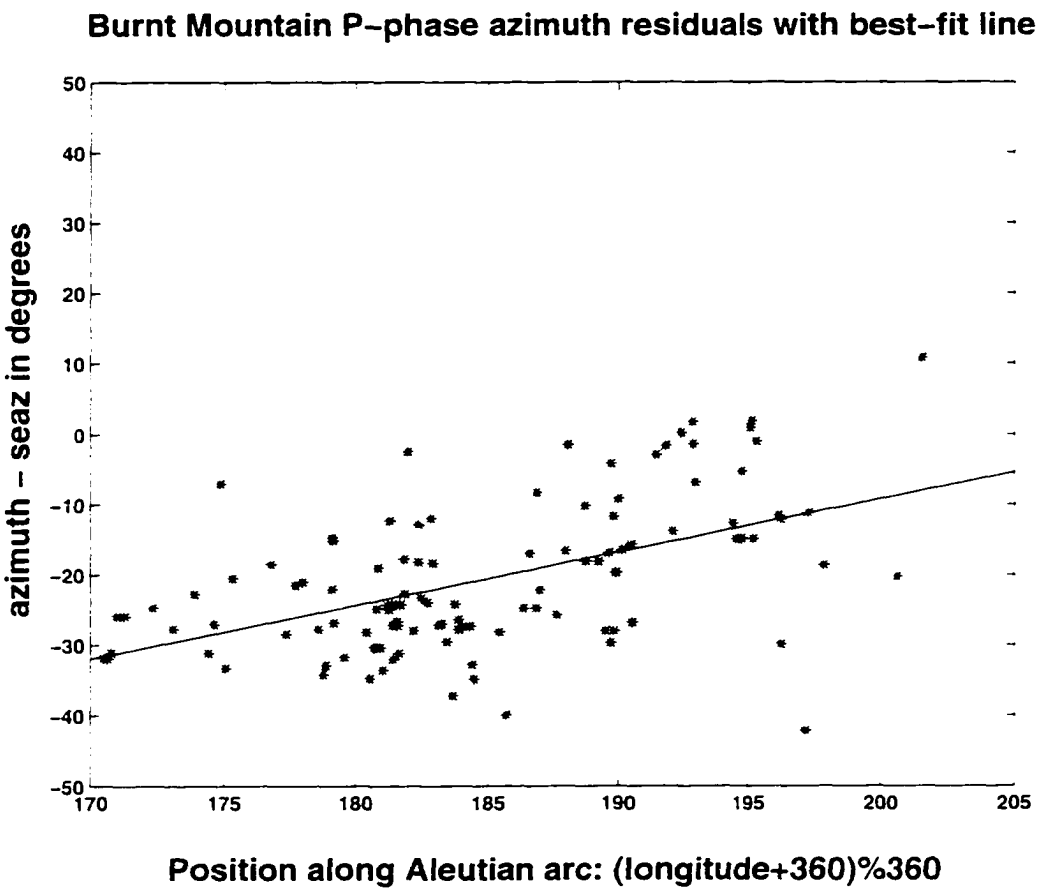

Figure 4.14 c

This figure shows azimuth residuals observed at the Burnt Mountain array for P-phases incident from the earthquakes in Figure 4.12, plotted vs. longitudinal position of the epicenter along the Aleutian arc. The line is a least-squares fit to the data. For discussion, see Section 4.9 of the text.

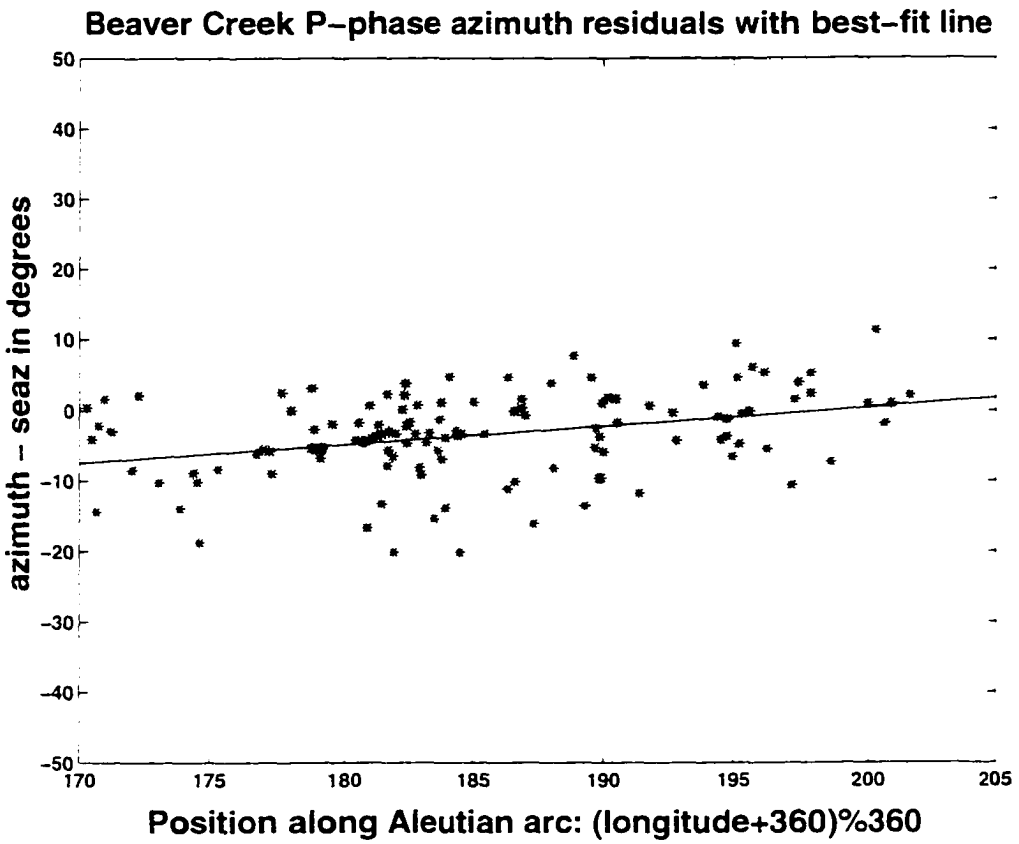

Figure 4.14 d

This figure shows azimuth residuals observed at the Beaver Creek array for P-phases incident from the earthquakes in Figure 4.12, plotted vs. longitudinal position of the epicenter along the Aleutian arc. The line is a least-squares fit to the data. For discussion, see Section 4.9 of the text.

explanation of the residuals will probably require three-dimensional wavefield modeling through the structural heterogeneities of the subducting Pacific slab. Since our goal in this work is the introduction of array processing for improvement of regional monitoring, further investigation of these residuals is left to future studies.

4.10 Automation of Array Detection of Events

Most of the events described so far in this chapter have been serendipitous discoveries in the data. In order to contribute to improved understanding of Arctic tectonics, however, we will need to detect events automatically, such that at the very least, an analyst can review the detections to produce an array-based seismicity catalog. One strategy is to form continuous beams to regions of interest in the world, applying an automatic picker to the computed beams. This is illustrated in Ringdal *et al.* [1989].

As an alternative but essentially equivalent strategy, which will result in global detection, we can follow a procedure which we illustrate by example. First, we will form a continuous, moving-window FK of the data from each array. We choose the segment of data from 2:00 to 2:30 UTC on October 11, 1997, which we know to contain an Aleutian event. To conduct the moving FK, we apply a one to three Hertz bandpass filter to the raw data. We FK-transform two seconds of data at a time, noting the peak power for each window of data. The peak power for each FK window will form a time-series, which can

be passed through a simple threshold-detection program to identify times at which the power exeeds a preset level. In Figure 4.15 we show these peak-power time series for all four arrays, together with the center elements of the arrays, for a time period during which an event occurred. Figure 4.16 illustrates a detection on the Burnt-Mountain power trace. Note that the continuous FK also yields time-series of azimuth and slowness, which we show in Figure 4.16. As the signal arrives, the azimuth and slowness time-series stabilize to values indicating the incidence direction of the incoming energy.

The detection times for the raw power trace form the basis for an FK around the incoming seismic phase. We form an FK plot for a three-second window of data around the power detections for each array, starting 0.5 seconds before the detection time. As an example, the result for the Burnt Mountain array is shown in Figure 4.17. FK processing around the power detection returns an azimuth and slowness for the best beam, which we form for a twenty-second window around the detection time for each array. Figure 4.17 also shows this best beam for the Burnt Mountain array.

While the detection time calculated from the continuous FK processing gives an approximate arrival time for the seismic phase at the array, our experience shows that this arrival time is often not aligned very well with the onset seen on the beam. For the Eielson array and for the earthquake currently under consideration, the detection time appears to be approximately two seconds after an analyst estimate of the first arrival on the Eielson beam. We apply an autoregressive onset-time estimator [Taylor *et al.*, 1992] to this best-beam to yield a more accurate arrival time. These autoregressive onset times, together with

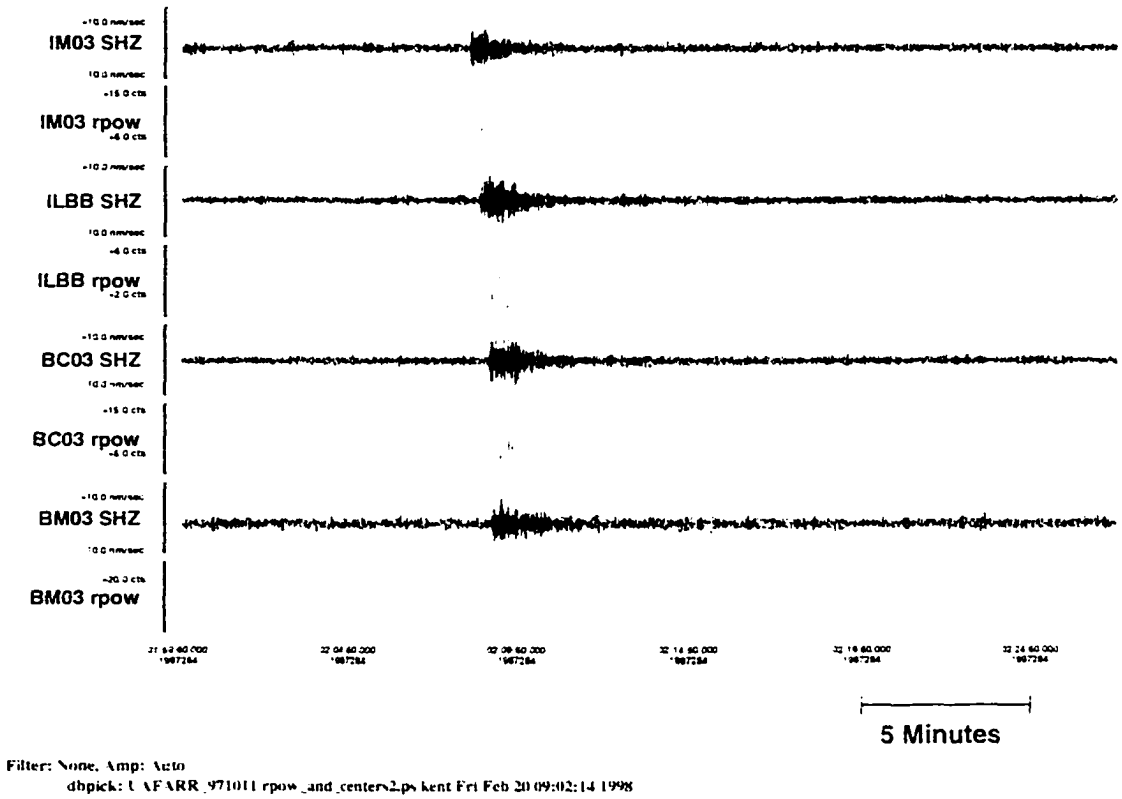

Filter: None, Amp: Auto
dbpick: C:\FARR_971011 rpow_and_centers2.ps kent Fri Feb 20 09:02:14 1998

Figure 4.15

This plot shows the center elements from each array (labelled as the SHZ component) plus peak-power time-series (labelled as the "rpow" component) from continuous FK processing, for automatic detection. For discussion see Section 4.10 of the text.

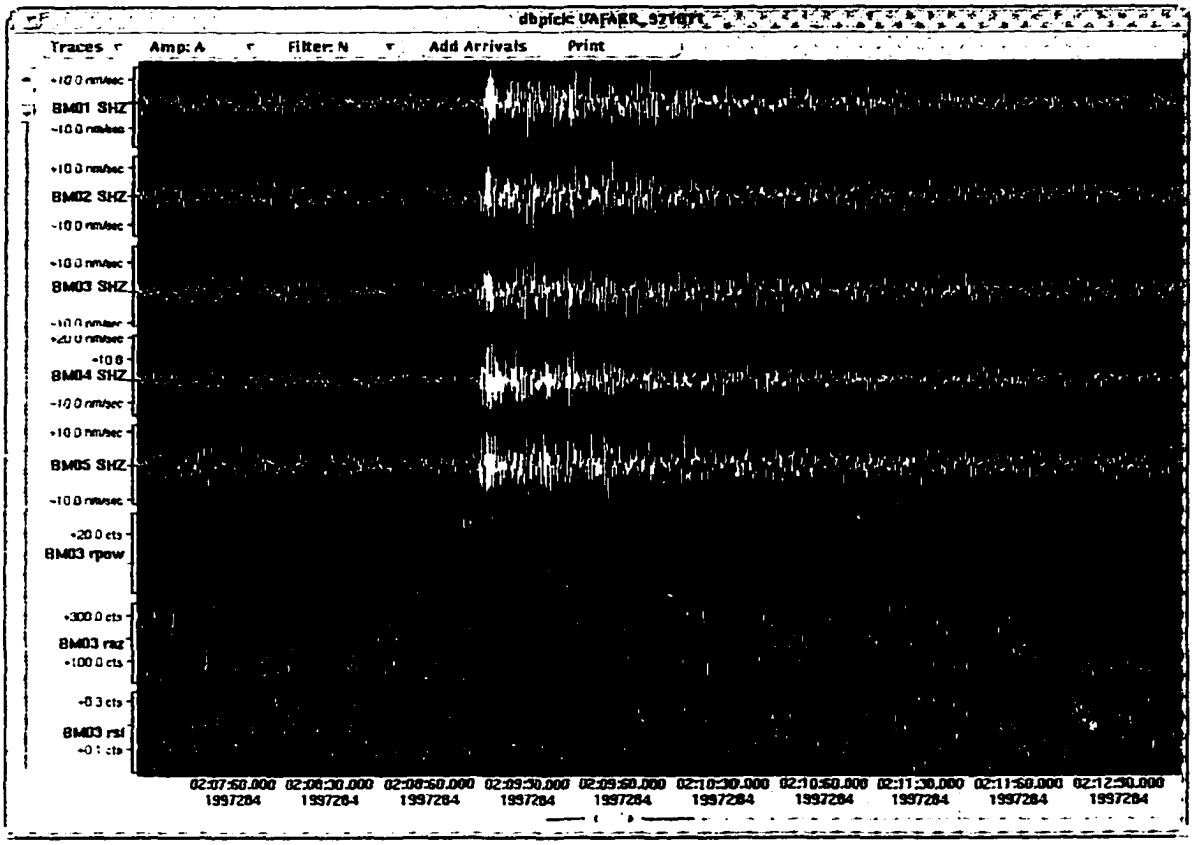

Figure 4.16

This plot shows the five elements of the Burnt Mountain array, plus the peak power, azimuth, and slowness time-series from continuous FK processing for a time window containing an incoming seismic phase. The detection flag on the power trace ("rpow") is an automated pick based on a preset threshold crossing. For discussion see Section 4.10 of the text.

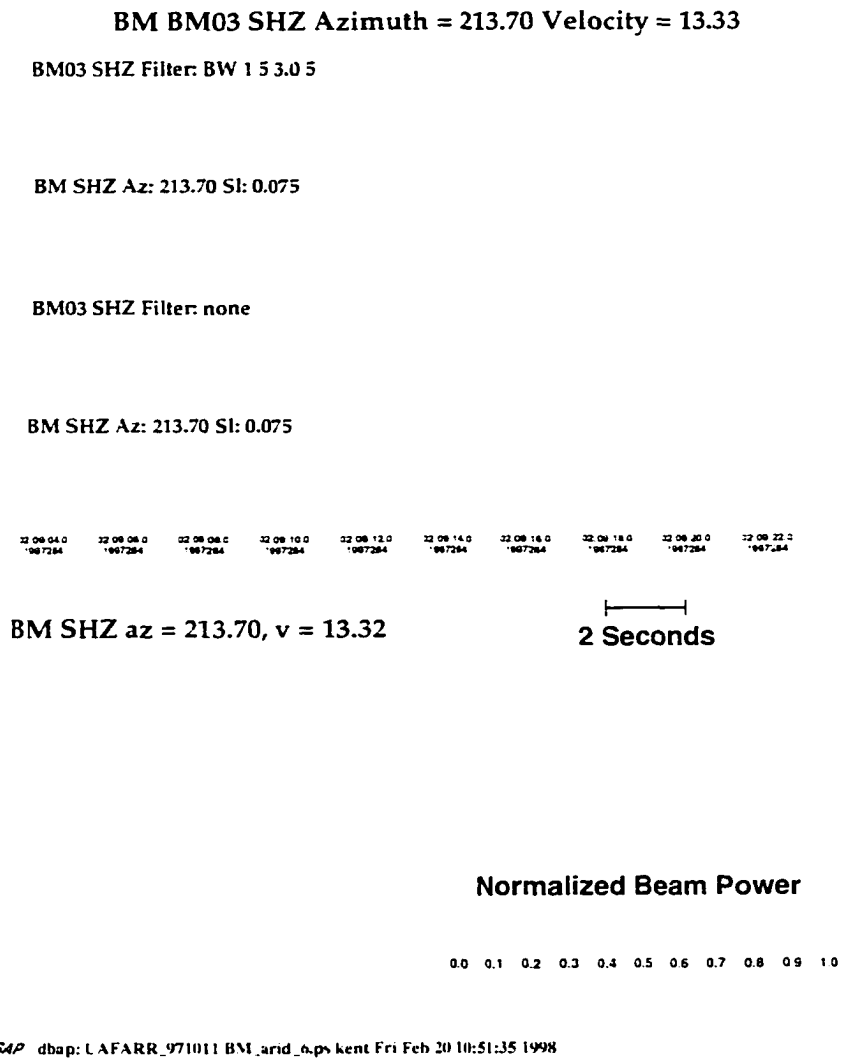

Figure 4.17

This plot shows array processing results for the time window around the detection shown in Figure 4.16. The elements of this figure are the same as in Figure 4.6b. with the exception that the filter bandpass is between one and three Hertz.

the azimuth and slowness information from the FK analysis, comprise the phase detection information for subsequent location of the event.

In this work, we simply locate the event with *dblocsat2*, based on the detected phases (adding P and S picks at FX01, and a P pick at the Tatalina station TT01). Our solution converges to within a degree of the REB solution, almost due south of it. Ultimately these phase detections will be put into an array-based associator such as the GA algorithm of the IDC [Bache *et al.*, 1990]; or the Generalized Beam-forming of Ringdal *et al.* [1989]. The core software-development to implement all of this automated phase detection and arrival estimation in near-real-time has essentially been completed, though some engineering details remain in order to incorporate this software into our current processing system. Nevertheless, what we have demonstrated here is the ability to automatically detect seismicity in the Aleutians, in continental Alaska, and in fact around the globe with the Alaskan array stations.

4.11 Summary

The work in this chapter sketches the outset of the application of array processing to Alaskan regional seismology. The high quality of the array stations improves monitoring of continental Alaskan earthquakes, revealing new microseismicity and providing reliable magnitudes for Alaskan earthquakes. Standard array analysis allows us to extend

Alaskan regional earthquake monitoring into the Aleutian Islands and the Bering Sea rim, with detection thresholds in some cases below M_L 3.0. In addition to the study of Aleutian events, this should contribute to seismic monitoring of active volcanoes in the Aleutians. The enhanced information provided by the arrays reveals evidence of the effects of heterogeneous structure on wavefields coming from Aleutian earthquakes, a subject which will be a rich source of study in the future. Finally, with the automated techniques sketched in section 4.10 combined with international collaboration amongst Nordic seismic installations, the Alaskan arrays open up the possibility of improved seismic monitoring of the entire Arctic region.

4.12 Acknowledgments

We would like to acknowledge the staff of the AEIC for their work in establishing the array data, especially Martin LaFevers for data handling help and Mitch Robinson for data acquisition. Janae Deverell helped greatly in our initial array studies, working through the NSF's Research Experience for Undergraduates program, NSF grant number EAR95-31601. Under the same contract, Cristyn Presley participated in the empirical magnitude-threshold detection study. Kaz Fujita kindly provided data from station Anadyr for the Chukchi sea event. The *Datascope Seismic Application Package (DSAP)* software from Danny Harvey and Dan Quinlan of the University of Colorado has been invaluable in this

work, especially the *dbap* array-processing toolbox of Danny Harvey. We thank them as well for useful discussion of software issues. Gary Pavlis of the University of Indiana provided *dbap* driver scripts which greatly aided the beginnings of this project.

4.13 References for Chapter 4

Abers, G.A. and G. Sarker (1996). Dispersion of regional body waves at 100-150 km depth beneath Alaska: In situ constraints on metamorphism of subducted crust. *Geophys. Res. Lett.* **23**, 1171-1174.

Aki, K. and P.G. Richards (1980). Quantitative Seismology, Theory and Methods, Vol. II., W.H. Freeman and Company: New York, 932 pp.

Bache, T.C., S.R. Bratt, J. Wang, R.M. Fung, C. Kobryn, and J. Given (1990). The Intelligent Monitoring System. *Bull. Seis. Soc. Am.* **80**, 1833-1851.

Bratt, S.R. and T.C. Bache (1988). Locating events with a sparse network of regional arrays. *Bull. Seis. Soc. Am.* **78**, 780-798.

Bame, D.A., M.C. Walck, and K.L. Hiebert-Dodd (1990). Azimuth estimation capabilities of the Noress regional seismic array. *Bull. Seis. Soc. Am.* **80**, 1999-2015.

Capon, J. (1969). High-resolution frequency-wavenumber spectrum analysis. *Proceedings of the IEEE* **57**, 1408-1419.

Estabrook, C.H., D.B. Stone, and J.N. Davies (1988). Seismotectonics of Northern Alaska. *J. Geophys. Res.* **93**, 12,026-12,040.

Filson, J. (1975). Array Seismology. *Ann. Rev. Earth Planet. Sci.* **3**, 157-181.

Fyen, J. (1996). NORSAR Array Data Processing: Draft Reference Guide. NORSAR: Kjeller, 37 pp.

Hansen, R.A. and K.G. Lindquist (1996). Array processing for a Cooperative Arctic Seismology Program, *in* Abstracts from the XXV General Assembly of the European Seismological Commission, Sept. 9-14, Reykjavik, Iceland.

Harvey, D. and R. Hansen (1994). Contributions of IRIS Data to Nuclear Monitoring. *IRIS Newsletter*, **XIII** No. 2, p.1.

Kvaerna, T. (1989). On exploitation of small-aperture NORESS type arrays for enhanced P-wave detectablility. *Bull. Seis. Soc. Am.* **79**, 888-900.

Lindquist, K.G., R.A. Hansen, and J. Deverell (1997). Application of seismic arrays to

automatic regional earthquake monitoring in Alaska and the Aleutian Islands. Eos Supplement **78**, No. 46, p. F46.

Mackey, K. G., K. Fujita, L. V. Gunbina, V. N. Kovalev, V. S. Imaev, B.s M. Koz'min, and L. P. Imaeva (1997). Seismicity of the Bering Strait Region: Evidence for a Bering Sea Block, *Submitted April 22 to Geology*.

Mykkeltveit, S., F. Ringdal, T. Kvaerna, and R. Alewine (1990). Application of regional arrays in seismic verification research, *Bull. Seis. Soc. Am.* **80**, 1777-1800.

Neidell, N.S. and M.T. Taner (1971). Semblance and other coherency measures for multichannel data. *Geophys.* **36**, 482-497.

Richter, C.F. (1935). An instrument earthquake magnitude scale. *Bull. Seis. Soc. Am.* **25**, 1-32.

Ringdal, F. and E.S. Husebye (1982). Application of arrays in the detection, location, and identification of seismic events. *Bull. Seis. Soc. Am.* **72**, S201-S224.

Ringdal, F. and T. Kvaerna (1989). A multi-channel processing approach to real time net-

work detection, phase association, and threshold monitoring. *Bull. Seis. Soc. Am.* **79**, 1927-1940.

Taber, J.J., S. Billington, and E.R. Engdahl (1991). Seismicity of the Aleutian Arc, *in* Slemmons, D.B., Engdahl, E.R., Zoback, M.D. and Blackwell, D.D., eds., Neotectonics of North America: Boulder, Colorado, Geological Society of America, Decade Map Volume I.

Taylor, D.W.A., H.A.A. Ghalib, and R.H. Kimmel (1992). Autoregressive analysis for seismic signal detection and onset-time estimation: Final technical report, delivery order TT-91-15, prepared for Air Force Technical Applications Center, Ensco, Inc.: Melbourne, 68 pp.

Chapter 5

Conclusion

5.1 Summary

This thesis work has brought near-real-time seismology to Alaska. We have contributed to regional seismology an automated system with relational-database technology; integration of diverse data streams into a common real-time processing environment; and an infrastructural framework for the automated extraction of data from seismic wavefields. We have applied this technology to begin assembling a long-term data set for the calibration of Alaskan magnitude scales; and we have computed a preliminary, regionalized local-magnitude scale for Alaska. Finally, we have introduced seismic array processing to Alaskan regional seismology for improved sensitivity for Alaskan earthquake detection; expanded geographic coverage of Alaskan earthquake monitoring into the Aleutians; and the extraction of more sophisticated information from Alaskan seismic wavefields. In this conclusion we attempt to sketch out some of the many directions which the thesis work presented here makes possible.

5.2 Future Directions

5.2.1 Integrating Real-time Source Mechanisms with Three-dimensional Propagation Modelling for Improved Hazard Response

Progress in the community has been made in near-real-time fault-plane solutions, moment-tensor inversions, and source extent and rupture determination. These should be integrated into the infrastructure we have established, which is now primed for such calculation. In addition, the prospect of making strong-ground shaking maps based on observed data is also quite close. In the near future we hope to incorporate accelerometer data from Anchorage into the Iceworm system, which will aid the generation of such maps. With quick, realistic estimates of the true ground motion in the aftermath of a large earthquake, the emergency response capability should be significantly improved. With quick estimates of detailed source parameters comes the possibility of more accurate ground-response calculations for rapid notification to aid earthquake disaster response. One could pre-compute Green's functions with a three-dimensional modelling code to predict ground response in areas of high population density such as the Anchorage basin. After a large event, near-real-time estimation of moment tensors combined with the realistic Green's functions could allow estimation of likely high damage. With a combination of observed data and forward modelling one should be able to publish peak accelerations and velocities after large earthquakes.

5.2.2 Arrival Time and Location Refinement Towards Releasable Locations

While the current system provides automatic locations that are good for first estimates of earthquake hazard and form a starting point for analyst review, the ultimate goal would be to construct automatic earthquake solutions that would be releasable to the public just seconds to minutes after the earthquake. In Alaska, this is important in applications such as monitoring the Alyeska oil pipeline as well as for urban areas. Part of this task can be accomplished by adding postprocessing to the earthquake location procedures and part requires an upgrade of the seismic network to include more thorough geographic coverage with modern instrumentation. For example, the Earthworm system includes an implementation of hypoinverse that can process the output of the associator. An important step to take in refining automatic locations, however, is to improve the quality of the automatic arrival-time picks. One possibility is to use the initial picks from the Rex Allen picker of the Iceworm system and refine them with autoregressive techniques. Further subjects to address include better handling of noise picks, as well as handling of A/VCO gain-ranging pulses and avoidance of false events built from them.

5.2.3 Monitoring of Arctic Seismicity Through COASP, the Cooperative Arctic Seismology Program

The communications and automatic-processing infrastructure described in this

work advances the potential for international cooperation in monitoring the earth, bridging the gap between traditional regional network seismology and traditional global seismology. The current knowledge of detailed seismicity patterns for the Arctic region is relatively limited as compared to many other regions on the Earth. A better knowledge of the seismicity of the Arctic would be of significant geophysical interest. There are quite a large number of arrays and seismic stations surrounding the Arctic region, but the data are unfortunately not processed jointly. These stations and arrays include the NORSAR and NORESS arrays in Norway; FINESSA in Finland; and the Yellowknife array in Canada. A number of stations from the Global Seismic Network could also contribute, including Magadan, Yakutsk, Lovozero, Bilibino, and Norilsk in Russia; Godhaven and Sondre Stromfjord in Greenland; Borgarfjordur in Iceland; and Kongsberg in Norway. Depending on the lower-latitude cutoff for the COASP collaboration, one could also include Arti and Obninsk from Russia and Eskadalemuir in Scotland. Additional stations from the Incorporated Research Institutions for Seismology (IRIS) that could contribute would be Tiksi, Russia; Alert, Canada and Flin Flon, Canada; and Ny-Alesund on Spitsbergen. These are all in addition to the Alaskan arrays and to the Alaskan stations at Adak, Kodiak, and College.

In 1994, Dr. Erik Hjortenberg of Denmark proposed to the International Arctic Science Committee (IASC) to establish an international Cooperative Arctic Seismology Program (COASP). Dr. Hansen, as a member of the working group, proposed an automatically processed, high-arctic seismic network [R. Hansen, *pers. comm.*, 1996]. This would

expand the catalogs of seismicity available for the entire Arctic region to much lower magnitude thresholds than available with global catalogs (as discussed in Chapter four), providing a more detailed picture of Arctic seismicity.

This monitoring would employ generalized beam-forming, a technique developed by Ringdal and Kvaerna [1989]. Generalized beam-forming (GBF) is less a single technique than it is a framework for processing data from multiple stations simultaneously. In conventional beam-forming, seismic traces from a number of different seismic stations, usually deployed in a tight array, are delayed and summed. The delays, and the beams, are computed for a number of different expected incoming wavefronts, and actual incoming wavefronts show a marked increase of signal amplitude over the incoherent noise for the appropriate beam. This technique relies on phase coherence of the signal across the array of stations. In Generalized Beam Forming, a number of beam-steering points are similarly defined over the geographical region of interest. The traces are not summed directly, however. Relevant features of the seismic traces are first extracted (often with coherent beam-forming of component arrays), and the sums of these extracted features are computed for "beams" aimed at each of the geographic beam-steering points of interest.

A single, hybrid system that involves sending NORSAR array-detection information to Alaska over the internet, integrating Alaskan parametric data in a hybrid associator running in Alaska, will probably be most efficient. This suggests an initial approach to the project of working cooperatively with NORSAR to demonstrate integrated processing between Alaska and Fennoscandia. After proven procedures are in place, additional stations

and arrays within the Arctic region can be added. Because of the emphasis on international collaboration, this project meshes well with the recent establishment, under the US-Japan Common Agenda, of an International Arctic Research Center on the campus of the University of Alaska, Fairbanks.

In order to implement the first stages of the COASP work, several major tasks must be undertaken. First, we need to implement NORSAR array processing software such that it is connected to the data streams from our Iceworm processing system. Then we need to establish the ability to run NORSAR-style processing functions on Iceworm data streams. This will include building single-component phase detections from Alaskan stations into the NORSAR associator. Second, we need to adapt the hybrid NORSAR/Iceworm GBF software to handle a spherical-geometry grid covering the Arctic region of interest, i.e. the North-polar cap, then study and implement the optimal grid configuration for the area. While this will require work, it is not likely that there will be any major technical obstacles to this task. Some experimentation will be required to establish the optimal association grid (the suite of beam-steering points) for observation of Arctic seismicity with the new system. Third, we need to set up the appropriate parametric data-exchange between participating countries and institutions, together with data connections and surrounding software to maintain them. Finally, we need to produce catalogs of the detected Arctic seismicity and compare them to existing catalogs from global networks and individual arctic networks and arrays (where there are Arctic institutions producing catalogs). This will include Alaskan catalogs, NORSAR catalogs, Russian catalogs, possibly Japanese

catalogs, possibly Canadian catalogs, as well as the USGS Preliminary Determination of Epicenters (PDE) catalog, and the Reviewed Event Bulletin (REB) put out by the International Data Centre of the Center for Monitoring Research.

5.2.4 Three-dimensional Heterogeneity Incorporated into Automatic Processing System

The work described in this thesis relies predominantly on models of the earth that are laterally homogeneous. However, technology is in hand at the University of Alaska to begin incorporating lateral heterogeneity into the automatic processing. There are three major avenues for this: first the pseudospectral modelling techniques of Archambeau/Orrey [Orrey, 1995], which are already being applied, in work with Hansen and Lindquist [unpublished], to three-dimensionally heterogeneous models in Alaska. Second is the Huygen's method wavefront-tracking method of Harvey/Kohl [B. Kohl, *writt. comm.*, 1994], which, close to a finite-difference scheme, is very attractive as a way to improve the Generalized Beam-Forming associator used in the detection and location of regional earthquakes. Third, the tau-p formulation [Buland *et al.*, 1983] is being extended for atmospheric wave-propagation in the the realm of lateral heterogeneity by Garcés [Garcés *et al.*, 1997], in ways that would very easily extend to the solid earth [R. Buland, *pers. comm.*, 1996].

5.2.5 Application of Array Data to Studies of Wavefield Propagation in Heterogeneous Structure

As demonstrated in Chapter four, the seismic array data allow the extraction of much more sophisticated data from the seismic wavefield than single seismographs. This information can reveal complexities of seismic wave propagation that are due to the lateral heterogeneity of the propagation environment, as demonstrated by the analysis of azimuth residuals from Aleutian events in Chapter four. Extensive modelling work will most likely be required to explain these observations. Work has also begun [Ratchkovsky *et al.*, 1997] to identify and explain anomalous phases in Alaskan seismic data.

5.2.6 Joint Infrasonic Array and Seismic Array Processing

We have shown in this work the joint acquisition of infrasonic data, namely the King Cove pressure sensor and several others; and seismic data with the same infrastructure. This infrastructure already includes tools to process seismic arrays, tools which can be transparently applied to infrasonic array data as well. Combined with the extensive experience and software already at the Geophysical Institute to handle infrasonic data, our system offers great promise for joint infrasonic and seismic array processing, which could be put to use both for Comprehensive Test-Ban Treaty (CTBT) verification work and for volcano monitoring, as well as other uses that generate both seismic and infrasonic waves.

5.2.7 More Extensive Use of Broadband, Three-component Data

With the increase in the intake of high-quality, three-component, broadband waveform data at the University of Alaska's Alaska Earthquake Information Center, much potential is opening up studies that involve full-waveform synthetics and information extraction from large parts of the waveform, rather than the travel-time-based studies that have formed the bulk of work with Alaskan data up to the present time. Application in near-real-time of the many possible techniques that require broadband, three-component data leaves worlds of opportunity for the development of the Iceworm system at the AEIC. One of the first to pursue will be the implementation of a robust, three-component picking algorithm that runs automatically, perhaps with inclusion of autoregressive refinement to improve the accuracy of initial picks. Automatic calculation of moment magnitudes is also a clear target of value, especially useful for larger earthquakes where the local-magnitude scale saturates. Near-real-time moment-tensor estimation has already been studied elsewhere [Pasyanos *et al.*, 1996], and merits implementation in Alaska.

5.2.8 Tsunami Calculations and Response to Large Earthquakes

With the tsunamigenic potential of the very large Alaskan subduction-zone events, there is importance to communities along the Pacific rim for accurate predictions of ocean behavior after large events. While the Alaska and Pacific Tsunami Warning Centers pro-

vide timely predictions of tsunamis from large Alaskan events, there is much to be improved in the modelling of the expected tsunamis generated. With high-quality data, we should be able to compute accurate, extended source mechanisms and, with coupled solid-earth and fluid-dynamic modelling of the tsunamigenic potential of these earthquakes, obtain much more useful models that will aid hazard predictions after large earthquakes.

5.2.9 Near-real-time Quiescence Detection

Recent work [e.g. Wiemer *et al.*, 1994] suggests the utility of seismic quiescence studies in strengthening our understanding of impending earthquakes in earthquake-prone regions. This problem is nearly ideal for real-time implementation into a system designed to automatically detect and catalog regional earthquakes. Running continuously, a process such as ZMAP (Wiemer et al.), modified to interact in near-real-time with the output of the Iceworm system, could watch over months for seismicity patterns and set off alarms upon the detection of significant quiescence episodes. Related to the task of detecting precursory episodes of seismic quiescence is the need to monitor system performance for artificial changes in seismicity. These can occur with loss of station performance, addition of new stations, problems with calibration information, and changes to the associator.

5.2.10 Near-real-time Tomography; Full-wavefield Tomography

Seismic tomography is usually a quite complex process, requiring extensive inter-

vention on the part of the scientist to make reasonable trade-offs to get models to converge. Tomography is by no means, at least in most cases, a simple task of blindly feeding a catalog of propagation data to an inversion code. Nevertheless, it seems quite possible that an existing model could be automatically, iteratively refined by a tomographic process implemented in a system such as Iceworm. This idea is especially attractive for the common but difficult task of monitoring a seismically unfamiliar volcano which suddenly develops unrest. A real-time process that made use of the high seismicity common at an active volcano could iteratively refine a starting plane-layered model for the volcano, as scientists made use of the automatic processing results from the starting models. Farther in the future is the prospect of full-wavefield tomography in a more automated regime, although work is just beginning on the theory itself of this type of tomography [Archambeau *et al.* 1996]. Note that the full-wavefield tomography integrates well with the three-dimensional modelling studies we have already begun.

5.2.11 Near-real-time Volcano Monitoring

There are a multitude of ways the Earthworm/Iceworm software can be applied to the monitoring of active volcanoes. One is to study associator tuning over very small grids, such as those that would be necessary to process volcanic swarms. This is related to the use of Iceworm to monitor subnets of stations, for example collecting aftershocks after large earthquakes. Note the utility of the relational database inputs for managing these subsetting

tasks easily. We have already applied the Iceworm system in a simpler way to the monitoring of Iliamna volcano, by subsetting all the picks made on the Iliamna network for later screening (a simple association process based on the proximity in time of picks on multiple stations) and location by hand. Swarm counting is also an important activity that would be very useful if automated. The volcano-monitoring environment is an ideal application for real-time tomography. Finally, spectral monitoring at volcanoes with the Iceworm system has already yielded significant successes during the 1996 eruption of Pavlof volcano [Lindquist *et al.*, 1996; 1997].

5.2.12 Near-real-time Feeds of Infrasonic and Seismic Signals from Volcanoes into Integrated, Quantitative Models of Volcano Dynamics

Recent work by Garcés [Garcés *et al.*, 1997] has developed wave-theoretical, seismoacoustic models of volcano dynamics that integrate multiple quantitative models of the dynamical processes at work in a volcano that is erupting or threatening to erupt. These integrated models have already been applied to the interpretation of the explosion and eruption tremor signals radiated by Pavlof volcano, Alaska, during the Fall 1996 eruption of that volcano. Given the flexibility to acquire and process both seismic and infrasonic data on volcanoes in near real time, i.e. the progress presented in the current work, there is significant potential to take advantage of integrated models such as that of Garcés *et al.* [1997] to improve the monitoring of active volcanoes with quantitative techniques.

5.2.13 More Extensive Real-time Use of Array Data

Of the many future directions that are open, perhaps the most promising is much more involved application of the Alaskan arrays to regional event detection and location, and Aleutian monitoring. This will follow after the implementation of an associator that makes full use both of the regional network stations and the array data. In fact, with the arrays we have the potential to automatically monitor the seismicity for the entire world. Altogether, these developments open up many options for real-time regional seismology in Alaska.

5.3 References for Chapter 5

Archambeau, C., J. Orrey, and B. Kohl (1996). 3-D Seismic Wave Synthesis and Full Wavefield Inversion, in Proceedings of the 18th Annual seismic research symposium on monitoring a comprehensive test-ban treaty, 4-6 September 1996, Philips Laboratory.

Buland, R. and C.H. Chapman (1983). The computation of seismic travel-times. *Bull. Seis. Soc. Am.* **73**, pp. 1271-1302.

Garcés, M.A., R.A. Hansen, S.R. McNutt, and J.C. Eichelberger (1997). Application of wave-theoretical seismoacoustic models to the interpretation of explosion and eruption tremor signals radiated by Pavlof Volcano, Alaska. Submitted to *J. Geophys. Res.*

Garcés, M.A., R.A. Hansen, and K.G. Lindquist (1997). Travel times for infrasonic waves propagating in a stratified atmosphere. Submitted to *Geophys. J. Intl.*

Hansen, R.A. and K.G. Lindquist (1996). Array processing for a Cooperative Arctic Seismology Program, in Abstracts from the XXV General Assembly of the European Seismological Commission, Sept. 9-14, Reykjavik, Iceland.

Lindquist, K.G., J.P. Benoit, and R.A. Hansen (1996). Advances to near-real-time spectral monitoring at volcanoes with an Iceworm-based implementation. *Eos Trans. Amer. Geophys. U.* **77**, No. 46, p. F451.

Lindquist, K.G., J.P. Benoit, and R.A. Hansen (1997). Near-real-time monitoring on a network of seismic stations with Iceworm: automatic alarms for and spectral signals of the 1996 eruptions of Pavlof volcano. *Seis. Res. Lett.* **68**, p. 332.

Orrey, J.L. (1995). A generalized Fourier pseudospectral method for elastodynamics. *Ph.D. Thesis, University of Colorado*, 231 pp.

Pasyanos, M.E., D.S. Dreger, and B.S. Romanowicz (1996). Toward real-time estimation of regional moment-tensors. *Bull. Seis. Soc. Am.* **86**, pp. 1255-1269.

Ratchkovsky, N.A., R.A. Hansen, and K. Lindquist (1997). Analysis of Crustal and Subduction Zone Alaskan earthquakes using seismic array data. *Eos Trans. Amer. Geophys. U.* **78**, No. 46 p. F444.

Ringdal, F. and T. Kvaerna (1989). A multi-channel processing approach to real time network detection, phase association, and threshold monitoring., *Bull. Seis. Soc. Am.* **79**,

1927-1940.

Wiemer, S. and M. Wyss (1994). Seismic Quiescence before the Landers (M = 7.5) and Big Bear (M = 6.5) 1992 Earthquakes. *Bull. Seis. Soc. Am.* **84**, pp. 900-916.

Appendix A

Glossary of Acronyms

A/D	Analog to Digital
AEIC	Alaska Earthquake Information Center
AH	Ad-Hoc seismic data format
ASCII	American Standard Code for Information Interchange
ATWC	Alaska Tsunami Warning Center
AVO	Alaska Volcano Observatory
CEDAR	CalTech Earthquake Detection And Recording
CMR	Center for Monitoring Research
COASP	COoperative Arctic Seismology Program
CPU	Central Processing Unit
CSS	Center for Seismic Studies
CUSP	CalTech-USGS Seismic Processing
CTBT	Comprehensive Test Ban Treaty
DP	Data Processor

DSAP	Datascope Seismic Application Package
EVA	Earthquake/Volcano Alarm
FK	Frequency-Wavenumber processing
GBF	Generalized Beam-Forming
GSETT	Group of Scientific Experts Technical Test
GUI	Graphical User Interface
IDA	International Deployment of Accelerometers
IDC	International Data Center
IP	Internet Protocol
IRIS	Incorporated Research Institutions for Seismology
JADE	Just Another Detector of Events
LTA	Long-Term Average
NOAA	National Oceanic and Atmospheric Administration
NORSAR	NORwegian Seismic ARray
NSF	National Science Foundation
ORB	Object-Ring Buffer
PC	Personal Computer
PDE	Preliminary Determination of Epicenters
PEPP	Princeton Earth Physics Project

RAID	Redundant Array of Independent Disks
RAM	Random Access Memory
RDBMS	Relational DataBase Management System
REB	Reviewed Event Bulletin
REDI	Rapid Earthquake Data Integration
RTP	Real-Time Picker
SAC	Seismic Analysis Code
SEED	Standard for the Exchange of Earthquake Data
SIL	South Iceland Lowlands
SPARC	Scalable Processor ARChitecture
STA	Short-Term Average
TCP	Transmission Control Protocol
UAF	University of Alaska, Fairbanks
UAFGI	University of Alaska, Fairbanks Geophysical Institute
UDP	User Datagram Protocol
UrEDAS	Urgent Earthquake Detection and Alarm System
USGS	United States Geological Survey
VCO	Voltage-Controlled Oscillator

Appendix B

Data Processing for Spurr M_L Inversion

B.1 Pickfile Extraction

The volcanic catalog data were obtained as three files, one per year for 1991, 1992, and 1993. Each of these was a concatenation of all the Hypoellipse pickfiles (archive phase files) for Alaskan volcanic events for the year. Information on the format of these pickfiles is available in Lahr (1994), referenced in Chapter 3.

The first task was to split the files into subsections, then split each subsection into pickfiles. Because of the limits of csplit, the following technique sacrifices 1% of the pickfiles in order to avoid complex programming. This loss was deemed acceptable because of the overabundance of data compared to the size of the inversions we could perform. The remove command in the middle eliminates some superfluous header material found at the beginning of two of the input files.

```
ugle% foreach  year (91 92 93)
foreach? sed "/^Syear/s/^/@/" /net/kiska/export/Kiska4/spurrSyear.pha > Syear.pha
foreach? awk 'BEGIN {i=0} /^@/ {print i $0; i=i+1} /^[^@]/ {print}' Syear.pha >
Syear.marked
foreach? csplit -k -f Syear\chunk. Syear.marked '/00@/' "{99}"
foreach? end

ugle% rm 91chunk.00 92chunk.00

ugle% foreach chunk (*chunk*)
```

```
foreach? set yr=`echo Schunk | sed 's@chunk...@@'`
foreach? set no=`echo Schunk | sed 's@..chunk.@@'`
foreach? sed 's/^.*@//' Schunk > temp
foreach? csplit -k -f pick_SyrSno temp "/^Syr/" "{99}"
foreach? /bin/rm temp
foreach? end
```

B.2 Conversion to Input Format for Magnitude Regression Program (*magqt*)

Conversion to the input format required by magqt, the magnitude regression program, was accomplished with the following tcl script. Three files were created, one for each year. This took approximately 15 minutes, using three Sparc 20's.

```
#!/sw/solaris/bin/dbtcl -f
#
# Reformat pickfiles from volcano catalog into AMPL.REPORT form for magqt
#
# K. Lindquist

proc bail {file} {
        echo Unable to process $file -- Continuing.
        return
}

proc check_summary {line} {
        if {! [regexp {^9[0-9][0-9 ][0-9][0-9 ][0-9][0-9 ][0-9][0-9 ][0-9]} $line]} {
                        return 0
        }
        if {! [regexp {.*[0-9].*} [string range $line 10 13]]} {return 0}
        if {! [regexp {[0-9][0-9]N.*[0-9].*} [string range $line 14 20]]} {return 0}
        if {! [regexp {.*[0-9].*W.*[0-9].*} [string range $line 21 28]]} {return 0}
        if {! [regexp {.*[0-9].*} [string range $line 29 33]]} {return 0}
```

```
        return 1

}

proc check_phase {line} {
        if {! [regexp {^[A-Z ]+} [string range Sline 0 3]]} {return 0}
        if {! [regexp {.*[0-9].*} [string range Sline 24 27]]} {return 0}
        if {! [regexp {.*[0-9].*} [string range Sline 47 49]]} {return 0}
        if {! [regexp {.*[0-9].*} [string range Sline 100 101]]} {return 0}
        return 1
}

proc xmag_to_WAamp {xmag dist depth} {

        if {Sdist < 200.0} {
                        set b1 0.15
                        set b2 0.80
        } else {
                        set b1 3.38
                        set b2 1.50
        }
        set range [expr Sdist*Sdist + Sdepth*Sdepth]
        set alogwmp [expr Sxmag + Sb1 - Sb2*log10(Srange)]

        return [expr pow(10.,Salogwmp)]
}

proc process {current_file outid} {
        set fileid [open Scurrent_file r]

        set line [gets Sfileid]

        if {! [check_summary Sline]} {
                        bail Scurrent_file
                        close Sfileid
                        continue
        }
```

```
    set year 19[string range Sline 0 1]
    set month [string range Sline 2 3]
    set day [string range Sline 4 5]
    set hour [string range Sline 6 7]
    set min [string range Sline 8 9]
    set sec [expr [string range Sline 10 13] / 100.]
      set epoch [exec h2e -y Syear -m Smonth -d Sday -H Shour -M Smin -S Ssec]
      set doy [string range [yearday Sepoch] 4 6]

    set latdeg [string range Sline 14 15]
    set latsign [string index Sline 16]
    set latmin [expr [string range Sline 17 20] / 100.]
    set lat [expr Slatdeg + Slatmin / 60.]
#     if {Slatsign == "S"} {set lat [expr Slat * -1.]}

    set londeg [string range Sline 21 23]
    set lonsign [string index Sline 24]
    set lonmin [expr [string range Sline 25 28] / 100.]
    set lon [expr Slondeg + Slonmin / 60.]
    if {Slonsign == "W"} {set lon [expr Slon * -1.]}

    set depth [expr [string range Sline 29 33] / 100.]

      set line [gets Sfileid]
      while {Sline != ""} {
                  if {! [check_phase Sline]} {set line [gets Sfileid]:continue}
                  scan [string range Sline 0 3] %s sta
                  set dist [expr [string range Sline 24 27] / 10.]
                  set per [expr [string range Sline 47 49] / 100.]
                  set xmag [expr [string range Sline 100 101] / 10.]
                  set WAamp [xmag_to_WAamp Sxmag Sdist Sdepth]

                  set out " Syear-"
                  append out [format "%3s:%2d.%2d.%5.2f " Sdoy Shour Smin Ssec]
                  append out [format "%-4s              " Ssta]
                  append out [format "%3.0f. 0.0000E+00 " Sdist]
```

```
                append out [format "%10.4E %10.4E %10.4E " Sper SWAamp
Sper]
                append out [format "%6.3f %8.3f %7.3f" Slat Slon Sdepth]

                puts Soutid Sout

                set line [gets Sfileid]
        }

        close Sfileid

}

if {Sargc < 1} {
        echo usage: Sargv0 pickfile \[pickfile...\]
        exit 1
}

if {[info exists env(REFORMAT_FILE)]} {
        set output_file Senv(REFORMAT_FILE)
} else {
        set output_file AMPL.REPORT
}

set outputid [open Soutput_file a]

loop i 0 [expr Sargc] {

        set current_file [lindex Sargv Si]

        if {[file size Scurrent_file] == 0} {
                bail Scurrent_file
                continue
        }

        catch "process Scurrent_file Soutputid"
}
```

close Soutputid

B.3 Winnowing

The magqt input files AMPL.REPORT_9* were concatenated and winnowed to choose only Spurr seismic stations, and observations with depth under 20 km and distances under 25 km.

```
ugle% egrep '(NCG|BGL|CKL|CPK|CKT|CKN|CRP|S PU|CGL)' AMPL.REPORT_cat >
AMPL.REPORT_Spurr
ugle% awk '$(NF-7) <= 25. && SNF <= 20. {print}' AMPL.REPORT_Spurr >
AMPL.REPORT_Spurr_win
```

Appendix C

Sample Program Input and Output for Spurr M_L Inversion

C.1 Input to *magqt*

The following is a sample input file for magqt. Comments do not appear in the original file.

```
5                   # Reference distance
0 20                # Minimum and maximum source depths
0                   # Source depth to use for calculations
1 25                # Minimum and maximum distances
1991 001 1993 365   # Minimum and maximum dates for observation
3                   # Minimum allowable number of observations (stations) per event
10                  # Minimum allowable number of observations per station
n                   # Area subsetting ("n" implies none used)
y                   # Invert for station corrections also
0                   # Allow geometric spreading factor to be determined from the
                      inversion
0                   # Allow attenuation parameter to be determined from the inversion
0                   # Allow standard error on observations to be determined from the
                      inversion
n                   # Residual zone selection ("n" implies this wasn't used)
```

C.2 Comprehensive Summary Output from *magqt*

The following is the output file of magqt, showing the number of earthquakes and

stations used, the magnitude and uncertainty of each earthquake from the inversion, the station corrections and their uncertainties from the inversion, the reference parameters, and the observed attenuation and Q values and uncertainties.

number of observ., stations, events, refdist, refmag: 485 5 129 5. 1.4

dim = 136 n = 485 statno(1) = 1

Variance and Standard error = 5.7487078295691D-02 0.23976463103571

Station	Magnitude Correction	# of Obs.
NCG	-0.14 +- 0.054	107
BGL	-0.38 +- 0.053	103
SPU	0.25 +- 0.054	97
CKL	0.15 +- 0.054	78
CRP	0.12 +- 0.055	100

Earthquake (origin time)		Magnitude	# of Obs.
1	1991-037:23:36	0.52 +- 0.137	4
2	1991-038:14:36	0.67 +- 0.149	3
3	1991-042: 3:10	0.36 +- 0.120	5
4	1991-062: 9:19	0.54 +- 0.107	7
5	1991-062: 9:43	-0.07 +- 0.132	4
6	1991-067: 1:56	0.35 +- 0.150	3
7	1991-067:17:28	0.84 +- 0.150	3
8	1991-067:18:23	0.26 +- 0.151	3
9	1991-067:21:33	0.39 +- 0.150	3
10	1991-067:23:26	1.10 +- 0.133	4
11	1991-068:14:12	0.45 +- 0.132	4
12	1991-069:14: 0	0.36 +- 0.150	3
13	1991-071:16:47	0.14 +- 0.121	5
14	1991-072: 0:22	0.57 +- 0.133	4
15	1991-080: 1:38	0.32 +- 0.150	3
16	1991-099: 7:13	0.19 +- 0.149	3

17	1991-102:20:52	0.14 +- 0.148	3
18	1991-112:20: 2	0.06 +- 0.149	3
19	1991-112:23: 1	1.19 +- 0.153	3
20	1991-121:10:13	-0.05 +- 0.121	5
21	1991-121:14:37	0.11 +- 0.133	4
22	1991-121:14:49	0.20 +- 0.149	3
23	1991-121:18:36	0.37 +- 0.132	4
24	1991-122: 6:22	0.59 +- 0.133	4
25	1991-123:15:27	0.59 +- 0.133	4
26	1991-125:19:48	-0.02 +- 0.121	5
27	1991-128:20:49	0.08 +- 0.121	5
28	1991-130:11:52	0.34 +- 0.133	4
29	1991-131:17:43	0.41 +- 0.133	4
30	1991-131:23: 3	-0.12 +- 0.132	4
31	1991-132:11:36	0.19 +- 0.130	4
32	1991-132:16:55	0.54 +- 0.121	5
33	1991-132:21:33	-0.03 +- 0.120	5
34	1991-133:18:13	-0.19 +- 0.149	3
35	1991-133:18:38	0.19 +- 0.133	4
36	1991-135: 1:11	0.06 +- 0.132	4
37	1991-135: 4: 0	-0.01 +- 0.133	4
38	1991-137:20: 8	0.16 +- 0.149	3
39	1991-143:17: 2	0.86 +- 0.133	4
40	1991-143:22:46	0.07 +- 0.148	3
41	1991-165:22:11	0.53 +- 0.131	4
42	1991-172:13: 5	0.30 +- 0.120	5
43	1991-178: 7:57	-0.02 +- 0.133	4
44	1991-179:22:30	0.78 +- 0.152	3
45	1991-180: 4:37	1.00 +- 0.155	3
46	1991-205: 8: 3	0.60 +- 0.133	4
47	1991-206: 7:42	0.76 +- 0.153	3
48	1991-209: 2:31	0.77 +- 0.121	5
49	1991-216: 3:18	0.93 +- 0.133	4
50	1991-217: 5:39	0.22 +- 0.132	4
51	1991-221: 3:23	0.17 +- 0.133	4
52	1991-226: 2:11	0.65 +- 0.132	4
53	1991-227:23:19	1.10 +- 0.150	3

54	1991-228: 0:18	0.40 +- 0.132	4
55	1991-228: 0:58	0.58 +- 0.132	4
56	1991-228: 1:33	0.40 +- 0.132	4
57	1991-228: 2:32	0.89 +- 0.149	3
58	1991-233: 6:29	0.79 +- 0.149	3
59	1991-233:22:28	1.03 +- 0.149	3
60	1991-234: 7:48	0.64 +- 0.112	6
61	1991-234: 8: 3	0.43 +- 0.105	7
62	1991-234:10:14	0.54 +- 0.132	4
63	1991-234:12:20	0.18 +- 0.132	4
64	1991-234:18:35	0.61 +- 0.149	3
65	1991-235: 3: 3	0.56 +- 0.120	5
66	1991-238: 7:15	0.20 +- 0.120	5
67	1991-238:18:10	1.16 +- 0.149	3
68	1991-239:17:25	0.23 +- 0.120	5
69	1991-239:18: 1	0.72 +- 0.148	3
70	1991-240: 7: 6	0.45 +- 0.132	4
71	1991-240:12:52	0.60 +- 0.131	4
72	1991-241: 4: 1	0.16 +- 0.149	3
73	1991-241:15:11	0.24 +- 0.149	3
74	1991-241:21: 7	0.50 +- 0.148	3
75	1991-242: 3: 7	0.42 +- 0.132	4
76	1991-242:14:54	0.44 +- 0.112	6
77	1991-243: 6:31	0.38 +- 0.148	3
78	1991-243: 8:44	0.30 +- 0.148	3
79	1991-244: 9:59	0.33 +- 0.133	4
80	1991-244:11:42	0.55 +- 0.149	3
81	1991-254:20:34	0.01 +- 0.120	5
82	1991-256: 4:12	0.14 +- 0.150	3
83	1991-256: 7: 4	0.19 +- 0.149	3
84	1991-263: 0: 3	0.23 +- 0.151	3
85	1991-271: 6:24	0.40 +- 0.150	3
86	1991-285: 4:14	1.14 +- 0.150	3
87	1991-291: 3: 6	0.38 +- 0.135	4
88	1991-293:23:57	0.56 +- 0.133	4
89	1991-297:10:44	0.29 +- 0.133	4
90	1991-297:19:22	0.27 +- 0.149	3

91	1991-297:19:51	0.31 +- 0.106	7
92	1991-297:20:15	0.24 +- 0.149	3
93	1991-301:21:55	0.68 +- 0.152	3
94	1991-302:16: 0	0.34 +- 0.120	5
95	1991-302:20:22	0.58 +- 0.150	3
96	1991-311: 2:33	-0.14 +- 0.149	3
97	1991-319:20:22	0.30 +- 0.150	3
98	1991-320: 3:48	0.43 +- 0.151	3
99	1991-325: 6:10	0.23 +- 0.131	4
100	1991-332: 4: 5	0.12 +- 0.149	3
101	1991-332: 9:19	0.52 +- 0.150	3
102	1991-334: 6:47	0.21 +- 0.149	3
103	1991-339:17:17	-0.02 +- 0.149	3
104	1991-340:16:27	0.68 +- 0.149	3
105	1991-340:21:54	0.57 +- 0.132	4
106	1991-341:23:26	-0.03 +- 0.149	3
107	1991-342: 5:28	0.14 +- 0.132	4
108	1991-342: 6: 3	-0.09 +- 0.149	3
109	1991-343: 3:15	0.27 +- 0.149	3
110	1991-344:11:53	0.15 +- 0.149	3
111	1991-344:12:15	0.28 +- 0.150	3
112	1991-345: 4:39	0.32 +- 0.151	3
113	1991-347: 8:15	1.04 +- 0.135	4
114	1991-347:12:32	-0.11 +- 0.132	4
115	1991-348: 1:41	0.22 +- 0.149	3
116	1991-348: 2:14	0.31 +- 0.112	6
117	1991-350:19:21	0.02 +- 0.132	4
118	1991-351: 9:48	0.10 +- 0.112	6
119	1991-354: 3:37	-0.17 +- 0.149	3
120	1991-354: 4:30	0.36 +- 0.132	4
121	1991-354: 8:53	0.05 +- 0.132	4
122	1991-355: 9:17	0.26 +- 0.150	3
123	1991-356:10:41	0.46 +- 0.149	3
124	1991-357: 2:31	0.14 +- 0.131	4
125	1991-358: 4:36	-0.12 +- 0.149	3
126	1991-358: 4:55	0.00 +- 0.132	4
127	1991-361:23:39	0.45 +- 0.148	3

128	1991-362: 1:38	-0.21 +- 0.149	3
129	1991-362:22: 4	0.03 +- 0.149	3

Reference Distance = 5.
Reference Magnitude = 1.38
Distance Range = 1.000 - 25.0000
Time Range =1991001 - 1993365
Minimum # of stations = 3
geometrical spreading = 0.825 +- 0.2680
attenuation = 0.02330 +- 0.011516
Q = 223. at 13.74 Hz
Q-low & Q-high (1 sdv)= 153. - 294.
for frequencies = 9.39 - 18.08 Hz

Appendix D

Implementation of General Recursive Filtering

In order to calculate synthetic Wood-Anderson traces from our input seismograms, we have implemented generic time-domain recursive filtering with digital modeling of arbitrary analog filters. This rewrites and expands on the implementation of digital, recursive time-domain Butterworth filtering by Danny Harvey [D. Harvey, *writt. comm.*, 1997]. The following theory presentation begins by following Bozic [1979].

For a general discrete-time, digital filter, the difference equation relating the output sequence y(k) to the input sequence x(k) where k is the index of the time series ($0 \le k < \infty$) is

$$y(k) + b_1 y(k-1) + \ldots + b_M y(k-M) = a_0 x(k) + a_1 x(k-1) + \ldots + a_N x(k-N)$$

Solving for y(k), we see we have a recursive filter definition, meaning that the k'th point of the filtered output sequence y(k) can be obtained from the current input x(k), all the previous inputs {x(i): i<k}, and all the previous outputs {y(i):i<k}:

$$y(k) = \sum_{n=0}^{N} a_n x(k-n) - \sum_{m=1}^{M} b_m y(k-m)$$

Our goal here is to determine the recursive coefficients a_n and b_m. Applying the z-transforms

$$Y(z) = \sum_{k=0}^{\infty} y(k)z^{-k}$$

and

$$X(z) = \sum_{k=0}^{\infty} x(k)z^{-k}$$

term-by-term to the time-series y(k) and x(k), we derive

$$\sum_{k=0}^{\infty} y(k)z^{-k} = \sum_{n=0}^{N} a_n \sum_{k-n=0}^{\infty} x(k-n)z^{-k} - \sum_{m=1}^{M} b_m \sum_{k-m=0}^{\infty} y(k-m)z^{-k}$$

Then

$$\sum_{k=0}^{\infty} y(k)z^{-k} = \sum_{n=0}^{N} a_n \sum_{k'=0}^{\infty} x(k')z^{-(k'+n)} - \sum_{m=1}^{M} b_m \sum_{k''=0}^{\infty} y(k'')z^{-(k''+m)}$$

where k'=k-n and k''=k-m. Factoring out z terms and relabelling indices, we have

$$\sum_{k=0}^{\infty} y(k)z^{-k} = \sum_{n=0}^{N} a_n z^{-n} \sum_{k=0}^{\infty} x(k)z^{-k} - \sum_{m=1}^{M} b_m z^{-m} \sum_{k=0}^{\infty} y(k)z^{-k}$$

or, with the definition of the z-transform above,

$$Y(z) = X(z) \sum_{n=0}^{N} a_n z^{-n} - Y(z) \sum_{m=1}^{M} b_m z^{-m}$$

Rewriting this to give the general recursive filter transfer function H(z), we get

$$H(z) = \frac{Y(z)}{X(z)} = \frac{\sum_{n=0}^{N} a_n z^{-n}}{1 + \sum_{m=1}^{M} b_m z^{-m}}$$

This is the most general form of the z-transform for Infinite Impulse Response (IIR) filters, providing at least one of the b_m is nonzero and all the roots of the denominator are not canceled exactly by the roots of the numerator [Rabiner *et al.*, 1975]. The goal is to determine the coefficients a_n and b_m that satisfy the filter specifications. We proceed by one of the standard techniques, which is to determine the analog filter transfer function H(s) and then to digitize this filter.

To explain the modeling of the analog transfer function H(s) in the digital domain as H(z) we follow Jackson [1989]. The transformation z=exp(sT), where T is the sampling interval, is many-to-one (due to 2π periodicity of $\exp(i\theta)$), causing frequency aliasing. To solve this we need a one-to-one mapping from the s-plane to the z-plane, obtained with a bilinear transformation which compresses the entire s-plane into the strip $-\pi/T \le \mathrm{Im}(s') \le \pi/T$ of the transformed, or s' plane:

$$s' = \frac{2}{T}\operatorname{atanh}\left(\frac{sT}{2}\right)$$

Examining the effect of this transformation on the $j\omega$ axis, we see that

$$\omega' = \frac{2}{T}\operatorname{atan}\left(\frac{\omega T}{2}\right)$$

This is also known as "frequency warping." To compensate for the effect of this we prewarp the continuous filter frequencies before applying the filter, i.e. we compute recursion

coefficients for the frequency

$$\omega = \frac{2}{T}\tan\frac{\omega' T}{2}$$

where ω' is the input frequency [e.g. Kaiser, 1966]. Combining the definition of z with the conformal mapping (bilinear transform) above, we obtain

$$s = \frac{1}{T}\left(\frac{1 - z^{-1}}{1 + z^{-1}}\right)$$

which, solved for z, becomes

$$z = \frac{1 + \frac{T}{2}s}{1 - \frac{T}{2}s}$$

This maps the jω axis into the unit circle.

Writing H(s) in terms of its poles and zeros,

$$H(s) = K\frac{\prod_{m=1}^{M}(s - \sigma_m)}{\prod_{k=1}^{N}(s - s_k)}$$

where K is a gain factor. Calculating the discrete equivalents of the zeros

$$z_m = \frac{1 + \frac{T}{2}\sigma_m}{1 - \frac{T}{2}\sigma_m}$$

and poles

$$p_k = \frac{1 + \frac{T}{2}s_k}{1 - \frac{T}{2}s_k}$$

and substituting s(z) algebraically into H(s) we have

$$H(z) = K'(1 + z^{-1})^{N-M} \cdot \frac{\prod_{m=1}^{M} (1 - z_m z^{-1})}{\prod_{k=1}^{N} (1 - p_k z^{-1})}$$

The K' coefficient is a gain factor, which can be obtained by equating the DC gains

$$H|_{z=1} = H|_{s=0}$$

For a single, real, first-order pole s_1 we have M=0, N=1 and

$$H(z) = K'(1 + z^{-1}) \frac{1}{1 - \left(\frac{1 + \frac{T}{2}s_1}{1 - \frac{T}{2}s_1} \right) z^{-1}}$$

yielding recursion coefficients

$$a_0 = K'$$

$$a_1 = K'$$

$$b_1 = -\frac{2 + Ts_k}{2 - Ts_k}$$

Equating gains at DC,

$$\frac{K}{s_1} = \frac{2K'}{1 - \left(\frac{1 + \frac{T}{2}s}{1 - \frac{T}{s}s} \right)}$$

or

$$K' = \frac{KT}{2 - Ts_1}$$

Normalizing H(s) to 1 at DC, $K=-s_1$.

Since we are putting in real signals and want real signals out, we want a real transfer function. All complex poles in our filters should therefore appear in complex-conjugate pairs $s_k=u+iv$, where u and v are both real constants. For the case of a single, complex-conjugate pair of first-order poles, M=0, N=2 and we obtain a z-plane transfer function of

$$H(z) = K'(1 + z^{-1})^2 \frac{1}{\left(1 - \left(\frac{1 + \frac{T}{2}(u - iv)}{1 - \frac{T}{2}(u - iv)} \cdot z^{-1} \right) \right) \cdot \left(1 - \left(\frac{1 + \frac{T}{2}(u + iv)}{1 - \frac{T}{2}(u + iv)} \cdot z^{-1} \right) \right)}$$

Expanding this out and simplifying,

$$H(z) = K' \frac{a_0 + a_1 z^{-1} + a_2 z^{-2}}{1 + b_1 z^{-1} + b_2 z^{-2}}$$

where, defining the term

$$den \equiv 4 - 4Tu + T^2(u^2 + v^2)$$

we have the recursion coefficients

$$a_0 = K'$$

$$a_1 = 2K'$$

$$a_2 = K'$$

$$b_1 = -\frac{8 - 2T^2(u^2 + v^2)}{den}$$

$$b_2 = \frac{4 + 4Tu + T^2(u^2 + v^2)}{den}$$

Here we find, again equating the DC gains,

$$\frac{K}{(-u - iv)\cdot(-u + iv)} = \frac{K'2^2}{\left(1 - \frac{1 + \frac{T}{2}(u - iv)}{1 - \frac{T}{2}(u - iv)}\right)\cdot\left(1 - \frac{1 + \frac{T}{2}(u + iv)}{1 - \frac{T}{2}(u + iv)}\right)}$$

or

$$K' = \frac{KT^2}{4 - 4Tu + T^2(u^2 + v^2)}$$

Normalizing H(s) to 1 at DC, $K=u^2+v^2$.

For a first-order, real zero of the transfer function σ_1, M=1, N=0 and

$$H(z) = K'(1 + z^{-1})^{-1}\left(1 - \left(\frac{1 + \frac{T}{2}\sigma_1}{1 - \frac{T}{2}\sigma_1}\right)z^{-1}\right)$$

By inspection, our recursion coefficients are therefore

$$a_0 = K'$$

$$a_1 = -K'\frac{1 + \frac{T}{2}\sigma_1}{1 - \frac{T}{2}\sigma_1}$$

$$b_1 = 1$$

Normalization of H(s) at DC gives $-K\sigma_1=1$ or $K=-1/\sigma_1$. Equating H(s) and H(z) at DC.

$$-K\sigma_1 = \frac{K'}{2}\left(1 - \frac{2 + T\sigma_1}{2 - T\sigma_1}\right)$$

which gives

$$K' = \frac{K(2 - T\sigma_1)}{T}$$

For a first-order, complex-conjugate pair of zeroes $\sigma_{1,2}$=u±iv, the z-plane transfer function is

$$H(z) = K'(1 + z^{-1})^{-2}\left(1 - \left(\frac{1 + \frac{T}{2}(u - iv)}{1 - \frac{T}{2}(u - iv)} \cdot z^{-1}\right)\right)\left(1 - \left(\frac{1 + \frac{T}{2}(u + iv)}{1 - \frac{T}{2}(u + iv)} \cdot z^{-1}\right)\right)$$

Once again expanding this out, we find

$$H(z) = K'\frac{a_0 + a_1 z^{-1} + a_2 z^{-2}}{1 + b_1 z^{-1} + b_2 z^{-2}}$$

This produces recursion coefficients

$$a_0 = K'$$

$$a_1 = K'\frac{8 - 2T^2(u^2 + v^2)}{den}$$

$$a_2 = K'\frac{4 + 4Tu + T^2(u^2 + v^2)}{den}$$

$$b_1 = 2$$

$$b_2 = 1$$

using the same definition of *den* as before. Again, equating DC gains

$$K(-u-iv)\cdot(-u+iv) = K'2^{-2}\left(1-\frac{1+\frac{T}{2}(u-iv)}{1-\frac{T}{2}(u-iv)}\right)\cdot\left(1-\frac{1+\frac{T}{2}(u+iv)}{1-\frac{T}{2}(u+iv)}\right)$$

or

$$K' = K\frac{4-4Tu+T^2(u^2+v^2)}{T^2}$$

where

$$K = \frac{1}{u^2+v^2}$$

Because differentiation with respect to time is a simple multiplication by s in the Laplace-transform domain, i.e.

$$y(t) = \frac{d}{dt}x(t) \Rightarrow Y(s) = sX(s)$$

we can represent differentiation with a transfer function H(s) = s, i.e. K=1 and a single zero at the origin. Since we have normalized the DC transfer function to one in the above presentation, however, the formulation must be modified. Also, the bilinear z-transform is not appropriate for a differentiator because the amplitude response of the continuous system is not piecewise constant [Rabiner *et al.*, 1975].Therefore, for a single, first-order zero at the origin we will use recursion coefficients for a first-order, backwards-first-difference differentiator:

$$a_0 = \frac{1}{T}$$

$$a_1 = -\frac{1}{T}$$

This corresponds to the mapping [Rabiner *et al.*, 1975]

$$s = \frac{1 - z^{-1}}{T}$$

or

$$z = \frac{1}{1 - sT}$$

Similarly,

$$y(t) = \int_0^t x(t)dt \Rightarrow Y(s) = \frac{X(s)}{s}$$

is a single, first-order pole at the origin with K=1. This can be represented with a trapezoid-rule integrator [e.g. Press *et al.*, 1992]

$$a_0 = \frac{T}{2}$$

$$a_1 = \frac{T}{2}$$

$$b_1 = -1$$

As an example of the types of filters that can be implemented with this formalism we take the Butterworth lowpass filter, which has the property that the magnitude characteristic is maximally flat at the origin of the s-plane [Rabiner *et al.*, 1975]. Following that reference, the squared-magnitude response of a Butterworth lowpass filter normalized to a cutoff frequency of 1 rad/sec is

$$|H(\Omega)|^2 = \frac{1}{1 + (\Omega)^n}$$

The integer n is called the order of the filter. By analytic continuation, we can write this

$$H(s)H(-s) = \frac{1}{1 + (-s^2)^n}$$

The poles of this transfer function lie at equally-spaced points on the unit circle in the s-plane. Associating the poles in the left-half plane with H(s) and those in the right half-plane with H(-s), we find

$$H(s) = \frac{k_0}{\prod_{k=1}^{n} (s - s_k)}$$

where

$$s_k = e^{j\pi\left[\frac{1}{2} + \frac{(2k-1)}{2n}\right]}, k = 1, 2, \ldots n$$

These lowpass filters can be constructed from the coefficients derived above for real, first-order poles and for complex-conjugate pairs of first-order poles.

To create high-pass, bandpass, and bandstop filters, standard frequency-transformations can be applied to the lowpass transfer functions [Rabiner *et al.*, 1975]. For example, to convert a lowpass filter normalized to 1 rad/sec to a highpass filter with cutoff frequency Ω_u, we apply the transformation

$$s \rightarrow \frac{\Omega_u}{s}$$

to the transfer function.

Applying a filter that consists of multiple stages is as simple as applying the first stage to the input data series, applying the second stage to that output, the third stage to the output of the second, and so on.

References

Bozic, S.M. (1979). Digital and Kalman Filtering, Bedford Square: Edward Arnold Ltd., 157 pp.

Hamming, R.W. (1983). Digital Filters, Second Edition, Englewood Cliffs: Prentice-Hall, 257 pp.

Jackson, L. B. (1989). Digital Filters and Signal Processing, Second Edition, Boston: Kluwer Academic Publishers, 410 pp.

Kanasewitch, E.R. (1975). Time Sequence Analysis in Geophysics, Second Revised Edition, Edmonton: The University of Alberta Press, 364 pp.

Kaiser, J.F., Digital Filters, in System Analysis by Digital Computer, Kuo, F.F. and J.F. Kaiser, eds., New York: John Wiley and Sons, Inc., 438 pp.

Lewis, L. J., D. K. Reynolds, F. R. Bergseth, and F. J. Alexandro Jr. (1969). Linear Systems Analysis, New York: McGraw-Hill, 489 pp.

Press, W. H., S. A. Teukolsky, W. T. Vetterling, and B. P. Flannery (1992). Numerical Recipes in C: The Art of Scientific Computing, Second Edition. Cambridge: Cambridge University Press, 994 pp.

Rabiner, L. R. and B. Gold (1975). Theory and Application of Digital Signal Processing. Englewood Cliffs: Prentice-Hall, 762 pp.

Robinson, E.A. and T.S. Durrani (1986). Geophysical Signal Processing. Englewood Cliffs: Prentice Hall, 481 pp.

Spiegel, M. R. (1965). Laplace Transforms, New York: McGraw-Hill, 261 pp.

Terrell, T. J. (1980). Introduction to Digital Filters, London: Macmillan Press Ltd., 222 pp.

IMAGE EVALUATION TEST TARGET (QA-3)

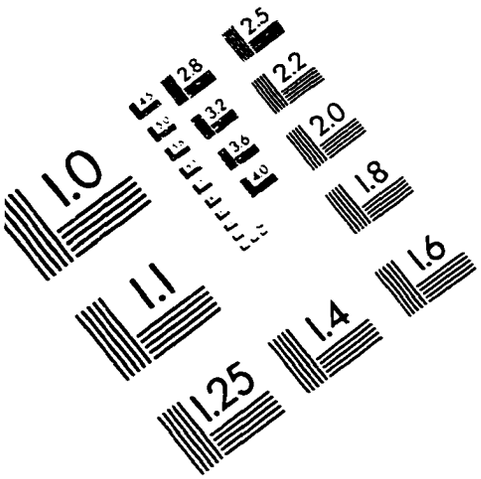

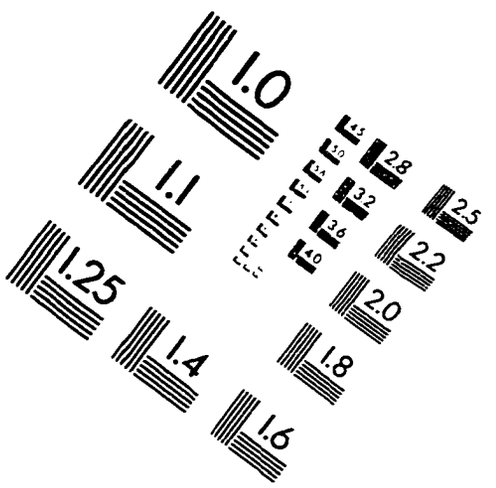

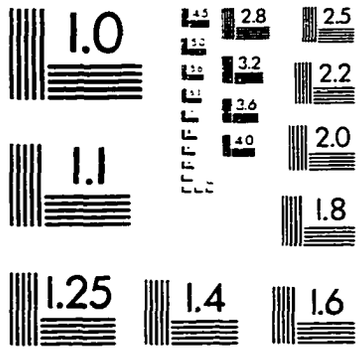

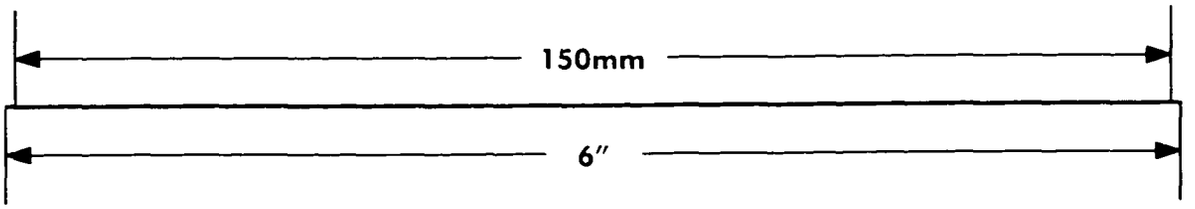

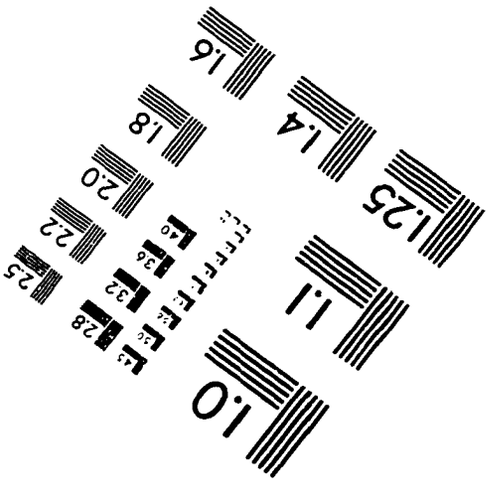

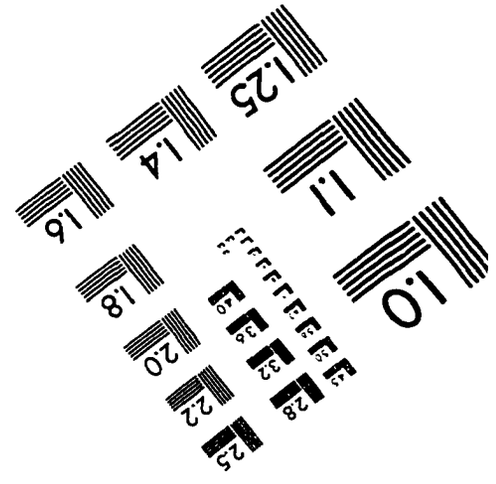

APPLIED IMAGE, Inc
1653 East Main Street
Rochester, NY 14609 USA
Phone: 716/482-0300
Fax: 716/288-5989